



**HAL**  
open science

# Regulation of actin assembly and mechanotransduction in cell-matrix adhesion complexes by the protein RIAM

Clémence Vigouroux

► **To cite this version:**

Clémence Vigouroux. Regulation of actin assembly and mechanotransduction in cell-matrix adhesion complexes by the protein RIAM. Biochemistry [q-bio.BM]. Université Paris-Saclay, 2020. English. NNT : 2020UPASL015 . tel-03872919

**HAL Id: tel-03872919**

**<https://theses.hal.science/tel-03872919v1>**

Submitted on 26 Nov 2022

**HAL** is a multi-disciplinary open access archive for the deposit and dissemination of scientific research documents, whether they are published or not. The documents may come from teaching and research institutions in France or abroad, or from public or private research centers.

L'archive ouverte pluridisciplinaire **HAL**, est destinée au dépôt et à la diffusion de documents scientifiques de niveau recherche, publiés ou non, émanant des établissements d'enseignement et de recherche français ou étrangers, des laboratoires publics ou privés.

# Regulation of actin assembly and mechanotransduction in cell-matrix adhesion complexes by the protein RIAM

**Thèse de doctorat de l'université Paris-Saclay**

École doctorale n° 577, Structure et dynamique des systèmes vivants (SDSV)  
Spécialité de doctorat : Sciences de la Vie et de la Santé  
Unité de recherche : Université Paris-Saclay, CEA, CNRS, Institute for Integrative  
Biology of the Cell (I2BC), 91198, Gif-sur-Yvette, France  
Réfèrent : Faculté des Sciences d'Orsay

**Thèse présentée et soutenue en visioconférence totale  
le 25 novembre 2020 par**

**Clémence VIGOUROUX**

## Composition du Jury

**Benoît LADOUX**

Directeur de Recherche, Institut Jacques Monod (Paris)

Président du jury

**Manuel THERY**

Chercheur CEA, Institut de Recherche Saint-Louis (Paris)

Rapporteur & Examineur

**Grégory GIANNONE**

Directeur de Recherche, Institut Interdisciplinaire de  
NeuroScience (Bordeaux)

Rapporteur & Examineur

**Fanny JAULIN**

Chargée de Recherche, Institut Gustave Roussy (Villejuif)

Examinatrice

**Christophe LE CLAINCHE**

Directeur de Recherche, I2BC (Gif-sur-Yvette)

Directeur de thèse

**Florence NIEDERGANG**

Directrice de Recherche, Institut Cochin (Paris)

Invitée

## ACKNOWLEDGEMENTS

---

Tout d'abord, je tiens à témoigner ma gratitude envers mon directeur de thèse, Christophe Le Clainche, qui m'a fait confiance accomplir cet ambitieux projet. Merci de m'avoir accompagnée et fait grandir tout au long de cette aventure. Merci pour ta disponibilité, pour discuter de toutes sortes de sujets, merci de nous transmettre ton enthousiasme pour la science au quotidien, et surtout, merci pour ton côté humain sans lequel cette thèse se serait passée différemment.

Je remercie chaleureusement notre collaboratrice et ma tutrice de thèse Florence Niedergang pour ses précieux conseils et son attention toute particulière tout au long de ma thèse.

Je tiens à remercier les membres du jury pour avoir pris le temps d'évaluer mon travail doctoral : Benoît Ladoux, Manuel Théry, Grégory Giannone, Fanny Jaulin.

Merci également aux autres membres de mon comité de thèse, Cécile Leduc et Zoher Gueroui, pour leurs discussions constructives, leurs conseils et le suivi de mon projet dans son ensemble.

J'exprime également ma gratitude envers Maud Gorbet et Frédéric Jaisser pour avoir contribué à mon développement scientifique.

Je remercie Louis Renault pour m'avoir accueillie dans l'équipe, pour son intérêt et ses conseils. Merci à tous les membres de l'équipe "ACTIN", actuels ou anciens : Christophe, Louis, Julien, Thanh, Marcelina, Hong, Violaine, Magda, Rayan, Véronique, Blandine, Anani... Merci pour tous ces moments passés ensemble. Julien, merci pour ton soutien, ton aide et tous tes précieux conseils au quotidien. Julien et Marcelina, merci pour les pains au chocolat après chaque sortie footing, et de vous être émerveillés avec moi devant les hérons et les cannetons de Gif. Violaine merci pour les shots tournés et émaillés avec soin. Aussi, je n'oublierai pas les bières l'été dans les buissons ! Hong, thank you for always being amazed at magnificent flowers with me, for the delicious dumplings for our New Year meals and all the good laughs we shared. Thanh, merci pour tous les bons plans quotidiens, jardinage ou autre, pour les ballades dans les jardins giffois et nos discussions sur la culture et cuisine vietnamienne.

Merci aussi à toutes les autres personnes que j'ai pu côtoyer au quotidien, au bâtiment 34, et à l'I2BC, pour avoir contribué à faire de ces années de thèse une période inoubliable de ma vie.

Je remercie également aux membres de la plateforme de microscopie photonique de Gif, Romain Lebars, Sandrine Lécart et Laëtitia Besse.

## Acknowledgements

J'aimerais également exprimer ma reconnaissance envers tous ceux qui me sont chers.

Merci à mes amis, de longue date, de TF, de l'UTC et d'ailleurs, pour embellir ma vie au quotidien.

Je n'oublie évidemment pas ma formidable famille qui m'a toujours soutenue. Merci à tous !  
Cảm ơn cả gia đình !

Mes derniers remerciements sont destinés tout particulièrement à mon mari. Merci de m'avoir encouragée et supportée tout au long de ce voyage. Je te remercie du fond du cœur pour ta patience, ton soutien dans les moments difficiles et pour être toujours à mes côtés ! Chồng yêu ơi, cảm ơn chân thành vì tình yêu vô điều kiện của anh ! Cảm ơn vì anh luôn luôn ủng hộ em và anh lúc nào cũng bên cạnh em !

# TABLE OF CONTENTS

---

RESUMÉ.....	7
SUMMARY .....	8
SYNTHÈSE EN FRANÇAIS .....	9
LIST OF ABBREVIATIONS .....	23
LIST OF FIGURES.....	27
<b>I INTRODUCTION .....</b>	<b>29</b>
<b>I.1 Migrating cells adapt to mechanical cues.....</b>	<b>29</b>
<b>I.2 Actin assembly and actomyosin contraction produce force for movement .....</b>	<b>34</b>
I.2.1 Actin assembly is tightly regulated in filopodia and lamellipodia .....	36
I.2.2 The contractile actomyosin stress fibers are associated to focal adhesions.....	41
<b>I.3 Cell-matrix adhesions couple the actin cytoskeleton and the extracellular matrix to allow cell migration</b>	<b>44</b>
I.3.1 Functions of cell-matrix adhesions.....	44
I.3.2 Diversity of cell-matrix adhesions .....	46
I.3.3 Integrins: the adhesive molecules of cell-matrix adhesions .....	47
I.3.4 A variety of adaptors regulate integrin activity and actin dynamics in cell-matrix adhesions .....	49
I.3.4.1 Talin .....	49
I.3.4.2 Kindlin.....	53
I.3.4.3 Filamin .....	54
I.3.4.4 Tensin .....	55
I.3.4.5 Vinculin .....	56
I.3.4.6 VASP .....	59
I.3.5 Nanoscale organization of focal adhesions.....	60
I.3.6 Dynamics of focal adhesions.....	63
<b>I.4 Cell-matrix adhesions sense and adapt to the actomyosin force.....</b>	<b>65</b>
I.4.1 Cell-matrix adhesions contain a variety of mechanosensors .....	65
I.4.1.1 The exposure of fibronectin RGD motifs is force-dependent .....	65
I.4.1.2 Integrin-ligand interactions behave as catch bonds.....	66
I.4.1.3 The zyxin- $\alpha$ -actinin-VASP complex repairs damaged stress fibers .....	67
I.4.1.4 The mechanosensitive phosphorylation of p130Cas controls signaling pathways.....	67

## Table of contents

I.4.2	Talin is the central mechanosensor of cell-matrix adhesions .....	68
I.4.2.1	The mechanical stretching of talin exposes cryptic vinculin- binding sites.....	68
I.4.2.2	Vinculin locks talin in its extended conformation .....	72
I.4.2.3	Vinculin activation by stretched talin contributes to actin anchoring .....	72
I.4.3	RIAM is a major regulator of talin function.....	74
I.4.3.1	RIAM belongs to the Mig-10 / RIAM / lamellipodin family .....	74
I.4.3.2	The Rap1-RIAM-talin complex activates integrins.....	75
I.4.3.3	The MRL protein-talin-integrin complex regulates actin dynamics.....	76
I.4.3.4	RIAM interacts with talin rod domain.....	78
I.4.3.5	RIAM precedes vinculin within maturing adhesions .....	79
II	AIM OF THE PHD THESIS .....	80
III	MATERIALS AND METHODS .....	82
<b>III.1</b>	<b>Proteins used in the study .....</b>	<b>82</b>
III.1.1	Talin .....	82
III.1.2	RIAM .....	84
III.1.3	VASP .....	86
III.1.4	Vinculin .....	87
<b>III.2</b>	<b>In vitro assays to study the regulation of actin assembly.....</b>	<b>88</b>
III.2.1	Actin polymerization assay .....	88
III.2.2	Actin bundling measurement by light scattering and epifluorescence microscopy observation .....	89
III.2.3	Observation and measurement of single actin filament elongation .....	89
<b>III.3</b>	<b>In vitro reconstitution of adhesion complexes at the surface of lipid vesicles .....</b>	<b>90</b>
III.3.1	Principle of the method .....	90
III.3.2	GUVs preparation.....	92
III.3.3	Reaction assembly.....	92
III.3.4	Microscopy observation and data analysis .....	93
<b>III.4</b>	<b>In vitro reconstitution of mechanosensitive protein complexes on a micropatterned surface.....</b>	<b>93</b>
III.4.1	Principle of the assay.....	93
III.4.2	Micropatterning .....	96
III.4.3	Reaction assembly.....	97
III.4.4	Optimization of the conditions and technical considerations.....	97
III.4.5	Microscopy observation and data analysis .....	98
IV	RESULTS.....	100
<b>IV.1</b>	<b>Article 1: The PIP<sub>2</sub>-talin-RIAM-VASP pathway controls actin polymerization and organization (in preparation).....</b>	<b>100</b>

## Table of contents

<b>IV.2 Article 2: Talin dissociates from RIAM and associates to vinculin sequentially in response to the actomyosin force (Vigouroux et al., 2020)</b> .....	<b>132</b>
<b>V DISCUSSION AND PERSPECTIVES</b> .....	<b>151</b>
<b>V.1 RIAM regulates actin assembly in nascent adhesions</b> .....	<b>151</b>
V.1.1 The MIT complex assembles at the tip of adherent protrusions.....	151
V.1.2 Formation of a PIP <sub>2</sub> -talin-RIAM-VASP complex requires the release of layers of autoinhibition .....	151
V.1.3 The talin-RIAM-VASP complex promotes actin polymerization .....	154
V.1.4 RIAM and lamellipodin have non-overlapping functions.....	157
V.1.5 Does the clustering of the multivalent proteins talin, RIAM and VASP influence actin assembly? ...	158
<b>V.2 RIAM controls the maturation of nascent adhesions into mature focal adhesions</b> .....	<b>159</b>
V.2.1 The actomyosin force destabilizes the talin-RIAM interaction.....	159
V.2.2 The various actin-binding domains of talin contribute differently to the mechanosensitivity of talin	161
<b>V.3 Talin controls the transition between polymerizing and contractile actin networks</b> .....	<b>162</b>
<b>V.4 Deciphering the talin code</b> .....	<b>162</b>
<b>BIBLIOGRAPHY</b> .....	<b>165</b>
<b>APPENDIX</b> .....	<b>183</b>
<b>Article 3: Integrin-bound talin head inhibits actin filament barbed end elongation (Ciobanasu et al., 2018)..</b>	<b>183</b>

## RESUMÉ

---

Pour migrer, les cellules étendent leur membrane vers l'avant, adhèrent à la surface et se contractent de manière coordonnée. Au cours de leur migration, les cellules ressentent les changements de propriétés mécaniques de leur environnement pour s'y adapter. Le cytosquelette d'actine joue un rôle central dans ce processus. La polymérisation de l'actine produit la force nécessaire à la déformation de la membrane en générant deux types de protrusions, plates ou effilées, appelées lamellipodes et filopodes respectivement. Les filaments d'actine s'associent également au moteur moléculaire myosine II pour former des structures contractiles qui tirent le corps cellulaire vers l'avant. Enfin, les complexes d'adhérence assurent le couplage mécanique des protrusions membranaires et du réseau contractile avec la matrice extracellulaire. Ce couplage mécanique est nécessaire pour que les réseaux d'actine génèrent de la force. Il permet également aux complexes d'adhérence de ressentir les forces intra- et extracellulaires.

Le but de ce projet était de comprendre les mécanismes moléculaires par lesquels les complexes d'adhérence à la matrice extracellulaire contrôlent la force produite par l'assemblage du cytosquelette d'actine, et codent l'information mécanique ressentie en réaction biochimique.

La première partie du projet montre que taline recrute séquentiellement les protéines RIAM et VASP à la surface de liposomes pour stimuler l'assemblage de l'actine. La combinaison de cinétiques de polymérisation d'actine en spectroscopie de fluorescence avec des observations de filaments d'actine uniques en microscopie à onde évanescente a révélé le mécanisme par lequel ce complexe stimule l'assemblage de l'actine. Outre VASP, qui était déjà connu pour contrôler la polymérisation de l'actine, cette étude montre que RIAM se lie directement aux filaments d'actine et bloque leur assemblage. L'addition de la profiline, qui interagit avec VASP, RIAM et l'actine, modifie l'activité des protéines et leur permet d'activer la polymérisation de l'actine de manière synergique.

La deuxième étude est basée sur la reconstitution de la machinerie mécano-sensible des complexes d'adhérence avec des protéines pures qui s'auto-organisent sur une surface micro-imprimée observée en microscopie de fluorescence. L'étude montre que les domaines étirables de la taline échangent leur partenaire RIAM contre la vinculine en réponse à la force produite par le cytosquelette. Cet échange se produit avec des efficacités et des mécanismes variables selon les différents domaines de la taline. La taline code donc l'information mécanique en recrutant des combinaisons de partenaires qui correspondent à son degré d'étirement.



## SUMMARY

---

To migrate, cells extend their membrane forward, adhere to the surface and contract in a coordinated manner. During their migration, cells sense changes in the mechanical properties of their environment and adapt to them. The actin cytoskeleton plays a central role in this process. Actin polymerization produces the force necessary to deform the membrane by generating two types of protrusions, flat or finger-like, called lamellipodia and filopodia respectively. Actin filaments also associate with the myosin II molecular motor to form contractile structures that pull the cell body forward. Finally, adhesion complexes ensure the mechanical coupling of the membrane protrusions and the contractile actin network with the extracellular matrix. This mechanical coupling is necessary for the actin networks to generate force. It also allows the adhesion complexes to sense the intra- and extracellular forces.

The aim of this project was to understand the molecular mechanisms by which cell-matrix adhesion complexes control the force produced by the assembly of the actin cytoskeleton, and encode mechanical information into biochemical reactions.

The first study shows that talin sequentially recruits the RIAM and VASP proteins on the surface of liposomes to stimulate actin assembly. The combination of actin polymerization kinetics in fluorescence spectroscopy with observations of single actin filaments in evanescent wave microscopy revealed the mechanism by which this complex stimulates actin assembly. Besides VASP, which was already known to control actin polymerization, this study shows that RIAM directly binds actin filaments and blocks their assembly. The addition of profilin, which interacts with VASP, RIAM and actin, modifies the activity of the proteins and allows them to activate actin polymerization synergistically.

The second part of this project is based on the reconstitution of the mechanosensitive machinery of cell-matrix adhesion complexes with pure proteins that self-organize on a micro-patterned surface observed in fluorescence microscopy. The study shows that talin stretchable domains exchange their partner RIAM for vinculin in response to the force generated by the actomyosin cytoskeleton. This exchange occurs with varying efficiencies and mechanisms for the different domains of talin. Talin therefore encodes mechanical information by recruiting combinations of partners that correspond to its degree of stretch.

# SYNTHÈSE EN FRANÇAIS

## I Introduction

### I.1 Les cellules qui migrent s'adaptent à des stimuli mécaniques

La migration cellulaire joue un rôle primordial dans de nombreux processus physiologiques, comme par exemple le développement embryonnaire, la cicatrisation ou la phagocytose (Foster et al., 2018; Gammill and Bronner-Fraser, 2003; Niedergang and Grinstein, 2018). Une capacité migratoire dérégulée peut conduire à de graves pathologies, ce qui est le cas notamment dans le développement de métastases cancéreuses (Yang et al., 2020).

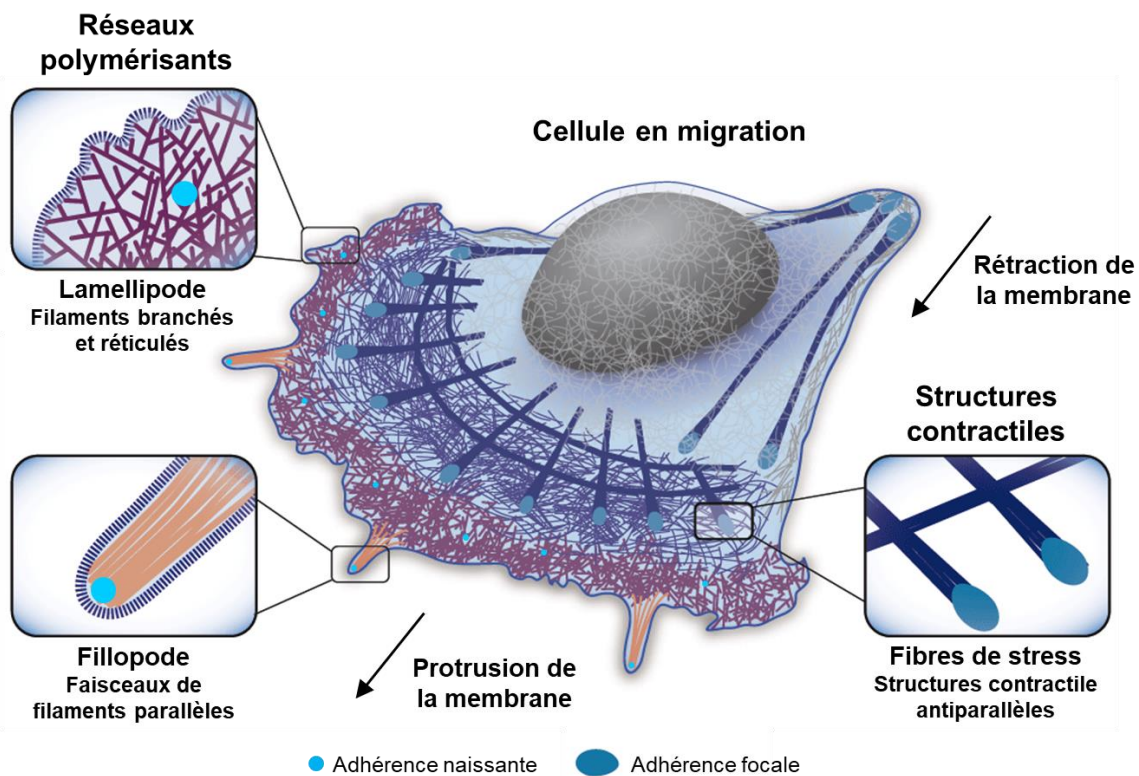


**Figure 1. Représentation des différents réseaux d'actine couplés aux adhésions cellule-matrice extracellulaire dans une cellule en migration.**

Adapté de (Letort et al., 2015).

Les cellules mésenchymateuses migrent en adoptant une polarisation avant-arrière. Tout d'abord, elles émettent de nombreuses protrusions membranaires riches en actine vers l'avant, grâce à l'assemblage de l'actine qui produit une force contre la membrane plasmique. Ces protrusions, plates ou effilées, sont appelées lamellipodes et filopodes respectivement. Des complexes d'adhérence naissants s'y forment (Figure 1). Très rapidement, ils se désassemblent ou mûrissent en adhésions focales sous l'effet de la force produite par les

## Synthèse en français

fibres de stress (Figure 1). Enfin, les adhérences focales à l'arrière de la cellule se détachent et les fibres de stress se contractent, afin de tirer le corps cellulaire dans la direction du mouvement. Dans ce mode de migration lent, la cellule adhère fortement au substrat. Les cellules s'adaptent aux propriétés mécaniques de leur environnement, mais également aux modifications de leur propre activité mécanique. Le cytosquelette contractile étant connecté à la matrice extracellulaire, via des complexes d'adhérence transmembranaires, les propriétés physiques de l'environnement et la contractilité intracellulaire sont extrêmement interdépendantes. Les complexes d'adhérence jouent donc un rôle central pour superviser la relation bidirectionnelle entre l'environnement et le comportement cellulaire. Les mécanismes moléculaires sous-jacents à l'adaptation des cellules aux stimuli physiques demeurent cependant peu compris.

### **I.2 L'assemblage de l'actine et la contraction actomyosine produisent de la force pour le mouvement**

L'actine est une des protéines les plus abondantes des cellules eucaryotes. Le cytosquelette d'actine résulte de l'assemblage dynamique d'actine monomérique ou globulaire (G-actine) en filaments hélicoïdaux (F-actine) polarisés avec deux extrémités structurellement différentes : une extrémité barbée (ou +) et une extrémité pointue (ou -). Les molécules d'ATP liées aux monomères sont hydrolysées en ADP afin de polariser les filaments en leur conférant des dynamiques d'assemblage différentes à chaque extrémité, de sorte que pour de l'actine pure en solution, l'extrémité barbée polymérise alors que l'extrémité pointue dépolymérise. Ce renouvellement, connu sous le nom de tapis-roulant, permet au filament de garder la même longueur tout en polymérisant contre la membrane (Blanchoin et al., 2014; Le Clainche and Carlier, 2008). Cependant, ce phénomène est trop lent pour expliquer à lui seul la grande rapidité de la migration cellulaire. L'addition de facteurs qui agissent de manière coordonnée permet d'accélérer le renouvellement des filaments. Tout d'abord, l'actine globulaire est liée à de la profiline dans les cellules, ce qui empêche la génération spontanée de filaments (nucléation) et dirige l'association des monomères vers l'extrémité barbée spécifiquement. L'ADF/cofiline dépolymérise les filaments à l'extrémité pointue pour augmenter la concentration d'actine monomérique en solution, ce qui accélère l'assemblage à l'extrémité barbée. Les protéines de coiffe bloquent l'élongation d'une majorité d'extrémités barbées, ce qui favorise l'allongement des filaments non-coiffés qui subsistent. De nouveaux filaments doivent donc être générés en continu par des protéines de nucléation pour compenser l'activité des protéines de coiffe.

## Synthèse en français

Les cellules contiennent différents types de réseaux d'actine, associés à des d'adhérences à différents stades de maturation. Au bord avant, où les adhérences naissantes se forment, les réseaux d'actine des filopodes et des lamellipodes polymérisent en réseau de filaments branchés et en faisceaux de filaments parallèles, respectivement (Figure 1). Plus proche du corps cellulaire, les fibres de stress associées aux adhérences focales matures sont des structures contractiles, formées par l'assemblage de filaments d'actine antiparallèles avec des filaments bipolaires du moteur moléculaire myosine II (Figure 1).

### **1.3 Les adhérences couplent le cytosquelette à la matrice extracellulaire**

La migration cellulaire exige que les adhérences subissent des cycles d'assemblage et de désassemblage et qu'elles régulent précisément la polymérisation et l'organisation des filaments d'actine. Les adhérences doivent donc contenir des protéines adhésives qui couplent l'extérieur à l'intérieur de la cellule, mais également des régulateurs de l'assemblage de l'actine.

La molécule adhésive des adhérences à la matrice extracellulaire est le récepteur transmembranaire intégrine. Il est composé de deux sous-unités  $\alpha$  et  $\beta$  associées de façon non-covalente en 24 combinaisons  $\alpha\beta$  différentes. Chaque hétéro-dimère est caractérisé par sa spécificité de liaison à des composants de la matrice extracellulaire, ses mécanismes de régulation et son expression tissulaire (Bachmann et al., 2019). Les intégrines peuvent être dans une conformation repliée inactive ou dans une conformation étendue active. Dans leur conformation active, elles couplent mécaniquement la matrice extracellulaire au cytosquelette via des protéines adaptatrices de liaison à l'actine telles que la taline.

La taline établit le premier lien entre les intégrines et le cytosquelette d'actine et ressent les forces transmises par le cytosquelette. Cette protéine de 2541 acides aminés se compose d'une tête FERM (four point one, ezrin, radixin, moesin) divisée en quatre sous-parties (F0 à F3) et d'un domaine en forme de tige allongée composé de treize faisceaux d'hélices  $\alpha$  (R1 à R13) (Figure 2). Le domaine F3 de la taline se lie à la partie cytoplasmique de la sous-unité  $\beta$  des intégrines pour induire leur conformation active. La taline est auto-inhibée par des interactions intramoléculaires entre ses domaines F3 et R9 et F2 et R12 (Dedden et al., 2019; Goult et al., 2013a, 2009). Cette autoinhibition doit être rompue pour que la taline active les intégrines. La taline contient également cinq domaines de liaison à RIAM (RBS) et onze domaines de liaison à la vinculine (VBS), ses deux partenaires majeurs. Enfin, elle effectue le lien avec le cytosquelette grâce à ses trois domaines de liaison à l'actine (ABD). La taline recrute donc de nombreuses protéines dans les adhérences focales, induisant une grande variété de réponses biochimiques.

## Synthèse en français

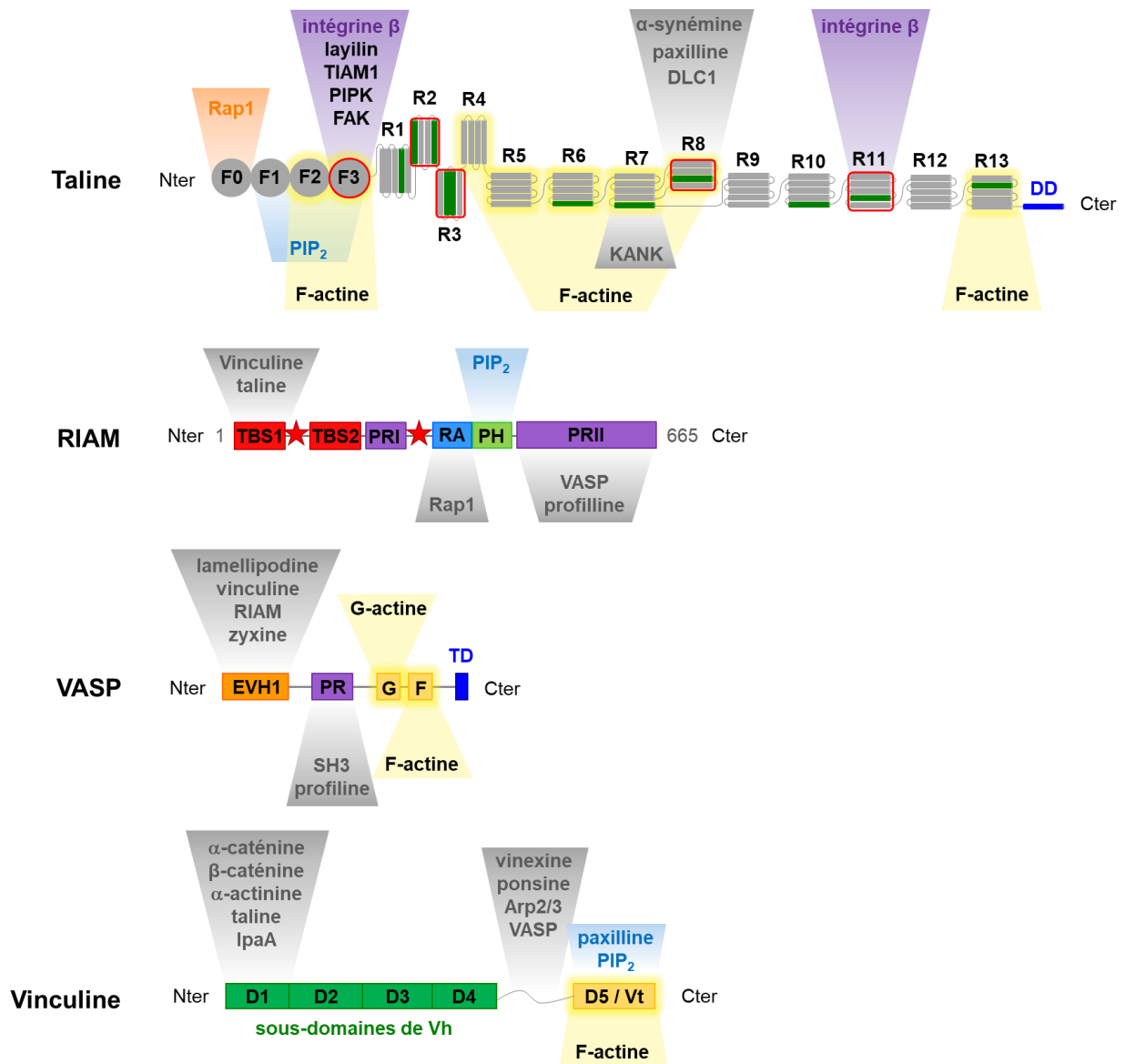


**Figure 2. Domaines et partenaires des protéines étudiées dans ce projet.**

La taline contient un domaine FERM (F0 à F3), une région de treize faisceaux d'hélices  $\alpha$  (R1 à R13), et un domaine de dimérisation (DD). Les domaines de liaison à la vinculine sont les hélices vertes et les domaines de liaison à RIAM sont entourés de rouge. RIAM se compose de deux domaines de liaison à la taline (TBS1 et 2), deux régions riches en proline (PRI et II), un domaine d'association aux GTPases Ras (RA) et un domaine d'homologie à la pleckstrine (PH). Les étoiles rouges indiquent les domaines en superhélice (coiled-coil). VASP contient un domaine d'homologie à Ena/VASP 1 (EVH1), une région riche en proline (PR), un domaine de liaison à l'actine monomérique (G) et aux filaments (F), et un domaine de tétramérisation (TD). La vinculine présente un domaine tête (Vh), sous-divisé en quatre (D1 à D4), et un domaine queue (Vt) séparés par une zone de liaison flexible.

### I.4 Les adhérences cellule-matrice ressentent les forces et s'y adaptent

La taline est une protéine étirable, ce qui en fait le capteur mécanique central au sein des adhérences. Des simulations de dynamique moléculaire ont tout d'abord prédit que les domaines de liaison à la vinculine (VBSs) sont enfouis au cœur des faisceaux d'hélices de la taline (Hytönen and Vogel, 2008). L'utilisation de pinces magnétiques a ensuite confirmé qu'un fragment R1-R2-R3 de la taline expose des VBSs cryptiques permettant la liaison de Vh à la

taline (Del Rio et al., 2009) (Figure 3). Un système reconstitué développé dans notre laboratoire a permis de démontrer que la force physiologique générée par le cytosquelette d'actomyosine, lié à la taline immobilisée sur une surface, est suffisante pour induire la fixation de la vinculine.

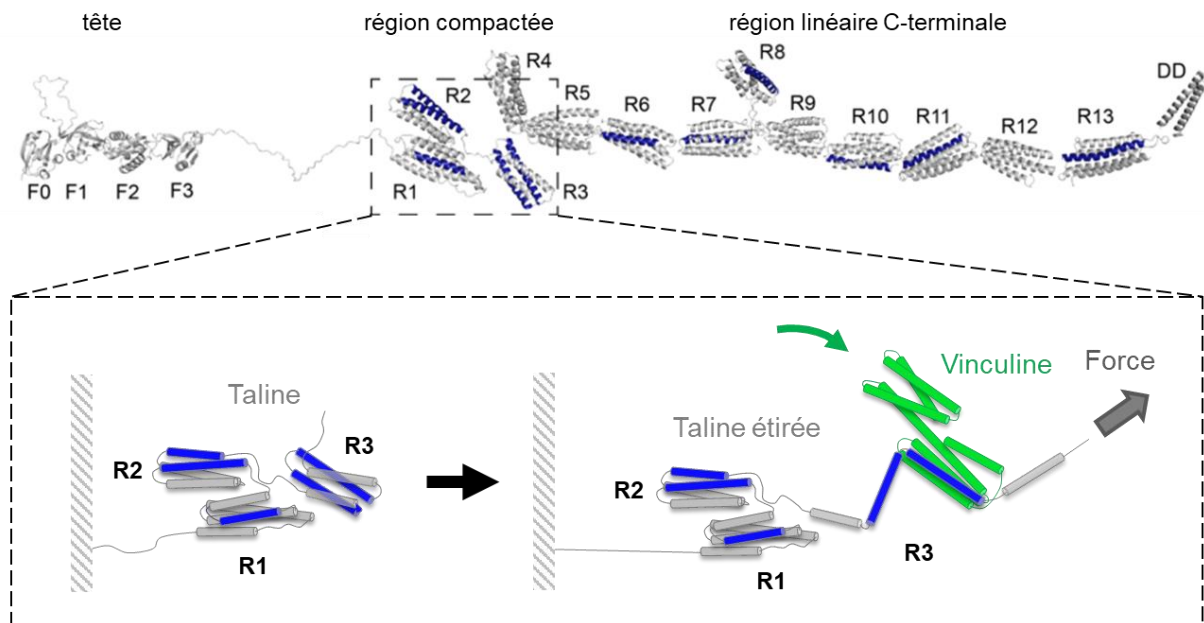


**Figure 3. L'étirement mécanique de la taline expose des domaines de liaison cryptiques à la vinculine.** (Haut) Représentation de la taline entière montrant les onze domaines de liaison à la vinculine colorés en bleu. Adapté de (Yao et al., 2014). (Bas) L'étirement de R1-R2-R3 expose deux domaines consécutifs de liaison à la vinculine dans R3. Par simplification, seulement la tête de la vinculine Vh est schématisée.

De plus, une fois la vinculine fixée à la taline, par son domaine tête (Vh), son domaine C-terminal (Vt) est libéré et peut recruter de nouveaux filaments d'actine, pour renforcer l'ancrage et contribuer à la croissance de l'adhérence focale (Ciobanasu et al., 2014) (Figure 2, Figure 4). Ce point a été confirmé par des études cellulaires (Atherton et al., 2015b). De plus, les auteurs ont montré que la dissociation de la vinculine limitait cinétiquement le retour de la taline étirée à son état de repos après le détachement du cytosquelette d'actomyosine, révélant un mécanisme par lequel la taline est capable de mémoriser de l'information mécanique pour une durée plus longue que celle de la stimulation mécanique. Cette conclusion a été confirmée par des expériences d'étirement de molécules uniques montrant que la taline étirée est bloquée dans cette conformation par la vinculine (Yao et al., 2016, 2014).

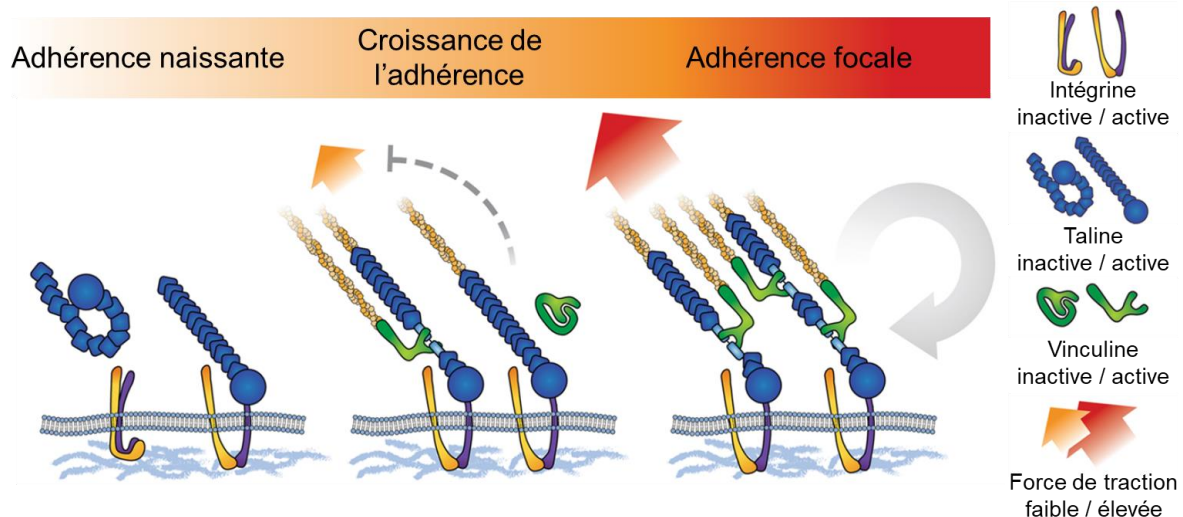


**Figure 4. La liaison de la vinculine à la taline sous l'effet de la force actomyosine renforce l'ancrage du cytosquelette d'actine au complexe d'adhérence.**

Le domaine tête de la vinculine est liée à la taline alors que le domaine queue recrute de nouveaux filaments d'actine pour approvisionner les fibres de stress et renforcer l'ancrage. Adapté de (Rahikainen et al., 2017).

L'autre partenaire majeur de la taline est la protéine Rap1-GTP-interacting adaptor molecule (RIAM). La partie N-terminale (TBS1 et 2) de RIAM se lie à plusieurs domaines de la taline (Chang et al., 2014; Goult et al., 2013b; Lee et al., 2009) (Figure 2).

Tout d'abord, en formant un complexe avec Rap1, RIAM recrute la taline à la membrane et stimule sa capacité à activer les intégrines (Lee et al., 2009). Une étude structurale montre que le domaine TBS1 de RIAM se lie au domaine F3 de la tête de la taline, ce qui briserait l'interaction entre F3 et R9 qui masque le site de liaison et d'activation de l'intégrine dans F3 (Yang et al., 2014). RIAM interagit également avec les domaines R2, R3, R8 et R11 de la partie tige de la taline (Goult et al., 2013b).

De plus, au bord avant des lamellipodes et au bout des filopodes, RIAM (ou son orthologue de la famille MRL (Mig-10 / RIAM / lamellipodine), la lamellipodine) forme un complexe avec la taline et l'intégrine, appelé MIT (protéine MRL-intégrine-taline) complexe (Lagarrigue et al., 2015) (Figure 5). Comme la partie C-terminale riche en proline (PR) de RIAM interagit avec VASP (Jenzora et al., 2005; Krause et al., 2004), connu pour stimuler l'assemblage de l'actine, il a été proposé que VASP confère à ce complexe la capacité de stimuler la polymérisation de l'actine (Figure 2, Figure 5). L'activité du complexe MIT produirait la force pour propulser des intégrines actives afin de sonder les propriétés de la matrice et guider la migration cellulaire (Galbraith et al., 2007; Lagarrigue et al., 2015). Dans ce complexe, la lamellipodine se lie directement aux filaments d'actine et contribue ainsi au contrôle de l'assemblage de l'actine (Hansen and Mullins, 2015). Cependant un rôle direct de RIAM sur la polymérisation de l'actine n'a jamais été rapporté.

## Synthèse en français

Dans les complexes d'adhérence, RIAM précède la vinculine (Lee et al., 2013). Cette observation pourrait être liée au fait que RIAM se lie constitutivement aux domaines étirables R2 et R3 de la taline, contrairement à la vinculine qui s'y lie en réponse à un stimulus mécanique (Goult et al., 2013b). Ces deux études suggèrent donc que la force appliquée par le cytosquelette d'actomyosine au complexe d'adhérence déclenche la transition entre adhérences naissantes et focales en contrôlant la liaison de RIAM et de la vinculine à la taline.

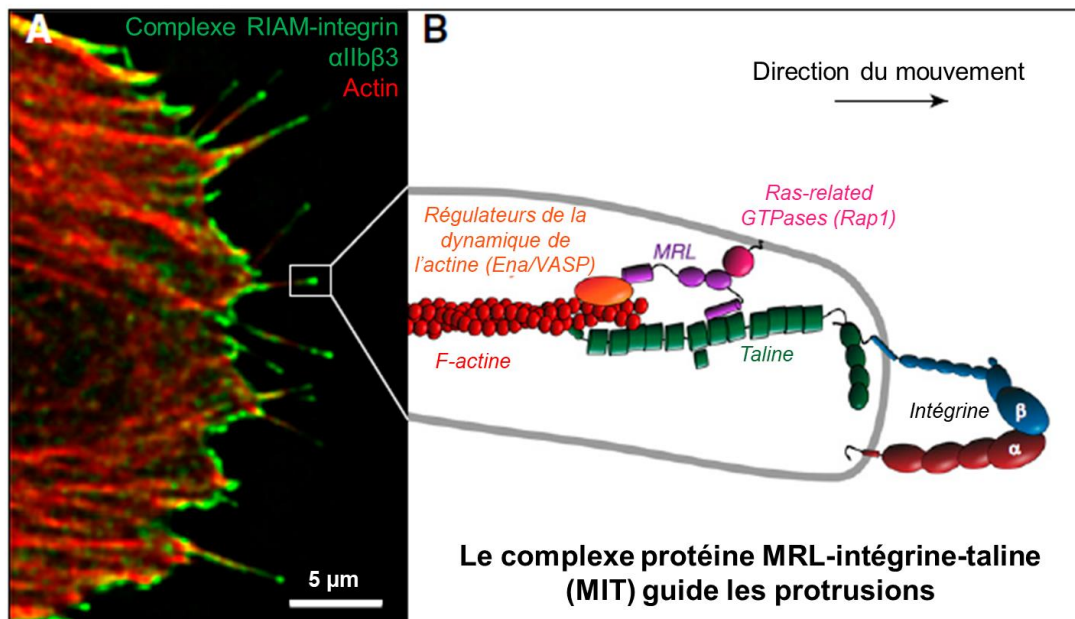


Figure 5. Le complexe protéine MRL-intégrine-taline régule l'assemblage de l'actine au bord avant des lamellipodes et au bout des filopodes.

Adapté de (Lagarrigue et al., 2017).

## II Objectifs de la thèse de doctorat

Pour avancer, les cellules en migration projettent des protrusions membranaires sous forme de filopodes et de lamellipodes. Au cours de ce processus, les adhérences naissantes couplent mécaniquement la polymérisation de l'actine aux adhérences cellules-matrice extracellulaire, afin de générer de la force contre la membrane plasmique. Dans les adhérences naissantes, la protéine de liaison à l'actine taline établit le premier lien entre la matrice extracellulaire, via les intégrines, et le cytosquelette. La taline recrute ensuite un membre de la famille Mig-10 / RIAM / lamellipodine (MRL) ce qui déclenche l'assemblage de l'actine dans les adhérences naissantes formées au bout des filopodes et au bord avant des lamellipodes. A ce jour, le mécanisme par lequel les protéines MRL contribuent à l'assemblage de l'actine est seulement partiellement compris. La protéine VASP, connu pour promouvoir l'assemblage de l'actine, se lie à des motifs spécifiques dans RIAM et la lamellipodine. L'hypothèse a donc été émise qu'il s'associe au complexe protéine MRL-intégrine-taline dans les adhérences naissantes afin d'y promouvoir la polymérisation de l'actine. En outre, la lamellipodine se lie aux filaments d'actine par des



## Synthèse en français

clusters d'acides aminés basiques, localisés dans sa partie C-terminale non structurée, et favorise l'activité de polymérisation d'actine de VASP. Cependant, un rôle direct de RIAM sur la dynamique de l'actine n'a jamais été rapporté et il n'est pas attendu que RIAM se lie aux filaments d'actine car, contrairement à la lamellipodine, il ne contient pas de clusters d'acides aminés basiques dans sa région C-terminale.

Les complexes d'adhérences à la matrice extracellulaire sont capables de ressentir des changements de propriétés mécaniques intra- et extracellulaires. Lors de la migration cellulaire, ces adhérences mûrissent en réponse à l'augmentation de la force actomyosine afin de renforcer la force d'adhésion et l'ancrage au cytosquelette. Au cours de ce processus, l'étirement mécanique de la taline expose des domaines de liaison cryptique pour la vinculine, ce qui permet au complexe taline-vinculine de renforcer l'ancrage de l'actine. Le changement de conformation de la taline qui dépend de la force pourrait être l'interrupteur initial qui déclenche la maturation des adhérences naissantes éphémères en adhésions focales stables. La liaison de RIAM à la taline pourrait réguler ce mécanisme. Cependant, la mécano-sensibilité de l'interaction taline-RIAM n'a jamais été étudiée. L'hypothèse d'une compétition entre RIAM et la vinculine pour la taline reste également à tester. Enfin, plusieurs faisceaux d'hélice de la taline qui interagissent à la fois avec RIAM et avec la vinculine pourraient réagir à la force de façon différente.

### III Matériel et méthodes

Dans la première étude, nous avons utilisé des méthodes biochimiques pour étudier la polymérisation de l'actine : les cinétiques de polymérisation d'actine-pyrène renseignent sur l'assemblage des monomères d'actine en filaments et la mesure de la diffusion de la lumière permet de suivre le regroupement des filaments en faisceaux au cours de la polymérisation. L'observation de filaments uniques en microscopie permet de lever les ambiguïtés dans les mécanismes suggérés par les études cinétiques. Nous avons également reconstitué un complexe talin-RIAM-VASP à la surface de vésicules unilamellaires géantes contenant du PIP<sub>2</sub>, observées en microscopie à épifluorescence.

Dans la deuxième étude, nous avons optimisé une reconstitution de complexes mécano-sensibles développée au laboratoire (Ciobanasu et al., 2015, 2014). La taline est immobilisée dans des disques micro-imprimés sur une surface de verre. La force générée par l'actomyosine dans les disques, étire la taline, ce qui révèle des sites cryptiques de fixation pour la vinculine. L'accumulation de fluorescence d'EGFP-vinculine dans les disques révèle l'étirement de la taline. Nous observons la dynamique de RIAM, la vinculine et l'actine, rendus fluorescents, en microscopie confocale spinning disk.

## IV Résultats

### **Article 1 : La voie PIP<sub>2</sub>-taline-RIAM-VASP contrôle la polymérisation et l'organisation de l'actine (en préparation)**

Nous combinons diverses techniques biochimiques afin d'élucider le rôle du complexe talin-RIAM-VASP localisé dans les adhérences naissantes sur la dynamique de l'actine. La reconstitution d'un complexe talin-RIAM-VASP à la surface de vésicules unilamellaires géantes a tout d'abord montré que la machinerie PIP<sub>2</sub>-talin-RIAM-VASP entraîne l'assemblage de l'actine à la surface des vésicules (Figure 6). Des cinétiques de polymérisation d'actine-pyrène ont ensuite déterminé que cette activité dépend de la profiline. De plus, des observations en microscopie par réflexion totale interne et spinning disk ont révélé que dans ce processus, RIAM coiffe l'extrémité barbée des filaments. Enfin, la mesure de diffusion de la lumière au cours de la polymérisation d'actine a indiqué que le complexe organise l'actine en large faisceaux de façon synergique.

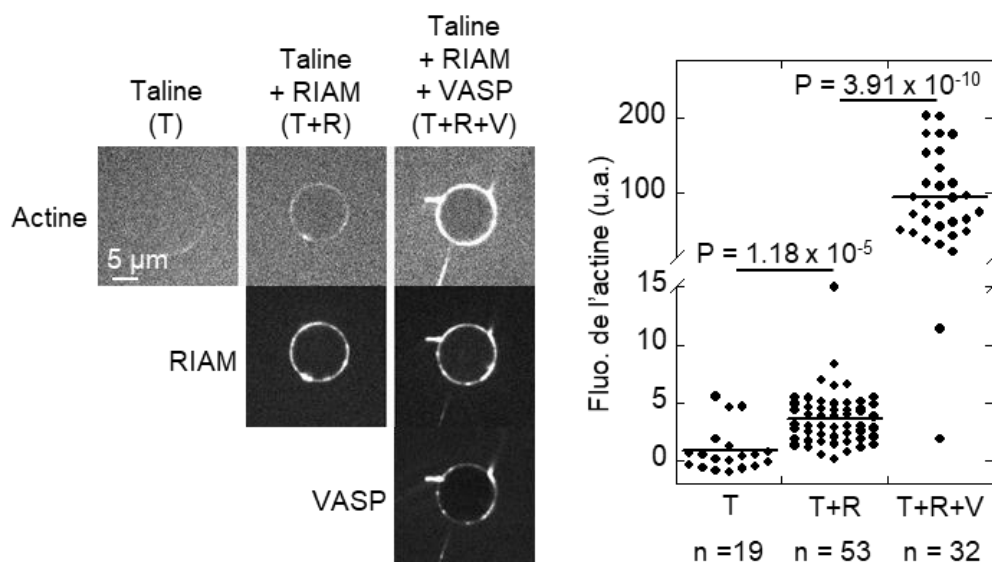


**Figure 6.** Le complexe talin-RIAM-VASP stimule l'assemblage de l'actine à la surface de vésicules unilamellaires géantes contenant du PIP<sub>2</sub>.

### **Article 2 : La taline se dissocie de RIAM et s'associe à la vinculine séquentiellement en réponse à la force actomyosine (Vigouroux et al., 2020)**

Pour déterminer la mécano-sensibilité, la séquence et l'interdépendance de la liaison de la taline à RIAM et à la vinculine, nous avons développé un essai reconstitué avec des protéines purifiées observé en microscopie. Dans ce système, la force générée par l'assemblage de l'actine et de la myosine contrôle la liaison de RIAM et de la vinculine à de la taline immobilisée sur des disques micro-imprimés sur une surface de verre. Nous avons révélé que la force générée par l'actomyosine est suffisante pour étirer mécaniquement la taline, casser son

## Synthèse en français

interface de liaison avec RIAM, ce qui induit sa dissociation. Nous avons aussi montré que l'actomyosine provoque l'échange séquentiel de RIAM pour la vinculine sur différents domaines de la taline (Figure 7). De plus, RIAM affecte de façon variable la mécano-sensibilité des domaines de la taline. En particulier, RIAM augmente le seuil de force nécessaire à l'étirement de certains domaines de la taline, et donc à l'exposition des domaines de liaison à la vinculine qui y sont inclus.

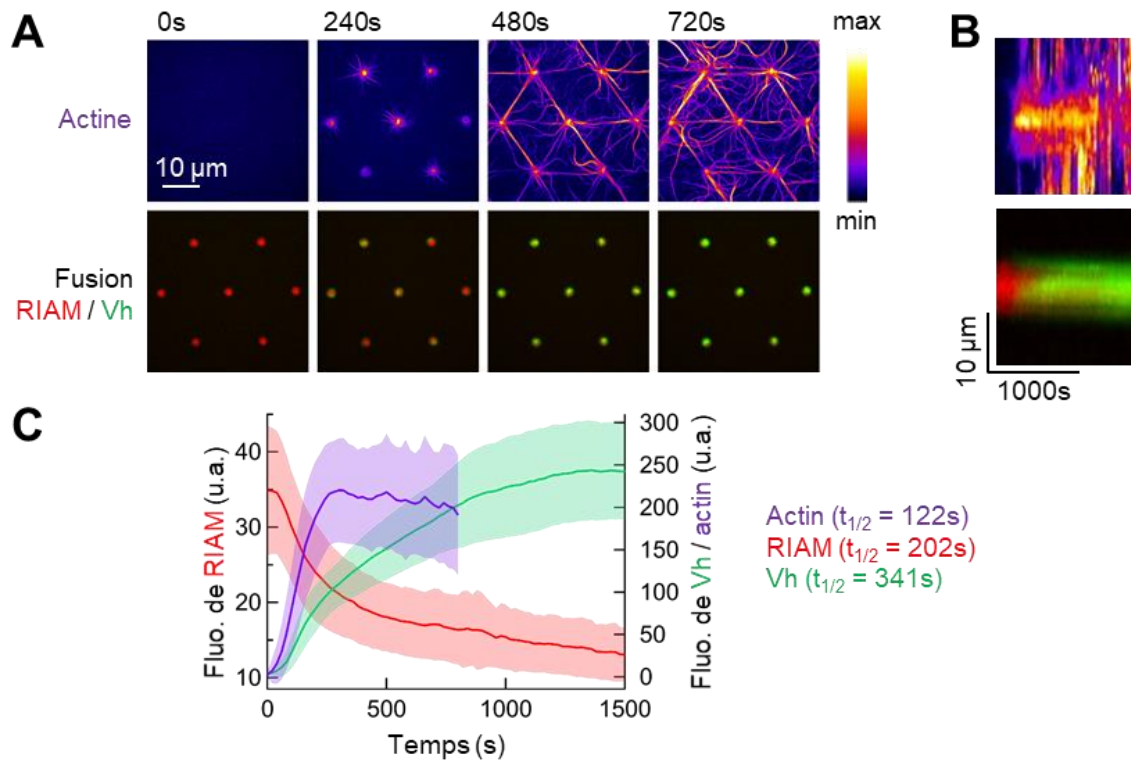


**Figure 7. L'actomyosine provoque l'échange séquentiel de RIAM pour la vinculine sur des disques recouverts de taline.**

(A) Images à différents intervalles de temps montrant que l'accumulation d'actine (haut) dans les disques recouverts de taline coïncide avec la dissociation de RIAM (rouge) et l'association de Vh (vert) (bas). Conditions : 100 nM de mCherry-RIAM 1-306, 100 nM d'EGFP-Vh, 2.4  $\mu$ M d'actine (marquée à 1% à l'Alexa Fluor-647), 50 nM de myosine II, 1  $\mu$ M de taline R1-R2-R3 (pendant l'étape d'incubation). (B) Kymographe le long d'une section d'un disque recouvert de taline montrant la fluorescence d'actine (haut) et une fusion des fluorescences RIAM / Vh (bas) dans les conditions décrites en (A). (C) Quantification de la fluorescence moyenne de chaque composant dans les disques recouverts de taline dans les conditions décrites en (A). Les données présentées sont la moyenne  $\pm$  écart-type.  $n = 63$  disques. La fluorescence d'actine est multipliée par 3.

## V Discussion

Les cellules doivent ressentir les variations de propriétés mécaniques des tissus dans lesquels elles migrent pour s'y adapter. Dans ce processus, les complexes d'adhérence, qui couplent la matrice extracellulaire au cytosquelette d'actine, sont primordiales. L'objectif global de ce projet était d'élucider les mécanismes moléculaires permettant l'initiation des adhérences naissantes couplées à de la polymérisation d'actine et leur progression en adhérence focales sous l'effet de la force produite par le cytosquelette d'actomyosine.

## Synthèse en français

Au bord avant des cellules en migration, le complexe MIT (protéine MRL-intégrine-taline) propulse des intégrines activées, mais non engagées avec la matrice extracellulaire, grâce à la polymérisation de l'actine (Galbraith et al., 2007; Lagarrigue et al., 2015) (Figure 8). Ce mécanisme permet de sonder les propriétés de la matrice pendant la migration. Lorsque l'intégrine reconnaît un ligand, une adhérence naissante se forme (Figure 8). VASP pourrait s'associer au complexe MIT pour stimuler la polymérisation de l'actine, contribuant ainsi à la formation de filopodes et lamellipodes au bord avant de la cellule (Lagarrigue et al., 2015) (Figure 8). Dans le premier article, nous avons découvert que RIAM favorise l'activité de polymérisation de l'actine de VASP. De plus, nous avons montré que RIAM lie les filaments d'actine *in vitro* par sa moitié C-terminale, et qu'il inhibe la polymérisation de l'actine en coiffant l'extrémité barbée des filaments. Cette découverte était inattendue. En effet, la lamellipodine, qui est l'orthologue de RIAM, interagit avec les filaments d'actine par des groupes d'acides aminés chargés positivement absents dans RIAM, et la lamellipodine inhibe la polymérisation de l'actine par un mécanisme différent de RIAM, probablement en séquestrant les monomères. Les protéines de la famille MRL possèdent donc des traits communs, comme l'organisation en domaine et la fonction, mais elles agissent sur le cytosquelette d'actine par des mécanismes d'action différents.

D'autre part, le complexe qui résulte de l'assemblage de dimères de taline, de dimères de RIAM et de tétramères de VASP présente de nombreux domaines de liaison à l'actine, et organise donc l'actine en large faisceaux. Cependant, le complexe MIT se forme au bout des filopodes et ne décore pas entièrement les filaments. Il pourrait donc servir à initier un regroupement en faisceaux à la membrane, alors que d'autres protéines viendraient rapprocher les filaments entre eux sur toute leur longueur.

Nous avons également découvert que l'activité du complexe taline-RIAM-VASP dépend de la profiline. La profiline agit probablement en apportant des monomères d'actine à VASP et RIAM en se liant à des motifs bien caractérisés le long de ces deux protéines. Des études précédentes avaient ainsi établi que l'activité d'élongation de VASP humain, contrairement à celle de VASP de *Dictyostelium*, est peu processive, mais elle est grandement favorisée par la profiline. Nos expériences suggèrent en outre que la profiline confère une activité de nucléation à RIAM, en plus de son activité de coiffe de l'extrémité barbée.



## Synthèse en français

Notre reconstitution a prouvé pour la première fois que la force physiologique de l'actomyosine est suffisante pour induire la dissociation de RIAM des domaines R2, R3 et R11 de la taline. Une étude cellulaire a montré que l'expression de constructions de talin contenant des régions étirables réduites à R1-R2-R3 ou R11 permet le renforcement des adhérences, confirmant l'importance de ces deux régions pour la mécanosensibilité de la taline (Rahikainen et al., 2019). Nous avons également montré que RIAM protège mécaniquement R1-R2-R3 de l'étirement, mais pas R11. Enfin, notre étude suggère que la force nécessaire à l'étirement du domaine R8 est plus grande que celle qui permet l'étirement de R1-R2-R3 et R11, car R8 est inséré dans R7 ce qui le protège de l'étirement (Figure 2).

Ce projet de thèse s'inscrit dans un enjeu plus global d'élucider le « code de la taline ». En effet, dans les cellules, la taline interagit avec de nombreuses autres protéines que celles décrites ici. Nous émettons l'hypothèse que ce grand nombre de combinaisons de partenaires liés à différents domaines de la taline, correspond à des niveaux d'étirement spécifiques de la taline. La cellule pourrait ainsi coder de façon extrêmement précise des variations de forces intra- et extracellulaires. Le changement de partenaire de la taline permet en particulier la progression des adhérences naissantes, associées à un réseau d'actine polymérisant, en adhérences focales, associées à un réseau d'actine contractile (Figure 8. La force produite par le cytosquelette d'actomyosine déclenche l'échange de partenaires de la taline au cours de l'évolution des adhérences naissantes en adhérences focales. Figure 8).

## Table des figures

Figure 1. Représentation des différents réseaux d'actine couplés aux adhérences cellule-matrice extracellulaire dans une cellule en migration.....	9
Figure 2. Domaines et partenaires des protéines étudiées dans ce projet. ....	12
Figure 3. L'étirement mécanique de la taline expose des domaines de liaison cryptiques à la vinculine.....	13
Figure 4. La liaison de la vinculine à la taline sous l'effet de la force actomyosine renforce l'ancrage du cytosquelette d'actine au complexe d'adhérence.....	14
Figure 5. Le complexe protéine MRL-intégrine-taline régule l'assemblage de l'actine au bord avant des lamellipodes et au bout des filopodes. ....	15
Figure 6. Le complexe taline-RIAM-VASP stimule l'assemblage de l'actine à la surface de vésicules unilamellaires géantes contenant du PIP <sub>2</sub> .....	17
Figure 7. L'actomyosine provoque l'échange séquentiel de RIAM pour la vinculine sur des disques recouverts de taline.....	18
Figure 8. La force produite par le cytosquelette d'actomyosine déclenche l'échange de partenaires de la taline au cours de l'évolution des adhérences naissantes en adhérences focales.....	20

## LIST OF ABBREVIATIONS

---

ABD: actin-binding domain

ABS: actin-binding site

ABP: actin-binding protein

ADF: actin depolymerizing factor

ADP: adenosine diphosphate

AFM: atomic force microscopy

APBB1IP: amyloid- $\beta$  precursor protein-binding, family B, member 1-interacting protein

Arp2/3: Actin-related protein 2/3

ATP: adenosine triphosphate

ATRA: all-trans retinoic acid

BME:  $\beta$ -mercaptoethanol

BSA: bovine serum albumin

Cas: Crk associated substrate

CCH: Cas-family C-terminal homology

CH: calponin homology

CP: capping protein

cryo-EM: cryo-electron microscopy

DD: dimerization domain

DLC1: deleted in liver cancer 1

DSF: dorsal stress fiber

ECM: extracellular matrix

EM: electron microscopy

EMT: epithelial-mesenchymal transition

Ena/VASP: Enabled/vasodilator-stimulated phosphoprotein

EPC (or Egg PC): L- $\alpha$ -phosphatidylcholine from chicken egg

EVH1: Ena/VASP homology 1



## List of abbreviations

FA: focal adhesion  
FAK: focal adhesion kinase  
FC: focal complex  
FERM: 4.1 / ezrin / radixin / moesin  
FH1: formin homology 1  
FMNL2: formin-like protein 2  
FN-III<sub>10</sub>: fibronectin type III 10<sup>th</sup> module  
FRAP: fluorescence recovery after photobleaching  
FRET: Förster resonance energy transfer  
F-actin: filamentous actin  
G $\alpha$ 13: guanine nucleotide-binding protein  $\alpha$  13  
GUV: giant unilamellar vesicle  
GST: glutathione-S-transferase  
G-actin: monomeric actin  
IBS: integrin-binding site  
Ig: immunoglobulin  
ITC: isothermal titration calorimetry  
Lpd: lamellipodin  
LUV: large unilamellar vesicle  
mDia1: mammalian diaphanous homologue 1  
MET: mesenchymal-epithelial transition  
MIT: MRL-integrin-talin  
MLC: myosin light chain  
MLR: Mig-10 / RIAM / lamellipodin  
NA: nascent adhesion  
NA: numerical aperture  
NCA: network contraction array  
NMR: nuclear magnetic resonance

## List of abbreviations

NPF: nucleation promoting factor

PREL1: proline-rich EVH1 ligand 1

PH: pleckstrin homology

PIP<sub>2</sub>: phosphatidylinositol(4,5)bisphosphate

PIP1 $\gamma$ : phosphatidylinositol phosphate kinase type 1  $\gamma$

PLL-g-PEG: Poly(L-lysine)-g-poly(ethylene glycol)

PR: proline-rich domain

PTB: phosphotyrosine-binding

PTP: protein tyrosine phosphatase

PVA: Polyvinyl alcohol

RA: Ras-association

Rap1: Ras-related protein 1

RBS: RIAM-binding site

RIAM: Rap1-GTP-interacting adaptor molecule

SAXS: small-angle X-ray scattering

SBD: substrate-binding domain

Scar: suppressor of cAMP receptor

SD: substrate domain

SH: Src homology

SMD: steered molecular dynamics

SR: serine-rich domain

SR101-DHPE: N-(Rhodamine 101 sulfonyl)-1,2-hexadecanoyl-sn-4-phosphoethanolamine

SUV: small unilamellar vesicle

TDA: transverse dorsal arc

THATCH: talin / HIP1R / Sla2p actin tethering C-terminal homology

TIAM1: T-lymphoma invasion and metastasis-inducing protein 1

TIRF: total internal reflection fluorescence

VASP: vasodilator-stimulated phosphoprotein

## List of abbreviations

VBS: vinculin-binding site

WASP: Wiskott-Aldrich Syndrome protein

WAVE: WASP-family verprolin-homologous protein

## LIST OF FIGURES

---

Figure 1. Cell migration plays an essential role in many physiological processes.....	30
Figure 2. Cells sense and adapt to the physical properties of their environment. ....	32
Figure 3. Formation of focal adhesion in response to external force.....	33
Figure 4. Structure of the actin monomer and its assembly into filaments. ....	35
Figure 5. Graphic representation of the distinct actin networks coupled to cell-matrix adhesions in a migrating cells.....	36
Figure 6. Overview of the molecular mechanisms controlling filopodial and lamellipodial actin dynamics.....	38
Figure 7. Initiation of filopodia from the lamellipodial network. ....	40
Figure 8. Myosin II assembles into bipolar mini-filaments to generate force. ....	42
Figure 9. Various types of stress fibers are present in mesenchymal cells.....	43
Figure 10. Downstream regulation of cell-matrix adhesions. ....	45
Figure 11. Organization of the cell-matrix adhesions and actomyosin cytoskeleton in a migrating cell. ....	46
Figure 12. Cell-specific integrin heterodimer combinations and their ligands. ....	47
Figure 13. Integrins domain organization and ligand-induced conformational change.....	49
Figure 14: Talin is localized in focal adhesions, anchor points of actin filaments.....	50
Figure 15: Talin is autoinhibited by two intramolecular contacts. ....	51
Figure 16: Talin-1 domain organization and interactions. ....	52
Figure 17: Kindlin-2 domain organization and binding partners.....	54
Figure 18: Filamin A domain organization and binding partners. ....	54
Figure 19. Tensin-1 domain organization and interactions.....	55
Figure 20: Vinculin domain organization and interactions. ....	56
Figure 21. Autoinhibited and active conformations of vinculin. ....	58
Figure 22: VASP domain organization and interactions.....	59
Figure 23. Clusters of VASP control the processive elongation of actin filaments.....	60
Figure 24. Lateral nanoscale organization of FAs. ....	61

## List of figures

Figure 25. Schematic model of the vertical nanoscale organization of focal adhesions. ....	62
Figure 26. The dynamics of single molecules of integrin and talin reveal the nanoscale organization of FAs.....	63
Figure 27. Cell-matrix adhesions act as a “molecular clutch” to convert the force generated by the actin cytoskeleton into protrusion.....	64
Figure 28. Fibronectin domain organization and interactions. ....	65
Figure 29: P130Cas domain organization and interactions.....	68
Figure 30. Simulation of the force-induced fragmentation of the talin rod fragment, containing helix 1 to helix 12, into $\alpha$ -helix sub-bundles.....	70
Figure 31. The mechanical stretching of talin. ....	72
Figure 32. The force-dependent binding of vinculin to talin reinforces actin anchoring. ....	73
Figure 33. RIAM and other MRL proteins domain organization and interactions. ....	75
Figure 34. The MRL protein-integrin-talin controls actin-based protrusions of the leading edge. ....	77
Figure 35. Localization of RIAM and vinculin in adhesions. ....	79
Figure 36. Talin constructs used in the study. ....	83
Figure 37. RIAM constructs used in the study. ....	85
Figure 38. VASP constructs used in the study. ....	87
Figure 39. Overview of the lipid membrane model systems.....	90
Figure 40. Principle of the formation of giant unilamellar vesicles (GUVs) by the spontaneous gel swelling technique. ....	91
Figure 41. Experimental methods to study stretchable proteins. ....	94
Figure 42. Principle of the in vitro assay used to study mechanosensitive protein complexes. ....	95
Figure 43. The sequential steps to fabricate a micropatterned glass coverslip. ....	96
Figure 44. The actomyosin force triggers the change of talin-binding partners during the maturation of nascent adhesions into focal adhesions. ....	152
Figure 45. Autoinhibited (off) and activated (on) forms of RIAM. ....	153
Figure 46. The talin code: talin domains interact with various proteins. ....	163

# I INTRODUCTION

---

## I.1 MIGRATING CELLS ADAPT TO MECHANICAL CUES

Cell migration is one of the major characteristics of metazoan cells. This locomotion function plays a critical role in many physiological processes (Figure 1). For instance, after a skin injury, cells of the immune system, such as leucocytes and macrophages, move to infectious sites to eliminate pathogens. During this process, macrophages eliminate pathogens by phagocytosis (Niedergang and Grinstein, 2018), while other cell types, fibroblasts for example, travel to the wound to secrete extracellular matrix to help repair the lesion (Figure 1A). Other processes, like the growth of neuronal axons, also require the ability to migrate over very long distances (Lowery and Vactor, 2009). Finally, during vertebrate embryonic development, a population of neural crest cells leaves its location to colonize distant tissues and differentiate into various cell types (Gammill and Bronner-Fraser, 2003). These examples do not constitute an exhaustive list of the physiological processes involving migration, but they illustrate its crucial importance. When triggered in organized tissues like epithelia or deregulated, cell migration can cause serious pathologies. The most striking example is obviously cancer. After accumulating several mutations, some cells lose their identity as immobile epithelial cells and become mesenchymal cancer cells with migratory capacity. This epithelial-mesenchymal transition (EMT) causes cancer cells to invade deeper tissues where they reach and penetrate blood vessels. Following the blood flow, they then access distant tissues where they metastasize (Yang et al., 2020) (Figure 1B).

Cell migration is not ruled by a universal mechanism. However, two main modes of migration, called amoeboid and mesenchymal, are widely accepted. Amoeboid cells have a single migration front and adhere poorly to the surface, allowing them to reach high speeds. Their moving force comes from the contraction of the back of the cell. Mesenchymal cells migrate by emitting numerous flat membrane protrusions, called lamellipodia, or finger-like protrusions, called filopodia, in various directions. The force at the origin of the movement of these cells results from the assembly of the actin cytoskeleton pushing against the plasma membrane. This migration mode is slow because the cells adhere strongly to the underlying extracellular matrix (ECM). Because we are interested in mechanisms that couple actin assembly and adhesion in this study, our work focusses on the mesenchymal migration mode. How these cells assemble dynamic actin cytoskeletal structures, associated to adhesion complexes, to produce the force necessary for movement will be detailed later (See I.2). Besides, many cell types do not move

## Introduction

individually, but collectively, forming more or less cohesive cohorts by interacting via intercellular contacts (Haeger et al., 2015; Ladoux and Mège, 2017).

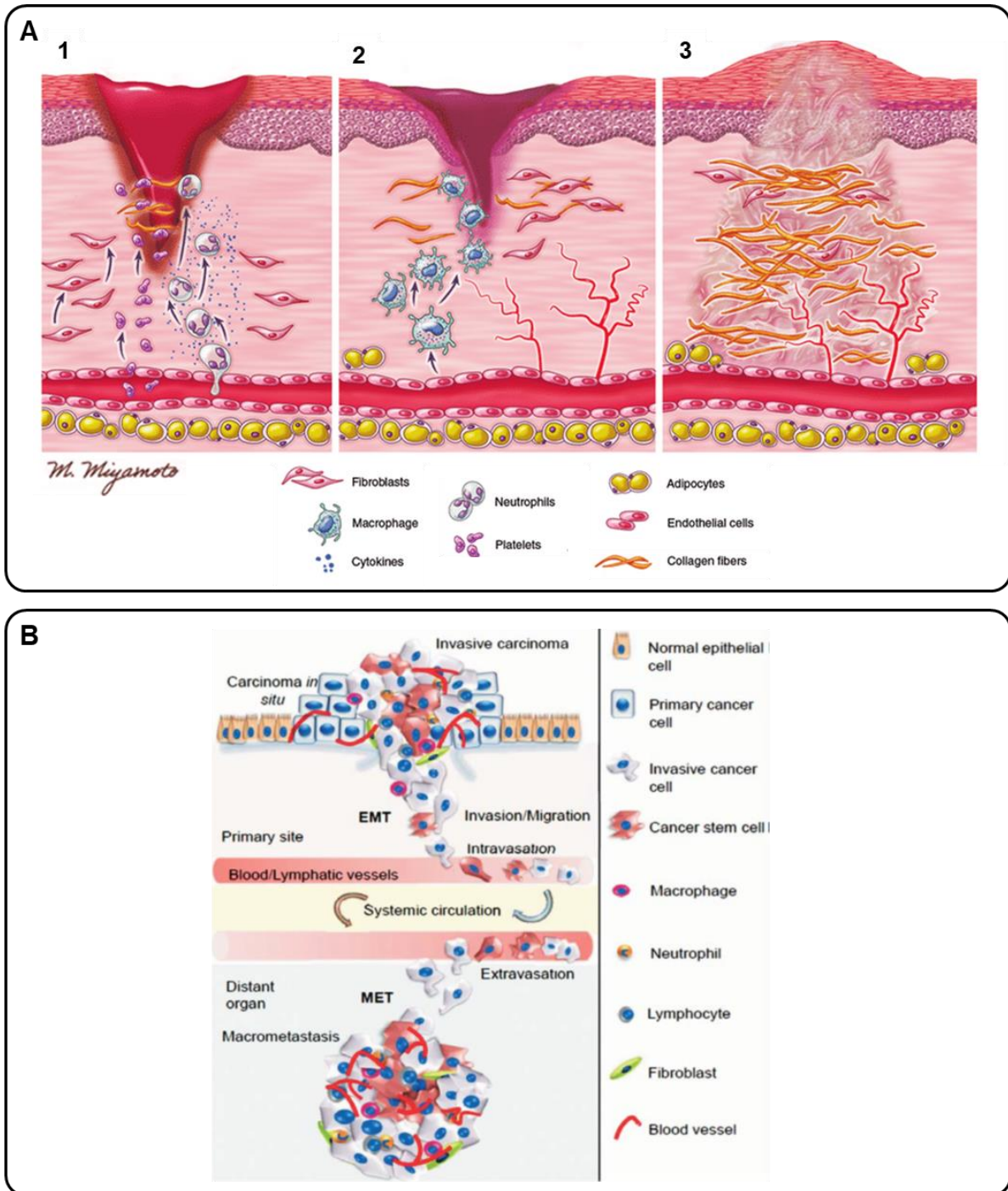


**Figure 1. Cell migration plays an essential role in many physiological processes.**

**(A)** Wound healing involves migration of several types of cells. **(1)** After injury, platelets first cross the endothelium of a blood vessel to form a clot at the injury site. Neutrophils cross the endothelium by diapedesis to move to the wound and release cytokines. Fibroblasts are recruited to the wound to contribute to repair the damaged tissue. **(2)** Macrophages then migrate to phagocytose pathogens and clear dead tissue. Keratinocytes migrate to cover the superficial wound area. New blood vessels form in the wound bed. Fibroblasts begin to secrete new extracellular matrix. **(3)** Lastly, the extracellular matrix is remodeled (Adapted from Foster et al., 2018). **(B)** The epithelial-mesenchymal transition (EMT) leads to the invasion of deeper tissues by cancer cells. The mesenchymal-epithelial transition (MET) then allows these cancer cells to colonize distant tissues and generate secondary tumors (Franco-Chuaire et al., 2013).

## Introduction

The migration mode and its speed do not only depend on the cell type. Indeed, cells are able to adapt their migratory properties to many chemical and physical signals. Chemotaxis allows a cell to migrate in the direction of a concentration gradient of a chemoattractant. During wound healing, for example, fibroblasts are attracted by several substances (Figure 1A). The topography of the surface to which the cells adhere also changes their behavior. Thus, the micrometric curvatures, density or spatial distribution of proteins of the extracellular matrix are information that influences the speed of migration. Although the study of the interaction between cells and 2D surfaces has proved to be a rich source of information, the cellular microenvironment remains much more complex. Immune cells must adopt strategies to deform in order to overcome three-dimensional constrictions. This need is particularly obvious during diapedesis, which requires that leukocytes cross the endothelial barrier of blood vessels to respond to an inflammatory stimulus (Figure 1A). Recent studies show that cells are able to cross passages narrower than their nucleus by disrupting their nuclear envelope transiently (Thiam et al., 2016). In addition to these geometrical characteristics, cells adapt to the mechanical properties of their environment. Cells that migrate on surfaces covered with deformable micro-pillars prefer areas with rigid pillars, where they migrate efficiently (Trichet et al., 2012) (Figure 2A, B). As evidenced by the above descriptions, the study of the biomechanics of migrating cells has greatly benefited from the development of new technologies (Garcia-Arcos et al., 2019). The development of photolithography has enabled imposing specific shapes to cells, by making them attach to adhesive micro-patterns of variable geometry (Théry et al., 2006) (Figure 2D, E). Besides, it is possible to measure the forces applied by cells to their substrates using elastic surfaces or deformable micro-pillars (Figure 2A-C, F).

Cells adapt not only to the mechanical properties of their environment, but also to the modifications of their own mechanical activity. One of the historical experiments that revealed this behavior is the addition of a drug, which destroys the intracellular architecture of the contractile actomyosin cytoskeleton. Indeed, it destabilizes cell-matrix adhesion complexes. Another striking assay showed that the application of a traction force to an adherent cell using a micropipette induces the reinforcement of cell-matrix adhesion complexes, even when cell contractility is inhibited (Riveline et al., 2001) (Figure 3). These experiments clearly revealed that the cell has the ability to adapt the strength of its adhesion to its own contractile force.



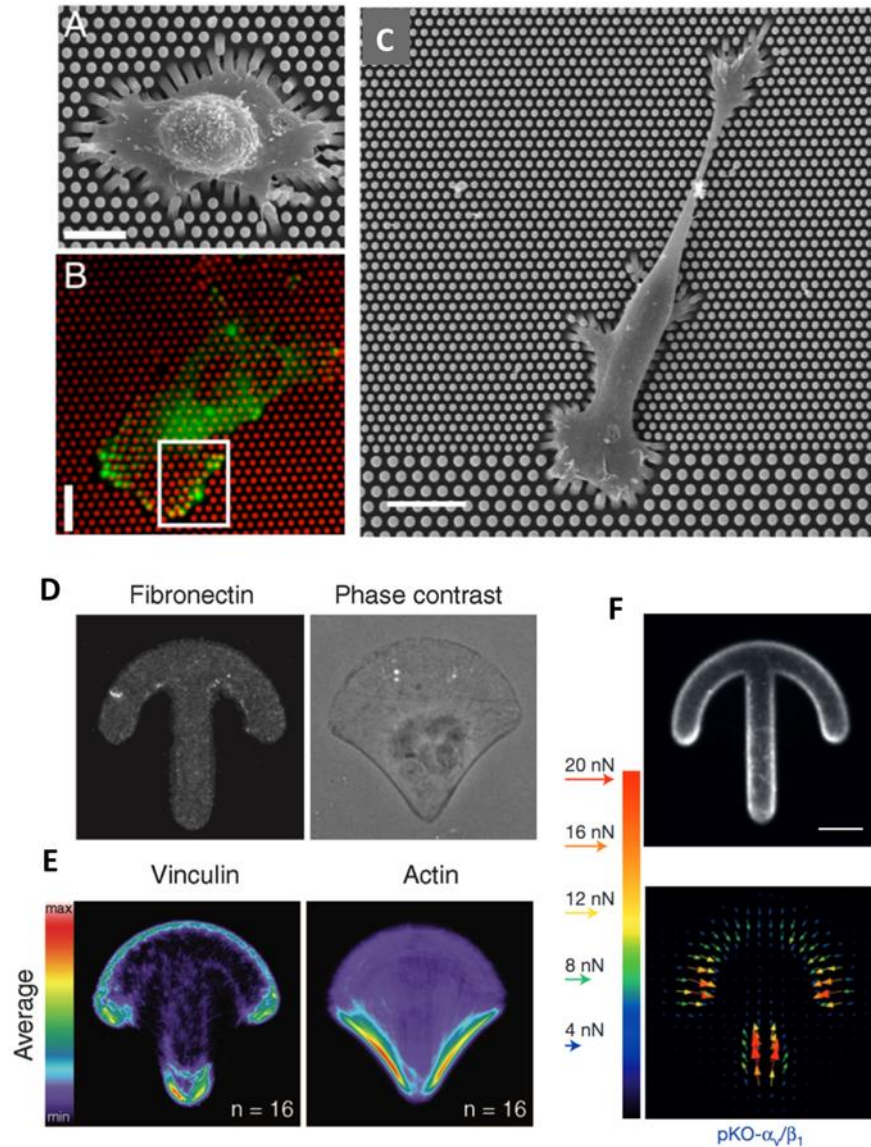


**Figure 2. Cells sense and adapt to the physical properties of their environment.**

(A-C) Adhesion and traction forces developed by fibroblasts on micropillar substrates (Trichet et al., 2012). (A) Electron microscopy image of a typical fibroblast on a micropillar substrate. Scale bar = 15  $\mu\text{m}$ . (B) A fibroblast deforming micropillars. Cy3-fibronectin is in red and YFP-paxillin-rich adhesions are in green. Scale bar = 15  $\mu\text{m}$ . (C) Electron microscopy image of a typical fibroblast spreading between micropillar surfaces of different stiffness. Scale bar = 10  $\mu\text{m}$ . (D) RPE1 cell plated on a fibronectin-coated crossbow micropattern. The left panel shows the fibronectin and the right panel shows the cell in phase contrast. (E) Labeling of vinculin and F-actin from multiple cells were averaged. (F) Average traction-force fields of fibroblasts expressing  $\alpha_v\beta_1$  integrins plated on a fibronectin-coated crossbow micropattern. Scale bar = 10  $\mu\text{m}$ . (D, E) (Théry et al., 2006) (F) (Schiller et al., 2013)

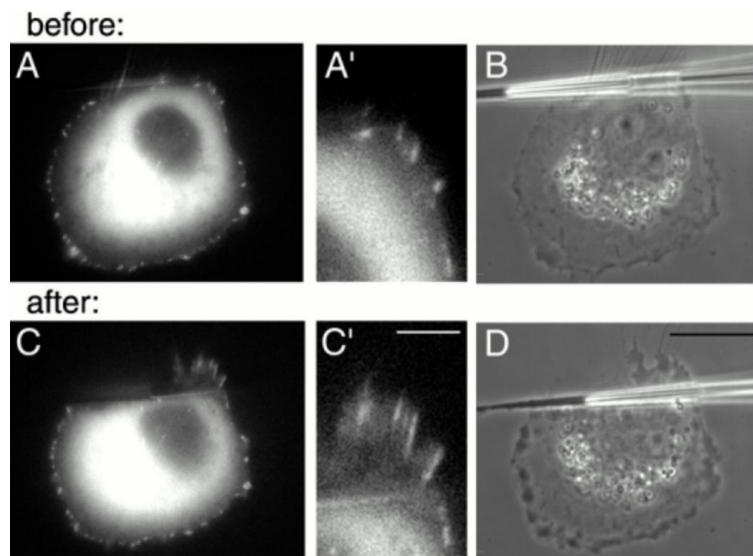


**Figure 3. Formation of focal adhesion in response to external force.**

GFP-vinculin-transfected SV-80 cells are shown before (**A-B**) and after (**C-D**) application of a pulling force produced by a micropipette. (**A, A', C, C'**) GFP-vinculin. (**B, D**) Phase contrast of the same cell. A' and C' represent higher magnifications of A and C. Scale bar = 5  $\mu\text{m}$  in (C') and 20  $\mu\text{m}$  in (D) (Riveline et al., 2001).

The tensile actomyosin cytoskeleton being connected to the extracellular matrix via transmembrane adhesion complexes, the mechanical properties of the environment and the intracellular contractility are highly interdependent. Adhesion complexes thus play a central role in monitoring the bidirectional relationship between the environment and the cellular behavior. Although many observations described the adaptation of cells to variations in their intra- and extracellular mechanical properties, the underlying molecular mechanisms remain poorly understood. The following chapters detail the current knowledge on the molecular aspects of the organization and dynamics of the actin cytoskeleton (See I.2), involved in force production, and the molecular mechanisms by which cell-matrix adhesion complexes control mechanotransduction (See I.3 and I.4).

### I.2 ACTIN ASSEMBLY AND ACTOMYOSIN CONTRACTION PRODUCE FORCE FOR MOVEMENT

The actin cytoskeleton performs a wide range of functions in diverse cell types, such as protruding and contracting membranes for motility, differentiation or cell division, but it also contributes to the movement of intracellular organelles and vesicles. Actin is one of the most abundant proteins in eukaryotic cells and is well conserved among eukaryotes, underlying its crucial importance. Actin exists in three different isoforms in vertebrate, named  $\alpha$ -,  $\beta$ - and  $\gamma$ -actin. The generation and disassembly of actin filaments has to be a very dynamic process in order to fulfill the diversity of actin-associated functions, the major one being the production of force for movement. An individual actin filament is quite flexible, whereas in cells, the association of filaments with actin regulatory proteins produces a variety of architectures that give them specific mechanical properties.

The cellular actin cytoskeleton results from the assembly of a 42 kDa monomeric or globular actin (G-actin), of around 5.5 nm in diameter, into double helical filaments (F-actin). Actin filaments are polar, with two structurally different ends: a slow-growing pointed end (or – end) and a fast-growing barbed end (or + end) (Figure 4). The kinetics of actin polymerization are limited by the nucleation step, consisting in the formation of an actin dimer and then a trimer, which can further be elongated into a filament very rapidly as soon as a trimer is assembled. Actin filament elongation can occur if the concentration of actin monomers available for incorporation in a filament is above what is called the critical concentration. Furthermore, actin polymerization is a dissipative biochemical process, as it is quickly followed by hydrolysis of the ATP carried by the actin subunits inside the filaments into ADP. Thus, it creates a difference between the critical concentration of the ATP-bound barbed end and the ADP-bound pointed end. After depolymerization from the pointed end, the ADP-bound monomers are re-charged with ATP to be further re-incorporated at the barbed end. For pure polymerized actin, the steady state is characterized by a constant concentration of unpolymerized monomeric actin of 0.1  $\mu$ M, implying that the barbed end elongation balances the pointed end depolymerization, so that on average the filament keeps the same length and moves forward. This process is known as “actin treadmilling” (Blanchoin et al., 2014; Le Clainche and Carlier, 2008). Its resulting force pushes the membrane at the leading edge of the lamellipodium, thus allowing the initiation of cell migration. Therefore, the control of actin depolymerization at the pointed end and polymerization at the barbed end determines the protrusive force. However, the treadmilling of actin alone is too slow to account for the speed of cell migration. Thus, a set of regulatory actin-binding proteins cooperate to accelerate the treadmilling. The in vitro study of pathogens, such as *Listeria*, *Shigella* or the vaccinia virus, that hijack the actin

## Introduction

polymerization machinery of host cells to propel themselves, initially allowed the identification of these actin-binding proteins (Cossart and Kocks, 1994; Frischknecht et al., 1999; Loisel et al., 1999; Tilney and Portnoy, 1989).

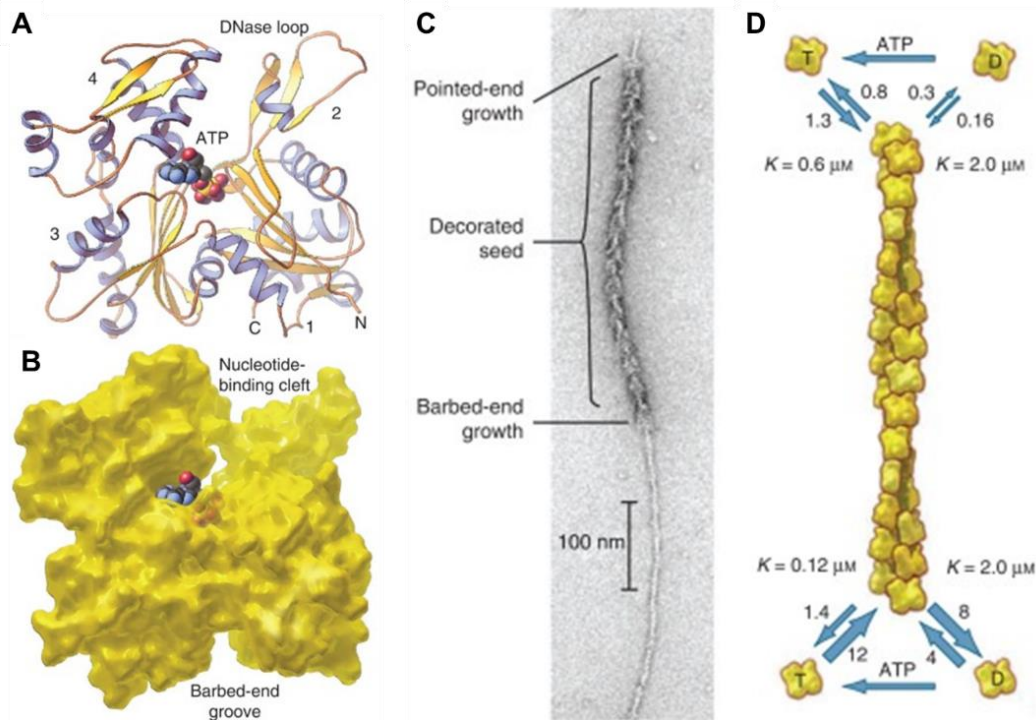


**Figure 4. Structure of the actin monomer and its assembly into filaments.**

(A) Ribbon representation of an actin monomer bound to one molecule of ATP (PDB: 1ATN). (B) Space-filling representation of an actin monomer bound to one molecule of ATP. (C) Electron micrograph of a negatively stained actin filament. (D) Rate constants for actin association and dissociation at the two ends of an actin filament. The pointed end is at the top and the barbed end is at the bottom. The association rate constants are expressed in  $\mu\text{M}^{-1}\text{s}^{-1}$  and the dissociation rate constants in  $\text{s}^{-1}$ . The critical concentration ( $K$ ) values are the ratios of dissociation rate constants to association rate constants. T and D represent ATP-bound and ADP-bound actin, respectively (Adapted from Pollard, 2016).

During cell migration, actin assembles at the front of the cell to extend the flat membrane protrusions, called lamellipodia, and finger-like protrusions, named filopodia. At the tip of filopodia and at the leading edge of the lamellipodium, cells form nascent adhesions (NAs) that connect the extracellular matrix to the actin cytoskeleton to anchor the protrusion (Figure 5). NAs mature into focal adhesions (FAs) in response to the force generated by actomyosin stress fibers. To move forward, the cell retracts its trailing edge by combining actomyosin contractility and disassembly of the focal adhesions at the back of the cell.

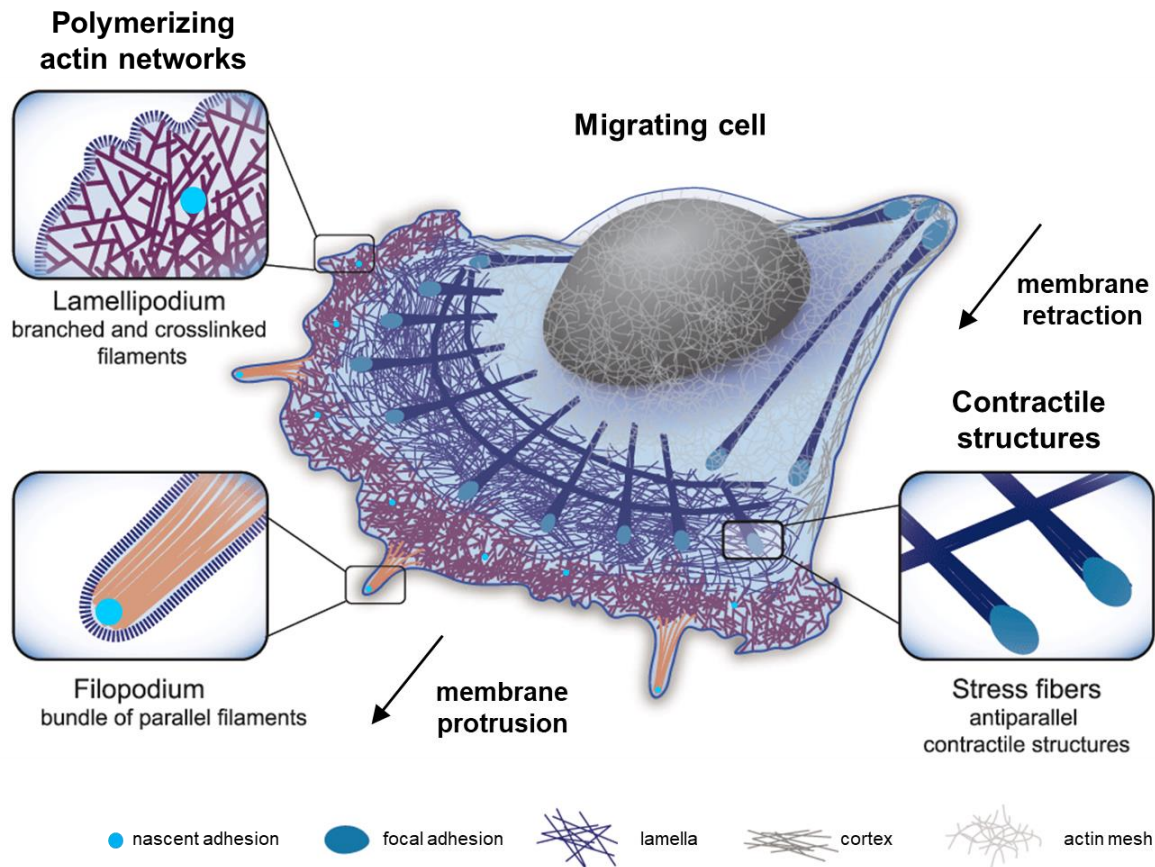


**Figure 5. Graphic representation of the distinct actin networks coupled to cell-matrix adhesions in a migrating cells.**

To move forward, cells extend membrane protrusions at the front and retract the membrane at the rear. The protruding actin structure filopodia and lamellipodia are coupled to nascent adhesions, while the contractile stress fibers are anchored to focal adhesions (Adapted from Letort et al., 2015).

### 1.2.1 Actin assembly is tightly regulated in filopodia and lamellipodia

The assembly of the lamellipodial actin networks is triggered by specific signaling pathways and maintained in rapid turnover by the synergistic action of a set of actin-binding proteins (Blanchoin et al., 2014; Le Clairche and Carlier, 2008).

One of the major actin binding proteins (ABPs) that accelerates actin turnover, or treadmilling, is the Actin Depolymerizing Factor (ADF), also known as cofilin. ADF binds to the side of ADP-actin filaments and favors their disassembly by enhancing the depolymerization of their pointed end (Figure 6). The binding of ADF to filaments also weakens the contacts between actin subunits, which results in their severing, which contributes to the overall disassembly of the actin network (Carlier et al., 1997; Maciver et al., 1991). More recent studies also show that the actin filaments saturated by ADF/cofilin depolymerize from their barbed end in addition to

## Introduction

the pointed end ([Wioland et al., 2017](#)). The concentration of available G-actin thus increases, then allowing a faster barbed end elongation ([Le Clainche and Carlier, 2008](#)).

In cells, the pool of G-actin is predominantly bound to profilin, which plays an important role in actin homeostasis. The profilin-actin complex associates to the barbed end exclusively ([Le Clainche and Carlier, 2008](#); [Pollard and Cooper, 1984](#); [Pring et al., 1992](#)). Profilin thus directs the actin monomers released from the filaments by ADF/cofilin towards the growing barbed end, which produces force against the membrane. Furthermore, profilin enhances the exchange of ADP for ATP to recycle actin monomers and controls actin assembly by preventing the spontaneous formation of actin trimers ([Pollard and Cooper, 1984](#)). Profilin also plays an important role in assisting the elongation machineries, like the Ena/VASP proteins and formins ([Pernier et al., 2016](#); [Romero et al., 2004](#)) (further detailed in the following paragraphs).

Finally, capping proteins block the barbed end of actin filaments. Many proteins have been described as barbed end cappers. Capping protein (CP), the homolog of the striated muscle protein CapZ, is the major barbed end capper in non-muscle cells. CP is enriched in the lamellipodium, where it binds to free barbed ends with a very high affinity. By controlling the length of the filaments, capping proteins contribute to determining the mechanical properties of the lamellipodial actin network. In addition, by blocking a large portion of the free barbed ends, capping proteins help direct the monomers released through ADF-induced depolymerization to the few remaining free barbed ends ([Shekhar et al., 2016](#)).

Ultimately, capping proteins will block all the actin filaments and ADF/cofilin will depolymerize them. To maintain the size and dynamics of the lamellipodial actin network, the cell must therefore constantly generate new filaments to compensate for the action of capping proteins and ADF/cofilin. The process of generating new actin filaments is named nucleation. The major actin nucleator that feeds the lamellipodium with new filaments is a 7-subunits complex, comprising the two actin-related proteins Arp2 and Arp3, called Arp2/3. At the leading edge of lamellipodia, the Arp2/3 complex generates new filaments by branching a daughter filament onto a pre-existing filament, creating a tree-like web (Figure 6). The Arp2/3 complex first needs to be activated by a nucleation promoting factor (NPF) at the plasma membrane. Scar/WAVE (suppressor of cAMP receptor / WASP-family verprolin-homologous protein) is the NPF that activates the Arp2/3 complex at the leading edge of the lamellipodium. Scar/WAVE is in fact a subunit of the WAVE complex, which is under the control of Rac signaling. In this cascade, the catalytic domain of WAVE, called VCA, plays a central role. This domain is made of a verprolin homology sequence (V) that binds monomeric actin, a central domain (C) and an acidic (A) sequence that binds the Arp2/3 complex. VCA makes a complex with a preexisting filament,

## Introduction

the Arp2/3 complex and an actin monomer to initiate the formation of a lateral actin branch (Machesky et al., 1999) (Figure 6).

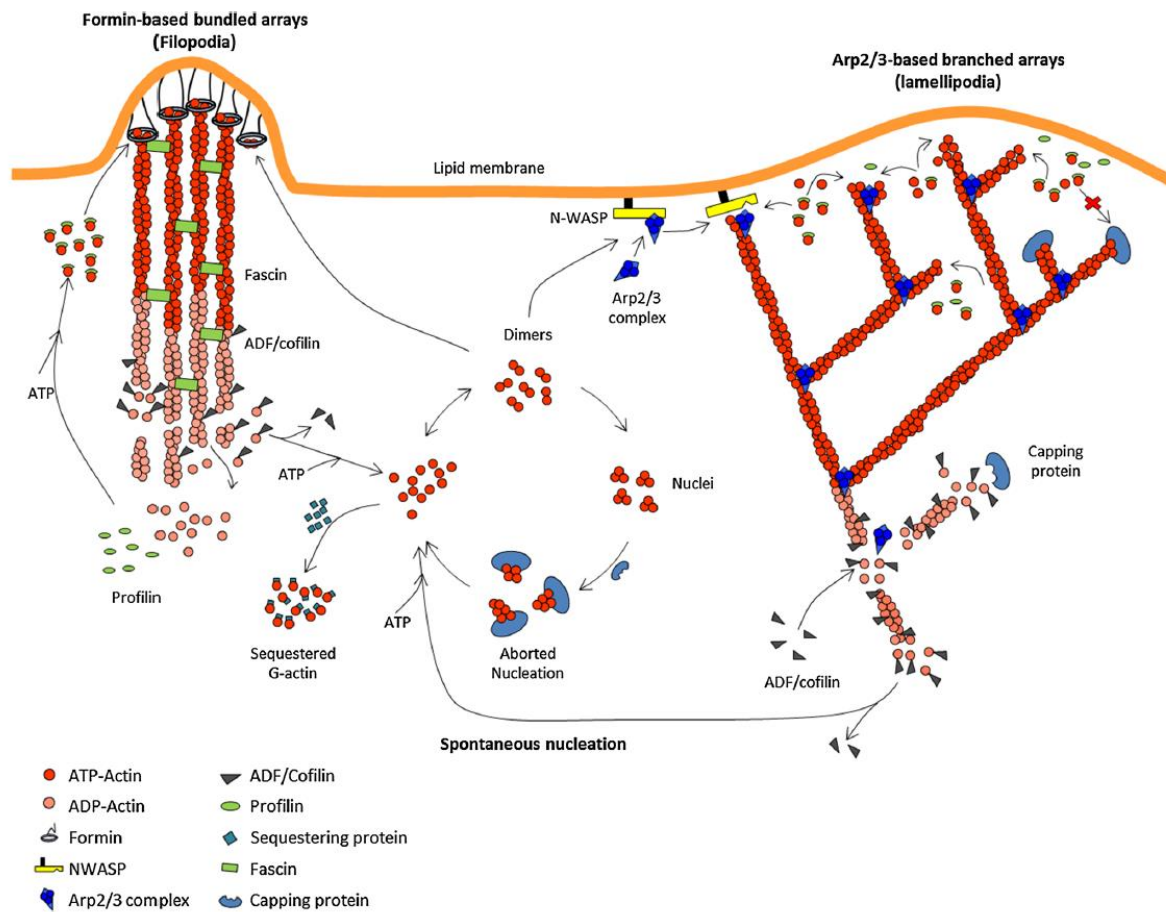


**Figure 6. Overview of the molecular mechanisms controlling filopodial and lamellipodial actin dynamics.**

This sketch features the elongation of actin filaments by formin in filopodia (left), and the branching of actin filaments by the Rac-WAVE-Arp2/3 pathway at the lamellipodium (right) by the combined actions of capping protein, ADF/cofilin and profilin. Spontaneous nucleation of ATP-actin is aborted by capping protein and locally facilitated by nucleators. In the lamellipodium, a balanced number of barbed ends is maintained by the equal frequency of “birth” by branching and “death” by capping. Capping protein is also required for regulating the length of formin-induced filament in filopodia. For simplicity, only the protein machineries responsible for filament branching (WASP family of proteins) and for processive individual filament assemblies (formins) are drawn (Carrier, 2015).

Other major players in lamellipodial actin dynamics are the proteins of the Ena/VASP (Enabled/vasodilator-stimulated phosphoprotein) family, which are found at the leading edge of moving cells and associated with protruding lamellipodia but not with retracting lamellipodia (Rottner et al., 1999) (more details on VASP in section I.3.4.6). VASP is not a specific regulator of lamellipodial actin dynamics since it is also localized in focal adhesions and filopodia.

Finally, lamellipodial actin assembly is also enhanced by members of the formin family (Faix and Rottner, 2006; Rottner et al., 2017; Svitkina et al., 2003). However, as described in the following paragraphs, the role of formins has been more documented in filopodia than in lamellipodia. The significant role of filopodia components in the protrusion of lamellipodia is

## Introduction

not surprising, since both structures are interdependent, as exemplified by the formation of filopodia in Arp2/3-null cells (Suraneni et al., 2012).

During migration, cells also extend finger-like protrusions, called filopodia, beyond the leading edge of protruding lamellipodia to explore the environment and initiate adhesions to the substrate. These protrusions do not contain CP nor Arp2/3. They are composed of unbranched, parallel, bundled actin filaments with their growing barbed ends facing the plasma membrane. Several mechanisms have been put forward to explain the initiation and elongation of filopodia. In the first mechanism proposed for filopodia formation, the filopodial actin bundles result from the reorganization of the lamellipodial branched network by crosslinkers, such as fascin, while the elongation of actin filament barbed ends is enhanced by Ena/VASP proteins located at the tip of filopodia (Svitkina et al., 2003) (Figure 7). In vitro studies have discovered that VASP might promote the elongation by protecting actin filaments against the action of capping proteins (Bear et al., 2002). VASP clusters could also enhance the elongation of actin filament barbed ends in a processive-like manner (Breitsprecher et al., 2011; Hansen and Mullins, 2010). However, it is currently unclear whether this activity of VASP is involved in the elongation of filopodia, since its efficiency to enhance the elongation speed of actin filaments varies greatly from one species to another. Explaining these differences probably requires considering the elongation machinery as composed of VASP and its ligand profilin, rather than VASP alone. *Dictyostelium* VASP is highly processive but insensitive to profilin (Breitsprecher et al., 2008), while human VASP is poorly processive but its activity is highly enhanced by profilin (Hansen and Mullins, 2010). More recent studies suggest that actin filament barbed ends elongation in filopodia is accelerated by the formin mDia2. Formins are characterized by their formin homology 1 and 2 domains (FH1 and FH2). The FH2 domain nucleates actin filaments while the FH1 domain recruits profilin-actin complexes to elongate the FH2-bound filament in a processive manner (Figure 6, left) (Kovar et al., 2006; Paul and Pollard, 2008; Romero et al., 2004). Alternatively, by binding transiently to the barbed end, formins can accelerate the dissociation of profilin from the barbed end, which limits elongation (Funk et al., 2019).



## Introduction

Although the rearrangement of lamellipodia is generally admitted as a mechanism for filopodia formation, it is important to mention that different types of filopodia may co-exist in cells, and the mechanisms of their formation could vary from one cell type to another. The observation that filopodia form in Arp2/3-null cells supports the existence of these alternative mechanisms (Steffen et al., 2006).

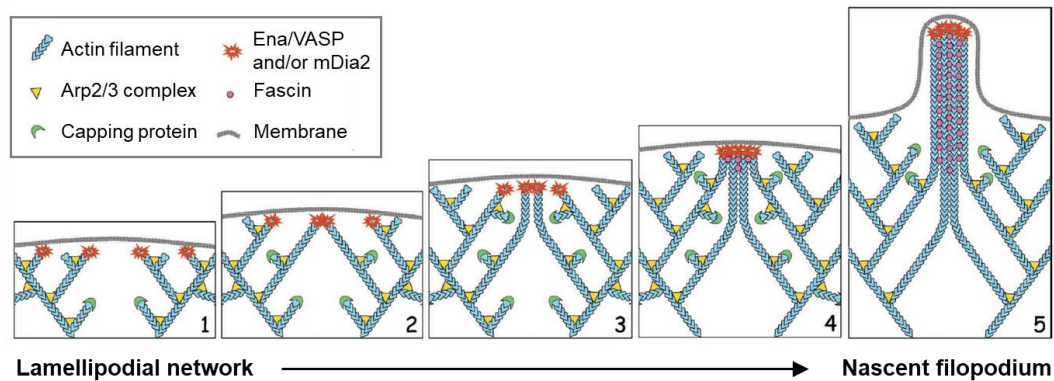


**Figure 7. Initiation of filopodia from the lamellipodial network.**

(1) The lamellipodial actin network is branched by the Arp2/3 complex. Capping protein blocks the elongation of some barbed ends in the network. A tip complex containing Ena/VASP proteins is located at the end of non-capped barbed ends and allows them to elongate continuously. (2) The Ena/VASP-bound barbed ends drift laterally during their elongation and come into contact with each other. Ena/VASP mediates the clustering of these barbed ends upon collision. (3) The filaments that converged continue to elongate together. (4) Ena/VASP proteins recruit fascin, which initiates filament cross-linking. (5) The bundling and elongation of the filaments in the growing filopodia continue (Adapted from Svitkina et al., 2003).

As mentioned at the beginning of this introduction, the mechanical coupling between actin assembly and cell-matrix adhesion determines the protrusion efficiency during cell migration. Moreover, the leading edge of migrating cells needs to initiate adhesions in order to sense the ECM and guide cell migration. Interestingly, several observations link both the lamellipodial and filopodial actin networks to nascent cell-matrix adhesions (Romero et al., 2020).

First, the Arp2/3 complex transiently interacts with the adhesion protein vinculin by a direct binding (more details on vinculin in section 1.3.4.5). This interaction is sufficient to recruit the Arp2/3 complex to integrin-rich sites at the leading edge (DeMali et al., 2002). More recently, a hybrid complex containing vinculin and 4 subunits of the Arp2/3 complex has been identified by mass spectrometry (Chorev et al., 2014). Similarly, the integrin regulator kindlin-2 and the focal adhesion kinase (FAK) interact with Arp2/3 (Böttcher et al., 2017; Romero et al., 2020; Serrels et al., 2007; Swaminathan et al., 2016). These interactions are required for lamellipodium protrusion. Whether vinculin, kindlin-2 and FAK contribute to anchor the branched actin network of the lamellipodium to nascent adhesions is an intriguing possibility that remains to be determined.

## Introduction

In addition to these Arp2/3-dependent mechanisms, a multiprotein complex located in both lamellipodial and filopodial protrusions couples actin and adhesion. This complex is composed of the cell-matrix adhesion receptor integrin, the actin-binding protein talin, which activates integrins, and a protein of the Mig-10 / RIAM / lamellipodin (MRL) family. This MRL protein-integrin-talin (MIT) complex localizes at the tip of filopodia, suggesting a role in actin assembly. This hypothesis is further supported by the impaired cell protrusions observed after disruption of the MIT complex by RIAM knockdown ([Lagarrigue et al., 2015](#)). The mechanism by which MRL proteins contribute to actin assembly in membrane protrusions is described and discussed later (See 1.4.3.3).

### 1.2.2 The contractile actomyosin stress fibers are associated to focal adhesions

In addition to lamellipodia and filopodia, mesenchymal cells contain another type of actin network, called stress fibers. These actomyosin tensile structures are anchored to FAs and allow the cell to pull its body during migration. The organization and dynamics of stress fibers vary greatly from one cell type to another: some cells have almost no stress fibers because they migrate very rapidly and do not form mature focal adhesions, while others organize their actin network to form numerous contractile fibers associated to prominent focal adhesions.

The force generated by stress fibers comes from the activity of the non-muscle myosin II. Unlike many myosins, the dimer of non-muscle myosin II is not processive because the two myosin motor heads do not walk along the actin filaments in a coordinated manner. In order to generate force, multiple molecules of non-muscle myosin II must assemble into bipolar mini-filaments (Figure 8A, B). Myosin II generates force through a conformational change that pulls the actin filament. This mechanism, called power stroke, is fueled by ATP hydrolysis. The power stroke occurs when phosphate is released from the actin-bound myosin head after ATP hydrolysis (Figure 8C). The binding of a new molecule of ATP induces the dissociation of myosin from the actin filament to start a new cycle.

## Introduction

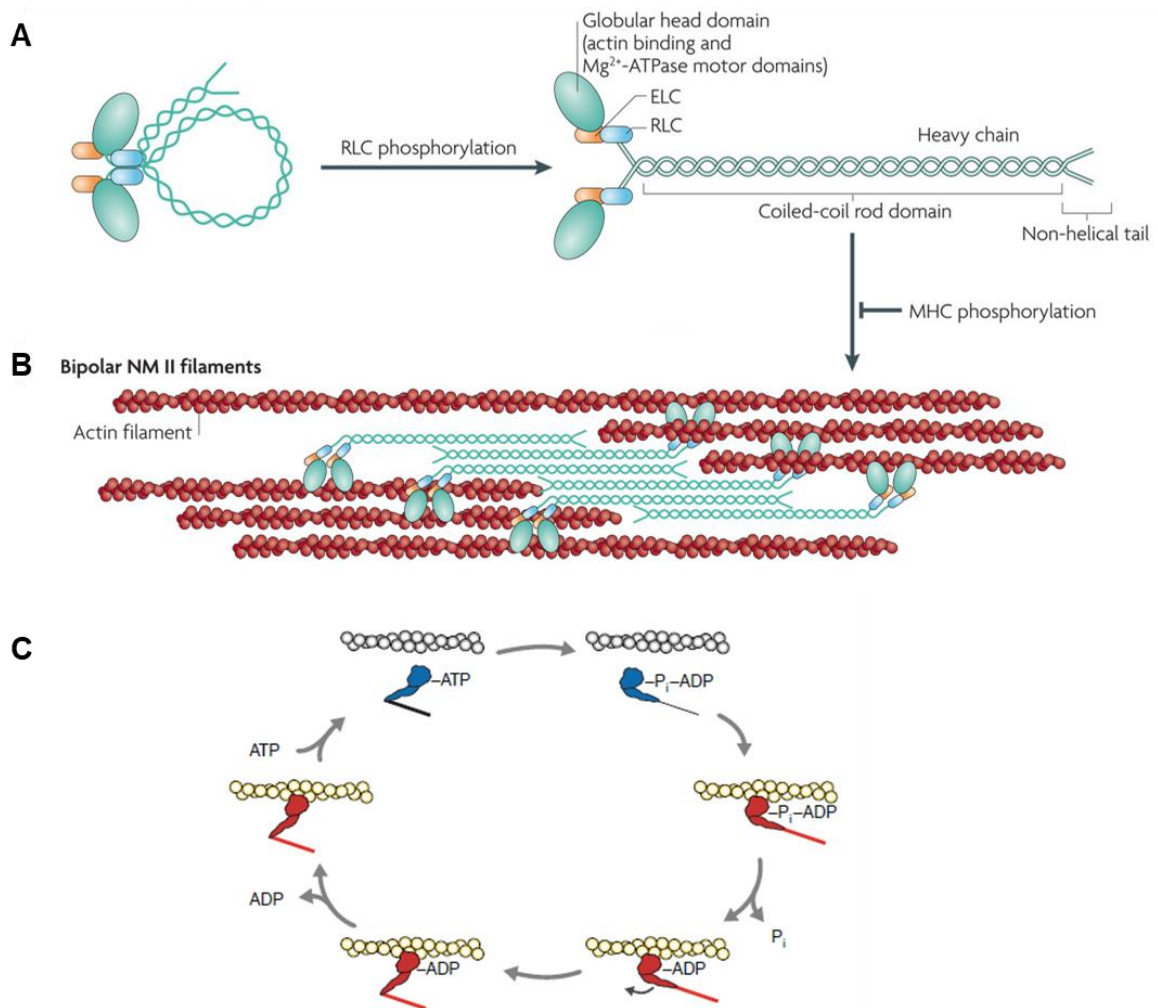


**Figure 8. Myosin II assembles into bipolar mini-filaments to generate force.**

**(A)** Non-muscle myosin II (NM II) is made of a motor head domain and an elongated heavy chain (tail). In its autoinhibitory conformation, the myosin II tail folds onto the head and blocks its motor activity. Phosphorylation of the regulatory light chain (RLC) induces its unfolding, releasing the motors. ELC (essential light chain), MHC (myosin heavy chain). **(B)** Phosphorylated monomers can polymerize into bipolar filaments. **(A, B)** (Vicente-Manzanares et al., 2009) **(C)** The myosin motor head undergoes an ATPase cycle in the presence of actin (Murphy et al., 2001).

Contractile stress fibers are excluded from the lamellipodia and filopodia region, but are present throughout the rest of the cell. Stress fibers can be divided into three classes depending on their orientation and interaction with focal adhesions: transverse arcs, ventral stress fibers and dorsal stress fibers (Figure 9). Transverse arcs are curved actomyosin structures that flow from the leading edge towards the center of the cell, parallel to the leading edge. They are not anchored to focal adhesions and display a periodic  $\alpha$ -actinin and myosin II pattern. Transverse arcs assemble through the endwise link of myosin II with both short actin bundles, nucleated at the plasma membrane by Arp2/3 and crosslinked by  $\alpha$ -actinin, and tropomyosin-bound actin filaments nucleated by the formin mDia2 (Figure 9). Tropomyosins are essential for stabilizing these filaments and for recruiting myosin II into these structures (Tojkander et al., 2011). These different actin structures undergo lateral fusion during their flow towards the center of the cell and straighten as a result of contraction (Hotulainen and Lappalainen, 2006; Tojkander et al.,

2011). Dorsal stress fibers do not contain myosin II and are thus not contractile. They elongate processively from FAs towards the center of the cell through actin polymerization. In this mechanism, short unipolar filaments are polymerized in a formin mDia1-dependent mechanism and simultaneously crosslinked by  $\alpha$ -actinin (Figure 9). Dorsal stress fibers interact with transverse arcs, and thus link them to FAs (Hotulainen and Lappalainen, 2006; Tojkander et al., 2011). Ventral stress fibers are tensile bundles anchored to focal adhesions at both sides. Pre-existing transverse arcs and dorsal stress fibers serve as precursors for forming ventral stress fibers. They fuse with each other into thicker more contractile actomyosin bundles.

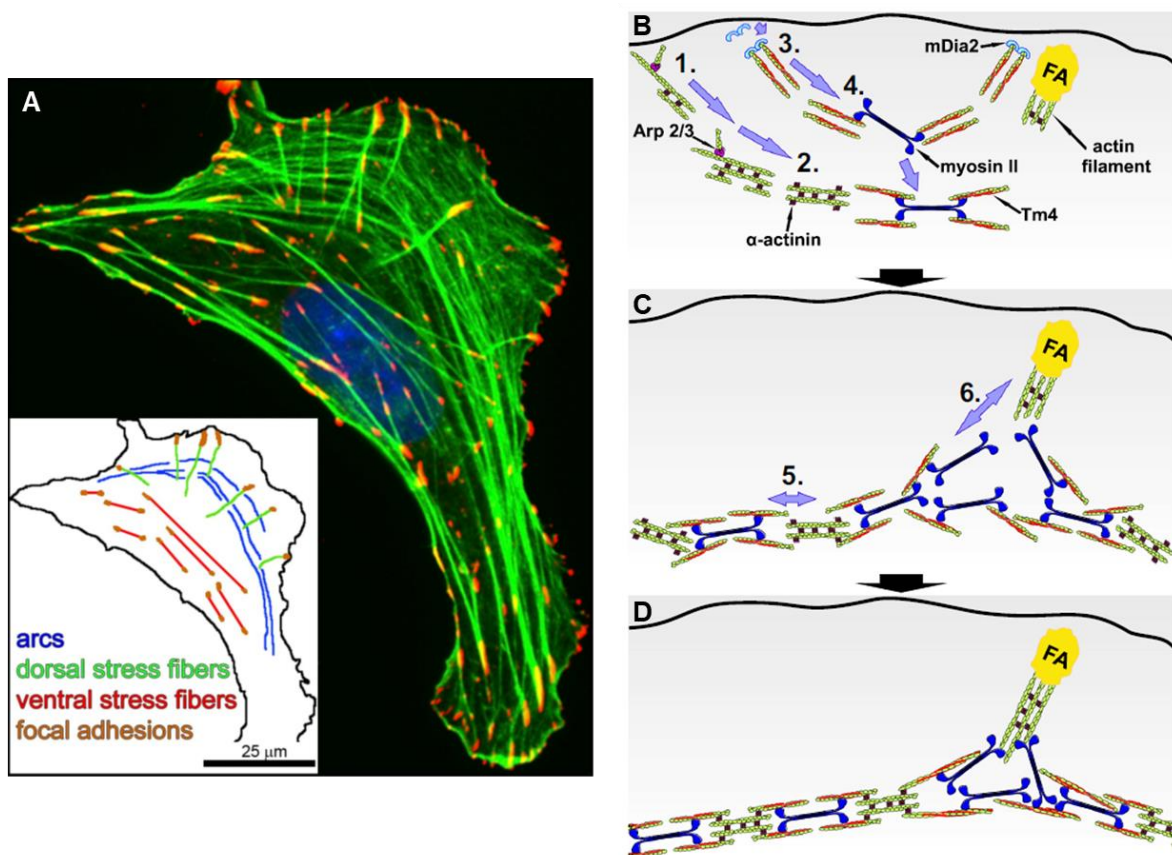


**Figure 9. Various types of stress fibers are present in mesenchymal cells.**

(A) Stress fibers can be divided in transverse arcs, ventral stress fibers and dorsal stress fibers (Burridge and Wittchen, 2013). (B-D) Model for the generation of contractile stress fibers. (B) Arp2/3-branched actin filaments associate to  $\alpha$ -actinin-crosslinked filaments. In parallel, the formin mDia2 initiates the formation of tropomyosin (Tm4)-decorated actin filaments, to which myosin II binds. (C) Actomyosin bundles assemble with  $\alpha$ -actinin-crosslinked filaments to form transverse arcs. The transverse arcs interact with dorsal stress fibers elongating from focal adhesions. (D) Actomyosin contractility allows the compaction of the stress fibers anchored at the focal adhesion. (C-D) (Tojkander et al., 2011)

## Introduction

Actin polymerization at the end of stress fibers controls the force that they generate. Ventral stress fibers elongate less rapidly than dorsal stress fibers, but they generate a higher force, suggesting that the elongation of actin filaments releases actomyosin tension. In addition, the myosin II-dependent tension generated by ventral stress fibers inactivates VASP, which inhibits actin filament elongation (Tojkander et al., 2015). Altogether, these observations suggest the existence of a feedback loop, in which the increase in tension and the inhibition of the actin assembly favor each other. Although several studies support a role for formins in the nucleation and elongation of the actin filaments composing stress fibers. It is still unclear, however, whether this activity takes place in nascent adhesions or focal adhesions, since formins have never been clearly localized in these structures.

### I.3 CELL-MATRIX ADHESIONS COUPLE THE ACTIN CYTOSKELETON AND THE EXTRACELLULAR MATRIX TO ALLOW CELL MIGRATION

#### I.3.1 Functions of cell-matrix adhesions

The primary role of cell-matrix adhesion complexes is to physically attach the cell to the ECM. They also fulfill a wide variety of functions besides connecting the external environment to the cytoskeleton. Cell-matrix adhesions play an important role in the detection, production and bi-directional transmission of forces, but also in the regulation of many other regulatory signals (Lock et al., 2008). Indeed, cell-matrix adhesions are essential for cytoskeletal organization, cell migration, proliferation, differentiation and survival, gene regulation and tissue organization. Thus, they play a central role in embryonic development, tissue remodeling, tissue and organ homeostasis, and wound healing (Figure 10). The immune system also heavily relies on integrin-based adhesions, for example during leukocyte trafficking from the bloodstream, for immune cells migration within tissues, for immune synapse formation and in phagocytosis. Cell-matrix adhesions induce signals that cooperate with other cell surface receptors and other cellular pathways to regulate an even wider range of biological processes, functions and phenotypes.

## Introduction

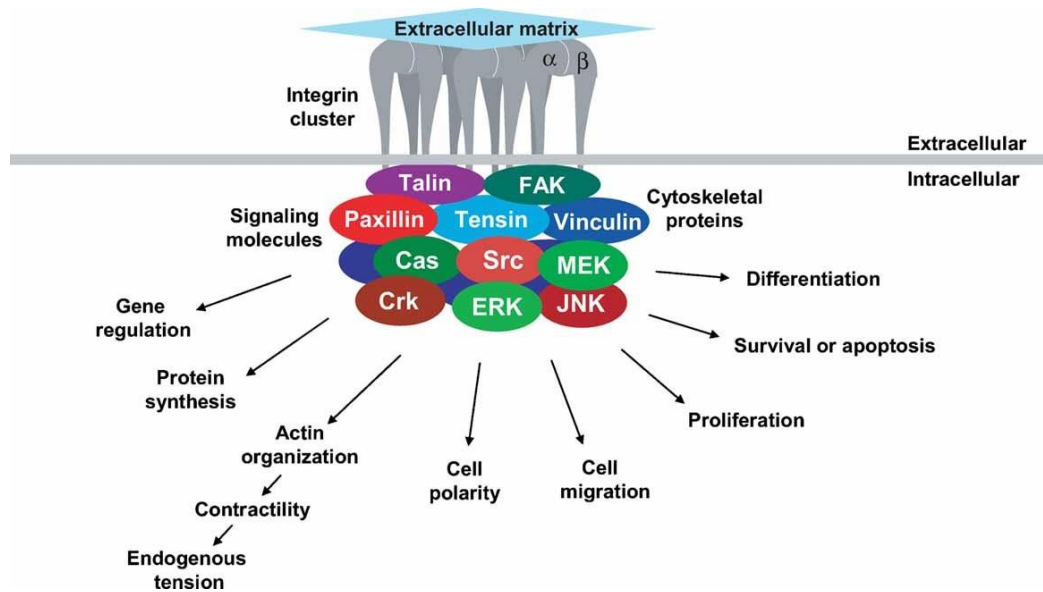


**Figure 10. Downstream regulation of cell-matrix adhesions.**

A myriad of signaling molecules associate to cell-matrix adhesion to induce various downstream signals controlling a tremendous number of cellular functions (Berrier and Yamada, 2007).

The mechanotransduction at the cell-matrix interface is subdivided into modules with different roles: a mechanosensitive module, an actin regulatory module, and a mechanosignaling module (Jansen et al., 2017). The clustering of integrins following their binding to the ECM promotes the localized concentration of signaling molecules inside the cell, such as FAK or paxillin, in the signaling module. Integrin clustering activates tyrosine kinases and phosphatases. These signaling pathways induce post-translational modifications in various adhesion proteins to trigger various downstream signaling cascades (Berrier and Yamada, 2007; Hervy et al., 2006; Li et al., 2005) (Figure 10).

Adhesion complexes do not only transmit external stimuli to the cell. In fact, integrins allow a bi-directional transmission of mechanochemical information across the membrane. Adhesions transmit information, like a change in substrate stiffness, via integrins, which then induces the rearrangement of the actin cytoskeleton or the regulation of intracellular signaling. This process is referred to as outside-in signaling. Conversely, endogenous tension or intracellular signals can induce changes in integrin conformation that alter its ligand-binding activity and modify the ECM stiffness, in a process termed inside-out signaling (Ginsberg et al., 2005; Luo et al., 2007) (integrin regulation will be further detailed in sections I.3.3 and I.3.4). Thus, integrin engagement with the matrix generates bi-directional signals that can regulate both endogenous and exogenous tension, and modify the composition of the matrix.

### I.3.2 Diversity of cell-matrix adhesions

Various types of integrin-based adhesion complexes exist. Hemidesmosomes link the basal lamina to intermediate filaments in epithelial cells. They therefore contribute to maintain the architecture of the epithelium. Other types of integrin-based cell-matrix adhesions link the extracellular matrix to the actin cytoskeleton in migrating cells. They vary in size, shape, distribution, number, and depending on the cell type. Podosomes are invasive structures made of polymerizing actin and adhesion components. Nascent adhesions (NAs), or slightly bigger focal complexes (FCs), are small newly-formed adhesions that link the lamellipodial actin to the ECM (Figure 11). These NAs quickly disassemble. However, when they are submitted to higher traction forces, they become larger adhesion sites, called focal adhesions (FAs) (Figure 11). FAs are elongated towards the direction in which the stress fibers pull on them. Some adhesions survive longer and become elongated fibrillar adhesions (Lock et al., 2008).

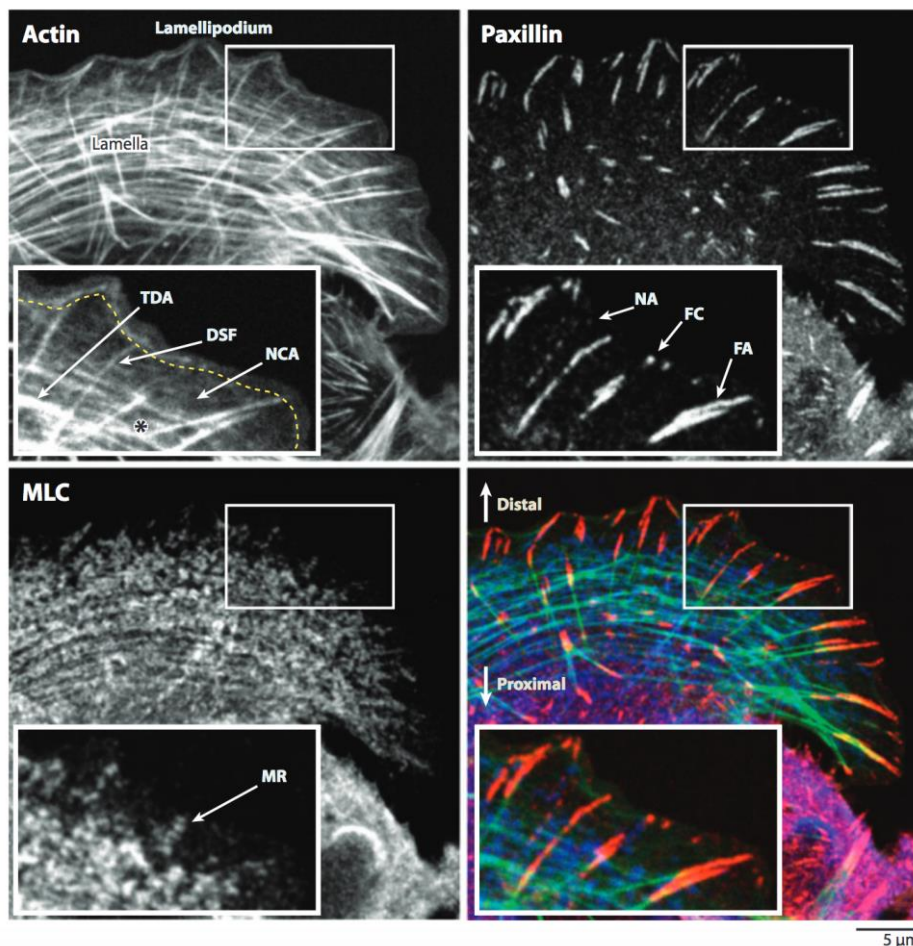


**Figure 11. Organization of the cell-matrix adhesions and actomyosin cytoskeleton in a migrating cell.**

Paxillin (red) and myosin light chain (MLC, blue) are revealed by immunofluorescence in human osteosarcoma (U2OS) cells. Actin filaments are revealed by phalloidin (green). TDA (transverse dorsal arc), DSF (dorsal stress fiber), NCA (network contraction array), NA (nascent adhesion), FC (focal complex), FA (focal adhesion), MR (myosin II ribbon) (Gardel et al., 2010).

### 1.3.3 Integrins: the adhesive molecules of cell-matrix adhesions

The transmembrane adhesion receptors integrins link the ECM to the actin cytoskeleton. Integrins are non-covalent heterodimers composed of  $\alpha$  and  $\beta$  subunits. There are many  $\alpha$  and  $\beta$  subunits, and many possible combinations between them, with specific binding affinities. There are 18 different  $\alpha$  chains and 8 types of  $\beta$  subunits in humans, which can assemble into 24 different integrin heterodimers (Kechagia and Ivaska, 2019). Each combination is characterized by its specificity of binding to extracellular matrix proteins, its mode of regulation and its tissue expression (Figure 12). Both subunits cross the plasma membrane, with a large modular extracellular domain (or ectodomain) that binds to specific components of the ECM (or in some cases, to receptors on the surface of other cells), and a small intracellular tail involved in the coupling with the cytoskeleton.

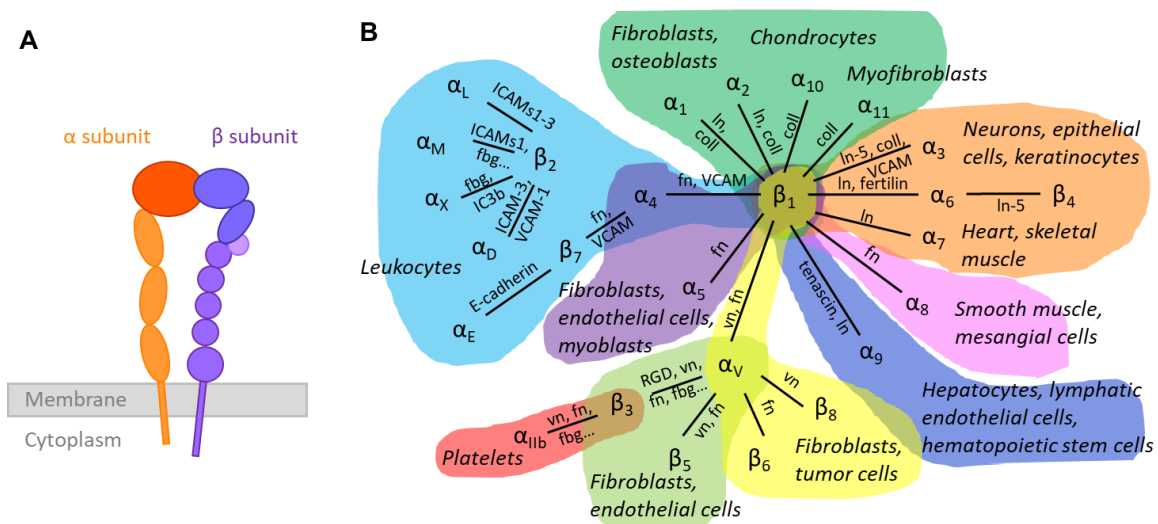


**Figure 12. Cell-specific integrin heterodimer combinations and their ligands.**

**(A)** Organization of an  $\alpha\beta$  integrin heterodimer. **(B)** In humans, there are 24 different combinations of  $\alpha\beta$  integrins with various ligand specificities. These  $\alpha\beta$  combinations are also found in different cell types. vn (vitronectin), fn (fibronectin), fbg (fibrinogen), coll (collagen), In (lanimin).

Due to the multiple roles of integrins in numerous cellular functions, a defect in one of the  $\alpha$  or  $\beta$  chain leads to severe pathologies. For instance, the  $\beta_1$  integrin associates with 12 distinct  $\alpha$  chains. Mice that cannot synthesize  $\beta_1$  integrins die during embryonic development. The ECM ligand for  $\alpha_7\beta_1$  integrin is laminin. Mutant mice that cannot synthesize the  $\alpha_7$  subunit, which combines with  $\beta_1$  in muscles, can survive but present very severe muscular dystrophy, similarly to the mice that are not able to produce laminin. Another example is the  $\beta_3$  integrin, which is found in platelets and binds several matrix proteins, including the blood clotting factor fibrinogen. Deficiency in  $\beta_3$  integrin leads to the Glanzmann's disease, characterized by defects in blood clotting and excessive bleeding (Wehrle-Haller and Imhof, 2003).



## Introduction

The extracellular domains of integrins binds specific amino-acid sequences in the proteins of the extracellular matrix. The best characterized sequence is the RGD peptide (Arg-Gly-Asp), found mainly in fibronectin and vitronectin. A high number of  $\beta_1$  and  $\beta_5$  integrins binds to this RGD motif. Other integrins recognize LDV sequences (Leu-Asp-Val). While the  $\beta$  subunit binds ECM ligands, the  $\alpha$  subunit provides ECM specificity, but also regulates the  $\beta$  subunit. For example, the  $\beta_1$  subunit is well known for binding to fibronectin when paired with the  $\alpha_5$  subunit, but it interacts with various collagens when combined with the  $\alpha_2$  subunit (Doyle and Yamada, 2013) (Figure 12). The short intracellular parts of both subunits bind to a complex of cytoskeleton-associated proteins, which plays a role in the regulation of integrins.

In order to decipher the multiple physiological roles of integrins, it is necessary to understand the link between the structural organization of integrins and their adhesive function. X-ray crystallography, electron microscopy and conformational antibodies have deciphered the structural organization of the  $\alpha$  and  $\beta$  subunits and have revealed that integrins exist in different conformations, corresponding to different states of activation (Bachmann et al., 2019). When integrins bind to a ligand, they switch from an inactive to an active conformation. In the bent-closed inactive state, integrin  $\alpha$  and  $\beta$  subunits are wrapped up together into a compact structure by an interaction between the  $\alpha$ -propeller and the  $\beta$ -I-like domain of the extracellular parts (Figure 13A) (Bachmann et al., 2019). In this state, integrins are not engaged with a ligand. After binding to a cytoplasmic ligand such as talin and/or kindlin, the ectodomains both unfold and extend. The integrin adopts an extended-closed low affinity conformation (Figure 13B). When integrins bind simultaneously to an ECM ligand and an activating cytoplasmic actin-associated adapter, their intracellular tails separate to adopt the extended-open active state (Michael and Parsons, 2020) (Figure 13C). Switching from the low-affinity inactive state to the high-affinity active state can be induced by many mechanisms and is regulated bi-directionally. In some cases, activation occurs by binding to matrix ligands in a process called “outside-in” activation, leading to the exposure of binding sites for adaptors in the intracellular  $\beta$  tails. These adaptors can then recruit actin filaments. Integrins can also be activated in a reverse way, in a process called “inside-out” activation, when intracellular signals stimulate the ability of cytoplasmic adaptors to recognize the  $\beta$  tails of the integrin. It thus separates the  $\alpha$  and  $\beta$  tail linkage, allowing the two legs of the integrin dimer to spring apart and bind matrix ligands. The importance of intracellular ligands is further highlighted, as they can either favor or inhibit integrin activation. For example, the large actin-binding protein talin, together with kindlin, activates integrins whereas the actin-crosslinking protein filamin inhibits them (Figure 13A) (Doyle and Yamada, 2013).

## Introduction

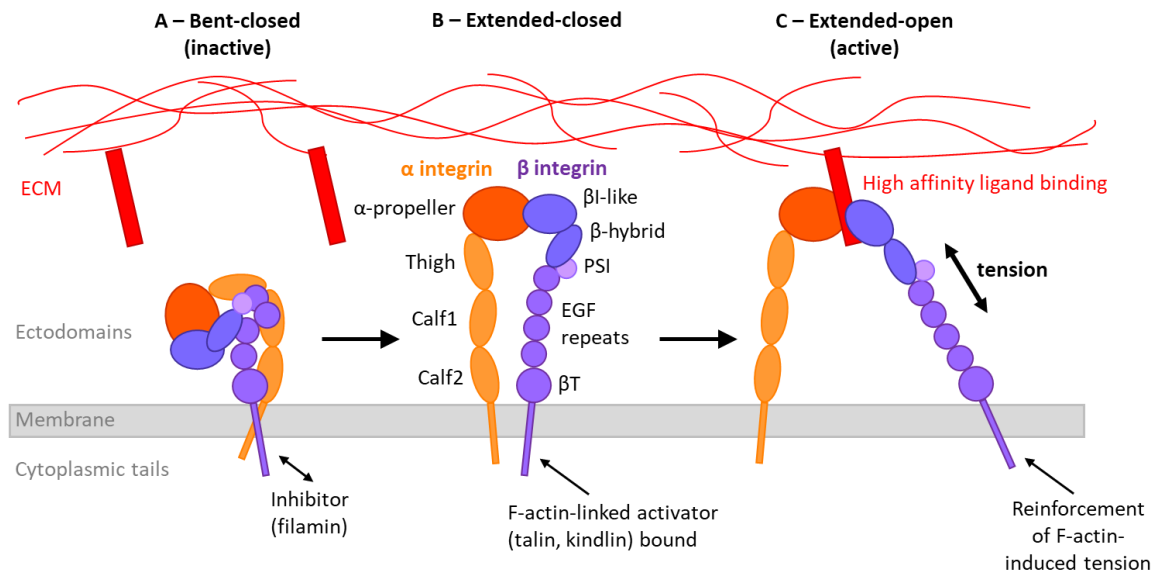


**Figure 13. Integrins domain organization and ligand-induced conformational change.**

Integrins are transmembrane heterodimers made up of an  $\alpha$  and a  $\beta$  subunit, each one containing specific domains. Integrins switch from **(A)** an inactive bent-closed conformation to **(B)** an extended-closed conformation upon ligand binding and finally to **(C)** an active extended-open conformation under the traction force exerted by the actomyosin cytoskeleton. The ligands which can activate integrins can be intracytoplasmic, such as talin and/or kindlin, or extracellular, such as RGD motifs in the extracellular matrix.

### 1.3.4 A variety of adaptors regulate integrin activity and actin dynamics in cell-matrix adhesions

The major role of cell-matrix adhesions is to connect the extracellular matrix to the actin cytoskeleton via integrins. Adhesions thus contain a variety of actin binding proteins including side binding proteins, capping proteins and nucleators. They are necessary for actin networks rearrangement and stress fibers assembly and function.

#### 1.3.4.1 Talin

- Talin domain organization and regulation

Talin was initially purified from chicken gizzard and earliest findings localized it in adhesion plaques and ruffling membranes (Burrige and Connell, 1983) (Figure 14). The two isoforms talin-1 and talin-2 share 74% sequence identity. While talin-1 is ubiquitously expressed, talin-2 is absent in endothelial cells. Mice lacking talin-1 fail to complete gastrulation (Monkley et al., 2000), while mice lacking talin-2 are viable and fertile (Chen and Lo, 2005; Debrand et al., 2012). Cellular studies revealed that talin-1 knockout cells show a compensatory upregulation of talin-

## Introduction

2, and depletion of talin-2 in talin-1 deficient cells abolishes the ECM-integrin-cytoskeleton linkage, cell spreading and adhesion, and severely impaired FA assembly, FAK signaling and traction force generation (Zhang et al., 2008). Because most studies focused on the role of talin-1 in adhesion, the role of talin-2 remains unclear.

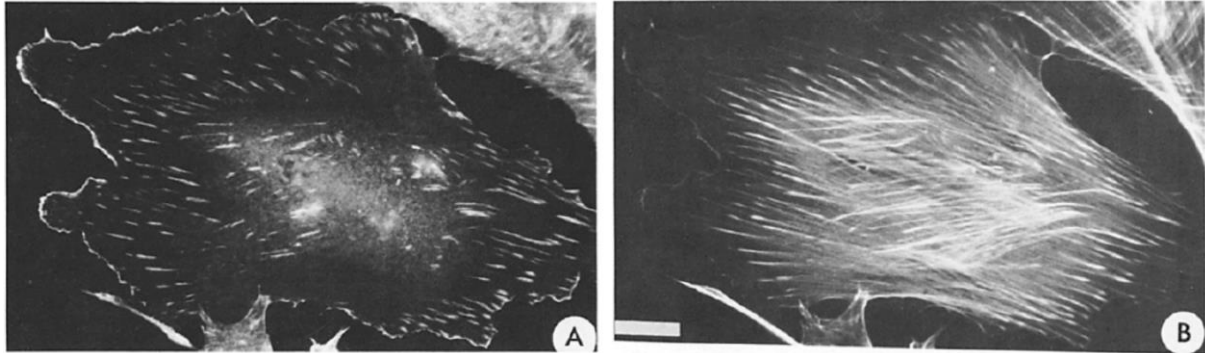


**Figure 14: Talin is localized in focal adhesions, anchor points of actin filaments.**

Chicken embryo fibroblasts were stained with (A) a primary rabbit anti-talin antibody followed by a rhodamine-labeled secondary antibody and (B) nitrobenzoxadiazol-phalloidin to localize actin filaments (Burridge and Connell, 1983).

Human talin is a large protein (270 kDa) comprising 2541 amino acids. This multidomain protein is composed of a globular N-terminal head domain (50 kDa), containing a FERM (4.1 / ezrin / radixin / moesin) domain, a flexible linker, a large rod domain (200 kDa) made of 13 consecutive bundles of four to five  $\alpha$ -helices, and a C-terminal dimerization domain (Critchley, 2009; Goult et al., 2018) (Figure 15A). Talin is regulated by intramolecular interactions, that need to be released to allow talin function. The inhibitory contact between the F3 subdomain of the FERM domain and the R9 helical bundle of the rod was first described by nuclear magnetic resonance (NMR) studies (Goksoy et al., 2008) (Figure 15A).

Talin being a large protein displaying flexible domains, attempts to crystallize the full-length protein have failed. However, Goult and his colleagues have proposed a first model obtained by fitting the known structures of the different domains into the density map of a dimer of talin-1 obtained by electron microscopy (Goult et al., 2013a). More recently, the high-resolution structure of a talin-1 monomer was resolved by cryo-electron microscopy (cryo-EM). This structure reveals that talin is in fact kept inactive by two intramolecular interactions between F3 and R9, as described above, but also between F2 and R12 (Dedden et al., 2019) (Figure 15B).

## Introduction

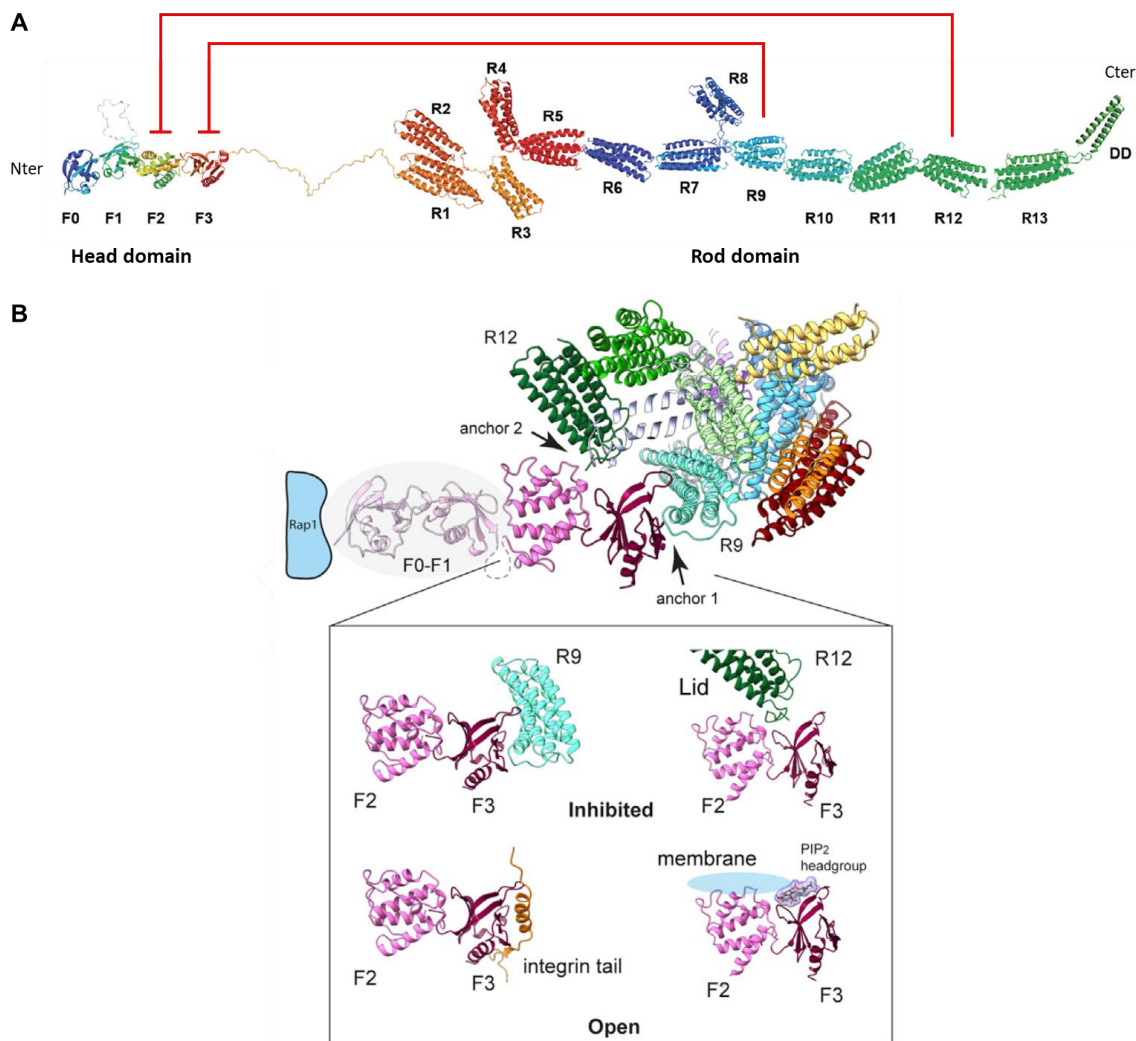


**Figure 15: Talin is autoinhibited by two intramolecular contacts.**

**(A)** Schematic representation of talin, showing the structure of the isolated domains. The domains have been juxtaposed to simplify the presentation but this does not correspond to the folded structure of talin. This scheme indicates the position of the F0, F1, F2 and F3 domains of the FERM domain, the 13 helical bundles (R1 to R13) of the rod and the dimerization domain (DD). The red arrows indicate the auto-inhibitory contacts between R9 and F3 and between R12 and F2 (Adapted from Goult, Zacharchenko, et al., 2013). **(B)** High resolution structure of full-length talin after molecular fitting of talin to the cryo-EM density map. The F0 and F1 subdomains were not visualized in this structural analysis due to the flexibility of the F1-F2 linker. The binding site of the small GTP Rap1 on F0 is shown in blue. The lower panel displays the isolated structures of the F3-R9 and F2-R12 contacts in the inhibited closed structure. This lower panel also shows how this two interactions must be disrupted to allow integrin binding to F3 and PIP<sub>2</sub> binding to F2-F3 (Dedden et al., 2019).

## Introduction

- Talin interacts with numerous proteins

As a link between integrins and the cytoskeleton, talin has three actin-binding domains (ABD): F2 and F3 in the head domains, the R4 to R8 bundles and the C-terminal THATCH (talin / HIP1R / Sla2p actin tethering C-terminal homology) domain (Hemmings et al., 1996) (Figure 16).

Talin F3, also known as phosphotyrosine-binding (PTB)-like domain, interacts with the cytoplasmic tail of  $\beta$  integrins. A secondary integrin-binding site has then been located in R11, but its function remains unclear. The auto-inhibitory contact between talin R9 and F3 masks the interaction site for  $\beta$  integrins in F3 (Figure 15B). Thus, breaking this contact is necessary for integrin binding. In addition to F3, the other subdomains of talin head contribute to maintain integrin in its high affinity conformation (Bouaouina et al., 2008). The binding of F1, F2 and F3 to the membrane phosphoinositide phosphatidylinositol(4,5)bisphosphate (PIP<sub>2</sub>) increases the affinity of talin for  $\beta$  integrins (Anthis et al., 2009; Saltel et al., 2009) (Figure 15B). In addition, talin has been shown to be targeted to the membrane by an interaction between the F0 subdomain of its head and the small GTPase Rap1 (Goult et al., 2010) (Figure 15B). The F3 subdomain of the head interacts with other proteins, including FAK, layilin, RIAM and TIAM1 (Calderwood et al., 2013) (Figure 16).

The talin rod displays eleven vinculin-binding sites (VBS) (Gingras et al., 2005), making vinculin its major partner. Talin rod also displays four RIAM-binding sites (RBS). In addition, R7 has been shown to interact with the KANK family of proteins (Bouchet et al., 2016), and R8 binds DLC1 (Li et al., 2011), paxillin and  $\alpha$ -synemin (Sun et al., 2008).

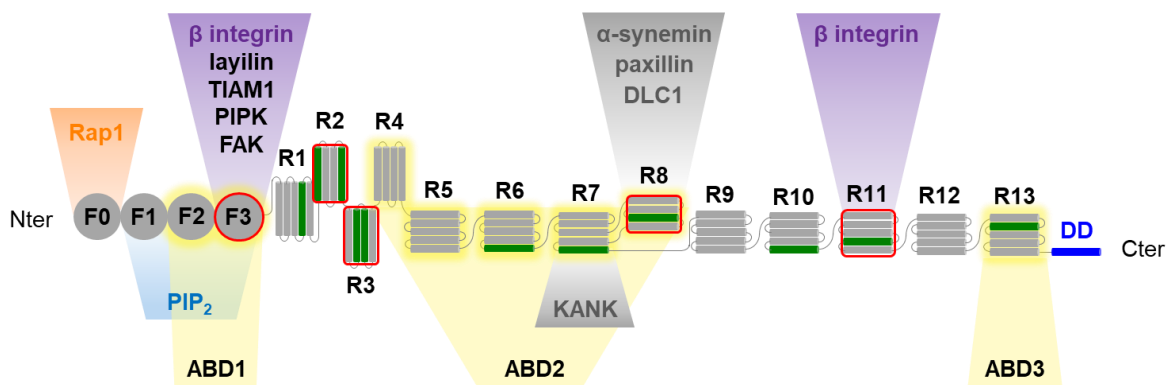


**Figure 16: Talin-1 domain organization and interactions.**

The 11 vinculin-binding sites (VBSs) are represented as green bars. The 5 RIAM-binding sites (RBSs) are highlighted by red boxes. F1 to F3 (FERM domain 1 to 3), R1 to R13 (rod domain 1 to 13), DD (dimerization domain), ABD (actin-binding domain).

## Introduction

- Talin activates integrin

As mentioned earlier, talin is required for both integrin activation and clustering. A crucial part in integrin activation by the “inside-out” mechanism is the unclasping of the  $\alpha$  and  $\beta$  subunits (See 1.3.3). The F3 subdomain of talin head contains a PTB-like domain that interacts with the proximal NPXY motif of the cytoplasmic  $\beta$  integrin tail. Although interactions between talin F3 and  $\beta$  integrin tails are required for integrin activation, they are not sufficient. Interaction of talin head with the membrane is in fact crucial. Talin F1, F2 and F3 harbor clusters of basic residues that bind PIP<sub>2</sub> in the membrane. Mutations of the basic residues in F2 (Anthis et al., 2009), or an insertion in F1 (Goult et al., 2010), impair talin binding to the membrane and its ability to activate integrins. The interaction between talin and the membrane can disrupt the autoinhibitory contacts in talin, and orient talin in order to optimize its binding with the integrin tail. The membrane-bound Rap1-RIAM complex has also been shown to activate and recruit it to the membrane where it can activate integrins (more details in section 1.4.3.2).

### 1.3.4.2 Kindlin

The kindlin family comprises 3 members. While kindlin-2 is expressed ubiquitously outside of the hematopoietic system, kindlin-1 is mainly present in epithelial cells and kindlin-3 can only be found in the hematopoietic system (Sun et al., 2019). The three isoforms show a similar organization (Figure 17), with 53% identity between kindlin-2 and 3. All kindlins contain a FERM domain with an additional N-terminal F0 subdomain, similarly to talin FERM domain. However, the particularity of kindlin is the insertion of a pleckstrin homology (PH) domain in F2 (Liu et al., 2011). This PH domain binds to lipids, which helps target kindlin to the membrane, where it can regulate integrin activation. Mutations in F3 that impair integrin binding do not abolish all the functions of kindlin, revealing that kindlin has multiple roles other than integrin activation (Plow and Qin, 2019). The F0 domain of kindlin interacts with actin filaments, which might be required for cell spreading (Bledzka et al., 2016). Kindlin-2 also promotes cell spreading by interacting with the Arp2/3 complex, via its F1 domain, and with paxillin through several binding sites (Böttcher et al., 2017). In fact, more than 20 kindlin partners have been identified (Plow and Qin, 2019). Among them, kindlin recruits other proteins involved in integrin regulation such as the integrin inhibitor SHARPIN and integrin-linked kinase (ILK).

## Introduction

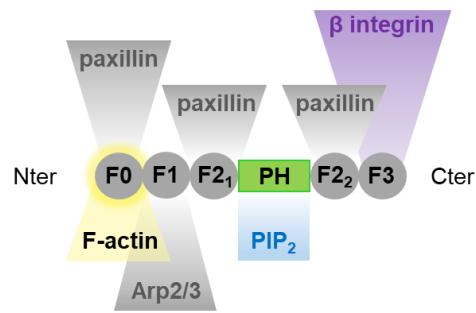


**Figure 17: Kindlin-2 domain organization and binding partners.**  
F0 to F3 (FERM domain 1 to 3), PH (plekstrin-homology domain).

Kindlin and talin cooperate to activate integrins (Sun et al., 2019). However, these two proteins have different roles. Talin is involved in mechanosensing, whereas kindlin contributes to initiate signaling downstream of integrins. Talin binds to the proximal NPXY motif of the  $\beta$  integrin cytoplasmic tail, whereas kindlin binds to a more distal NXXY motif. In vitro, talin binding is sufficient to induce the extension of integrin ectodomains. However, in cells, kindlin knockdown and knockout, together with the mutation of the kindlin-binding site in integrins, affects talin-dependent integrin activation (Kadry and Calderwood, 2020). The mechanism by which kindlin assists talin to activate integrins is not fully understood. Talin and kindlin may bind integrins cooperatively (Theodosiou et al., 2016). Alternatively, kindlin may help talin to fully destabilize the  $\alpha$  and  $\beta$  chain inhibitory salt bridge interaction in the membrane (Haydari et al., 2020). Some studies have also suggested that kindlin promotes the clustering of talin-activated integrins (Ye et al., 2013).

### 1.3.4.3 Filamin

Filamin is a large actin filament cross-linking protein that forms homodimers through a C-terminal interaction (Ciobanasu et al., 2013) (Razinia et al., 2012). The filamin family consists of filamin A, B and C. The A and B isoforms are expressed ubiquitously while filamin C is present mainly in cardiac and skeletal muscles. In non-muscle cells, filamins are associated with actin-rich structures including lamellipodia, filopodia, stress fibers and focal adhesions.



**Figure 18: Filamin A domain organization and binding partners.**  
CH (calponin homology domain), Ig (Immunoglobulin domain), DD (dimerization domain).

## Introduction

The N-terminal part of filamin A interacts with actin filaments via two calponin homology (CH) domains. This actin-binding site is followed by a rod of 23 immunoglobulin (Ig) domains (Figure 18). The C-terminal 24<sup>th</sup> Ig domain (IgFLNa24) mediates filamin dimerization (DD), allowing it to orthogonally crosslink actin filaments. Filamin interacts with  $\beta$  integrin tails via its 21<sup>st</sup> Ig subdomain (IgFLNa21) IgFLNa21 (Ciobanasu et al., 2013; Razinia et al., 2012). Interestingly this interaction does not activate integrins. Filamin acts as an inhibitor that prevents talin to activates integrins, because filamin- and talin-binding sites overlap on the cytoplasmic tail of  $\beta$  integrin tails. Filamin, like other integrin inhibitors, may control integrin inactivation or retention of the inactive form during cyclical adhesion periods observed at the leading of migrating cells (Bouvard et al., 2013). The recent NMR structure of  $\alpha_{IIb}\beta_3$  integrin bound to IgFLNa21 reveals that IgFLNa21 not only binds to the  $\beta$  integrin tail, but also interacts with the  $\alpha_{IIb}$  subunit. This mechanism allows filamin to keep integrin in an inactive state (Jianmin Liu et al., 2015).

### 1.3.4.4 Tensin

Tensins form a family of four proteins. Tensin-1 to 3 have an N-terminal F-actin binding domain, and a C-terminal Src homology 2 (SH2) domain, followed by a PTB domain that binds  $\beta$  integrin tails (Blangy, 2017; Ciobanasu et al., 2013; Lo et al., 1994). Only tensin-1 comprises an addition central ABD that caps the barbed ends of actin filaments (Figure 19). Tensin-4, also known as C-terminal tensin-like (CTEN), is shorter and lacks the N-terminal domains.

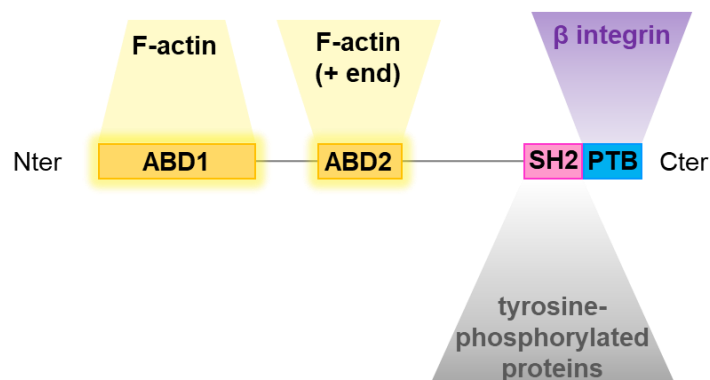


**Figure 19. Tensin-1 domain organization and interactions.**

ABD (actin-binding domain), SH (Src homology domain), PTB (phosphotyrosine-binding domain).

Like talin, tensin connects integrins to the actin cytoskeleton. Although tensin-1 is present in focal adhesions, it is more enriched in fibrillar adhesions, known for reorganizing the ECM through fibronectin fibrillogenesis.

At the molecular level, the PTB domain of tensin-1, like the one of talin, activates integrins by directly binding to the NPXY motif of a variety of intracellular  $\beta$  integrin tails (McCleverty et al.,



## Introduction

2007). The tensin PTB domain binds to soluble peptide corresponding to  $\beta$  integrin tails with a higher affinity than talin (Anthis et al., 2010; McCleverty et al., 2007). Surprisingly, the ability of tensin-1 and tensin-3 to activate integrins depends on talin expression. Since talin and tensin bind to same motif on  $\beta$  integrin tails (McCleverty et al., 2007), these observations imply the existence of a talin-tensin switch in fibrillar adhesions (Georgiadou and Ivaska, 2017). However, the mechanism that triggers the replacement of talin by tensin is unclear. Talin binds the integrin NPXY motif when the tyrosine is not phosphorylated, while tensin binding does not depend on phosphorylation. The replacement of talin by tensin in fibrillar adhesions could therefore result from tyrosine phosphorylation in the NPXY motif adhesions (McCleverty et al., 2007).

### 1.3.4.5 Vinculin

Vinculin (117 kDa) is a highly conserved ubiquitously expressed protein that localizes both in cell-cell and cell-matrix adhesions (Bays and DeMali, 2017; Ciobanasu et al., 2013; Romero et al., 2020). Vinculin knockout mice die in early embryogenesis, suggesting that vinculin is required for the highly complex cell movements and contacts needed for embryonic development. Vinculin-null fibroblasts are less adherent, more motile and have fewer and smaller adhesions than wild-type cells (Xu et al., 1998).

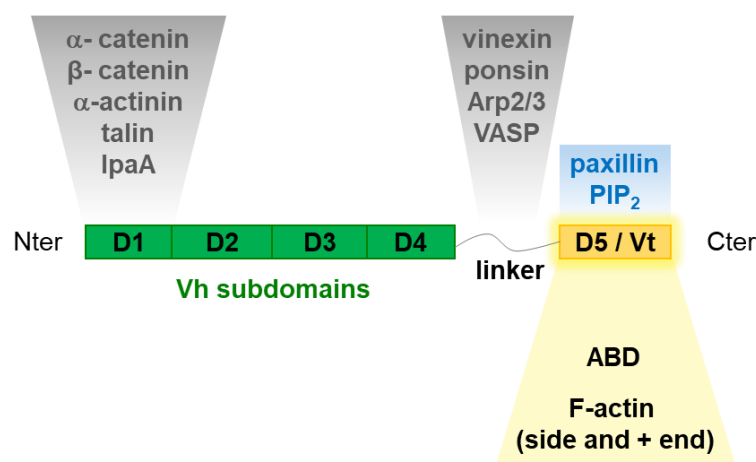


**Figure 20: Vinculin domain organization and interactions.**

Vh (vinculin head), D1 to D5 (vinculin head subdomain 1 to 5), Vt (vinculin tail), ABD (actin-binding domain).

Vinculin is composed of a 95 kDa head domain (Vh), subdivided into four subdomains, D1 to D4, and a 30 kDa tail domain (Vt or D5) separated from the head by a flexible 61 amino acids proline-rich linker (Ciobanasu et al., 2013) (Figure 20). D1 interacts with talin,  $\alpha$ -catenin,  $\alpha$ -actinin, and IpaA. The proline-rich linker binds VASP, Arp2/3, vinexin and ponsin, while Vt binds actin filaments, PIP<sub>2</sub> and paxillin. In muscle cells, vinculin is co-expressed with a splice variant known as metavinculin, which is characterised by the presence of an insertion in Vt.

## Introduction

Metavinculin reinforces the mechanical coupling between actin filaments and muscle-specific adhesion sites (Thoss et al., 2013).

Vinculin exists in an open, active state and a closed, auto-inhibited conformation in which Vt interacts with the D1 and D4 subdomains of the head (Figure 20). These intramolecular contacts prevent the binding of talin to D1 and F-actin to Vt (Johnson and Craig, 1995, 1994). Various FRET probes inserted in vinculin detected the active extended state in FAs, whereas the inactive conformation remains in the cytoplasm (Chen et al., 2005). In cells, point mutations that disrupt the head-tail interaction lead to increased talin binding and actin recruitment (Humphries et al., 2007), demonstrating that this autoinhibition needs to be disrupted to display vinculin functions. As the head binds the tail with high affinity ( $K_d \sim 50$  nM) (Johnson and Craig, 1994), vinculin might be activated by a combinatorial mechanism (Bakolitsa et al., 2004; Chen et al., 2006), to ensure its activation only at sites of cell adhesion. Vinculin activation thus requires simultaneous binding of talin to Vh and actin filaments to Vt. The observation that vinculin recruitment to FAs is abolished in cells lacking talin, underline talin requirement for vinculin activation. In addition, the expression of a vinculin point mutant (A50I) that inhibits talin binding in vinculin-null cells prevents FA growth and force generation (Cohen et al., 2006). This model is also supported by the observation that vinculin and the talin rod domain, which contains 11 VBSs, are found at the same position along the z-axis in FAs (Kanchanawong et al., 2010). An alternative pathway for vinculin recruitment to FAs has been proposed, in which the force-dependent recruitment of vinculin involves the phosphorylation of paxillin. However, vinculin and paxillin do not colocalize in FAs (Humphries et al., 2007), and Vh alone, that does not contain the paxillin binding site, is efficiently targeted to FAs (Carisey et al., 2013).

Cellular experiments have shown that vinculin is recruited to FAs by mechanical stimuli (Hirata et al., 2014). The recruitment of vinculin to talin stabilizes FAs and promotes integrin clustering and adhesion enlargement (Cohen et al., 2006; Humphries et al., 2007). Overexpression of Vh is sufficient to induce FA growth independently of Vt (Humphries et al., 2007), probably by stabilizing talin in its extended conformation. Vinculin then recruits other core FA components that contribute to the growth of the adhesion.

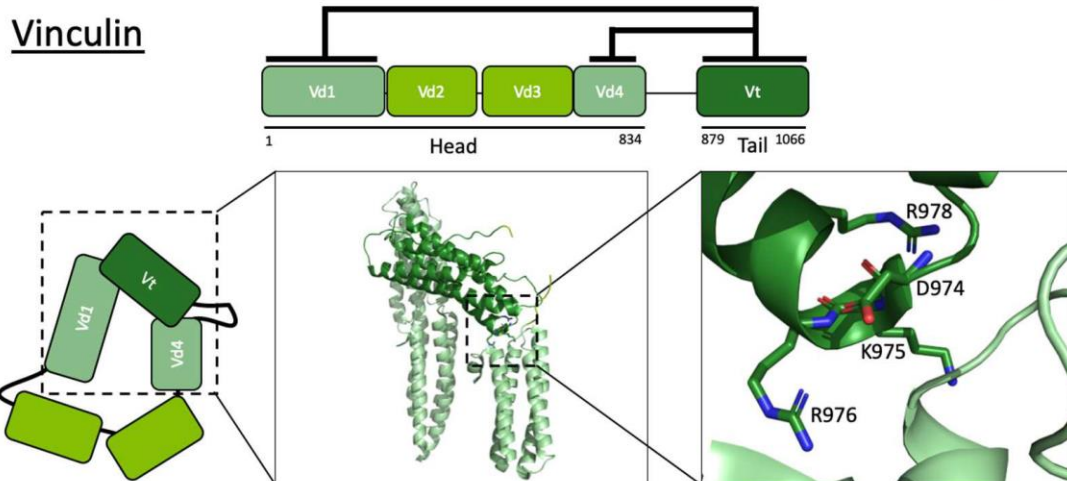


**Figure 21. Autoinhibited and active conformations of vinculin.**

The vinculin tail (Vt) interacts with both Vd1 and Vd4 domains of the head to form a strong autoinhibitory conformation. The bottom panel features the structure of the key amino acids involved in the D4-Vt interface (Khan and Goult, 2019). Adapted from crystal structure PDB ID: 1TR2 (Borgon et al., 2004).

Once localized in FAs, vinculin remains sensitive to forces, as demonstrated by the fact that full-length vinculin remains associated with FAs only during the application of force, and that the presence of the actin binding tail is required (Dumbauld et al., 2013). The use of a vinculin FRET sensor supports this view (Grashoff et al., 2010). Constitutively active forms of vinculin, obtained by point mutations that weaken the head-tail interaction (vinT12) (Figure 21) or deletion of Vt (vin880 or vin258), show reduced rate of turnover compared with the full-length protein (Humphries et al., 2007). The expression of these constitutively active mutants of vinculin trigger the formation of bigger FAs (Humphries et al., 2007). These vinculin mutants remain in FAs even after treatment with actin-destabilizing drugs (Carisey et al., 2013). Altogether, these data imply that the head-to-tail interaction plays a central role to control vinculin turnover in FAs, since, without the possibility to reform an inactive vinculin conformation, vinculin is more tightly associated to FAs.

The insertion of a FRET sensor between vinculin head and tail confirmed the existence of a myosin-dependent tension across vinculin (Grashoff et al., 2010). The combination of a vinculin FRET sensor with micropillar arrays of various substrate stiffness further determined a strong spatiotemporal correlation between the molecular tension that vinculin undergoes in FAs and traction forces exerted by the cell on its substrate, demonstrating that vinculin can sense both the force generated by the actomyosin and the ECM mechanical properties (Sarangi et al., 2017).

## Introduction

In vitro reconstitution showed that Vt can cross-link and bundle actin filaments (Shen et al., 2011). It can also nucleate new filaments, inhibit actin barbed end elongation by a capping mechanism (Le Clairche et al., 2010), modify existing actin bundles and stimulate the formation of new bundles (Wen et al., 2009). In cells, the expression of a vinculin point mutant defective for F-actin binding revealed that Vt is required for coupling the actin retrograde flow to the ECM, but is dispensable for the growth of FAs (Thievessen et al., 2013). Hence, vinculin establishes new actin structures, regulates the organization and dynamics of pre-existing actin networks and mechanically couple them to FAs.

### 1.3.4.6 VASP

The Ena/VASP (Enabled/vasodilator-stimulated phosphoprotein) family of proteins is composed of the three paralogs Evl, VASP and Mena. Ena/VASP proteins are characterized by a N-terminal EVH1 (Ena/VASP homology 1) domain, followed by a central proline-rich (PR) region and a C-terminal EVH2 domain which contains both a G-actin binding domain and a F-actin binding domain (Figure 22). The C-terminal domain (TD) mediates the tetramerization of the protein. The EVH1 interacts with FPPPP motifs, also present in the proteins zyxin, RIAM, lamellipodin and vinculin. The proline-rich domain interacts with profilin and SH3 domains.

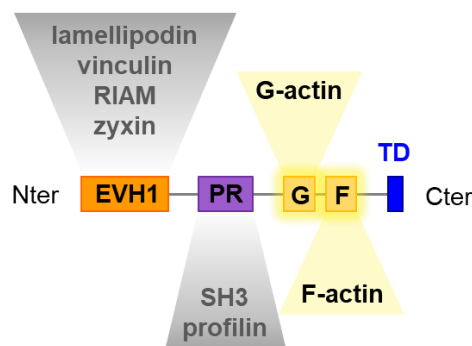


**Figure 22: VASP domain organization and interactions.**

EVH (Ena/VASP homology domain), PR (proline-rich region), G (G-actin-binding domain), F (F-actin-binding domain), TD (tetramerization domain).

Ena/VASP proteins localize at the leading edge of lamellipodia, at the tip of filopodia, in cell-matrix adhesions and in cell-cell junctions, where they control actin-dependent processes. The CRISPR/Cas9-mediated inactivation of the three paralogs Evl, VASP and Mena in melanoma cells revealed that Ena/VASP proteins are required to build the architecture of the lamellipodial actin network (Damiano-Guercio et al., 2020). In addition, Ena/VASP proteins control the formation of microspikes, often referred to as filopodia, emanating from this lamellipodial actin network while playing no role in the formation of the Arp2/3-independent filopodia. Finally, the loss of Evl impairs FA growth, cell spreading and traction force generation. Ena/VASP may

## Introduction

also play a role at the tip of adhesive filopodia, called sticky fingers. As discussed in details in the previous section describing actin dynamics in filopodia (See I.2.1), the MIT complex, made of MRL proteins, integrins and talin, could additionally recruit Ena/VASP proteins at the tip of filopodia to stimulate actin assembly (Lagarrigue et al., 2015).

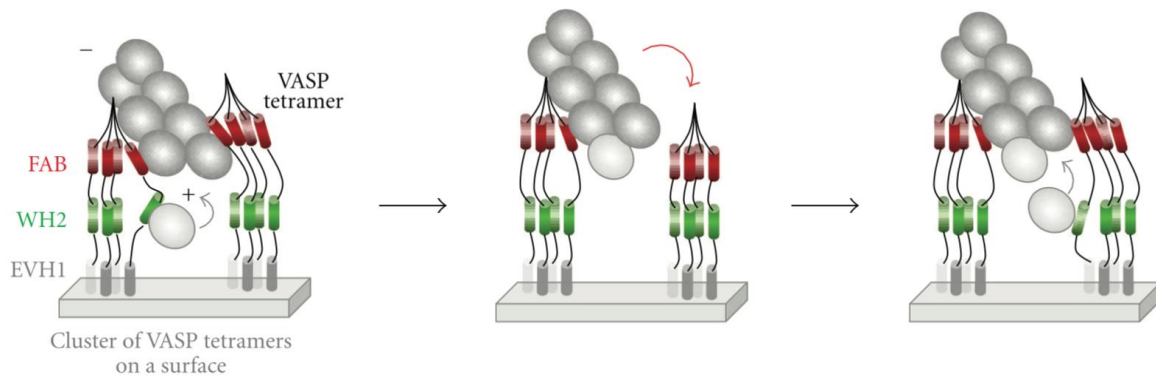


**Figure 23. Clusters of VASP control the processive elongation of actin filaments.**

Clusters of VASP tetramers allow the G-actin binding domains (GABs), called WH2 domains here, of several VASP molecules to deliver actin monomers to the barbed end. Between actin association events, VASP remains bound to the growing filament via its F-actin binding domain (FAB). (Ciobanasu et al., 2012)

Ena/VASP proteins have been proposed to regulate actin polymerization by a variety of mechanisms. In vitro, VASP has the ability to nucleate actin filaments in a pyrene-actin polymerization assay. However, targeting VASP at mitochondria did not coincide with an accumulation of F-actin on mitochondria (Bear et al., 2000). Like formins, Ena/VASP proteins elongate actin filament barbed ends in a processive manner (Breitsprecher et al., 2011, 2008; Hansen and Mullins, 2010). This activity requires the formation of dense clusters of VASP (Figure 23) and it is only efficient for *Dictyostelium* VASP. In these conditions, the barbed ends that elongate processively from VASP clusters are protected from the action of capping proteins (Breitsprecher et al., 2011, 2008; Brühmann et al., 2017). Although human VASP is poorly processive, the recruitment of profilin-actin complexes to its PR domain enhances this activity (Hansen and Mullins, 2010). Ena/VASP also bundle actin filaments, which requires both its ability to bind F-actin and to form tetramers (Bachmann et al., 1999). In contrast to other bundling proteins, such as fascin, VASP is not found along the entire length of actin bundles, but only localized at the tip of filopodia.

### I.3.5 Nanoscale organization of focal adhesions

Nascent adhesions are difficult to image with fluorescence microscopy, as they are small and very dynamic, such that upon formation, they quickly disassemble or grow into mature FAs. They also have many components in common with the lamellipodial network, making them

## Introduction

difficult to observe using fluorescence microscopy. Thus, most studies have focused on FAs rather than NAs. FA size vary from less than 0.2 to 10  $\mu\text{m}$ , with a more elongated shape as they grow.

Cell-matrix adhesions are dense heterogeneous plaques made of stackings of various proteins. To characterize these structures, studies first focused on making an inventory of their specific components. Traditional biochemical methods pointed out the most abundant components: integrins, vinculin and talin. Screening techniques, like yeast 2-hybrid or co-affinity purification, then allowed identifying additional members of the adhesion proteome, sometimes referred to as adhesome. More recently, proteomic analysis revealed up to thousands more proteins at least transiently associated to FAs (Geiger and Zaidel-Bar, 2012; Kuo et al., 2011; Schiller et al., 2013).

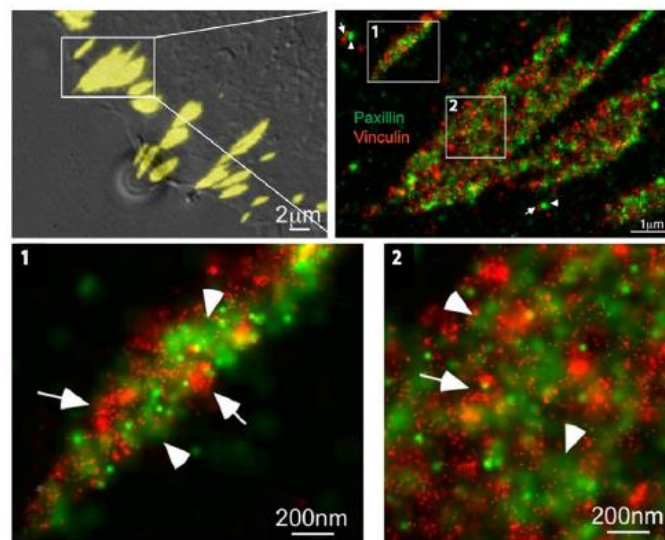


**Figure 24. Lateral nanoscale organization of FAs.**

Parallel arrays of interwoven paxillin (green) and vinculin (red) aggregates along the length of an adhesion (Shroff et al., 2007).

Although there is plenty of knowledge about the composition of these structures, their complex molecular architecture remained poorly studied, until recent technical advances allowed addressing this issue. The resolution of conventional light microscopy being limited to 200 nm, electron microscopy provided a much higher resolution (Chen and Singer, 1982). Later, cryo-EM observations revealed that the membrane-cytoskeleton coupling at focal adhesions is mediated by doughnut-shaped particles with a typical diameter of 20 to 30 nm (Patla et al., 2010). However, the molecular composition of these particles remains unclear. The development of super-resolution fluorescence microscopy and single-protein tracking allowed us to revise the organization of FA components. For example, proteins such as vinculin as paxillin appear colocalized in confocal microscopy but they localize to distinct nanostructures when observed in super-resolution microscopy (Shroff et al., 2007) (Figure 24).

## Introduction

Kanchanawong and colleagues also used a complex 3D iPALM super-resolution method to localize FA components along the vertical axis (Kanchanawong et al., 2010). They described a 40 nm gap between the intracellular integrin tails and the actin filaments that consists of organized layers of FA proteins (Figure 25). The membrane-proximal layer, close to the integrins, is a signaling layer containing the highly phosphorylated signaling proteins FAK (focal adhesion kinase) and paxillin. Talin and vinculin, adapter proteins that link the integrins to the actomyosin machinery, are localized in the following layer, termed force-transduction layer. Talin spans over the whole layer, with its head binding integrins and its rod binding actin, up to 30 nm away on the z-axis. The most distal layer, up to 60 nm away from integrins, is the actin regulatory and actin stress fiber layer, containing actin-associated proteins such as VASP, zyxin and  $\alpha$ -actinin (Kanchanawong et al., 2010; Jaron Liu et al., 2015).

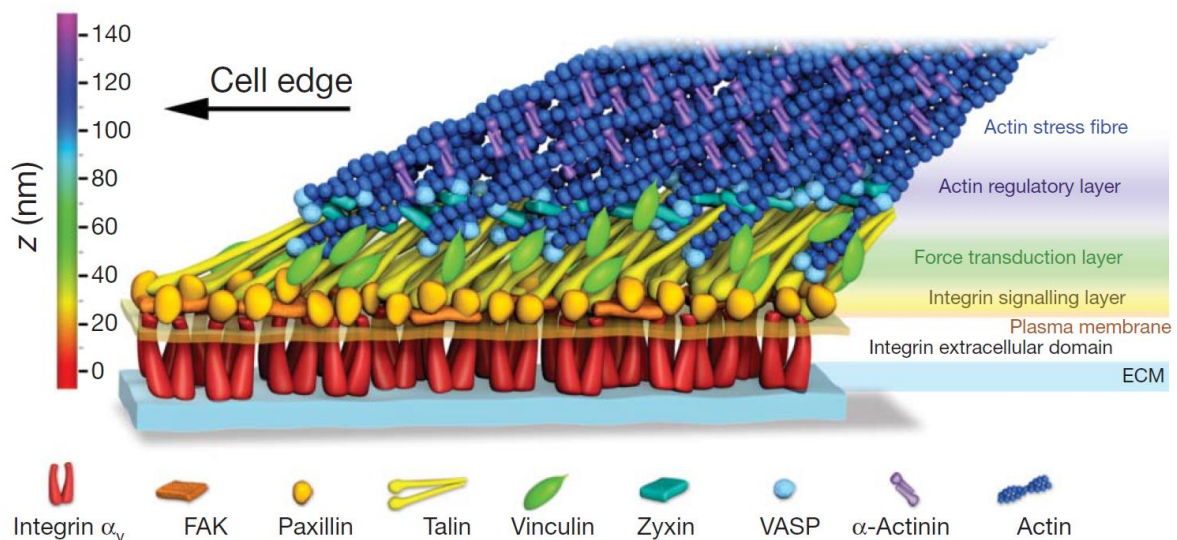


**Figure 25. Schematic model of the vertical nanoscale organization of focal adhesions.**  
(Kanchanawong et al., 2010)

### I.3.6 Dynamics of focal adhesions

Unraveling the vertical stratification of proteins in the adhesive plaque brought new insight into the global functioning of cell-matrix adhesions and the relative role of each of their components. However, determining the dynamics of the components inside FAs was also critical to understand their contribution to force transmission. The combination of single-protein tracking with super-resolution microscopy revealed the nanoscale organization and the dynamics of integrins and talin in FAs. This approach showed how integrins diffuse into the membrane before being trapped in FAs, whereas talin is recruited to FAs from a soluble pool in the cytoplasm. The analysis of integrin immobilization times in FAs, which reflects their activation, indicates that different integrins, co-existing in the same FA, coupling the cytoskeleton to the extracellular matrix with different efficiencies (Rossier et al., 2012) (Figure 26).

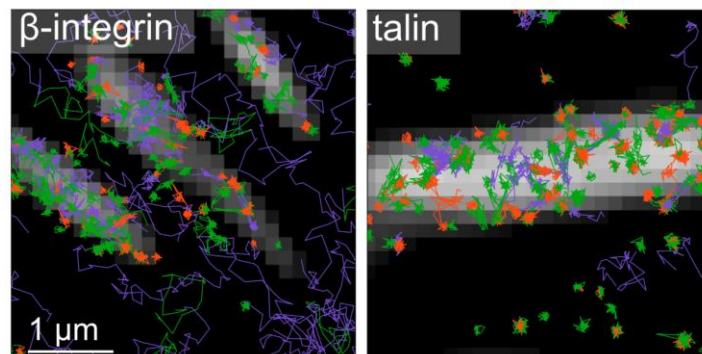


**Figure 26. The dynamics of single molecules of integrin and talin reveal the nanoscale organization of FAs.** Trajectories obtained by sptPALM outside and inside FAs (labeled with paxillin-GFP in grey) for  $\beta$ 3 integrin (left) and talin (right) (Rossier et al., 2012).

Furthermore, correlation fluorescence speckle microscopy allows measuring the coupling of FA proteins to actin filaments (Hu et al., 2007). This technique revealed that the transmission of motion from the actin filaments to the FA components follows a hierarchical slippage that correspond to the stratification observed by 3D iPALM (Kanchanawong et al., 2010). The differential transmission of actin-generated force decreases from actin-binding proteins, in the actin regulatory layer, to the FA core proteins, to integrins. The “molecular clutch” theory has been used to conceptualize force transmission in FAs. In this model, the degree of force transmission is determined by the association and dissociation rates of the protein-protein interactions along the actin-FA-ECM pathway (Elosegui-Artola et al., 2018; Kechagia and Ivaska, 2019) (Figure 27).



## Introduction

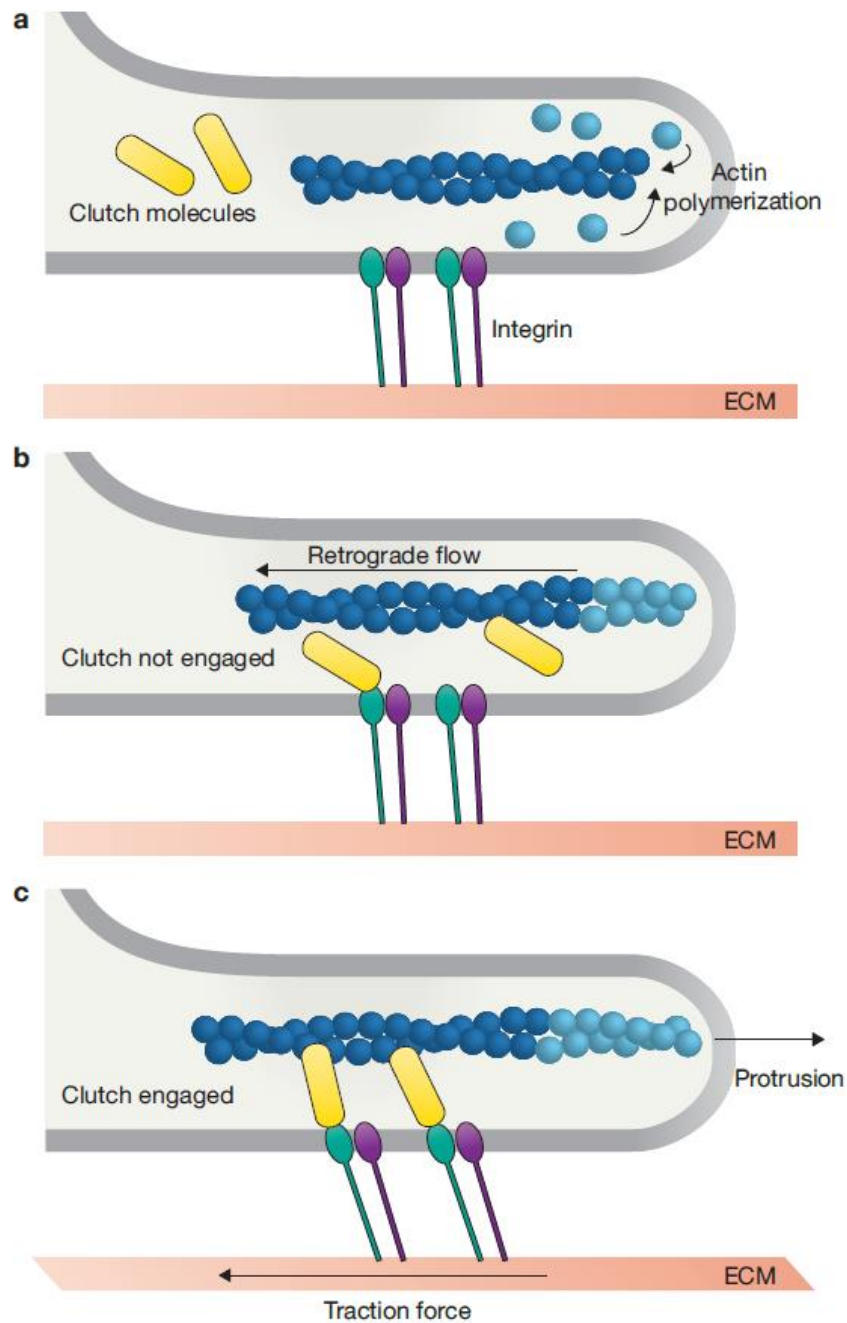


**Figure 27. Cell-matrix adhesions act as a “molecular clutch” to convert the force generated by the actin cytoskeleton into protrusion.**

**(a)** Actin polymerizes towards the membrane. **(b)** When the molecular clutch is disengaged, the pushing actin cytoskeleton is not anchored. Thus, it will not generate force on the membrane, but it will move backwards as a retrograde flow. **(c)** When the clutch is engaged, adhesion anchors the pushing actin cytoskeleton, so that protrusion can occur instead of retrograde flow. ECM (extracellular matrix) (Case and Waterman, 2015).

## I.4 CELL-MATRIX ADHESIONS SENSE AND ADAPT TO THE ACTOMYOSIN FORCE

### I.4.1 Cell-matrix adhesions contain a variety of mechanosensors

To understand cellular mechanotransduction, it is crucial to decipher the molecular mechanisms that control how forces are being sensed by cells and how these mechanical stimuli are transduced into appropriate biochemical responses. Force-induced conformational change of specific proteins in specific locations of the cell are key molecular mechanisms that controls both processes (Bao, 2013).

#### I.4.1.1 The exposure of fibronectin RGD motifs is force-dependent

The fibronectin fibrils, to which the cells associate, do not form an inert matrix. The ability of fibronectin to adapt to the traction forces generated by the cells makes them a major element in maintaining mechanical homeostasis throughout tissues.

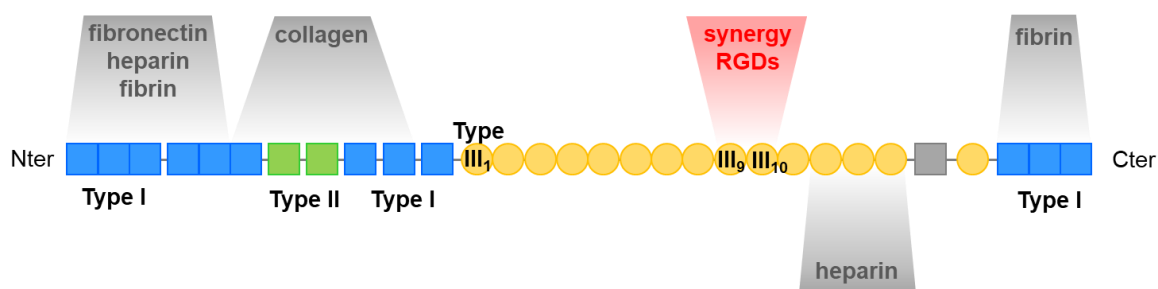


**Figure 28. Fibronectin domain organization and interactions.**  
RGD (Arg-Gly-Asp).

Integrin binds to the tripeptide RGD (Arg-Gly-Asp) loop of fibronectin, located on the tenth type III module (FN-III<sub>10</sub>), and also to a nearby site on the ninth type III module (FN-III<sub>9</sub>) (Figure 28). The molecular basis of fibronectin mechanosensitivity involves the mechanical exposure of the cryptic RGD buried inside FN-III<sub>10</sub> in the native state of the protein. This mechanism was first predicted by steered molecular dynamics (SMD) simulations (Krammer et al., 1999). Experiments using GFP-tagged fibronectin revealed that cells can stretch fibronectin fibers up to four times their native length (Ohashi et al., 1999), confirming that the type III modules of fibronectin experience sufficient stretching to expose their RGD motifs.

At the molecular level, force acts on the structure of the RGD loop of the FN-III<sub>10</sub> module. This loop needs to be extended from the protein surface for optimal integrin binding (Vogel et al., 2001). SMD simulations suggest that force application is sufficient to extend the RGD loop of FN-III<sub>10</sub> (Krammer et al., 1999). This model predicts that integrin affinity for the RGD loop first

increases with force until the loop is overextended, which reduces its affinity for integrin. The mechanical exposure of two consecutive RGD motifs in fibronectin increases integrin affinity. Indeed, integrin binding to the RGD loop of FN-III<sub>10</sub> is enhanced 40-fold when the synergy site of FN-III<sub>9</sub> is also exposed (Aota et al., 1994). In addition to the synergistic RGD sites along individual fibronectin molecules, the assembly of fibronectin into fibrils creates clusters of RGD motifs, which promotes integrin binding (Vogel et al., 2001).

### *1.4.1.2 Integrin-ligand interactions behave as catch bonds*

Most protein-protein interactions behave as slip bonds, which means that the strength and the lifetime of the bond are reduced with force application. Integrins, however, do not always follow this behavior. Some integrin-ligand interactions are strengthened by a pulling force, resulting in a prolonged bond lifetime. This process is referred to as catch bond. But integrin-ligand interactions are most likely catch-to-slip bonds.

In a catch-to-slip bond, force first strengthens the bond (catch regime), but once a sufficiently high tension is reached, the bond starts to weaken (slip regime). The best example to illustrate this physical principle is the picture of two interconnected hooks. At rest, they are loosely attached to one another. Once force starts to pull the hooks apart, they are locked in place. But if the force exceeds a sufficiently high threshold, the hooks themselves start to deform and they eventually separate from each other. The complex integrin-ECM interaction can be affected by force in many different ways, explaining this peculiar behavior (Kechagia and Ivaska, 2019). Such a catch-to-slip bond behavior has been described between the RGD loop of fibronectin and  $\alpha_5\beta_1$  integrin (Kong et al., 2009) and then for  $\alpha_v\beta_3$  integrin (Elosegui-Artola et al., 2018).

During their activation process, integrins first switch from a bend-closed to an open-closed conformation, and they finally transition to an open-extended conformation under force application. Structural data have shown that in their extended conformation, the transition of integrins from extended-closed to extended-open increases their affinity for RGD ligands in the matrix (Figure 13). Force applied to integrins could reduce fluctuations in integrin conformation and lock them in their open state, which would increase their affinity for RGD ligands in the matrix and prolong the lifetime of the bond with the ECM (Kechagia and Ivaska, 2019).

Finally, it is interesting to note that the force-dependent properties of the integrin-RGD bonds have been extensively studied, whereas the interaction between integrins and non-RGD matrix components, such as collagen or laminin, have been addressed to a much smaller extent. Their

response to a tensile load still needs to be elucidated, although indirect elements suggest that they could be catch bonds ([Kechagia and Ivaska, 2019](#)).

### *1.4.1.3 The zyxin- $\alpha$ -actinin-VASP complex repairs damaged stress fibers*

Several machineries contribute to the formation, reinforcement and maintenance of SFs. When cells are submitted to a sustained mechanical stress, SFs are occasionally damaged. Zyxin rapidly accumulates along SFs at sites of thinning or damage. Once there, zyxin promotes the recruitment of the actin regulatory proteins  $\alpha$ -actinin and VASP. This ternary complex induces actin polymerization to repair the damage, in order to maintain the tension exerted by the SF ([Smith et al., 2010](#)). However, to date, the mechanism by which zyxin is relocated to the damaged sites and the contribution of the individual proteins of the ternary complex to actin polymerization remains unknown.

### *1.4.1.4 The mechanosensitive phosphorylation of p130Cas controls signaling pathways*

The 130 kDa scaffold protein p130Cas is an adaptor from the Cas (Crk associated substrate) family. P130Cas can dimerize. It contains a N-terminal SH3 domain, which binds the polyproline motifs of several proteins including FAK and vinculin. This SH3 domain is followed by a large substrate domain (SD) containing 15 repetitions of the tyrosine phosphorylation site YxxP. The C-terminal Src-binding domain (SBD) binds SH2 and SH3 domains upon tyrosine phosphorylation ([Janoštiak et al., 2014b](#)) (Figure 29).

Cytoplasmic p130Cas is recruited to NAs by  $\beta$  integrin tail-bound FAK, after FAK activation by Src. The mechanical unfolding of p130Cas, both in vitro by atomic force microscopy (AFM) and magnetic tweezers and in cells, induces the exposure of tyrosine residues, which are normally masked, resulting in phosphorylation of these residues by the FAK-Src complex ([Lu et al., 2013](#); [Sawada et al., 2006](#)) (Figure 29). The interaction of signaling molecules, such as the Crk-C3G complex, with the activated substrate domain of p130Cas leads, in turn, to the activation of Rap1, ERK and other components of major signaling pathways ([Sawada et al., 2006](#)) (Figure 29). Force-dependent p130Cas phosphorylation sites are associated with both positive and negative effects, allowing fine tuning p130Cas signaling in time and space. The phosphorylation of tyrosine 410 in the substrate domain turns on p130Cas when adhesions experience force. On the contrary, the delayed phosphorylation of tyrosine 12 in the SH3 domain switches p130Cas off, by weakening its affinity for FAK and vinculin, which uncouples p130Cas from adhesions experiencing high forces ([Janoštiak et al., 2014a](#)).

## Introduction

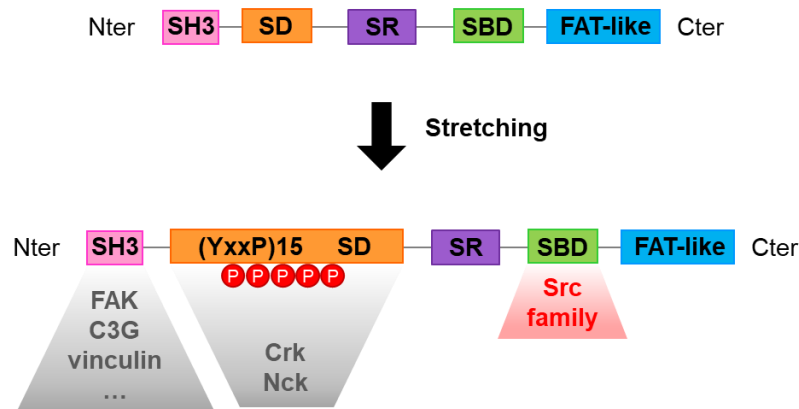


**Figure 29: P130Cas domain organization and interactions.**

P130Cas stretching induces the exposure of phosphorylation sites. SH3 (Src homology 3 domain), SD (substrate domain), P (phosphorylation sites), SR (serine-rich region), SBD (substrate-binding domain), FAT (focal adhesion-targeting domain).

P130Cas serves as a hub for connecting the force transmission machinery with the biochemical signaling cascades in mechanically-induced cellular responses, such as FA reinforcement and durotaxis. The interaction of p130Cas with vinculin in NAs could help stabilize vinculin in the opened conformation and thus promote the stabilization and enlargement of the adhesion (Janoštiak et al., 2014a). One of the Src family member, Fyn, which phosphorylates the unfolded substrate domain of p130Cas, is more active when the substrate is stiffer, and thus increases the phosphorylation of p130Cas (Kostic and Sheetz, 2006). Furthermore, a positive feedback loop involving myosin II could also contribute to durotaxis. Force-dependent activation of p130Cas results in increased myosin II activity, which generates higher traction forces on the adhesion, and in turn increases the amount of unfolded phosphorylated p130Cas. It can then recruit Crk to stimulate Rac-dependent lamellipodia formation, thus promoting protrusions of the leading edge towards stiffer substrate (Chodniewicz and Klemke, 2004).

### 1.4.2 Talin is the central mechanosensor of cell-matrix adhesions

#### 1.4.2.1 The mechanical stretching of talin exposes cryptic vinculin-binding sites

- Talin is a stretchable protein

The idea that talin could be a mechanosensor was suggested at an early stage because it is ideally positioned between the adhesion machinery and the contractile cytoskeleton to serve this function. The N-terminal head of talin binds integrins at the membrane, while the C-terminal ABD interacts with the actomyosin stress fibers. Talin thus forms a 2 pN bond between

## Introduction

the fibronectin extracellular matrix and the actin cytoskeleton (Jiang et al., 2003). Finally, talin is required for the force-dependent reinforcement of the integrin-actin link (Giannone et al., 2003).

Steered molecular dynamics (SMD) was first used to support the idea that talin could be stretched mechanically. The first in silico experiments suggested the existence of stable intermediate conformations during the mechanical stretching of the  $\alpha$ -helix bundles of a talin fragment corresponding to R1-R2-R3 (Hytönen and Vogel, 2008; Lee et al., 2007) (Figure 30). Later on, the stretching of single molecules of talin fragments by atomic force microscopy or magnetic tweezers confirmed that  $\alpha$ -helix bundles are unfolded at physiological forces (Del Rio et al., 2009; Yao et al., 2016). These experiments allowed determining the force required to unfold a structured bundle. Comparison of several isolated bundles of talin pointed out that most of them unfold at forces ranging from 5 to 25 pN (Haining et al., 2016b; Yao et al., 2016). R3, which unfolds at 5 pN, is the most fragile, implying that it would be the first one to unfold along the talin rod in response to a mechanical stimulus (Yao et al., 2014) (Figure 30). R8 differs from all other talin bundles because it is protected from mechanical unfolding by its insertion in R7 (Gingras et al., 2010) (Figure 16).

These single molecule studies are also supported by cellular observations. By inserting a calibrated FRET sensor between the head and the rod, the forces applied to talin were measured between 7 and 10 pN (Austen et al., 2015), consistent with single molecule experiments. In cells, high-resolution fluorescence microscopy was used to determine the length of talin molecules, by fusing it to a different fluorophore at each end. Measurements showed that the C-terminal end of talin extends 250 nm from the N-terminal end, while the length of talin is limited to 60 nm after inhibition of myosin (Margadant et al., 2011). Such an extension of talin requires the unfolding of several bundles along its rod. iPALM super-resolution microscopy observations of talin with distinct fluorescent markers at each end revealed that the talin extends from 97 nm at an angle of 15° to the plasma membrane (Jaron Liu et al., 2015).

Altogether, these experiments confirm that talin senses a broad range of forces by unfolding its domains sequentially. It might then induce different signaling cascades depending on which of its domains unfold and which proteins associate to them.

## Introduction

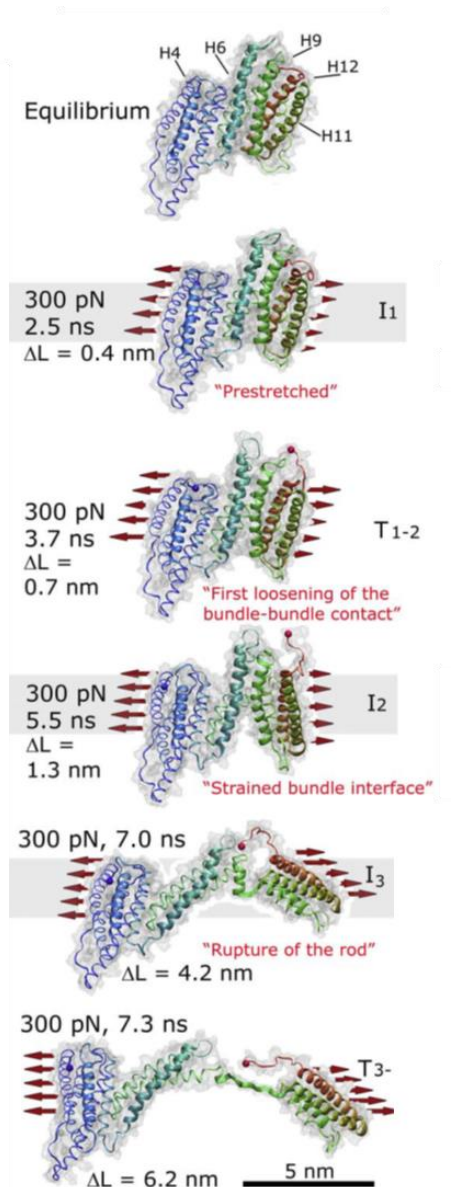


**Figure 30. Simulation of the force-induced fragmentation of the talin rod fragment, containing helix 1 to helix 12, into  $\alpha$ -helix sub-bundles.**

Sequential structural snapshots of the mechanically strained talin H1-H12 part of the rod are displayed. The pulling force of 300 pN was used in the depicted steered molecular dynamics simulation. The extension (increase in the length of the H1-H12 as compared to the equilibrium state) is shown as  $\Delta L$ . Three intermediate states are observed (I1, I2, I3) (Adapted from Hytönen and Vogel, 2008).

- The vinculin-binding sites are buried inside talin bundles

The mechanosensing abilities of talin rely primarily on its force-dependent interactions with its binding partners. In cells, the observation that FAs are enriched in vinculin when stress fibers exert an increasing tension on them supports a model in which the actomyosin force applied on talin is necessary for binding vinculin.

The binding of vinculin head (Vh) to talin was tested for all the  $\alpha$ -helices of the talin rod individually. It revealed the existence of eleven vinculin-binding sites (VBSs) (Gingras et al.,

## Introduction

2005) (Figure 16). At the molecular level, NMR and crystal structures of talin R3 showed that the VBSs are buried inside the folded  $\alpha$ -helix bundle, suggesting that vinculin binding requires talin unfolding (Fillingham et al., 2005). The observation that the deletion of the last helix of R3 dramatically increases the affinity of talin for Vh confirms this hypothesis (Patel et al., 2006).

- The mechanical stretching of talin induces the exposure of its vinculin-binding sites

The demonstration that mechanical stretching of talin allows vinculin binding required the combination of single molecule stretching experiments and fluorescence microscopy. A fragment of talin corresponding to R1-R2-R3, bound to a surface on one side and to a magnetic bead on the other side, was stretched by magnet forceps in the presence of Vh fused to the fluorescent protein GFP. During force application, the stepwise photobleaching of the GFP-Vh molecules bound to single talin molecules determined the number of Vh molecules bound per talin (Del Rio et al., 2009). This series of experiments revealed that three Vh molecules can simultaneously bind to the R1-R2-R3 fragment of talin subjected to a force of 12 pN, while only one Vh binds to this unstretched talin fragment. It is important to keep in mind that although the majority of VBSs are masked in talin, this experiment demonstrates that some VBSs can be exposed in the absence of force.

Although these studies used physical techniques to reveal the mechanosensitive interaction between talin rod bundles and Vh, they did not demonstrate that the physiological force generated by the actomyosin contraction was sufficient to stretch talin bundles, expose cryptic VBSs and recruit vinculin. Demonstrating this point remained crucial, because in the physical devices used to stretch single molecules of talin, the protein is almost covalently anchored at both ends. In cells, there is no evidence that the bond between talin and the actomyosin contractile cables is able to withstand the force required to unfold talin. Our laboratory developed an in vitro reconstituted assay in which the self-assembly of actomyosin cables induced the association of Vh to full-length talin immobilized in disc-shaped islands micropatterned on a glass surface (Ciobanasu et al., 2015, 2014). This experiment proved that actomyosin is sufficient to induce the strong accumulation of EGFP-Vh in the talin-coated micropatterns, whereas a weak accumulation of EGFP-Vh was observed in the absence of actomyosin.



## Introduction

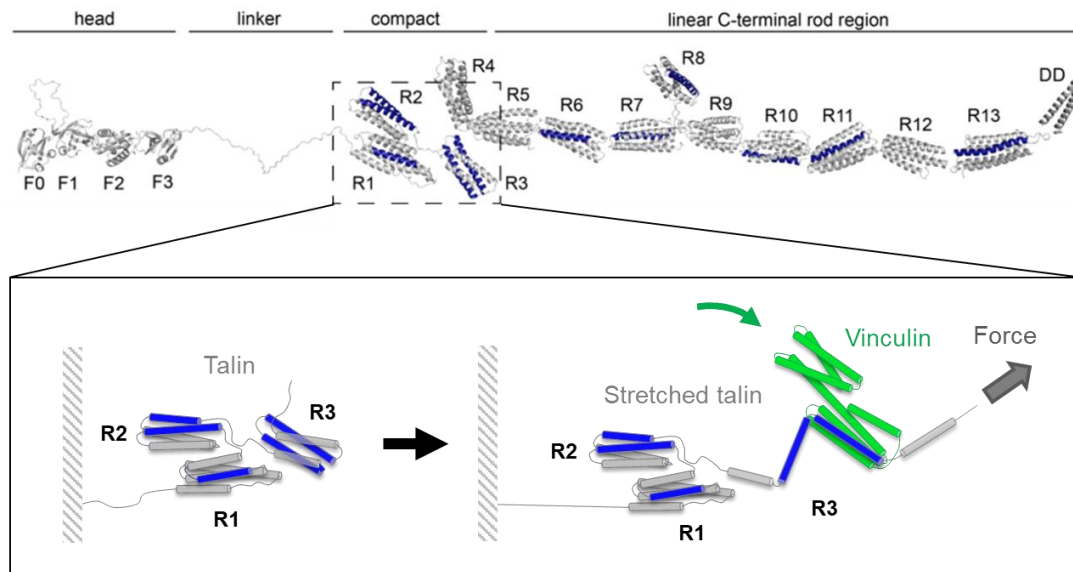


**Figure 31. The mechanical stretching of talin.**

(Top) Representation of full-length talin with the eleven vinculin-binding sites (VBSs) highlighted in blue (Yao et al., 2014). (Bottom) The well-documented stretchable region of talin comprising R1, R2 and R3. The stretching of R3 exposes two consecutive cryptic VBSs (blue).

### 1.4.2.2 Vinculin locks talin in its extended conformation

The study of talin unfolding in the presence of vinculin provided important information on the stability of the talin-vinculin complex. In the presence of Vh, the first unfolding cycle displays jumps that reflect the sequential dissociation of the helices from the bundles. After force release, the following stretching cycle no longer show these jumps, indicating that vinculin did not dissociate between the two cycles and that vinculin kept talin locked in its stretched conformation (Yao et al., 2016, 2014). In our in vitro reconstituted assay described previously, the rate of Vh dissociation from talin after an actomyosin cable detaches from a talin-covered micropattern is the same as the rate of Vh dissociation from stretched talin in the presence of actomyosin measured by fluorescence recovery after photobleaching (FRAP). The fact that vinculin dissociation is not affected by the release of force confirms that vinculin locks talin in a stretched conformation (Ciobanasu et al., 2014). These observations reveal a mechanism for talin to memorize the mechanical information for a longer time than the duration of the mechanical stimulation.

### 1.4.2.3 Vinculin activation by stretched talin contributes to actin anchoring

A question that remains relatively unexplored, even until now, is how the talin-vinculin complex behaves and responds after its formation. The ability of isolated vinculin to bind, cap, nucleate and bundle actin filaments, described in the previous paragraphs (See 1.3.4.5), must influence

## Introduction

the dynamic anchoring of stress fibers to FAs. In the *in vitro* assay that reconstitutes the formation of the talin-vinculin complex in response to the actomyosin force, the binding of full-length vinculin to talin, which releases its actin-binding tail  $V_t$ , stabilizes the anchoring of the actomyosin cables, whereas under the same conditions,  $V_h$  that cannot bind actin does not allow actomyosin to anchor durably (Ciobanasi et al., 2014). Similarly, in cells expressing  $V_h$ , the actin network moves backwards over talin-containing FAs, whereas in cells expressing full-length vinculin, actin is stably anchored to FAs (Hirata et al., 2014). Altogether, these biochemical and cellular studies show that the force-dependent vinculin binding to talin reinforces actin anchoring to FAs (Figure 32). In addition, single molecule experiments showed that the binding of vinculin tail to an actin filament is enhanced by force in a direction-dependent manner, providing the first demonstration of a directionally sensitive catch bond (Huang et al., 2017). This asymmetric catch bond behavior could contribute to organizing the polarity of the actin cytoskeleton in response to external and internal mechanical stimuli during directed migration, in addition to enhancing overall resistance to tension.

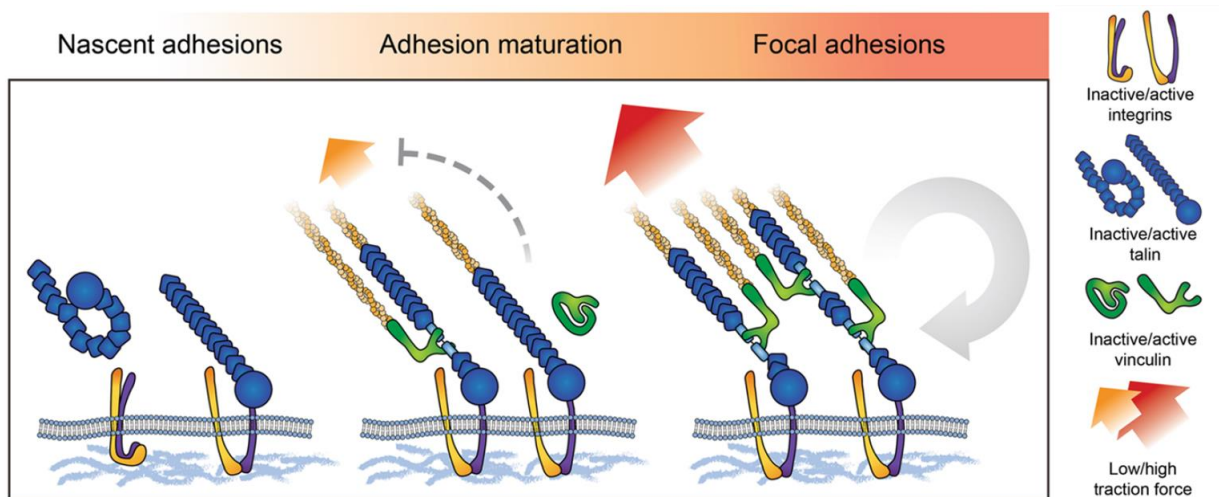


**Figure 32. The force-dependent binding of vinculin to talin reinforces actin anchoring.**

The recruitment of vinculin to mechanically stretched talin contributes to feed the stress fibers with new actin filaments and thus reinforces their anchoring to the adhesion complex (Adapted from Rahikainen et al., 2017).

## Introduction

Stabilization of the focal adhesion-actin bond is undoubtedly not the only response of the force-dependent talin-vinculin complex. The observation that Vh stabilizes FAs suggests that the formation of this complex is an initial nucleus on which many additional components assemble to initiate various signaling pathways (Carisey et al., 2013). Most of these signaling pathways influence cell adhesion on the very short term, but the talin-vinculin complex, like FA components in general, could also induce a long-term cell adaptation, as suggested by the requirement of vinculin for the nuclear translocation of the transcription factors YAP/TAZ on a stiff ECM (Kuroda et al., 2017; Rausch and Hansen, 2020).

### I.4.3 RIAM is a major regulator of talin function

#### I.4.3.1 RIAM belongs to the Mig-10 / RIAM / lamellipodin family

Mig-10 (abnormal cell migration protein 10), RIAM (Rap1-GTP-interacting adaptor molecule) and lamellipodin belong to the MRL (Mig-10 / RIAM / lamellipodin) family of multidomain adaptor molecules. Mig-10 was characterized as the *Caenorhabditis elegans* ortholog of the MRL proteins, whereas Pico is the *Drosophila* ortholog. The present study will focus on RIAM. The protein is known by different names depending on how it was discovered. Before being referred to as RIAM when it was identified as an interactor of the small GTPase Rap1 in a yeast two-hybrid screen (Lafuente et al., 2004), the protein was first termed amyloid- $\beta$  (A4) precursor protein-binding, family B, member 1-interacting protein (APBB1IP), because it interacts with the WW (tryptophan-tryptophan) domain of APBB1 via its proline-rich domain (Ermeikova et al., 1997). Another group named it retinoic acid-responsive proline-rich protein 1 (RARP1) because it is transcriptionally induced in response to all-trans retinoic acid (ATRA) (Inagaki et al., 2003). Finally, another independent study identified RIAM as a binding partner of Ena/VASP proteins, and named it proline-rich EVH1 ligand 1 (PREL1) (Jenzora et al., 2005).

The MRL proteins share a N-terminal coiled-coiled region (red star on Figure 33), a central Ras-association (RA) and a pleckstrin homology (PH) domain, followed by a C-terminal proline-rich (PR) region containing multiple putative EVH1-binding motifs (D/E)(F/L/W/Y)PPPPX(D/E)(D/E), abbreviated FPPPP, as well as XPPPPP motifs that interact with profilin and SH3-binding motifs (Coló et al., 2012; Niebuhr, 1997; Patsoukis et al., 2017) (Figure 33).

## Introduction

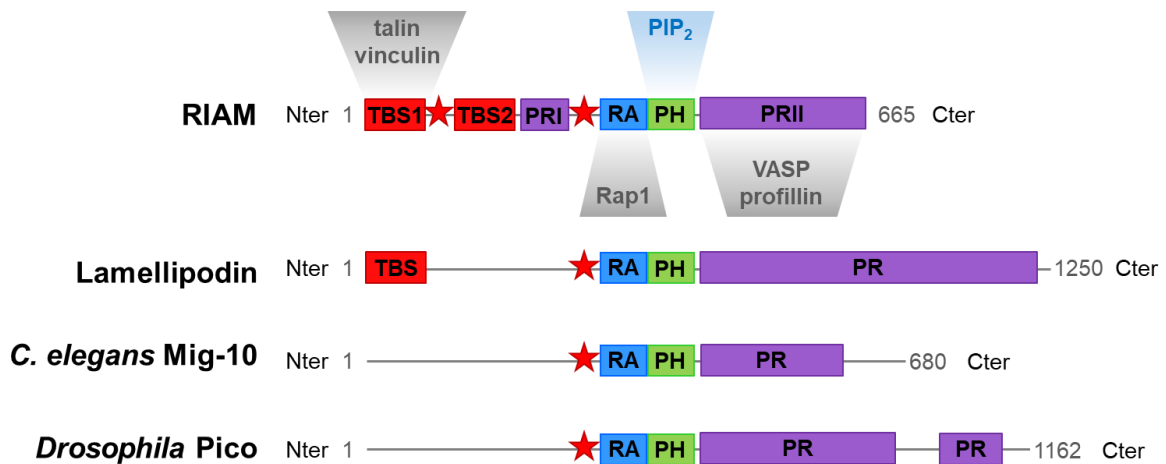


**Figure 33. RIAM and other MRL proteins domain organization and interactions.**

TBS (talin-binding site), PR (proline-rich region), RA (Ras-association domain), PH (pleckstrin homology domain). The red stars represent coiled-coiled regions.

While the RA and PH domains of RIAM and lamellipodin are conserved, their C-terminal region is not. Although both paralogs can bind talin via their N-terminal talin-binding site (TBS) (Figure 33), in contrary to other MRL proteins, only RIAM contains an additional N-terminal coiled-coiled and proline-rich domain that contains a putative profilin-binding motif and two FPPPP motifs. In the C-terminal PR region, RIAM comprises five putative profilin-binding motifs and four FPPPP motifs, while lamellipodin only displays one C-terminal PR domain, which is much longer and contains six putative FPPPP motifs, three profilin-binding motifs and eight potential SH3-binding sites (Coló et al., 2012). Individually, all the FPPPP motifs of lamellipodin interact with Ena/VASP proteins (Krause et al., 2004). Another difference between RIAM and lamellipodin is their localization. RIAM is expressed broadly, with higher levels in hematopoietic cells, while lamellipodin is expressed mainly in the brain, heart, ovaries and developing embryos. Furthermore, lamellipodin oligomerizes through a unique configuration that does not involve the coiled-coiled region, while RIAM lacks this interactions in both crystallographic and solution studies (Chang et al., 2013).

### 1.4.3.2 The Rap1-RIAM-talin complex activates integrins

Among the various functions of MRL proteins, several studies highlighted their crucial role in integrin activation and in promoting cell adhesion.

Bimolecular fluorescence complementation (BiFC) revealed that in living cells, RIAM overexpression stimulates  $\beta_3$  integrin activation, while RIAM knockdown blocks it (Watanabe et al., 2008). Overexpression of RIAM in T cells also induces  $\beta_1$  and  $\beta_2$  integrin activation, favors cell adhesion and cell spreading, while RIAM knockdown displaces Rap1 from the plasma

## Introduction

membrane and abolishes Rap1-dependent adhesion (Lafuente et al., 2004). The disruption of the interaction between the RA domain of RIAM and Rap1 also leads to a loss of cell adhesion (Zhang et al., 2014). Moreover, the consecutive RA and PH domains of RIAM operate as a proximity detector for Rap1 and PIP<sub>2</sub> respectively, which is necessary to localize and anchor the Rap1-RIAM complex to the plasma membrane (Wynne et al., 2012). Altogether, these observations support the view that the recruitment of the Rap1-RIAM complex at the plasma membrane is important for integrin activation.

In parallel, Han and colleagues showed that Rap1 is involved in  $\beta_3$  integrin activation in platelet through the formation of an integrin-associated complex containing talin and RIAM. In this complex, RIAM is required for talin-mediated integrin activation (Han et al., 2006). RIAM interacts with the F3 subdomain (PTB) of talin head, which disrupts the F3-R9 autoinhibitory interaction, allowing F3 to bind and activate integrin (Yang et al., 2014) (Figure 16). In addition to F3, RIAM binds to the R2, R3, R8 and R11 bundles of talin (Goult et al., 2013b) (Figure 16). Structural studies also suggested that the binding of RIAM to talin R8 contributes to the disruption of the F3-R9 autoinhibitory interaction (Chang et al., 2014; Zhang et al., 2016b).

Altogether these observations suggest that, in the Rap1-RIAM-talin complex, the function of Rap1 is mainly to target RIAM at the membrane, while the function of RIAM is to recruit and activate talin, which in turn activates integrin. Consistent with this hypothesis, a protein composed of the talin binding site (TBS1) of RIAM fused with the membrane targeting domain of Rap1 is sufficient to target talin to the membrane where it activates integrins (Lee et al., 2009).

Whether lamellipodin and RIAM both participate in the mechanisms described above or whether these proteins have distinct activities remains to be clarified. Some studies support a role for a Rap1-lamellipodin complex in talin-induced integrin activation (Lee et al., 2009). However, RIAM knockdown, but not lamellipodin knockdown, blocks talin recruitment and  $\alpha_{IIb}\beta_3$  activation induced by Rap1 in platelets (Watanabe et al., 2008).

### *1.4.3.3 The MRL protein-talin-integrin complex regulates actin dynamics*

A recent report identified a complex containing either RIAM or lamellipodin, integrins and talin, localized at the tip of filopodia and the leading edge of lamellipodia (Lagarrigue et al., 2015) (Figure 34). Disruption of this complex impairs actin assembly and the protrusion of both lamellipodia and filopodia. The mechanism by which this complex promotes actin assembly is not fully understood.

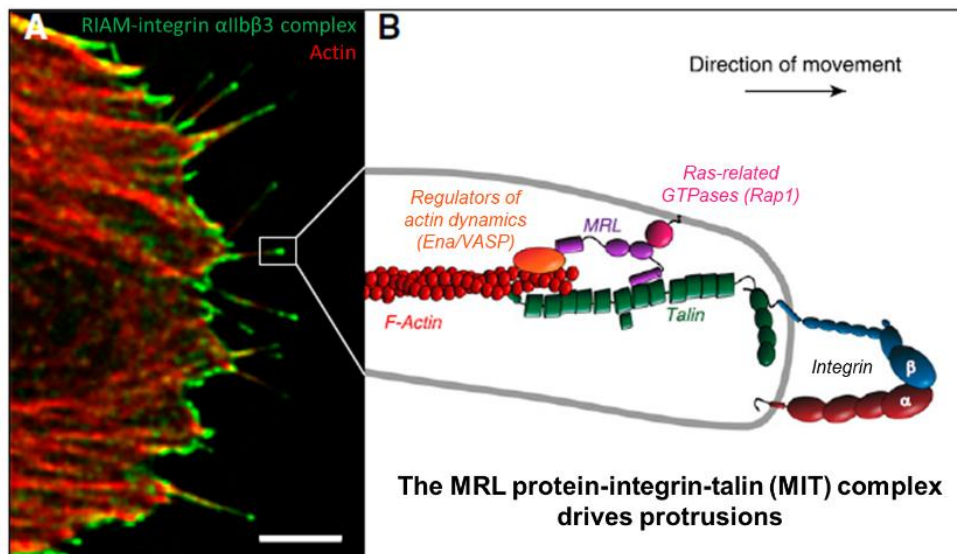


**Figure 34. The MRL protein-integrin-talin controls actin-based protrusions of the leading edge.**

**(A)** The MRL protein-integrin-talin (MIT) complex, visualized by bimolecular fluorescence complementation (green) between RIAM and  $\alpha_{11b}\beta_3$  integrin, is enriched at the tips of growing actin filaments (red) in the protrusions of a migrating cell. Scale bar = 5  $\mu\text{m}$ . **(B)** The N terminus of MRL proteins binds talin, which in turn activates integrin. The C terminus of MRL proteins would promote actin assembly by recruiting actin regulators, including Ena/VASP proteins (Adapted from Lagarrigue, Kim and Ginsberg, 2017).

Interestingly, VASP binds several FPPPP motifs in the C-terminal half of RIAM and lamellipodin (Jenzora et al., 2005; Krause et al., 2004). In vitro, VASP nucleates, elongates and bundles actin filaments (Breitsprecher et al., 2008; Hansen and Mullins, 2010; Laurent et al., 1999). It was therefore proposed that VASP, which is also localized at the leading edge of lamellipodia and at the tip of filopodia (Galbraith et al., 2007; Rottner et al., 1999; Svitkina et al., 2003), associates with the MRL protein-integrin-talin (MIT) complex to control actin assembly (Lagarrigue et al., 2015) (Figure 34).

Alternatively, the proline-rich motifs of lamellipodin bind to the SH3 domain of the Abi subunit of the WAVE complex, which promotes the formation of Arp2/3-dependent branched networks in lamellipodia (Law et al., 2013).

Finally, lamellipodin could also contribute to the actin polymerization activity of the MIT complex by a direct interaction with actin filaments and by promoting the VASP-mediated processive elongation of actin filaments (Hansen and Mullins, 2015). However, it is not known whether RIAM could interact with actin filaments, since the clusters of basic amino acids in the C-terminal part of lamellipodin that mediate this interaction do not exist in RIAM.

### *1.4.3.4 RIAM interacts with talin rod domain*

NMR studies determined that the talin-binding site 1 (TBS1) of RIAM, corresponding to the N-terminal residues 6-30, binds to the helix bundles R2, R3, R8 and R11 of the talin rod (Goult *et al.*, 2013). In agreement with these observations, a RIAM peptide, carrying mutations in 4 conserved hydrophobic residues of TBS1, fails to colocalize with talin in cells (Lee *et al.*, 2009). In addition, a second fragment of RIAM, corresponding to residues 45-127 interacts with talin R3, showing the existence of a second talin binding site, called TBS2 (Goult *et al.*, 2013) (Figure 16, Figure 32, Figure 33).

Interestingly, RIAM TBS1 interacts with talin R3 with a low affinity ( $K_d = 36 \mu\text{M}$ ), while a RIAM construct encompassing both TBS1 and TBS2 binds to talin R2-R3 with a much higher affinity ( $K_d = 2 \mu\text{M}$ ) (Goult *et al.*, 2013). NMR spectra revealed that a RIAM TBS1-TBS2 fragment binds to a talin R2-R3 fragment with a 2:2 stoichiometry (Goult *et al.*, 2013). Although this observation suggests that the high affinity binding of RIAM to talin requires a bipartite site, other studies have reached different conclusions. Using pull-down assays, Chang and colleagues found that TBS1 alone and TBS1-TBS2 interact with R2-R3 with similar affinities ( $K_d = 3 \mu\text{M}$  and  $2.6 \mu\text{M}$  respectively) (Chang *et al.*, 2014).

This study also shows that only TBS1 is capable of targeting talin to the plasma membrane, and this interaction occurs mainly through the R8 bundle of talin (Chang *et al.*, 2014). The comparison of the TBS1 domain of RIAM with the TBS of lamellipodin reveals that lamellipodin lacks a critical kink in the TBS1  $\alpha$ -helix, resulting in a low affinity for talin R8.

The interaction between RIAM and the isolated talin R11 bundle would need to be further studied, as no structural or biochemical data about this interaction have been reported so far. It is interesting to note that R11 also contains an integrin-binding site. The role of R11 in integrin activation, as well as the possible competition between RIAM and integrin for R11, remain unknown.

### 1.4.3.5 RIAM precedes vinculin within maturing adhesions

Cellular observations revealed that RIAM is more enriched in small nascent adhesions at the leading edge, whereas vinculin is strongly localized in force-dependent mature focal adhesions (Lee et al., 2013) (Figure 35). Structural and biochemical studies suggest that RIAM and vinculin binding to talin might be mutually exclusive because RIAM-binding sites and vinculin-binding sites overlap in talin R2, R3 and R8 (Goult et al., 2013b). In addition, RIAM and vinculin have very different modes of interaction with talin. Working models suggest that RIAM binds to the compacted conformation of talin, while vinculin recognizes its cryptic binding sites after talin stretching. Altogether, these observations suggest that the force generated by the actomyosin stress fibers triggers the mechanosensitive transition between nascent adhesions and force-bearing focal adhesions by controlling the binding of RIAM and vinculin to talin.

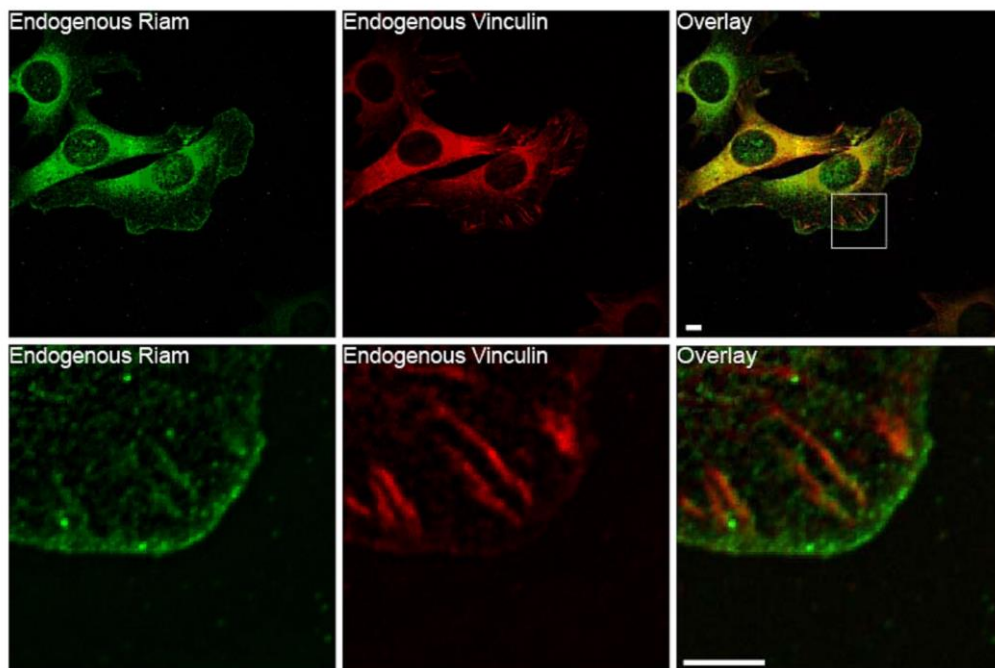


**Figure 35. Localization of RIAM and vinculin in adhesions.**

Immunofluorescence of endogenous RIAM (green) and vinculin (red) in NIH 3T3 fibroblasts plated on fibrinogen. Scale bar = 5  $\mu\text{m}$  (Lee et al., 2013).



## II AIM OF THE PHD THESIS

---

In order to migrate, mesenchymal cells extend membrane protrusions forward, adhere to the extracellular matrix, contract their body in a coordinated manner and retract the cell rear. During this process, cells are constantly subjected to variations in intracellular and extracellular mechanics. They are able to sense and transduce these mechanical stimuli into an appropriate biochemical response in order to adapt their shape, dynamics, adhesion and functions. The actin cytoskeleton plays a central role in this process. Actin polymerization produces the force necessary to deform the membrane by generating flat protrusions called lamellipodia and finger-like protrusions called filopodia. Actin filaments also associate with the myosin II molecular motor to form contractile structures that pull the cell body forward. Finally, adhesion complexes, containing transmembrane integrins and actin-binding proteins, ensure the mechanical coupling of the protrusive and contractile actin networks with the extracellular matrix. This mechanical coupling is necessary for the actin networks to generate force, but it also allows the adhesion complexes to sense intra- and extracellular forces.

The **two objectives** of this project were to understand the molecular basis of the **control of actin assembly by adhesion complexes** and the molecular mechanisms by which these complexes **encode the mechanical information into biochemical reactions**.

MRL proteins, and in particular RIAM, are good candidates to control actin assembly, adhesion initiation and reinforcement, and mechanosensitivity. First, RIAM binds to talin, which activates integrins at the tip of adhesive filopodia and at the leading edge of lamellipodia. Several lines of evidence also indicate that a talin-RIAM-VASP complex is recruited to the membrane to control actin assembly (Lagarrigue et al., 2015). However, many issues remain open. Talin and RIAM contain FERM and PH domains respectively that bind to membrane PIP<sub>2</sub>, but it is not known which PIP<sub>2</sub>-binding domain initiates the recruitment of the components of the complex. The ability of MRLs proteins to regulate actin assembly is based on the study of lamellipodin. However, it is not known whether RIAM also has this activity. The actin polymerization activity of the talin-RIAM-VASP complex and its ability to organize actin filaments are also difficult to predict. In the first part of my PhD thesis, **I combined the observation of single actin filaments in TIRF microscopy, kinetic assays of actin polymerization and in vitro reconstitution of actin assembly on GUVs to address these issues**.

The role of RIAM in actin assembly addressed in the first part is associated with early events that occur in nascent adhesions. RIAM also appears to control the maturation of these nascent adhesions into force-bearing focal adhesions that recruit vinculin and form actomyosin contractile stress fibers. Numerous observations suggest that the role of RIAM in the formation of focal adhesions is intimately related to the mechanical stretching of talin. In response to the actomyosin force, talin rod bundles unfold, exposing cryptic binding sites for vinculin, the other

## Aim of the PhD thesis

major partner of talin in focal adhesions. The binding of vinculin to talin induces the irreversible maturation of focal adhesions. By reinforcing actin anchoring, the actin-binding protein vinculin also increases the ability of focal adhesions to transmit force to the extracellular matrix. Cellular observations have showed that newly formed nascent adhesions are enriched in RIAM, which is gradually replaced by vinculin in force-dependent mature focal adhesions (Lee et al., 2013). Structural and biochemical studies have reported that the talin residues interacting with RIAM are located on the surface of talin bundles (Chang et al., 2014; Goult et al., 2013b), whereas vinculin-binding sites are buried inside the bundles (Fillingham et al., 2005; Gingras et al., 2005) and require the mechanical stretching of talin to be exposed (Del Rio et al., 2009; Hytönen and Vogel, 2008; Yao et al., 2016, 2014). These data suggest that RIAM and vinculin have opposite modes of binding to talin. Altogether, these observations support the hypothesis that the actomyosin force induces the mechanosensitive transition from nascent adhesions to focal adhesions by controlling the binding of RIAM and vinculin to the stretchable protein talin. However, the mechanosensitivity of the talin-RIAM interaction has never been determined. Whether RIAM binding to talin controls the mechanosensitive formation of the talin-vinculin complex also remains unknown. In addition, several bundles of talin, that interact with RIAM and vinculin, may respond to force differently. In the second part of my PhD thesis, I **determined the mechanosensitivity, sequence and interdependence of these talin-associated reactions.** To this aim, I designed an in vitro microscopy assay with purified proteins, inspired by a previous work of the laboratory (Ciobanasu et al., 2015, 2014). **In this in vitro assay, the actomyosin force controls the binding of RIAM and vinculin to a micropatterned surface coated with talin constructs, which contain variable RIAM- and vinculin-binding sites.**

## III MATERIALS AND METHODS

---

### III.1 PROTEINS USED IN THE STUDY

Throughout my PhD work, I generated new molecular tools, more specifically talin and RIAM constructs. I also used proteins that were already available in our laboratory, such as human full-length VASP and EGFP-VASP, and EGFP-vinculin head. Finally, I worked with proteins that are already well characterized in the field and whose purification protocols have already been published: rabbit skeletal muscle actin ([Wiesner, 2006](#)), rabbit skeletal muscle myosin II ([Pollard, 1982](#)) and profilin ([Le Clairche and Carlier, 2004](#)). Pyrenyl- and Alexa Fluor-labeled actin were prepared as previously described ([Ciobanasu et al., 2015](#); [Kouyama and Mihashi, 1981](#)). Spectrin-actin seeds were purified from human erythrocytes as described by Casella ([Casella et al., 1986](#)).

#### III.1.1 Talin

The stoichiometry of the talin-RIAM interaction is very complex (Figure 36). Talin contains five RIAM-binding sites (RBSs) located in one subdomain of the head and in four helical bundles of the rod, whereas RIAM includes two consecutive talin-binding sites (TBSs). We thus decided to simplify the talin-RIAM interaction to investigate the mechanosensitivity of RBSs independently. To this aim, we designed three talin constructs. Note that in our micropatterned assay, the F3 subdomain of talin head is not available to interact with RIAM, therefore we only studied the binding of RIAM to talin rod domains. These three talin constructs contain the F2-F3 part of the head, which anchors talin to the surface of the micropatterns ([Ciobanasu et al., 2014](#)) (See III.4.4), and the actin-binding R13 bundle, which allows actomyosin force to stretch talin. Between these two parts, we inserted the R2-R3, R7-R8 or R11 subdomains of the talin rod, each one containing one or two RBSs (Figure 36). We can therefore study the mechanosensitive interaction between RIAM and R2-R3, R7-R8 and R11 independently. The RIAM-binding R2 and R3 bundles were not separated because they were defined as a bipartite site for RIAM TBS1-TBS2 ([Goult et al., 2013b](#)), and because the affinity of RIAM for R2 alone is too low to be examined ([Chang et al., 2014](#)). Similarly, R7 and R8 were kept together as the R8 bundle is inserted inside R7 ([Gingras et al., 2010](#)).

All talin constructs are derived from a cDNA encoding for human talin-1. The talin proteins used for the present project lack the F0 and F1 domain of the head, because this subpart of talin drastically reduces the expression quality in our hands and is not involved in the binding of

## Materials and methods

RIAM or vinculin. Talin R1-R2-R3, corresponding to F2-F3-R1-R2-R3-R13, was cloned into a pETM plasmid with a N-terminal StrepTagII and a C-terminal His<sub>6</sub> tag. Talin R11, corresponding to F2-F3-R11-R13 and talin R7-R8, corresponding to talin F2-F3-R7-R8-R13 were cloned into a pET-29a(+) plasmid with a N-terminal StrepTagII and a C-terminal His<sub>6</sub> tag. The enhanced green fluorescent protein (EGFP)-tagged talin F2-F3 and F2-R8, used with PIP<sub>2</sub>-containing giant unilamellar vesicles, were already available in the lab. They were cloned in a pGEX-6P1 (GE Healthcare), with a N-terminal cleavable glutathione-S-transferase (GST) tag followed by an EGFP (Figure 36). EGFP-talin F2-R8 also has a C-terminal His<sub>6</sub>-tag.

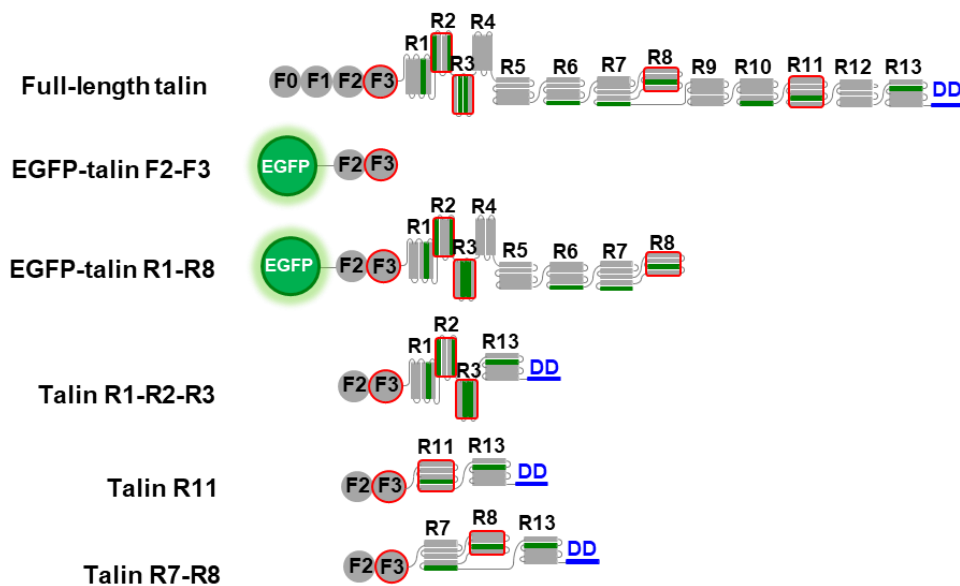


**Figure 36. Talin constructs used in the study.**

Vinculin-binding sites (VBSs) are represented as green bars. RIAM-binding sites (RBSs) are highlighted by red boxes. F0 to F3 (FERM domain 0 to 3), R1 to R13 (rod domain 1 to 13), DD (dimerization domain), EGFP (enhanced green fluorescent protein).

Talin constructs were expressed in *Escherichia coli* (BL21 DE3, Invitrogen) as previously described (Ciobanasu et al., 2015).

Talin R1-R2-R3, R11 and R7-R8 were bound to Ni-NTA (Ni<sup>2+</sup>-nitrilotriacetic acid)-Agarose (Macherey-Nalgen), washed with 50 mM Tris pH 7.8, 500 mM NaCl, 20 mM imidazole, 1 mM  $\beta$ -mercaptoethanol (BME), eluted with 50 mM Tris pH 7.8, 500 mM NaCl, 250 mM imidazole, 1 mM BME, dialyzed in 20 mM Tris pH 7.8, 100 mM KCl, 1 mM DTT, frozen in liquid nitrogen and stored at -80°C. The StrepTagII in talin R1-R2-R3, R11 and R7-R8 is not available to interact with the Streptactin resin during the purification process, probably because talin head is highly charged and likely masks the StrepTagII interface with Streptactin. However, the expression levels of these proteins are extremely high and the purification via the His<sub>6</sub>-tag only yields good quality and sufficient quantity. We thus did not need another purification step.

## Materials and methods

EGFP-talin F2-F3 was bound to Glutathione Sepharose, cleaved by PreScission protease and purified by gel filtration chromatography (Superdex 200, 16/60, GE Healthcare) in 20 mM Tris pH 8.5, 150 mM KCl, 1 mM  $\beta$ -mercaptoethanol (BME). EGFP-talin F2-R8 was bound to Ni-NTA-Agarose, cleaved by PreScission protease and purified by gel filtration chromatography (Superdex 200, 16/60, GE Healthcare) in 20 mM Tris pH 8, 150 mM KCl, 5 mM BME.

### III.1.2 RIAM

The study of the force-dependent interplay between talin, RIAM and vinculin using the micropatterned assay was achieved with a mCherry-fused mouse RIAM 1-306 construct. Note that this study is presented in the second part of this manuscript, though it was performed first. At the start of the project, this RIAM construct was the only one available in the laboratory in a sufficient amount with a good purity. The boundaries of this construct (1-306) have already been validated for its interaction with talin ([Yang et al., 2014](#)). The protein is tagged with a mCherry to allow the simultaneous microscopy observation with EGFP-Vh.

However, to explore the role of RIAM on actin regulation, in complex with talin and VASP, we used the human protein. We purified the full-length RIAM protein, because RIAM interaction with VASP is mediated by a series of EVH1-binding motifs, among which four are located in the C-terminal proline-rich domain of RIAM (Figure 37). RIAM 1-306 does not include this C-terminal proline-rich region. So far, the recombinant full-length form of RIAM, and that of its paralog lamellipodin, have never been purified. RIAM contains a high number of rare codons, which usually leads to stops in mRNA translation and to the subsequent release of a truncated protein. However, optimization of the sequence to remove these rare codons in *E. Coli* did not improve the expression. Numerous attempts to purify the protein have failed, even using specific affinity tags at both ends of the protein. One of the reasons for this peculiar behavior is probably the presence of dimerization domains in RIAM that allow the binding of truncated proteins to full-length proteins. These products could therefore also not be separated according to size by gel filtration. In addition, RIAM comprises an unstructured C-terminal portion rich in proline, which leads to its precipitation. We attempted different strategies to solubilize the protein. The use of a thioredoxin or Halo tags did not improve the solubility of the protein. However, the presence of the fluorescent mCherry tag finally proved beneficial. For all these reasons, it was challenging to purify the whole protein in reasonable quantity and quality.

We finally succeeded in purifying full-length human RIAM fused to a mCherry. After the discovery that RIAM binds to actin filaments, we designed another RIAM construct to map

## Materials and methods

more precisely the actin-binding domain of RIAM. All the RIAM constructs have a N-terminal cleavable GST-tag followed by a mCherry, and a C-terminal His<sub>6</sub>-tag. Full-length RIAM (1-665) includes binding sites for talin, VASP and profilin. mCherry-RIAM 1-306 contains the two talin-binding sites TBS1 and TB2, the first proline-rich region and the RA domain (Figure 37). The complementary RIAM 307-665 construct comprises the PH domain and the C-terminal proline-rich domain that contains four EVH1-binding motifs (FPPPP) (Figure 37).

The mouse cDNA encoding for RIAM 1-306 was cloned into a homemade pGEX-6P2-mCherry plasmid with a C-terminal His<sub>6</sub>-tag. Similarly, the human cDNA encoding for human RIAM 1-665 and 1-306 were cloned into the same homemade pGEX-6P2-mCherry plasmid with a C-terminal His<sub>6</sub>-tag. The pGEX-P2-mCherry RIAM 307-665 plasmid was created by deletion in the pGEX-P2-mCherry RIAM 1-665 plasmid using natural restriction sites and replacement by synthetic genes (Genscript).

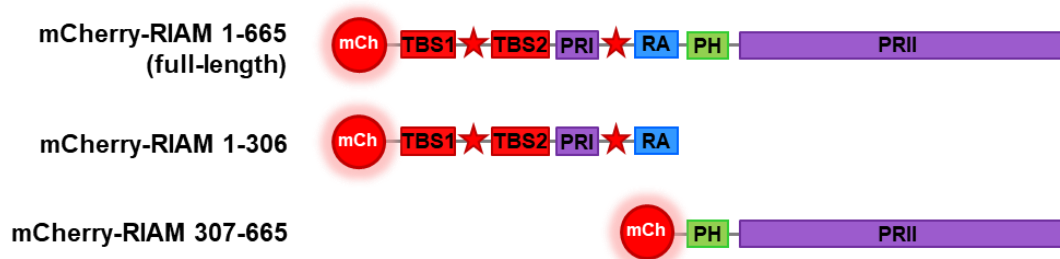


**Figure 37. RIAM constructs used in the study.**

mCh (mCherry), TBS (talin-binding site), PR (proline-rich region), RA (Ras-association domain), PH (pleckstrin homology domain). The red star represents coiled-coiled regions.

All RIAM constructs were expressed in *Escherichia coli* as previously described (Ciobanasu et al., 2015).

Mouse mCherry-RIAM 1-306 was bound to Glutathione Sepharose (GE Healthcare), washed with 50 mM Tris pH 7.8, 500 mM NaCl, and eluted with 50 mM Tris pH 7.8, 500 mM NaCl and 50 mM reduced L-Glutathione (Sigma-Aldrich). GST was cleaved by PreScission protease (GE Healthcare) in 50 mM Tris pH 7.8 and 500 mM NaCl, and eliminated by Glutathione Sepharose chromatography. The protein was then bound to Ni-NTA-Agarose, washed with 50 mM Tris pH 7.8, 500 mM NaCl, 20 mM imidazole, eluted with 50 mM Tris pH 7.8, 500 mM NaCl, 250 mM imidazole. Finally, it was dialyzed in 20 mM Tris pH 7.8, 100 mM KCl, 1 mM DTT, frozen in liquid nitrogen and stored at -80°C.

Human mCherry-RIAM 1-665 (full-length) was bound to Glutathione Sepharose, washed with 50 mM Tris pH 7.8, 500 mM NaCl, 10% glycerol, and eluted with 50 mM Tris pH 7.8, 500 mM NaCl, 10% glycerol and 50 mM reduced L-Glutathione. The procedure was repeated seven additional times with the previous flowthrough of the Glutathione Sepharose, as little of the

## Materials and methods

protein was depleted from the lysate at each purification step. GST was then cleaved by PreScission protease in 50 mM Tris pH 7.8, 500 mM NaCl and 10% glycerol, and eliminated by Glutathione Sepharose chromatography. The protein was then bound to Ni-NTA-Agarose, washed with 50 mM Tris pH 7.8, 500 mM NaCl, 10% glycerol, 20 mM imidazole, and eluted with 50 mM Tris pH 7.8, 500 mM NaCl, 10% glycerol and 250 mM imidazole. Human mCherry-RIAM 1-665 was dialyzed in 20 mM Tris pH 7.8, 500 mM NaCl, 2% glycerol, 1 mM DTT, frozen in liquid nitrogen and stored at -80°C. For specific experiments, the protein was further dialyzed in 20 mM Tris pH 7.8, 200 mM KCl, 2% glycerol, 1 mM BME.

Human mCherry-RIAM 1-306 and 307-665 were bound to Ni-NTA-Agarose, washed with 50 mM Tris pH 7.8, 500 mM NaCl, 10% glycerol, 20 mM imidazole, and eluted with 50 mM Tris pH 7.8, 500 mM NaCl, 10% glycerol and 250 mM imidazole. They were dialyzed in 20 mM Tris pH 7.8, 250 mM NaCl, 1 mM BME and incubated overnight with Glutathione Sepharose. The resin was then washed with 20 mM Tris pH 7.8, 250 mM NaCl, 1 mM BME. GST was cleaved by PreScission protease in the same buffer. The protein released by cleavage was dialyzed in 20 mM Tris pH 7.8, 200 mM KCl, 2% glycerol, 1 mM BME. Finally, RIAM 1-306 and 307-665 were frozen in liquid nitrogen and stored at -80°C.

### III.1.3 VASP

Interpreting experiments in the presence of VASP is challenging because the protein has multiple competing activities contributing to actin networks formation, such as processive actin filament barbed end elongation, nucleation, anti-capping and bundling. For example, VASP can nucleate actin filaments and simultaneously elongate and bundle them. When adding other actin regulators in the assay, such as RIAM and talin, results are even more complex to understand. It is crucial to keep this point into consideration when interpreting the data.

Because human VASP is a weakly processive actin polymerase, most studies on VASP have been carried out with the *Dictyostelium* protein, which is a much more potent processive elongator (Breitsprecher et al., 2011, 2008; Hansen and Mullins, 2010). However, the relevance of working with a *Dictyostelium* protein is debatable here. Thus, all experiments presented in this manuscript were performed using human full-length VASP.

The human cDNA encoding for human full-length VASP was cloned into a pGEX-6P1 plasmid to produce the pGEX-6P1-VASP and pGEX-6P1-EGFP-VASP plasmids, with an additional N-terminal EGFP for the pGEX-6P1-EGFP-VASP plasmid (Figure 38).

## Materials and methods

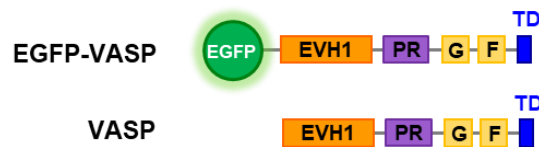


**Figure 38. VASP constructs used in the study.**

EGFP (enhanced green fluorescent protein), EVH1 (Ena/VASP homology 1), PR (proline-rich domain), G (G-actin-binding domain), F (F-actin-binding domain), TD (tetramerization domain).

Both proteins were expressed in *Escherichia coli* as previously described (Ciobanasu et al., 2015).

Human full-length EGFP-VASP was first bound to Glutathione Sepharose in 50 mM Tris pH 7, 150 mM NaCl, 1 mM EDTA, 1mM DTT and cleaved from GST by PreScission protease in the same buffer. The protein was purified by monoQ chromatography in 20 mM Tris pH7, 100 mM NaCl, 1mM BME, eluted from monoQ by a 100-500 mM NaCl linear gradient, purified by gel filtration chromatography (Superdex 200, 16/60, GE Healthcare) in 20 mM Tris pH 8.5, 150 mM NaCl, frozen in liquid nitrogen and stored at  $-80^{\circ}\text{C}$ . Human full-length VASP was first bound to Glutathione Sepharose in 50 mM Tris pH 7, 500 mM NaCl, 1 mM EDTA, 1mM DTT and cleaved from GST by PreScission protease in 50 mM Tris pH 7, 150 mM NaCl, 1 mM EDTA, 1mM DTT. The protein was dialyzed in 20 mM Tris pH 7.8, 100 mM KCl, 1 mM DTT, frozen in liquid nitrogen and stored at  $-80^{\circ}\text{C}$ .

### III.1.4 Vinculin

To study the mechanosensitive talin-vinculin complex, we used an EGFP-tagged vinculin head (1-851) construct, because in contrast with the auto-inhibited full-length vinculin, vinculin head (Vh) interacts constitutively with exposed vinculin-binding sites (VBSs). It thus behaves as a conformation sensor of talin stretching, that binds to newly exposed VBSs. Most single molecule studies have used the talin-binding D1 subdomain of Vh, but we choose to use the whole Vh moiety of vinculin because its size is more similar to that of full-length vinculin.

The pGEX-6P1-EGFP-Vh plasmid encoding for EGFP-Vh was created as previously described (Ciobanasu et al., 2015). The protein was also expressed and purified as previously described (Ciobanasu et al., 2015).



## III.2 IN VITRO ASSAYS TO STUDY THE REGULATION OF ACTIN ASSEMBLY

Various techniques are available to test the effect of a protein on actin assembly and organization in vitro. First, kinetics of actin polymerization provide a global idea in solution on the mechanism by which the protein of interest acts on actin assembly. Then, the observation of single actin filaments in microscopy then allows to refine the mechanism.

### III.2.1 Actin polymerization assay

Actin polymerization was monitored by the increase in fluorescence of pyrene-labeled actin over time. Pyrene being highly sensitive to its environment, fluorescence increases when pyrene-labeled G-actin is incorporated into F-actin. Pyrene is covalently bound to the C-terminal actin cysteine, which corresponds to the profilin binding site, thus altering profilin activity. To reduce the effect of pyrene on profilin, pyrenyl-actin was reduced from 10% to 4% in the presence of profilin. Actin polymerization was induced by the addition of 25 to 100 mM KCl, 1 mM MgCl<sub>2</sub>, and 0.2 mM EGTA to a solution of pyrenyl-labeled G-actin containing the proteins of interest. Experiments containing RIAM alone were performed at 100 mM KCl but experiments containing full-length VASP were performed at 50 mM KCl to favor its nucleation activity. Profilin was added to the reaction to prevent spontaneous nucleation. Spectrin-actin seeds were added to the reaction to measure the barbed end elongation specifically. As soon as actin was added, the mix was cautiously transferred to a quartz cuvette and the fluorescence intensity was measured every 20s with a Safas Xenius FLX spectrofluorimeter (Safas, Monaco). Excitation and emission wavelengths were 366 nm and 407 nm, respectively, with 10 nm excitation and emission slits. Polymerization curves were normalized to 0 at the start time. To measure the affinity of mCherry-RIAM 1-665 for barbed ends, the initial elongation rate was taken as a measure of free barbed ends (BE). The following equation was used to fit the data. [C<sub>0</sub>] and [R<sub>0</sub>] are the total concentrations of barbed ends and RIAM respectively, and K represents the equilibrium dissociation constant of the barbed end-RIAM complex. The fraction of free barbed ends is:

$$BE = 1 - ( ( [C_0] + [V_0] + K - ( ( [V_0] + [C_0] + K)^2 - 4 [V_0] [C_0] )^{1/2} ) / 2 [C_0] )$$

The graphs were assembled with Excel or Kaleidagraph.

### III.2.2 Actin bundling measurement by light scattering and epifluorescence microscopy observation

The actin bundling activity of the proteins was assessed by light scattering using a Safas Xenius FLX spectrophotometer (Safas, Monaco) at a wavelength of 400 nm (10 nm excitation and emission slits). Actin polymerization was induced by the addition of 20 mM KCl, 40 mM NaCl, 1mM MgCl<sub>2</sub>, and 0.2 mM EGTA to a solution of G-actin (2% Alexa488-labeled for observation in microscopy) containing the proteins of interest. The graphs were assembled with Excel. When the reaction measured in light scattering reached the steady state, a sample was taken for epifluorescence microscopy observation. Images were acquired with an Olympus IX71 microscope equipped with a 60X oil immersion objective (Olympus, 1.45 NA) and coupled to an EMCCD camera (Cascade, Photometrics). Images were acquired with MicroManager and assembled with ImageJ.

### III.2.3 Observation and measurement of single actin filament elongation

The protocol is a modification of the protocol used to study talin activity ([Ciobanasu et al., 2018](#)). Glass coverslips (22 × 32 mm, Thermo Scientific/Menzel-Glaser) were first washed with milliQ water, sonicated in ethanol, washed with milliQ water and irradiated for 1 min under a deep UV lamp (Ossila). The coverslips were then incubated for 2h in 0.1 mg.mL<sup>-1</sup> PLL-g-PEG (SuSoS) dissolved in 10 mM HEPES pH 7.4 and washed with milliQ water. A chamber was created by attaching a passivated coverslip to a glass slide (Super Frost, Thermo Scientific) with double-sided adhesive tape, with a typical volume of 50 µL. The chamber was first saturated with 1% bovine serum albumin (BSA) for 5 min and then washed with a wash buffer (5 mM Tris pH 7.8, 200 µM ATP, 10 mM DTT, 1 mM MgCl<sub>2</sub>, 100 mM KCl). The final reaction was then injected in the chamber. A typical reaction is composed of 0.6-1 µM G-actin (5-10% Alexa Fluor 488-labeled) in 5 mM Tris pH 7.8, 200 µM ATP, 0.4% methyl-cellulose, 1 mM 1,4-diazabicyclo(2,2,2)-octane (DABCO), 100 mM KCl, 1 mM MgCl<sub>2</sub>, 200 µM EGTA, 10 mM DTT, supplemented with the protein of interest. Finally, the chamber was sealed with VALAP (1:1:1 mixture of vaseline, lanolin and paraffin) or oil. Images were acquired with a Nikon Ti Eclipse microscope equipped with a spinning disk (Yokogawa CSU-X1-A1), a 60X oil immersion objective (Apochromat, 1.49 NA) and coupled to a sCMOS camera (Photometrics, Prime 95B) or an Olympus IX71 microscope equipped with a 60X oil immersion objective (Olympus, 1.45 NA) and coupled to an EMCCD camera (Cascade, Photometrics). Alexa488-actin and mCherry-RIAM constructs were excited with 488 and 561 lasers, respectively.

Images were acquired with MetaMorph or MicroManager and analyzed with ImageJ. The colocalization data were quantified by measuring the mean fluorescence along a filament, with background subtraction. The ratio of the fluorescence of mCherry-RIAM to the fluorescence of Alexa488-actin was plotted. The rates of barbed end elongation were calculated by measuring the elongation of a filament overtime, expressed in actin subunits incorporated into a filament per second. Each dot represents a filament. The bar indicates the mean. The dot plots were assembled with KaleidaGraph. P-values were obtained by performing two-tailed t-tests with Excel.

### III.3 IN VITRO RECONSTITUTION OF ADHESION COMPLEXES AT THE SURFACE OF LIPID VESICLES

#### III.3.1 Principle of the method

Cell adhesions anchor the actin cytoskeleton to the membrane via transmembrane receptors and adapters. Cellular studies have provided enormous knowledge on cell adhesions. In vitro reconstitutions with minimal components can isolate key molecular mechanisms, which control cell adhesion dynamics, mechanotransduction and cytoskeleton remodeling. Therefore, reconstituting adhesion complexes associated to membrane model systems appears physiologically relevant and critical to the molecular understanding of adhesion assembly and the role of the actin cytoskeleton in this process. Various membrane model systems for studying the lipid membrane have already been used under various conditions, such as two-dimensional lipid bilayers or various types of vesicles (Figure 39).

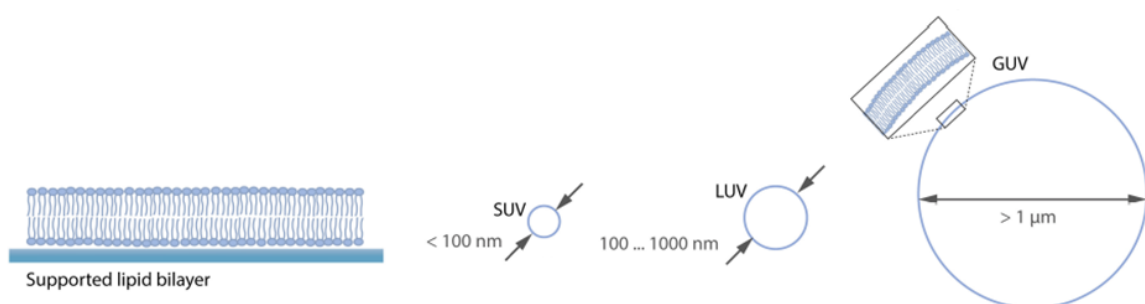


**Figure 39. Overview of the lipid membrane model systems.**

SUV (small unilamellar vesicle), LUV (large unilamellar vesicle), GUV (giant unilamellar vesicle) (Adapted from Stein et al., 2017).

We decided to reconstitute the assembly of the talin-RIAM-VASP complex, described to initiate actin assembly in nascent adhesions, on the surface of giant unilamellar vesicles (GUVs). Due to their large cell-like dimensions, GUVs can be observed and manipulated to allow the direct observation of relevant biochemical phenomena at the single membrane level. In addition to their size, these vesicles preserve key parameters of cells, such as the curvature and deformability of the membrane, with the possibility to perfectly control the composition of the mimetic membrane, and the buffers inside and outside of the vesicles. We thus reconstituted actin-associated minimal adhesion complexes at the surface of PIP<sub>2</sub>-containing GUVs. Different techniques allow the formation of giant unilamellar vesicles, such as natural swelling, electroformation on platinum wires or on indium tin oxide-coated glass, or spontaneous gel-assisted swelling. We used the gel-assisted swelling technique to produce GUVs. The polymer-assisted swelling aims at making a membrane swell from a preordered bilayer film. It thus requires the buffer to penetrate into the membrane stacks without any disruption of the membrane. The advantages of this technique are its efficiency and rapidity of production. Most of the obtained vesicles are unilamellar without any visible defect.

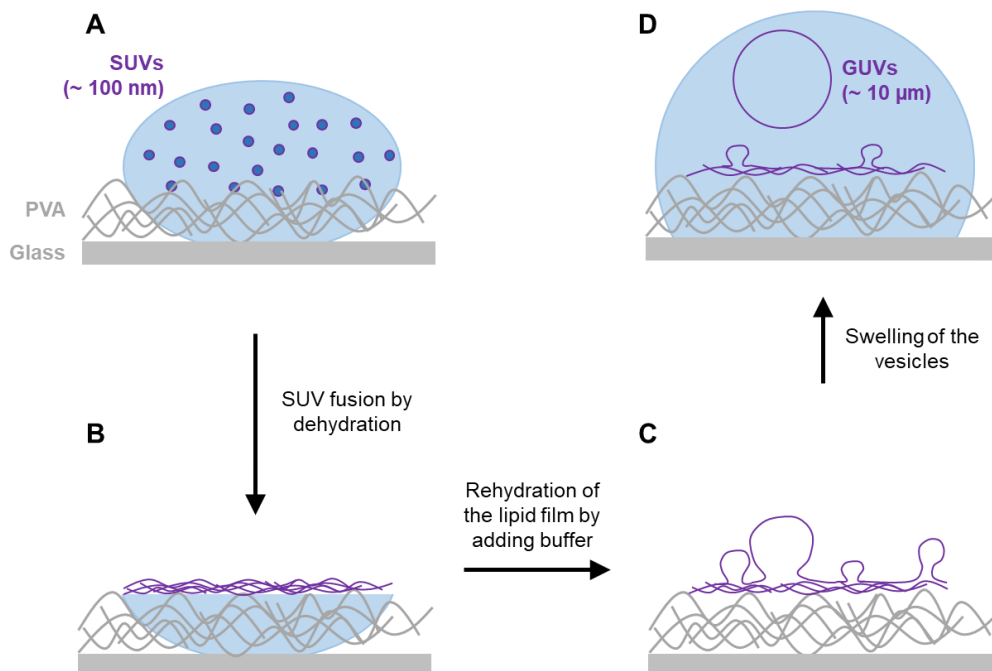


**Figure 40.** Principle of the formation of giant unilamellar vesicles (GUVs) by the spontaneous gel swelling technique.

## Materials and methods

First, a lipid mixture containing small unilamellar vesicles (SUVs) or proteoliposomes is deposited onto a dried gel (Figure 40A). The gel can be low melting agarose or polyvinyl alcohol (PVA). The lipids are then dried to create a thin lipid film (Figure 40B). Rehydration of the film by a specific buffer allows the spontaneous swelling of lipid vesicles from the film (Figure 40C), resulting in the formation of big liposomes (Figure 40D). The advantage of using PVA instead of agarose is the obtainment of bigger vesicles than with other techniques. Furthermore, PVA does not dissolve in solution at room temperature. Thus, the swollen vesicles do not contain residues of PVA.

### III.3.2 GUVs preparation

Our protocol is a modified version of the protocol used by Weinberger et al. ([Weinberger et al., 2013](#)). Briefly, polyvinyl alcohol (PVA) (Merck) was dissolved at 5% (w/w) in a 280 mM D(+)-saccharose (sucrose) (Euromedex) solution containing 20 mM Tris pH 7.5, by continuous stirring at 150°C for 30 min. The PVA solution was spread onto 22 × 22 mm glass coverslips (Thermo Scientific/Menzel-Glaser) previously cleaned by sonication in MilliQ water, ethanol and MilliQ water sequentially. The PVA-coated coverslips were dried at 50°C for 45 min. Lipids were mixed in chloroform at a concentration of 1 mg.mL<sup>-1</sup>. Lipid mixtures contain EPC (or Egg PC) lipids (L- $\alpha$ -phosphatidylcholine from chicken egg) (Avanti Polar Lipids) alone, or supplemented with 10 mole% PIP<sub>2</sub> (L- $\alpha$ -phosphatidylinositol-4,5-bisphosphate from porcine brain, ammonium salt) (Avanti Polar Lipids), and/or 0.1 mole% SR101-DHPE lipids (N-(Rhodamine 101 sulfonyl)-1,2-hexadecanoyl-sn-4-phosphoethanolamine, triethylammonium salt) (Interchim). Each lipid mixture was spread onto PVA-coated coverslips. The lipids were dried under vacuum for 1h at room temperature to remove residual chloroform. Liposomes were formed by incubating in growth buffer (200 mM sucrose) for 4h at room temperature. After incubation, the liposomes were collected, centrifuged at 18,000 × g for 30 min, and stored in glass vials at 4°C to be used within 3 days. The osmolarity inside the vesicles is 200 mOsmol.

### III.3.3 Reaction assembly

Glass coverslips (22 × 32 mm, Thermo Scientific/Menzel-Glaser) were washed with milliQ water, sonicated in ethanol, washed with milliQ water and irradiated for 1 min under a deep UV lamp (Ossila). The coverslips were incubated for 2h in 0.1 mg.mL<sup>-1</sup> mPEG-silane (SuSoS) dissolved in 10 mM HEPES pH 7.4 and washed with milliQ water. A chamber was created by attaching a passivated coverslip to a glass slide (Super Frost, Thermo Scientific) with double-sided adhesive tape, with a typical volume of 25  $\mu$ L. To maintain the GUVs stability, the experiments were performed in a final buffer of 200 mOsmol, containing 50 mM salt (KCl and

NaCl). Typically, the GUVs solution was diluted two-fold in a fluorescent mix (5 mM Tris pH 7.8, 32 mM NaCl, 18 mM KCl, 0.01% NaN<sub>3</sub>, 1 mM MgCl<sub>2</sub>, 0.2 mM EGTA, 0.2 mM ATP, 10 mM DTT, 1 mM DABCO) supplemented with the proteins of interest. Finally, the solution was injected into the chamber, and the chamber was sealed with oil.

### III.3.4 Microscopy observation and data analysis

Images were acquired with an Olympus IX71 microscope equipped with a 60X oil immersion objective (Olympus, 1.45 NA) and coupled to an EMCCD camera (Cascade, Photometrics), or with a Nikon Ti Eclipse microscope equipped with a spinning disk (Yokogawa CSU-X1-A1), a 60X oil immersion objective (Apochromat, 1.49 NA) and coupled to a sCMOS camera (Photometrics, Prime 95B). Alexa488-actin (and EGFP fusion proteins), mCherry-RIAM constructs (or SR101-DHPE) and Alexa647-actin were excited with 488, 561 and 642 nm lasers, respectively. Images were acquired with MicroManager or MetaMorph and analyzed with ImageJ. The data were quantified by measuring the mean fluorescence around a vesicle, with background subtraction. The dot plots were assembled with KaleidaGraph. Each dot represents a vesicle. The bar indicates the mean. P-values were obtained by performing two-tailed t-tests with Excel.

## III.4 IN VITRO RECONSTITUTION OF MECHANOSENSITIVE PROTEIN COMPLEXES ON A MICROPATTERNED SURFACE

### III.4.1 Principle of the assay

The functional study of mechanosensitive proteins has long been a major obstacle. Several techniques have already been used to study stretchable proteins. Förster resonance energy transfer (FRET), a powerful technique for studying molecular interactions inside living cells, is a physical process in which energy is transferred from an excited fluorophore (the donor) to another fluorophore (the acceptor) depending on their proximity, typically 3 to 6 nm. FRET sensors inserted in proteins have proven to be valuable tools to measure force across talin and vinculin in cellular studies ([Austen et al., 2015](#); [Chen et al., 2005](#); [Grashoff et al., 2010](#)). Atomic force microscopy and magnetic tweezers are the reference techniques for unfolding proteins at the scale of the single molecule in response to force (Figure 41). Single-molecule approaches are very precise, but most physical devices for stretching proteins require the protein to be hooked at both ends in a quasi-covalent manner. In this experimental configuration, the

## Materials and methods

protein is always stretched. However, in the cell, the force is generated by the cytoskeleton linked to an actin-binding domain of the stretchable protein. Whether this linkage is strong enough to resist the force necessary for the mechanical stretching of the protein is not easy to anticipate. If not, the stretching of a protein observed *in vitro* may simply not exist in the cell.

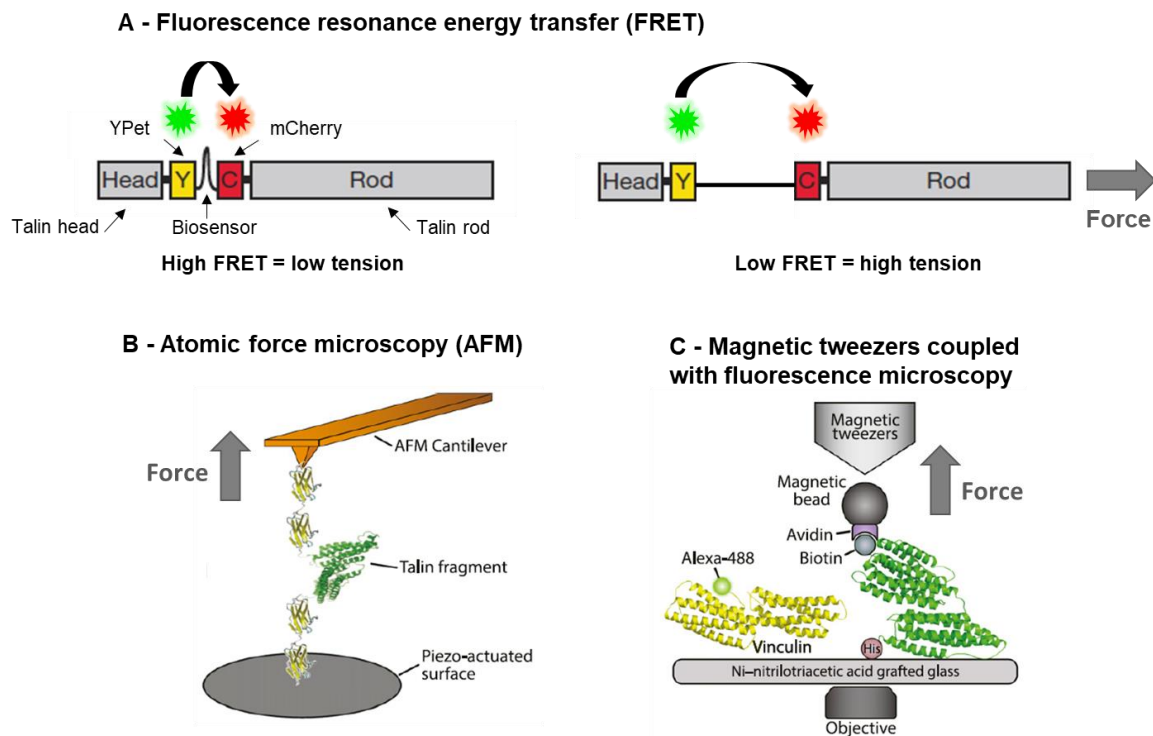


**Figure 41. Experimental methods to study stretchable proteins.**

**(A)** In cells, a FRET sensor inserted between talin head and talin rod domain revealed that talin experiences a range of forces around 7-10 pN during cell adhesion (Adapted from Austen et al., 2015). **(B)** Atomic force microscopy (AFM) was used to reveal the unfolding of talin. **(C)** Magnetic tweezers and fluorescent microscopy were combined to observe the force-induced recruitment of vinculin to stretched talin. **(B, C)** (Haining et al., 2016a).

Therefore, the laboratory developed an *in vitro* assay, with pure proteins. In this assay, the actomyosin cytoskeleton applies force on talin immobilized on disk-shaped islands micropatterned on a glass surface. The actomyosin force applied to the actin-binding domain of talin stretches the talin helical bundles, leading to the exposure of cryptic vinculin-binding sites. The binding of fluorescent EGFP-vinculin to stretched talin is visualized in TIRF microscopy (Ciobanasu et al., 2015, 2014). We adapted this technique to study how the actomyosin force controls the interaction of talin with both RIAM and vinculin.

## Materials and methods

Single molecule techniques, such as AFM or magnetic tweezers, enabled studying the kinetics of talin stretching and refolding (Del Rio et al., 2009; Yao et al., 2014), but they did not allow the observation of the mechanosensitive talin-vinculin complex in real time. The novelty of the assay developed in our laboratory thus relies in the direct observation of the coupling between the physiologically relevant actomyosin stimulus with the dynamics of the mechanosensitive talin-vinculin complex. Furthermore, the use of a micropatterned surface allows the standardization of shapes and the isolation of specific components, resulting in an easier understanding of the molecular mechanisms involved. The quantification of the fluorescent mechanosensitive response is easy and fast. The present method could also allow a clear interpretation of the changes induced by mutations in proteins or by drugs that target the cytoskeleton.

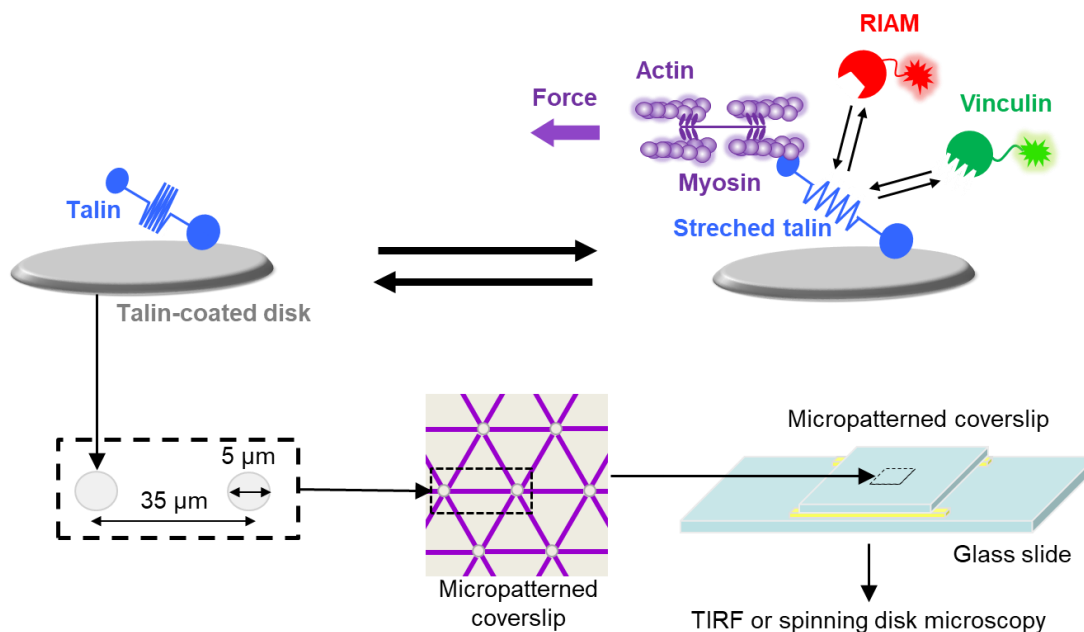


**Figure 42. Principle of the in vitro assay used to study mechanosensitive protein complexes.**

Talin is immobilized in disks micropatterned on a glass coverslip. The self-assembly of actin and myosin into cables, anchored to talin-coated disks, stretches talin, which allows the recruitment of vinculin. A chamber is created by attaching the micropatterned coverslip to a glass slide. The reaction is followed by TIRF or spinning disk confocal microscopy (Protocol from Ciobanasu, Faivre and Le Clairche, 2015).

The reconstitution of geometrically-controlled actomyosin networks with purified proteins on micropatterned surfaces was popularized by Reymann et al. (Reymann et al., 2010, 2012). The authors generated various architectures of actin networks derived from actin nucleators-coated micropatterns. The parameters arising from these studies, such as the area of actin nucleation, the contractility of actomyosin networks and the orientation of actin filaments, could be used to modulate the mechanosensitive response of talin in our assay.



### III.4.2 Micropatterning

Micropatterning was achieved by surface photolithography (Figure 43). The glass coverslips first need to be passivated, so that proteins will not interact with the surface non-specifically. To achieve this step, we use Poly(L-lysine)-g-poly(ethylene glycol) (PLL-g-PEG), a polymer that strongly interacts with the glass surface through its charged poly-L-lysine-chain, and exposes its non-charged PEG extremity. After exposure to deep UV (180 nm), PEG exhibits chemical modifications, which induces a strong adsorption of proteins (Azioune et al., 2009). Using a photolithography mask harboring specific designs, it is possible to control the geometry of the micropatterns to which the proteins will bind. For our project, we designed a photolithography mask with 5  $\mu\text{m}$ -diameter disks regularly spaced by 35  $\mu\text{m}$ , which is in the high range of focal adhesion and stress fiber dimensions (Figure 42). Deep UV radiation crosses the quartz layer, except in the chromium covered areas of the mask. Thus, deep UV radiation reaches PLL-g-PEG only on the disc-shaped chromium-free areas, creating reactive discs with a diameter of 5  $\mu\text{m}$ , where talin is strongly anchored.

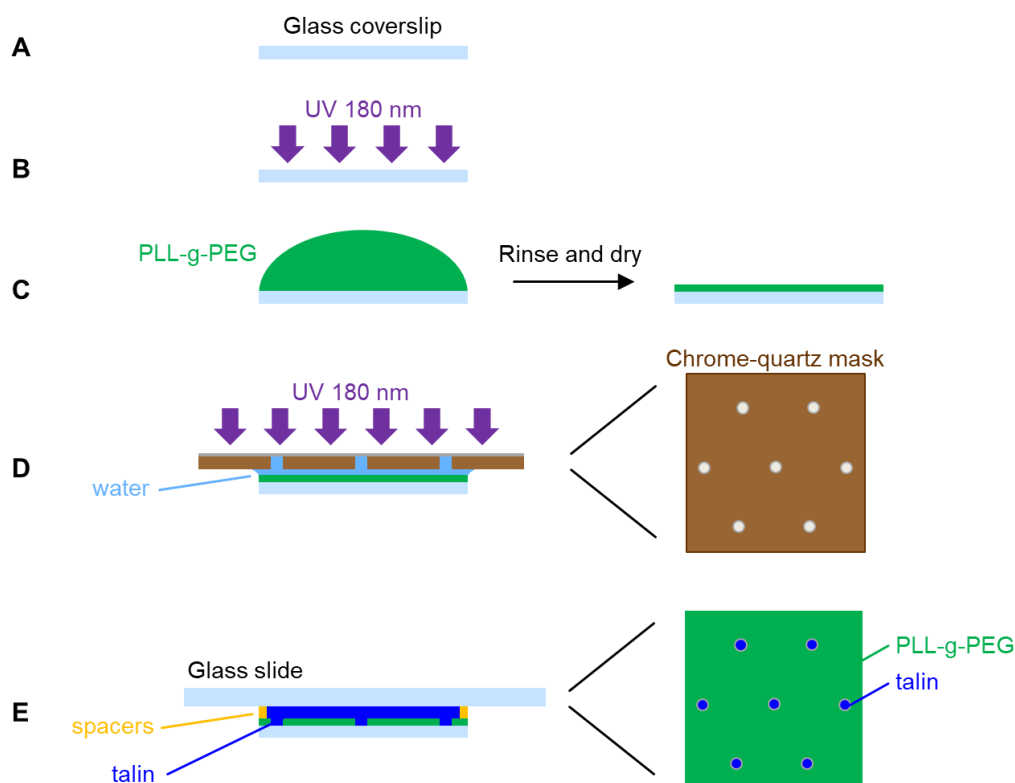


**Figure 43. The sequential steps to fabricate a micropatterned glass coverslip.**

(A) A glass coverslip is (B) submitted to deep UV for 1 min. (C) It is then incubated for 2h with PLL-g-PEG (0.1  $\text{mg}\cdot\text{mL}^{-1}$ ) and washed with milliQ water. (D) The coverslip is placed in contact with the chrome-quartz mask using a water drop. Then the sandwich is placed upside-down under UV (180 nm) for 3 min to oxidize the PLL-g-PEG under transparent areas. (E) A chamber is assembled between the micropatterned coverslip and a glass slide using double-sided adhesive tape. The coverslip is incubated for 5 min with talin (1  $\mu\text{M}$ ) (Drawn from a figure from Azioune et al., 2010).

## Materials and methods

Micropatterning was performed by modifying an existing method as follows (Azioune et al., 2010, 2009) (Figure 43). Glass coverslips (22 × 32 mm, Thermo Scientific/Menzel-Glaser) were washed with milliQ water, sonicated in ethanol, washed with milliQ water and irradiated for 1 min under a deep UV lamp (Ossila). The coverslips were then incubated for 2h in 0.1 mg.mL<sup>-1</sup> PLL-g-PEG (SuSoS) dissolved in 10 mM HEPES pH 7.8 and washed with milliQ water. The chrome-quartz photomask (Toppan, France), was cleaned by deep UV irradiation for 1 min, placed on the PLLg-PEG-coated coverslip, and exposed to deep UV for 3 min. Finally, a flow chamber was created by attaching a micropatterned coverslip to a glass slide (Super Frost, Thermo Scientific) with double-sided adhesive tape. The volume of a typical chamber was 50 µL.

### III.4.3 Reaction assembly

The flow chamber was first incubated with talin (1 µM) for 5 min at room temperature. Unbound talin was washed out with 200 µL of wash buffer (10 mM Tris pH 7.8, 25 mM KCl, 1mM Mg Cl<sub>2</sub>, 0.2 mM Ca Cl<sub>2</sub>, 1mM DTT). The surface of the disks was passivated with 100 µL of wash buffer containing 10% BSA for 5 min at room temperature and washed with 200 µL wash buffer. Finally, 100 µL of the reaction was added and the chamber was sealed with VALAP (1:1:1 mixture of vaseline, lanolin, and paraffin). A typical reaction contained: 2.4 µM actin (containing 1% Alexa647-labeled or 2% Alexa488-labeled or 2% Alexa594-labeled actin), 50 nM myosin II, 1% BSA, a salt mix (2 mM MgCl<sub>2</sub>, 0.2 mM EGTA, and 25mM KCl), and an ATP regenerating mix (2 mM ATP, 2 mM MgCl<sub>2</sub>, 10 mM creatine phosphate, 3.5 U.mL<sup>-1</sup> creatine kinase) in fluorescence buffer (10 mM Tris pH 7.8, 0.2 mM CaCl<sub>2</sub>, 0.4% methylcellulose, 5 mM DABCO and 20 mM DTT), supplemented with the proteins of interest, such as EGFP-Vh and mCherry-RIAM 1-306. The short gelsolin-capped actin filaments have been prepared by mixing the barbed end capping protein gelsolin with actin filaments at a 1:600 gelsolin:actin molar ratio (Ciobanasu et al., 2015).

### III.4.4 Optimization of the conditions and technical considerations

In this assay, G-actin slowly polymerizes and assembles with myosin II filaments. The delay of actomyosin accumulation in the disks helps the self-organization of the system and makes the start of force application easy to correlate with force-dependent events, which is crucial for the present project.

Furthermore, the viscous methylcellulose mimics the molecular crowding of cells, which confines the actomyosin network in close vicinity to the surface. The potassium ions neutralize

charges at the surface of actin monomers, which limits their repulsion and facilitates their assembly into F-actin. Actin polymerization thus requires a high ionic strength, while myosins assemble into microfilaments in the absence of KCl. A concentration of 25 mM KCl is a good compromise that allows the assembly of both polymers.

The ATP regenerating mix contains ATP, creatine phosphate and creatine phosphokinase, which constantly re-phosphorylate ADP into ATP. A high concentration of ATP is necessary to maintain the catalytic cycle of myosin II motors driven by ATP hydrolysis. Because the system depends on myosin activity, this ATP regenerating mix allows the reaction to persist over time until it establishes a steady state.

The orientation of talin on the micropatterns was determined by taking advantage of the high affinity calpain-2 cleavage site between amino acids Q433 and Q434 (between talin head and talin rod) (Bate et al., 2012). The calpain-2-induced cleavage of a talin construct tagged with EGFP on its C-terminal extremity, provoked both the loss of the EGFP fluorescence and the dissociation of the actomyosin network from the talin-coated disks (Ciobanasu et al., 2014). This result indicates that the N-terminal part of talin is bound to the surface, while its C-terminal actin-binding domain interacts with actin filaments. Similar experiments (not published) performed with fluorescent RIAM, instead of fluorescent actin, led to the same conclusion. A similar orientation of talin was observed in FAs (Kanchanawong et al., 2010), with the N-terminal part of talin close to the membrane, and the C-terminal extremity pointing toward the actin-enriched zone.

### III.4.5 Microscopy observation and data analysis

Images were acquired with a Nikon Ti Eclipse E microscope equipped with a 60X oil immersion objective (Apochromat, 1.49 NA) and coupled to a sCMOS camera (Photometrics, Prime 95B or Hamamatsu, Orca Flash04), using the spinning disk mode (Yokogawa CSU-X1-A1) or the TIRF mode. EGFP-Vh (or Alexa488-Actin), mCherry-RIAM 1-306 (or Alexa594-actin) and Alexa647-actin were excited with 488, 561, and 642 nm lasers, respectively. Images were acquired with MetaMorph and analyzed with ImageJ.

Kinetics were obtained by averaging kinetics of the mean fluorescence of a large number of single disks, after background subtraction. To observe vinculin recruitment to talin-coated disks, only background subtraction and averaging of the kinetics of single disks were processed. To observe RIAM dissociation from talin-coated disks, the data were first normalized to 1 as the maximal mCherry-RIAM 1-306 fluorescence and synchronized using this maximal value as  $t_0$ , before being averaged. To observe simultaneously RIAM, vinculin and actin accumulation in

## Materials and methods

talin-coated disks, the data were only synchronized by using the maximal mCherry-RIAM 1-306 fluorescence value as  $t_0$ , before being averaged. For steady-state data, each point of the dot plots represents the mean fluorescence of a single disk (background subtracted). The bar indicates the mean. The graphs were assembled using Igor Pro or Kaleidagraph. Statistical analysis was performed using two-tailed t-tests with Microsoft Excel.

## IV RESULTS

---

### IV.1 ARTICLE 1: THE PIP<sub>2</sub>-TALIN-RIAM-VASP PATHWAY CONTROLS ACTIN POLYMERIZATION AND ORGANIZATION (IN PREPARATION)

To move forward, migrating cells propel actin-rich membrane protrusions in the form of filopodia or lamellipodia. In this process, nascent adhesions mechanically couple the polymerizing actin networks to cell-matrix adhesions components to produce force against the plasma membrane. In nascent adhesions, the actin-binding protein talin establishes the first link between the extracellular matrix, via integrins, and the actin cytoskeleton. Talin then recruits members of the Mig-10 / RIAM / lamellipodin (MRL) family, which form a complex that triggers actin assembly in the nascent adhesions that form at the tip of filopodia and at the leading edge of lamellipodia. The mechanism by which MRL proteins contribute to actin assembly is only partially understood. The actin nucleator, elongator and bundler VASP binds FPPPP motifs in RIAM and lamellipodin, and has thus been proposed to associate with MRL protein-integrin-talin complexes in nascent adhesions to promote actin polymerization. Furthermore, lamellipodin binds actin filaments via clusters of basic amino acids in its C-terminal unstructured region and promotes the processive elongation of actin filaments by VASP. A direct role of RIAM on actin dynamics has however never been reported.

Here, we combine various biochemical approaches to show that talin, RIAM and VASP cooperate to regulate actin assembly and organization. The reconstitution of a talin-RIAM-VASP complex on PIP<sub>2</sub>-containing giant unilamellar vesicles (GUVs) first showed that the PIP<sub>2</sub>-talin-RIAM-VASP machinery triggers actin assembly at the surface of GUVs. Kinetic assays further determined that this activity depends on profilin. Observations carried out in TIRF microscopy to clarify the role of RIAM in this process revealed that RIAM binds to actin filaments and controls their elongation. Finally, light scattering and microscopy showed that the three proteins of the complex synergize to organize actin filaments into large actin bundles.

I have carried out and analyzed all the experiments on GUVs and single actin filaments. I also performed actin polymerization kinetics and purified proteins. C. Le Clainche also performed some of the actin polymerization kinetics and the bundling experiments. V. Henriot, B. Faivre and C. Le Clainche designed cDNAs and purified proteins. J. Pernier and M. Cardoso Dos Santos supervised the preparation of giant unilamellar vesicles. This article is in preparation.

# **The PIP<sub>2</sub>-talin-RIAM-VASP pathway controls actin polymerization and organization.**

Clémence Vigouroux, Julien Pernier, Marcelina Cardoso Dos Santos,  
Véronique Henriot, Bruno Faivre and Christophe Le Clainche<sup>#</sup>

Université Paris-Saclay, CEA, CNRS,  
Institute for Integrative Biology of the Cell (I2BC),  
91198, Gif-sur-Yvette, France.

During cell migration, protein machineries associated with the actin cytoskeleton and cell-matrix components cooperate to form membrane protrusions such as lamellipodia and filopodia. Multiprotein complexes, containing regulators of actin dynamics and adhesion components, mechanically couple actin polymerization to adhesion, allowing force production against the plasma membrane. Several studies suggest that the actin-binding proteins talin and VASP, linked by the adaptor RIAM, regulate actin polymerization to form lamellipodia and filopodia associated to nascent adhesions. However, the actin polymerization activities of the individual proteins, and the activity of the ternary complex resulting from their association, remain poorly understood. In this study, in vitro reconstitution at the surface of giant unilamellar vesicles (GUVs) reveals that talin head binding to membrane PIP<sub>2</sub> triggers the hierarchical assembly of a PIP<sub>2</sub>-talin-RIAM-VASP pathway that stimulates actin assembly. This assay also shows that RIAM contributes to actin recruitment. The colocalization of fluorescent RIAM constructs with single actin filaments further indicates that RIAM binds directly to the side of actin filaments through its C-terminal domain. Kinetic assays and single filament observations then demonstrate that RIAM inhibits actin barbed-end elongation. In physiological conditions, where actin is bound to profilin, the combination of the three proteins stimulates actin assembly. Finally, talin, RIAM and VASP synergize to organize actin filaments into higher order bundles. This study paves the way towards understanding the coordination between cell-matrix adhesion and actin assembly.

<sup>#</sup> To whom correspondence should be addressed:  
[christophe.leclainche@i2bc.paris-saclay.fr](mailto:christophe.leclainche@i2bc.paris-saclay.fr)

## Introduction

Migrating cells project actin-rich membrane protrusions, such as filopodia and lamellipodia to move forward. This process requires the mechanical coupling between actin polymerization and cell-matrix adhesion complexes (Le Clairche and Carlier, 2008). Nascent adhesions (NAs) play a major role in actin assembly at the leading edge of lamellipodia and at the tip of filopodia (Galbraith et al., 2007). The numerous actin-binding proteins (ABPs) present in NAs control the assembly and ultrastructure of the actin networks in a coordinated manner (Ciobanasu et al., 2018).

In NAs, the protein talin establishes the first link between the extracellular matrix and the cytoskeleton via transmembrane integrins (Jiang et al., 2003). Talin is a large ABP composed of a N-terminal head, which anchors the protein to PIP<sub>2</sub>-rich membranes and activates integrins, followed by a rod domain subdivided into 13 helical bundles (R1 to R13), which contain 11 force-dependent cryptic vinculin-binding sites (Goult et al., 2018). Talin also interacts constitutively with proteins of the Mig-10 / Rap1-GTP-interacting adaptor molecule (RIAM) / lamellipodin (Lpd) (MRL) family (Lagarrigue et al., 2016). RIAM knockdown and overexpression revealed its role in membrane protrusion, cell spreading and actin polymerization (Lafuente et al., 2004). RIAM and Lpd play a central role in actin assembly in NAs, by forming a complex with talin and integrin, called MRL-Integrin-Talin (MIT). This complex co-localizes with actin filaments at the leading edge of lamellipodia and at the tip of filopodia called sticky fingers (Lagarrigue et al., 2015). RIAM interacts with the F3, R2, R3, R8 and R11 domains of talin through two N-terminal talin-binding sites (TBS1 and TBS2) (Chang et al., 2014; Goult et al., 2013; Vigouroux et al., 2020; Yang et al., 2014). MRLs are also characterized by the presence of Ras association (RA) and PIP<sub>2</sub>-binding pleckstrin homology (PH) domains and a non-structured C-terminal half containing several proline-rich motifs that interact with VASP, profilin and SH3 domains (Lagarrigue et al., 2016).

RIAM and Lpd are recruited to the membrane through two possible pathways. Talin, bound to PIP<sub>2</sub> (Goksoy et al., 2008; Martel et al., 2001; Saltel et al., 2009), can target RIAM and Lpd to the plasma membrane. Alternatively, RIAM and Lpd are targeted to the membrane by their PH and RA domains which interact with PIP<sub>2</sub> and lipid-anchored GTPase Rap1, respectively (Lafuente et al., 2004; Zhang et al., 2014).

The mechanism by which MRLs contribute to actin assembly in membrane protrusions is not fully understood. Interestingly, Ena/VASP proteins bind several proline-rich motifs (D/E)(F/L/W/Y)PPPPX(D/E)(D/E), abbreviated FPPPP, in the C-terminal half of RIAM and Lpd (Jenzora et al., 2005; Krause et al., 2004). In vitro, VASP nucleates, elongates and bundles actin filaments (Breitsprecher et al., 2008; Hansen and Mullins, 2010; Laurent et al., 1999). It was therefore proposed that VASP, which is also located at the leading edge of lamellipodia and at the tip of filopodia (Galbraith et al., 2007; Rottner et al., 1999; Svitkina et al., 2003), associates with the integrin-talin-MRL complex to control actin assembly (Lagarrigue et al., 2015). Alternatively, some of the proline-rich motifs of Lpd bind to the SH3 domain of the Abi subunit of the WAVE complex, which activates the branched actin nucleation by the Arp2/3 complex (Law et al., 2013). The direct contribution of MRL proteins to actin polymerization is unclear. Lpd binds actin filaments directly via clusters of basic amino acids in the C-terminal unstructured region and promotes the processive elongation of actin filaments by VASP (Hansen and Mullins, 2015). However, RIAM does not display this basic amino acid signature in its C-terminal region and has never been shown to interact with actin. RIAM and Lpd may therefore act on actin dynamics by different mechanisms.

Although the above observations suggest possible mechanisms by which the talin-RIAM-VASP complex is recruited to the membrane to control actin assembly, several issues remain open. Talin and RIAM contain FERM and PH domains respectively that bind to PIP<sub>2</sub> but it is not known which protein initiates the recruitment of the components of the complex to the membrane. The ability of MRLs proteins to regulate actin dynamics is based on the study of Lpd alone and it is not known whether RIAM also has this activity. The actin polymerization activity of the talin-RIAM-VASP complex and its ability to organize actin filaments are also difficult to predict. We combined the observation of single actin filaments in TIRF microscopy, kinetic assays for actin polymerization and in vitro reconstitution of actin assembly on giant unilamellar vesicles (GUVs) to address these issues.



## Results

### **In vitro reconstitution of the hierarchical assembly of a PIP<sub>2</sub>-talin-RIAM-VASP pathway at the surface of GUVs.**

Although it is well established that talin head can be targeted to the membrane by its interaction with PIP<sub>2</sub>, it is not entirely clear whether the binding of RIAM to talin is sufficient to target it to the membrane or whether anchoring of its PH domain to PIP<sub>2</sub> is also necessary as previously suggested (Wynne et al., 2012). In addition, although the 6 FPPPP motifs of RIAM are capable of binding the Ena/VASP homology 1 (EVH1) domain of VASP (Jenzora et al., 2005), it is unclear which of the 2 N-terminal and 4 C-terminal motifs are required for VASP recruitment. To address these issues, we reconstituted the assembly of a PIP<sub>2</sub>-talin-RIAM-VASP pathway at the surface of GUVs. We first demonstrated that an EGFP-talin F2-R8 fragment, encompassing the F2 and F3 subdomains of the head and the R1-R8 part of the rod (Supplementary Figure 1), is recruited to the surface of GUVs containing EPC (L- $\alpha$ -phosphatidylcholine) lipids and PIP<sub>2</sub>, but not to control EPC GUVs (Supplementary Figure 2A-C). To determine the relative importance of the talin binding sites and the PH domain of RIAM for its recruitment to a PIP<sub>2</sub>-containing membrane coated with talin, we compared the ability of mCherry-RIAM full-length to bind PIP<sub>2</sub>-containing EPC GUVs in the presence of EGFP-talin F2-R8, containing high affinity binding domains for RIAM, and EGFP-talin F2-F3 which does not contain them (Supplementary Figure 1). Our results show that mCherry-RIAM colocalizes with EGFP-talin F2-R8 on the surface of PIP<sub>2</sub>-containing GUVs but not with EGFP-talin F2-F3, although both talin constructs are equally recruited to the surface of the GUVs (Figure 1A, Supplementary Figure 3). These observations show that the N-terminal TBS1 and TBS2 of RIAM mediate RIAM recruitment to membrane-bound talin, whereas direct binding of the PH domain of RIAM to membrane PIP<sub>2</sub> does not play a role. Moreover, in these experimental setup RIAM only interacts with talin rod and not with the F3 subdomain of the head bound to PIP<sub>2</sub>. We then determined the ability of RIAM to recruit EGFP-VASP on talin R1-R2-R3-coated GUVs. The use of talin R1-R2-R3 allows us to bypass the need of relieving talin autoinhibition, because it does not contain the R9 and R12 bundles (Supplementary Figure 1). Furthermore, the stoichiometry of the interaction

between RIAM and talin is simplified. The fact that EGFP-VASP is only recruited to talin-coated GUVs in the presence of RIAM indicates a clear hierarchy in the assembly of the components of the ternary talin-RIAM-VASP complex (Figure 1B). The recruitment of RIAM depends on the binding of talin to PIP<sub>2</sub>-containing GUVs (Figure 1C), and the recruitment of VASP depends on the binding of RIAM to talin (Figure 1B). Because VASP is a tetramer (Breitsprecher et al., 2008; Hansen and Mullins, 2010), we determined whether it recruits RIAM molecules other than those already bound to talin. Our results show that, in our experimental conditions, VASP does not increase RIAM recruitment to talin-coated GUVs, suggesting that all the EVH1 domains of VASP might be already bound to talin-bound RIAM or not accessible to new RIAM molecules (Figure 1C). We then compared the ability of mCherry-RIAM 1-306, which contains only the two N-terminal FPPPP motifs, and mCherry-RIAM full-length (1-665), which contains 6 FPPPP motifs, to recruit EGFP-VASP at the surface of talin-coated GUVs. Although mCherry-RIAM full-length and mCherry-RIAM 1-306 are equally recruited to talin-coated GUVs (Supplementary Figure 4), EGFP-VASP only colocalizes with mCherry-RIAM full-length but not with mCherry-RIAM 1-306 (Figure 1D), indicating that the two first FPPPP are not involved in VASP binding.

### **The talin-RIAM-VASP complex stimulates actin assembly at the surface of PIP<sub>2</sub>-containing GUVs**

After setting up the conditions for the formation of the talin-RIAM-VASP complex on PIP<sub>2</sub>-containing GUVs, we determined whether this complex is capable of stimulating actin assembly as it seems to do in filopodia (Lagarrigue et al., 2015). To ensure that the actin filaments associated with GUVs result from a mechanism of nucleation by the complex on the surface of the GUVs and not by the capture of filaments formed in solution, spontaneous actin nucleation was blocked by the addition of a five-fold excess of profilin. We compared the ability of talin, talin-RIAM and talin-RIAM-VASP complexes to stimulate actin assembly at the surface of PIP<sub>2</sub>-containing GUVs. In these conditions, talin alone does not stimulate actin assembly, as evidenced by the low Alexa488-actin fluorescence around the GUVs. Surprisingly, the addition of RIAM results in a slight stimulation of actin assembly. In the presence of talin, RIAM and VASP, a robust actin polymerization occurs at the surface of GUVs (Figure 1E).

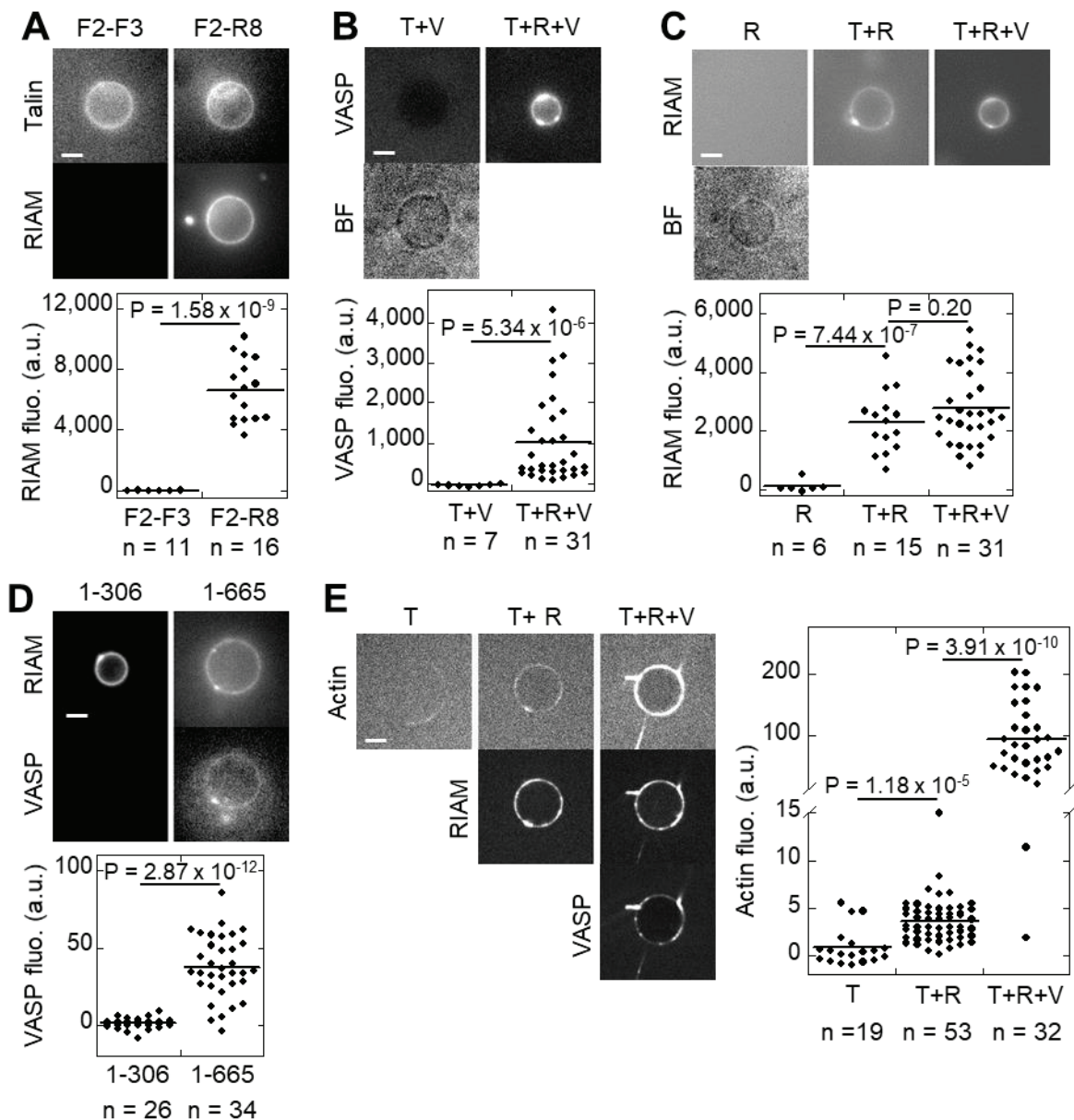


**Figure 1. In vitro reconstitution of the assembly of a PIP<sub>2</sub>-talin-RIAM-VASP pathway at the surface of GUVs.** (A) Representative epifluorescence images of mCherry-RIAM 1-665 (full-length) (0.125 μM) and EGFP-talin (5 μM) F2-F3 or F2-R8 incubated with PIP<sub>2</sub>-containing GUVs. (B) Representative epifluorescence and bright field (BF) images of PIP<sub>2</sub>-containing GUVs incubated with talin R1-R2-R3 (5 μM) and EGFP-VASP (0.125 μM) in the absence and presence of mCherry-RIAM 1-665 (0.125 μM). (C) Representative epifluorescence and BF images of PIP<sub>2</sub>-containing GUVs incubated with mCherry-RIAM 1-665 alone (0.125 μM), in the presence of talin R1-R2-R3 (5 μM), or in the presence of talin R1-R2-R3 and EGFP-VASP (0.125 μM). (D) Representative epifluorescence images of mCherry-RIAM 1-306 or 1-665 (0.2 μM) and EGFP-VASP (0.2 μM) incubated with talin R1-R2-R3 (3 μM) and PIP<sub>2</sub>-containing GUVs. (E) Representative spinning disk confocal images of the fluorescence of Alexa647-actin, mCherry-RIAM 1-665 and EGFP-VASP around PIP<sub>2</sub>-containing GUVs. Conditions: 2 μM actin (2% Alexa647-labeled, pre-incubated with 10 μM profilin), 3 μM talin R1-R2-R3, 0.2 μM mCherry-RIAM 1-665, 0.2 μM EGFP-VASP. (A-E) The final solutions contain 50 mM salt (KCl + NaCl) to maintain 200 mOsmol. Scale bar = 5 μm. The fluorescence of RIAM (A, C), VASP (B, D) and actin (E) around the GUVs is quantified. One point represents a vesicle, the bar indicates the mean. The P-value was obtained by a two-tailed t-test. In legends, talin, RIAM and VASP are abbreviated T, R and V respectively.

## **RIAM binds actin filaments through its C-terminal half and inhibits barbed end elongation**

To understand the mechanism by which the talin-RIAM-VASP complex initiates actin assembly, we studied the activity of these proteins by combining actin polymerization kinetic assays and observation of actin filaments in spinning disk confocal microscopy. We first tested the actin polymerization activity of isolated proteins. The activities of isolated talin and VASP are already known (Breitsprecher et al., 2008; Ciobanasu et al., 2018; Laurent et al., 1999). The mild stimulation of actin assembly induced by the addition of RIAM at the surface of talin-coated GUVs suggests that RIAM could interact with actin (Figure 1E). To test the binding of RIAM to actin filaments, we observed the localization of several mCherry-RIAM constructs along single Alexa488-labelled actin filaments. mCherry-RIAM full length (1-665) decorates actin filaments in a dose-dependent manner (Figure 2A, B). The observation that mCherry-RIAM 307-665 binds to actin filaments, while mCherry-RIAM 1-306 does not, indicate that the actin-binding domain is located in the C-terminal half of RIAM (Supplementary figure 1, Figure 2C). In this series of experiments, we also measured the elongation of single actin filaments in the presence of full-length RIAM and observed that it is frequently interrupted by pauses, as illustrated by kymographs (Figure 2D), indicating that RIAM caps actin filament barbed ends. In contrast, actin filaments growing in the absence of RIAM, or in the presence of the non-actin-binding fragment RIAM 1-306, show uninterrupted linear growth (Figure 2D, Supplementary movie 1). We confirmed that this inhibition of actin assembly corresponds to barbed end capping by showing that full-length RIAM, but not RIAM 1-306, inhibits the elongation of spectrin-actin seeds in a pyrenyl-actin assay (Supplementary figure 5A). In contrast with the RIAM paralogue Lpd (Hansen and Mullins, 2015), RIAM activity is insensitive to ionic strength (Supplementary figure 5B), indicating that RIAM and Lpd interact with actin differently. Altogether, these observations show that RIAM binds to the side of actin filaments and cap their barbed end.

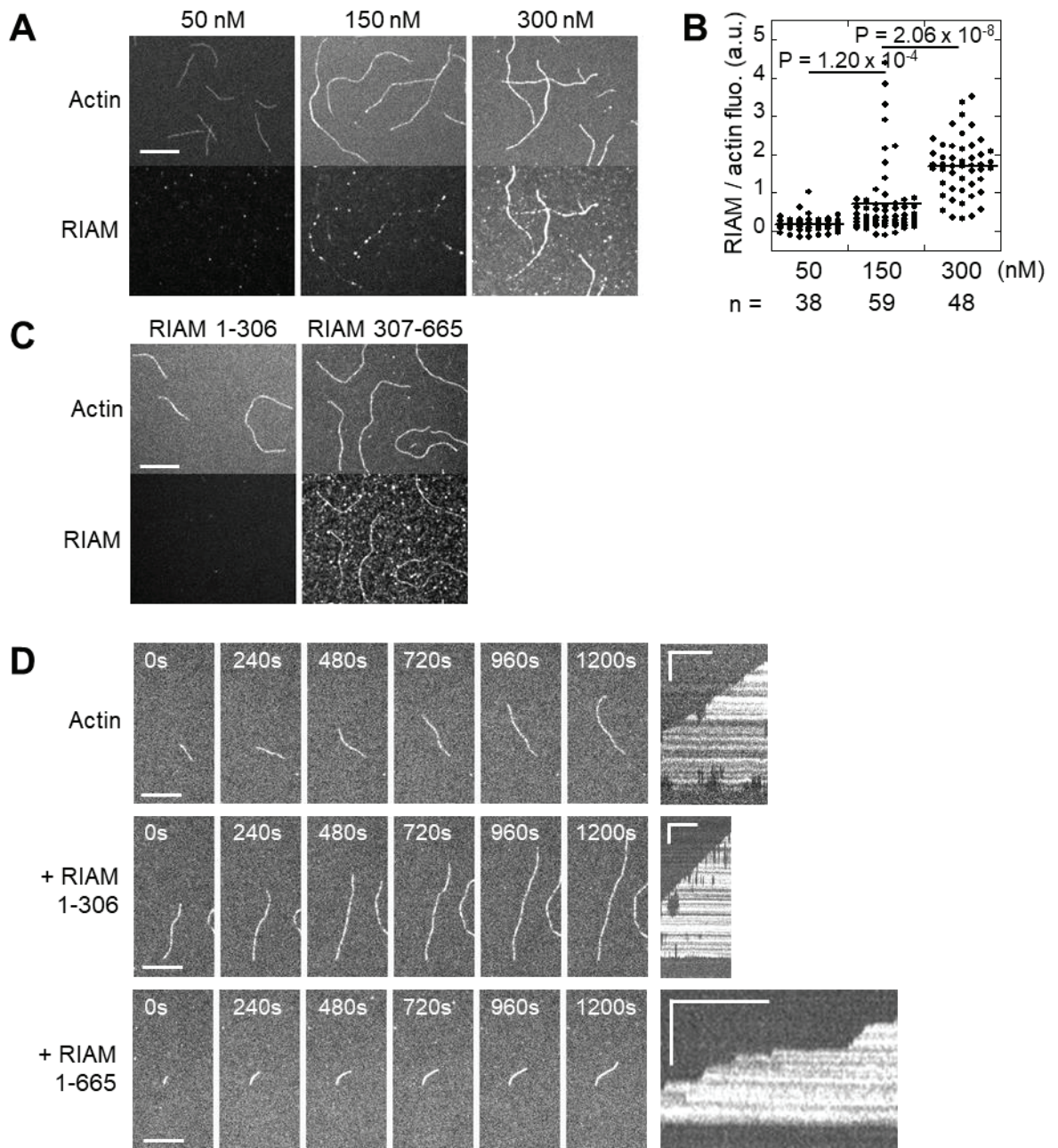


**Figure 2. RIAM binds actin filaments through its C-terminal half and inhibits barbed end elongation.** (A) Colocalization of mCherry-RIAM 1-665 with Alexa488-labelled single actin filaments observed in spinning disk confocal microscopy. Conditions: 50, 150 and 300 nM mCherry-RIAM 1-665, 0.6  $\mu$ M actin (5% Alexa488-labeled). The assay was performed in 100 mM salt (52 mM KCl, 48 mM NaCl). Scale bar = 5  $\mu$ m. (B) Quantification of the ratio of the fluorescence of mCherry-RIAM 1-665 to the fluorescence of Alexa488-actin. One point represents a filament, the bar indicates the mean. P-value obtained by a two-tailed t-test. (C) Colocalization of mCherry-RIAM 1-306 (left) or 307-665 (right) with Alexa488-labelled single actin filaments observed in spinning disk confocal microscopy. Conditions: 500 nM mCherry-RIAM constructs, 1  $\mu$ M actin (10% Alexa488-labeled). The assay was performed in 100 mM KCl. Scale bar = 5  $\mu$ m. (D) Time lapses and kymographs of single actin filaments (0.6  $\mu$ M, 5% Alexa488-labeled) observed in spinning disk confocal microscopy in the absence and presence of 300 nM mouse mCherry-RIAM 1-306 and human mCherry-RIAM 1-665. The assay was performed in 100 mM salt (52 mM KCl, 48 mM NaCl). In time lapses, scale bar = 5  $\mu$ m. In kymographs, horizontal bar = 500s, vertical bar = 5  $\mu$ m.

**Talin, RIAM and VASP form a complex that stimulates actin assembly in the presence of profilin.**

We then compared the actin polymerization activities of all the combinations of talin, RIAM and VASP, including isolated proteins, binary complexes and ternary complexes, by measuring kinetics of pyrenyl-actin polymerization. In these conditions, talin has no activity whereas RIAM inhibits actin assembly and VASP nucleates filaments (Figure 3A). The addition of RIAM to talin or VASP results in an inhibition of actin polymerization. Here, the three proteins simply combine their actin polymerization activities in an additive manner without synergy. Altogether these observations do not explain our previous observations that the talin-RIAM-VASP complex stimulates actin assembly at the surface of GUVs (Figure 1E). However, GUV experiments were carried out in the presence of profilin, which not only suppresses spontaneous actin nucleation but also modifies the actin polymerization activity of many proteins containing profilin-binding motifs. In this assay, both RIAM and VASP harbor several of these profilin-binding motifs (Supplementary figure 1). We therefore replicated the kinetic assays in the presence of profilin. Interestingly, profilin changed the activity of RIAM from an inhibitor to an activator of actin assembly. Talin itself has no activity but enhances the activity of RIAM. Finally, talin, RIAM and VASP stimulate actin assembly in a synergistic manner (Figure 3B), which explains our previous observations (Figure 1E).

In the presence of profilin, the activity of the talin-RIAM-VASP complex seems to depend mainly on the sensitivity of RIAM to profilin. Understanding the effect of profilin on RIAM activity should allow us to better understand the activity of the complex. We therefore determined how profilin affects the elongation of single actin filaments in the presence of RIAM. We did not observe significant differences in the frequency of elongation pauses in the presence of RIAM (Supplementary Figure 6A). Our quantifications also show that the average rate of elongation is lowered by RIAM in the same proportions in the absence and presence of profilin (Supplementary Figure 6B, C). Profilin does not seem to reverse the capping activity of RIAM nor does it seem to create a machinery that stimulates elongation. Overall our data converge towards the idea that profilin allows RIAM to nucleate actin filaments.

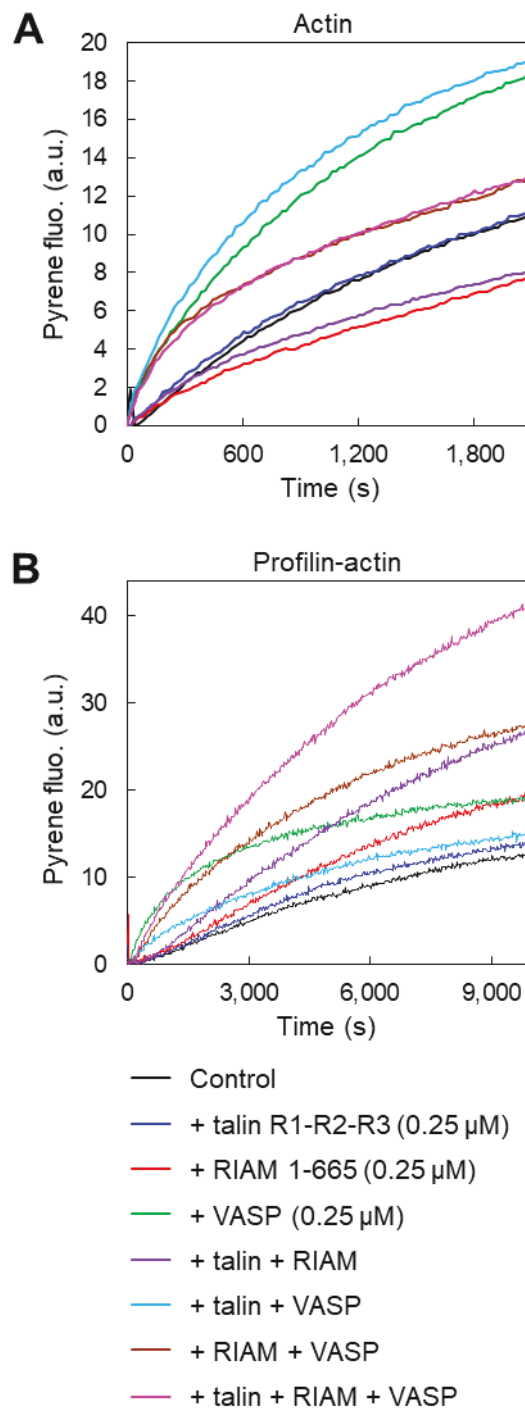


**Figure 3. Talin, RIAM and VASP nucleate actin filaments synergistically in the presence of profilin.** (A) Actin polymerization was measured alone and in the presence of all the combinations of talin R1-R2-R3, mCherry-RIAM 1-665 and VASP using a pyrene assay. (B) Profilin-actin assembly was measured in the same conditions as in (A). (A, B) Conditions: 3  $\mu$ M Mg-ATP-G-actin (10 % pyrenyl-labeled in the absence of profilin and 4 % pyrenyl-labeled in the presence of profilin), 6  $\mu$ M profilin, 0.25  $\mu$ M talin R1-R2-R3, 0.25  $\mu$ M mCherry-RIAM 1-665, 0.25  $\mu$ M VASP.

## **Talin, RIAM and VASP bundle actin filaments synergistically.**

In addition to controlling actin assembly, many ABPs contribute to shape actin networks by crosslinking actin filaments into large bundles. This property is often associated with the oligomerization of the proteins. Since RIAM contains a coiled-coil domain in the N-terminal part that mediates its dimerization (Chang et al., 2013) (Supplementary figure 1), it could induce the formation of actin bundles. VASP, which is a tetramer, is well known for bundling actin filaments in vitro (Laurent et al., 1999). Talin which contains 3 ABDs and a dimerization domain has also been described for cross-linking filaments (Zhang et al., 1996). We first used light scattering to determine the ability of the isolated proteins and their combinations to form higher order actin structures during actin polymerization. We only compared the final level reached by the kinetics because the bundling rate is greatly dependent on the rate of actin polymerization, which is influenced differently by proteins. In our experimental conditions, the bundling activity of talin is negligible, whereas VASP and RIAM display significant activities (Figure 4A). Although talin has no measurable activity in these conditions, it increases considerably the activity of its partner RIAM but not of VASP, to which it does not bind. The bundling activity measured in the presence of RIAM and VASP is higher than the sum of the activities of the two isolated proteins. Finally, maximum activity is observed in the presence of talin, RIAM and VASP (Figure 4A). We confirmed these results by directly observing the bundles in epifluorescence microscopy (Figure 4B).

## **Discussion**

The activity of the talin-RIAM-VASP complex described in this study is related to the activity of the complex called MIT (MRL-integrin-talin), which forms in response to Ras signaling at the leading edge of cells to induce the formation of actin-rich lamellipodia and filopodia (Lagarrigue et al., 2015) (Figure 6). In this process, the GTPase Rap1 plays an important role to recruit RIAM, which targets talin at the membrane where it activates integrins (Lafuente et al., 2004; Lee et al., 2009). However, a direct Rap1-talin interaction has been described as an alternative pathway to recruit talin to the membrane and induce integrin activation in cooperation with membrane PIP<sub>2</sub> (Bromberger et al., 2019, 2018). Our experimental system bypasses Rap1 requirement because our talin construct is activated by the deletion of the R9 and R12 domains, which normally prevents talin head to interact with PIP<sub>2</sub>-rich membranes.



RIAM also comprises a PH domain that can bind to membrane PIP<sub>2</sub>, but we did not detect this interaction in our in vitro reconstitution. The intramolecular contact between RIAM TBS2 and RA-PH domains might need to be released, maybe by Rap1 binding, to allow RIAM interaction with PIP<sub>2</sub> (Chang et al., 2019).

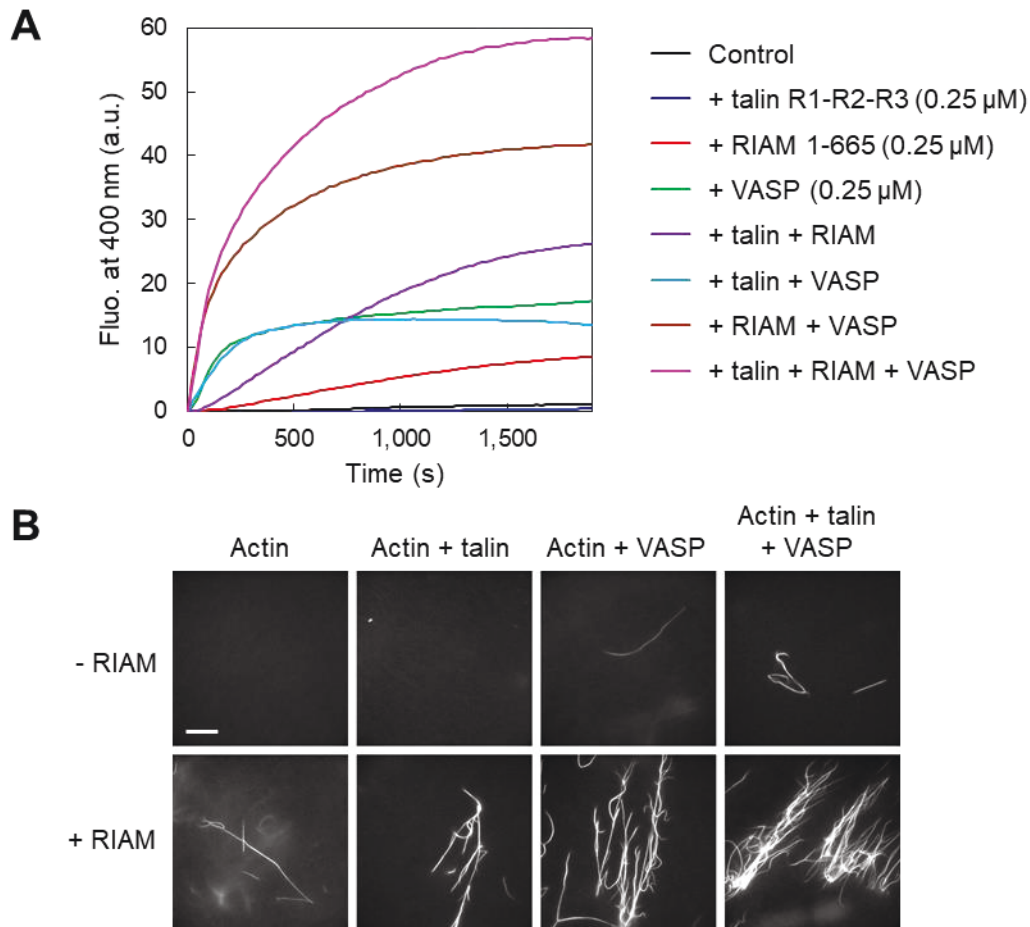


**Figure 4. Talin, RIAM and VASP bundle actin filaments synergistically.** (A) Light scattering was measured during the polymerization of actin alone and in the presence of all the combinations of talin R1-R2-R3, mCherry-RIAM 1-665 and VASP. (B) Representative epifluorescence images of Alexa488-actin filament bundles observed alone and in the presence of all the combinations of talin R1-R2-R3, mCherry-RIAM 1-665 and VASP. Bar = 25 μm. (A, B) Conditions: 3 μM G-actin (2 % Alexa488-actin), 0.25 μM talin R1-R2-R3, 0.25 μM mCherry-RIAM 1-665, 0.25 μM VASP.

Once assembled at the membrane, the MIT complex allows the actin-based propulsion of the tips of adhesive filopodia, called sticky fingers, to rapidly translocate active integrins and guide cell migration (Galbraith et al., 2007). Although Ena/VASP proteins were not identified in the MIT complex, the authors hypothesized that their binding to RIAM FPPPP motifs provides the actin polymerization activity to the MIT complex (Lagarrigue et al., 2015). In agreement with this hypothesis, the RIAM paralogue Lpd favors the formation of VASP clusters, which increases its barbed end elongation activity (Breitsprecher et al., 2008; Cheng and Mullins, 2020; Hansen and

Mullins, 2015). Although we confirmed that RIAM promotes the actin polymerization activities of VASP, we did not find strong evidence that this effect results from VASP clustering.

Multimeric actin filament side-binding proteins often organize actin networks into bundles. The complex resulting from the assembly of talin dimers, RIAM dimers and VASP tetramers harbors many actin-binding domains that bundle actin filaments efficiently. However, in the cellular context, it is well established that the MIT complex only forms at the tip of filopodia and does not decorate actin filaments along their entire length. This observation implies that the clustering activity of the complex is probably limited to the barbed ends of the filaments that have just been formed by the complex close to the membrane. The complex could therefore initiate bundling at the membrane, while other crosslinkers, such as fascin, bundle the filaments along their entire length.

Our discovery that profilin determines the actin polymerization activity of the talin-RIAM-VASP complex adds up to previous discoveries on the function of profilin. The profilin-actin complex associates to the barbed end, but not the pointed end, which directs actin monomers towards the growing barbed ends that produce force against the membrane (Le Clainche and Carlier, 2008; Pollard and Cooper, 1984; Pring et al., 1992). Profilin is also important for preventing spontaneous nucleation of filaments, allowing the spatio-temporal control of nucleation through signaling pathways. Another important role of profilin is to assist elongation machineries such as formins and Ena/VASP proteins. In the case of formins, several mechanisms have been proposed. The binding of profilin to proline-rich motifs along formin FH1 domain could concentrate actin monomers in the vicinity of the barbed ends and promote their elongation (Paul and Pollard, 2008; Pernier et al., 2016). Alternatively, formins could accelerate the dissociation of profilin from the barbed end which limits its elongation rate (Funk et al., 2019). The role of profilin in VASP-mediated barbed-end elongation varies from one species to another. *Dictyostelium* VASP is not sensitive to profilin (Breitsprecher et al., 2008), while human VASP activity is strongly enhanced by profilin (Hansen and Mullins, 2010). In the case of the talin-RIAM-VASP complex, both human RIAM and human VASP harbor profilin-binding motifs. Our experiments suggest that profilin confers a nucleation activity to RIAM, in addition to its capping activity (Figure 6). This observation explains why RIAM knockdown leads to a decrease of polymerized actin in cells (Lafuente et al., 2004). This nucleation activity then combines synergistically with that of VASP and is further enhanced by talin.

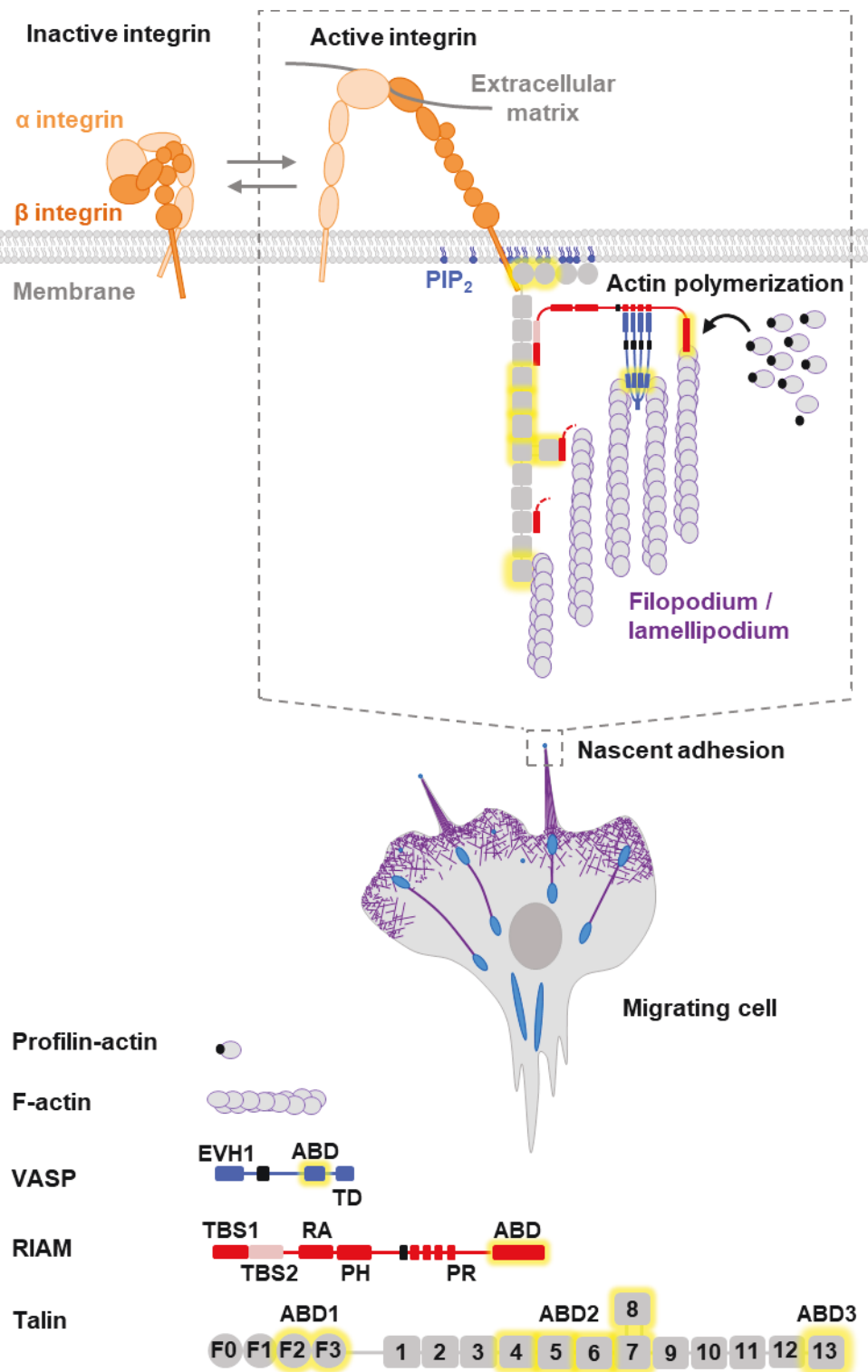


**Figure 5. Working model for the activity of the PIP<sub>2</sub>-talin-RIAM-VASP machinery.** RIAM contains two consecutive talin-binding sites (TBSs), a ras-association domain (RA), a pleckstrin-homology domain (PH) and a C-terminal proline rich region (PR) that contains four FPPPP, five profilin-binding motifs and the actin-binding domain (ABD). VASP contains an EVH1 (Ena/VASP homology 1) domain that interacts with RIAM FPPPP motifs, a profilin-binding domain, a G-actin and a F-actin-binding domain, and a tetramerization domain (TD). Profilin-binding sites in RIAM and VASP are represented in black. Talin FERM domains F0 to F3 and rod bundles 1 to 13 are indicated. The ABDs in all proteins are highlighted in yellow.

Our findings raise the question whether all MRLs act through the same mechanisms. Lpd and RIAM share many functions but important differences exist. Although the binding of RIAM and Lpd to talin at the end of filopodia has been established, only the interaction between RIAM and talin has benefited from a detailed mechanistic study (Goult et al., 2013; Vigouroux et al., 2020). The replacement of RIAM TBS1 by Lpd TBS greatly decreases the affinity of RIAM for talin and the ability of talin to activate integrins (Chang et al., 2014). This observation shows that talin-Lpd-VASP and talin-RIAM-VASP complexes do not have the same stability and suggest that their actin polymerization activity could be different. Also, it is not known whether Lpd binds to the same bundles (R2, R3, R8, R11) of talin as RIAM and whether these interactions occurs through two TBS1 and TBS2 motifs as for RIAM (Goult et al., 2013; Vigouroux et al., 2020), or only one. Lpd binds to actin filaments through its C-terminal domain and decreases the rate of actin assembly by sequestering actin monomers. This interaction is mediated by clusters of positively charged amino acids, which makes the interaction sensitive to ionic strength (Hansen and Mullins, 2015). RIAM was not predicted to interact with actin filaments directly because it does not contain this positively charged region. However, we found that RIAM interacts with the side of actin filaments, caps their barbed ends and promotes actin assembly. In contrast with Lpd, RIAM activity does not involve positively charged amino acids since it is not sensitive to ionic strength. Our findings suggest that RIAM and Lpd interact with actin filaments through different mechanisms, which is surprising for two evolutionary related genes. In conclusion, RIAM N-terminus can recruit talin at the membrane so that it can activate integrins, whereas its C-terminus promotes actin assembly to drive the rapid translocation of integrins at the tip of sticky fingers (Figure 6). In this process, the talin-RIAM-VASP complex coordinates actin nucleation and elongation machineries. RIAM thus mechanically couples adhesion to actin dynamics, allowing membrane protrusion.

## **Material and methods**

### **cDNA constructs**

Talin R1-R2-R3, corresponding to F2-F3-R1-R2-R3-R13, was cloned into a pETM plasmid with a N-terminal StrepTagII and a C-terminal His<sub>6</sub> tag. The enhanced green fluorescent protein (EGFP)-tagged talin 196-405 (F2-F3) was cloned into a pGEX-6P1

(GE Healthcare), with a N-terminal cleavable Glutathione-S-transferase (GST) tag followed by EGFP. EGFP-talin 196-1659 (F2-R8) was cloned into a pGEX-6P1 (GE Healthcare), with a N-terminal cleavable GST tag followed by EGFP, and a C-terminal His<sub>6</sub>-tag. The human cDNA encoding for RIAM 1-665 and 1-306 were cloned into a homemade pGEX-6P2-mCherry plasmid with a C-terminal His<sub>6</sub>-tag. The pGEX-6P2-mCherry RIAM 307-665 plasmid was created by deletion in the pGEX-P2-mCherry RIAM 1-665 plasmid using natural restriction sites and replaced by a synthetic cDNA (Genscript). The human cDNA encoding for human full-length VASP was cloned into a pGEX-6P1 plasmid to produce the pGEX-6P1-VASP and pGEX-6P1-EGFP-VASP plasmids, with an additional N-terminal EGFP for the pGEX-6P1-EGFP-VASP plasmid.

### **Protein purification**

Rabbit skeletal muscle actin (Wiesner, 2006), rabbit skeletal muscle myosin II (Pollard, 1982), profilin (Le Clainche and Carlier, 2004), pyrenyl- and Alexa488-actin (Ciobanasu et al., 2015; Kouyama and Mihashi, 1981), spectrin-actin seeds (Casella et al., 1986) were prepared as previously described.

All recombinant proteins were expressed in *Escherichia coli* (BL21 DE3, Invitrogen) as previously described (Ciobanasu et al., 2015).

Talin R1-R2-R3 was purified as previously described (Vigouroux et al., 2020). EGFP-talin 196-405 (F2-F3) was bound to Glutathione Sepharose, cleaved by PreScission protease and purified by gel filtration chromatography (Superdex 200, 16/60, GE Healthcare) in 20 mM Tris pH 8.5, 150 mM KCl, 1 mM  $\beta$ -mercaptoethanol (BME). EGFP-talin 196-1659 (F2-R8) was bound to Ni-NTA-Agarose, cleaved by PreScission protease and purified by gel filtration chromatography (Superdex 200, 16/60, GE Healthcare) in 20 mM Tris pH 8, 150 mM KCl, 5 mM BME.

Human full-length EGFP-VASP was first bound to Glutathione Sepharose in 50 mM Tris pH 7, 150 mM NaCl, 1 mM EDTA, 1mM DTT and cleaved from GST by PreScission protease in the same buffer. The protein was purified by monoQ chromatography in 20 mM tris pH7, 100 mM NaCl, 1mM BME, eluted from monoQ by a 100-500 mM NaCl linear gradient, purified by gel filtration chromatography (Superdex 200, 16/60, GE Healthcare) in 20 mM Tris pH 8.5, 150 mM NaCl, frozen in liquid nitrogen and stored at -80°C. Human full-length VASP was first bound to

Glutathione Sepharose in 50 mM Tris pH 7, 500 mM NaCl, 1 mM EDTA, 1mM DTT and cleaved from GST by PreScission protease in 50 mM Tris pH 7, 150 mM NaCl, 1 mM EDTA, 1mM DTT. The protein was dialyzed in 20 mM Tris pH 7.8, 100 mM KCl, 1 mM DTT, frozen in liquid nitrogen and stored at -80°C.

Human mCherry-RIAM 1-665 (full-length) was bound to Glutathione Sepharose, washed with 50 mM Tris pH 7.8, 500 mM NaCl, 10% glycerol, and eluted with 50 mM Tris pH 7.8, 500 mM NaCl, 10% glycerol and 50 mM reduced L-Glutathione. The procedure was repeated seven times because of the low affinity of this protein for Glutathione Sepharose. GST was then cleaved by PreScission protease in 50 mM Tris pH 7.8, 500 mM NaCl and 10% glycerol, and eliminated by Glutathione Sepharose chromatography. The protein was then bound to Ni-NTA-Agarose, washed with 50 mM Tris pH 7.8, 500 mM NaCl, 10% glycerol, 20 mM imidazole, and eluted with 50 mM Tris pH 7.8, 500 mM NaCl, 10% glycerol, 250 mM imidazole, dialyzed in 20 mM Tris pH 7.8, 500 mM NaCl, 2% glycerol, 1 mM DTT, frozen in liquid nitrogen and stored at -80°C. For specific experiments, the protein was further dialyzed in 20 mM Tris pH 7.8, 200 mM KCl, 2% glycerol, 1 mM BME.

Human mCherry-RIAM 1-306 and 307-665 were bound to Ni-NTA-Agarose, washed with 50 mM Tris pH 7.8, 500 mM NaCl, 10% glycerol, 20 mM imidazole, and eluted with 50 mM Tris pH 7.8, 500 mM NaCl, 10% glycerol and 250 mM imidazole. They were dialyzed in 20 mM Tris pH 7.8, 250 mM NaCl, 1 mM BME and incubated overnight with Glutathione Sepharose. The resin was then washed with 20 mM Tris pH 7.8, 250 mM NaCl, 1 mM BME. The protein was cleaved from GST by PreScission protease in the same buffer, dialyzed in 20 mM Tris pH 7.8, 200 mM KCl, 2% glycerol, 1 mM BME, frozen in liquid nitrogen and stored at -80°C.

### **Actin polymerization assay**

Actin polymerization was monitored by the increase in fluorescence of 10% pyrenyl-labeled actin. Pyrenyl-labeled actin was decreased to 4% in the presence of profilin. Actin polymerization was induced by the addition of 25 to 100 mM KCl, 1mM MgCl<sub>2</sub>, and 0.2 mM EGTA to a solution of pyrenyl-labeled G-actin containing the proteins of interest. Experiments containing RIAM alone were performed at 100 mM KCl but experiments containing full-length VASP were performed at 50 mM KCl to favor its nucleation activity. Profilin was added to the reaction to prevent spontaneous nucleation. Spectrin-actin seeds were added to the reaction to measure the barbed

end elongation specifically. Fluorescence measurements were carried out with a Safas Xenius FLX spectrophotometer (Safas, Monaco). Polymerization curves were normalized to 0 at the start time. To measure the affinity of mCherry-RIAM 1-665 for barbed ends, the initial elongation rate was taken as a measure of free barbed ends (BE). The following equation was used to fit the data.  $[C_0]$  and  $[R_0]$  are the total concentrations of barbed ends and RIAM respectively, and  $K$  represents the equilibrium dissociation constant of the barbed end-RIAM complex. The fraction of free barbed ends is:

$$BE = 1 - ( ([C_0] + [V_0] + K - ( ([V_0] + [C_0] + K)^2 - 4 [V_0] [C_0] )^{1/2} ) / 2 [C_0] )$$

The graphs were assembled with Excel or Kaleidagraph.

### **Actin bundling measurement by light scattering and microscopy observation**

The bundling of actin filaments accompanying actin polymerization was assessed by measuring light scattering at 400 nm in a Safas Xenius FLX spectrophotometer (Safas, Monaco). Actin polymerization was induced by the addition of 20 mM KCl, 40 mM NaCl, 1mM MgCl<sub>2</sub>, and 0.2 mM EGTA to a solution of G-actin (2% Alexa488-labeled) containing the proteins of interest. The graphs were assembled with Excel. When the reaction measured in light scattering reached the steady state, a 3  $\mu$ L sample was taken for epifluorescence microscopy observation. Images were acquired with an Olympus IX71 microscope equipped with a 60X oil immersion objective (Olympus, 1.45 NA) and coupled to an EMCCD camera (Cascade, Photometrics). Images were acquired with MicroManager and assembled with ImageJ.

### **Observation of single actin filament elongation**

The filaments were observed using a previously published method (Ciobanasu et al., 2018), with some modifications. Glass coverslips (22  $\times$  32 mm, Thermo Scientific/Menzel-Glaser) were first washed with milliQ water, sonicated in ethanol, washed with milliQ water and irradiated for 1 min under a deep UV lamp (Ossila). The coverslips were then incubated for 2h in 0.1 mg.ml<sup>-1</sup> PLL-g-PEG (SuSoS) dissolved in 10 mM HEPES pH 7.4 and washed with milliQ water. A chamber was created by attaching a passivated coverslip to a glass slide (Super Frost, Thermo Scientific) with double-sided adhesive tape, with a typical volume of 50  $\mu$ l. The chamber was first saturated with 1% bovine serum albumin for 5 min and then washed with a wash buffer

(5 mM Tris pH 7.8, 200  $\mu$ M ATP, 10 mM DTT, 1 mM  $MgCl_2$ , 100 mM KCl). The final reaction was then injected in the chamber. A typical reaction is composed of 0.6-1  $\mu$ M G-actin (5-10% Alexa Fluor 488-labeled) in 5 mM Tris pH 7.8, 200  $\mu$ M ATP, 0.4% methyl-cellulose, 1 mM 1,4-diazabicyclo(2,2,2)-octane (DABCO), 100 mM KCl (or 52 mM KCl and 48 mM NaCl), 1 mM  $MgCl_2$ , 200  $\mu$ M EGTA, 10 mM DTT, supplemented with the protein of interest. Finally, the chamber was sealed with VALAP (1:1:1 mixture of vaseline, lanolin and paraffin) or oil. Images were acquired with a Nikon Ti Eclipse microscope equipped with a spinning disk (Yokogawa CSU-X1-A1), a 60X oil immersion objective (Apochromat, 1.49 NA) and coupled to a sCMOS camera (Photometrics, Prime 95B) or an Olympus IX71 microscope equipped with a 60X oil immersion objective (Olympus, 1.45 NA) and coupled to an EMCCD camera (Cascade, Photometrics). Alexa488-actin and mCherry-RIAM constructs were excited with 488 and 561 lasers, respectively. Images were acquired with MetaMorph or MicroManager and analyzed with ImageJ. The colocalization data were quantified by measuring the mean fluorescence along a filament, with background subtraction. The ratio of the fluorescence of mCherry-RIAM to the fluorescence of Alexa488-actin was plotted. The rates of barbed end elongation were calculated by measuring the elongation of a filament overtime, expressed in actin subunits incorporated into a filament per second. Each dot represents a filament. The bar indicates the mean. The dot plots were assembled with KaleidaGraph. P-values were obtained by performing two-tailed t-tests with Excel.

### **GUVs preparation**

Giant unilamellar vesicles (GUVs) were prepared using the spontaneous gel-assisted swelling technique. Our protocol is a modified version of a previously published protocol (Weinberger et al., 2013). Polyvinyl alcohol (PVA) (Merck) was dissolved at 5% (w/w) in a 280 mM D(+)-saccharose (sucrose) (Euromedex) solution containing 20 mM Tris pH 7.5, by continuous stirring at 150°C for 30 min. The PVA solution was spread onto 22  $\times$  22 mm glass coverslips (Thermo Scientific/Menzel-Glaser) previously cleaned by sonication in water, ethanol and water sequentially. The PVA-coated coverslips were dried at 50°C for 45 min. Lipids were mixed in chloroform with a concentration of 1 mg.mL<sup>-1</sup>. Lipid mixtures contain EPC (or Egg PC) lipids (L- $\alpha$ -phosphatidylcholine from chicken egg) (Avanti Polar Lipids) alone, or supplemented with 10 mole% PIP<sub>2</sub> (L- $\alpha$ -phosphatidylinositol-4,5-bisphosphate from porcine brain,



ammonium salt (Avanti Polar Lipids), and/or 0.1 mole% SR101-DHPE lipids (N-(Rhodamine 101 sulfonyl)-1,2-hexadecanoyl-sn-4-phosphoethanolamine, triethylammonium salt) (Interchim). Each lipid mixture was spread onto PVA-coated coverslips and dried under vacuum for 1h at room temperature to remove residual chloroform. GUVs were formed by incubating in growth buffer (200 mM sucrose) for 4h at room temperature. After incubation, the GUVs were collected, centrifuged at  $14,000 \times g$ ,  $20^{\circ}\text{C}$  for 30 min, and stored in glass vials at  $4^{\circ}\text{C}$  to be used within 3 days. The osmolarity inside the vesicles is 200 mOsmol.

### **GUVs observation**

Glass coverslips ( $22 \times 32$  mm, Thermo Scientific/Menzel-Glaser) were washed with milliQ water, sonicated in ethanol, washed with milliQ water and irradiated for 1 min under a deep UV lamp (Ossila). The coverslips were incubated for 2h in  $0.1 \text{ mg}\cdot\text{mL}^{-1}$  mPEG-silane (SuSoS) dissolved in 10 mM HEPES pH 7.4 and washed with milliQ water. A chamber was created by attaching a passivated coverslip to a glass slide (Super Frost, Thermo Scientific) with double-sided adhesive tape, with a typical volume of  $25 \mu\text{L}$ . To maintain the GUV stability, the experiments were performed in a final buffer of 200 mOsmol, containing 50 mM salt (KCl + NaCl). Typically, the GUVs solution was diluted two-fold in a fluorescent mix (5 mM Tris pH 7.8, 32 mM NaCl, 18 mM KCl, 0.01%  $\text{NaN}_3$ , 1 mM  $\text{MgCl}_2$ , 0.2 mM EGTA, 0.2 mM ATP, 10 mM DTT, 1 mM DABCO) supplemented with the proteins of interest. Finally, the solution was injected in the chamber sealed with oil. Images were acquired with an Olympus IX71 microscope equipped with a 60X oil immersion objective (Olympus, 1.45 NA) and coupled to an EMCCD camera (Cascade, Photometrics), or with a Nikon Ti Eclipse microscope equipped with a spinning disk (Yokogawa CSU-X1-A1), a 60X oil immersion objective (Apochromat, 1.49 NA) and coupled to a sCMOS camera (Photometrics, Prime 95B). Alexa488-actin (and EGFP fusion proteins), mCherry-RIAM constructs (or SR1010-DHPE) and Alexa647-actin were excited with 488, 561 and 642 nm lasers, respectively. Images were acquired with MicroManager or MetaMorph and analyzed with ImageJ. The data were quantified by measuring the mean fluorescence around a vesicle, with background subtraction. The dot plots were assembled with KaleidaGraph. Each dot represents a vesicle. The bar indicates the mean. P-values were obtained by performing two-tailed t-tests with Excel.

## **Acknowledgements**

This work was supported by Agence Nationale pour la Recherche Grants ANR-16-CE13-0007-02 PHAGOMECANO and ANR ANR-18-CE13-0026-01 RECAMECA (to CLC). The present work has benefited from the Light Microscopy facility of Imagerie-Gif, (<http://www.i2bc.paris-saclay.fr>), member of IBIISA (<http://www.ibisa.net>), supported by “France- Biolmaging” (ANR- 10- INBS- 04- 01), and the Labex “Saclay Plant Sciences” (ANR-10-LABX-0040-SPS). We thank Florence Niedergang and the members of the “Cytoskeleton Dynamics and Motility” team for helpful discussions.

## **Author contributions**

CV purified proteins, performed the microscopy experiments, analyzed the data and prepared the figures. JP and MCDS supervised the preparation of GUVs. VH and BF cloned cDNAs and purified proteins. CLC performed bundling experiments, supervised the project and wrote the manuscript.

## **Conflict of interest**

The authors declare no conflicts of interest.

## References

- Breitsprecher D, Kieseewetter AK, Linkner J, Urbanke C, Resch GP, Small JV, Faix J. 2008. Clustering of VASP actively drives processive, WH2 domain-mediated actin filament elongation. *EMBO J* **27**:2943–2954. doi:10.1038/emboj.2008.211
- Bromberger T, Klapproth S, Rohwedder I, Zhu L, Mittmann L, Reichel CA, Sperandio M, Qin J, Moser M. 2018. Direct Rap1/Talin1 interaction regulates platelet and neutrophil integrin activity in mice. *Blood* **132**:2754–2762. doi:10.1182/blood-2018-04-846766
- Bromberger T, Zhu L, Klapproth S, Qin J, Moser M. 2019. Rap1 and membrane lipids cooperatively recruit talin to trigger integrin activation. *J Cell Sci* **132**:jcs.235531. doi:10.1242/jcs.235531
- Casella JF, Maack DJ, Lin S. 1986. Purification and initial characterization of a protein from skeletal muscle that caps the barbed ends of actin filaments. *J Biol Chem* **261**:10915–21.
- Chang Y-C, Su W, Cho E, Zhang H, Huang Q, Philips MR, Wu J. 2019. Molecular basis for autoinhibition of RIAM regulated by FAK in integrin activation. *Proc Natl Acad Sci* **116**:3524–3529. doi:10.1073/pnas.1818880116
- Chang Y-C, Zhang H, Brennan ML, Wu J. 2013. Crystal structure of Lamellipodin implicates diverse functions in actin polymerization and Ras signaling. *Protein Cell* **4**:211–219. doi:10.1007/s13238-013-2082-5
- Chang YC, Zhang H, Franco-Barraza J, Brennan ML, Patel T, Cukierman E, Wu J. 2014. Structural and mechanistic insights into the recruitment of talin by RIAM in integrin signaling. *Structure* **22**:1810–1820. doi:10.1016/j.str.2014.09.020
- Cheng KW, Mullins RD. 2020. Initiation and disassembly of filopodia tip complexes containing VASP and lamellipodin. *Mol Biol Cell* **31**:2021–2034. doi:10.1091/mbc.E20-04-0270
- Ciobanasu C, Faivre B, Le Clainche C. 2015. Reconstituting actomyosin-dependent mechanosensitive protein complexes in vitro. *Nat Protoc* **10**:75–89. doi:10.1038/nprot.2014.200
- Ciobanasu C, Wang H, Henriot V, Mathieu C, Fente A, Csillag S, Vigouroux C, Faivre B, Le Clainche C. 2018. Integrin-bound talin head inhibits actin filament barbed-end elongation. *J Biol Chem* **293**:2586–2596. doi:10.1074/jbc.M117.808204
- Funk J, Merino F, Venkova L, Heydenreich L, Kierfeld J, Vargas P, Raunser S, Piel M, Bieling P. 2019. Profilin and formin constitute a pacemaker system for robust actin filament growth. *Elife* **8**:1–34. doi:10.7554/eLife.50963
- Galbraith CG, Yamada KM, Galbraith JA. 2007. Polymerizing Actin Fibers Position Integrins Primed to Probe for Adhesion Sites. *Science (80- )* **315**:992–995. doi:10.1126/science.1137904
- Goksoy E, Ma YQ, Wang X, Kong X, Perera D, Plow EF, Qin J. 2008. Structural Basis for the Autoinhibition of Talin in Regulating Integrin Activation. *Mol Cell* **31**:124–133. doi:10.1016/j.molcel.2008.06.011
- Goult BT, Yan J, Schwartz MA. 2018. Talin as a mechanosensitive signaling hub. *J Cell Biol* **217**:3776–3784. doi:10.1083/jcb.201808061
- Goult BT, Zacharchenko T, Bate N, Tsang R, Hey F, Gingras AR, Elliott PR, Roberts GCK, Ballestrem C, Critchley DR, Barsukov IL. 2013. RIAM and Vinculin Binding to Talin Are Mutually Exclusive and Regulate Adhesion Assembly and Turnover. *J Biol Chem* **288**:8238–8249. doi:10.1074/jbc.M112.438119
- Hansen SD, Mullins RD. 2015. Lamellipodin promotes actin assembly by clustering Ena/VASP proteins and tethering them to actin filaments. *Elife* **4**:1–29. doi:10.7554/eLife.06585
- Hansen SD, Mullins RD. 2010. VASP is a processive actin polymerase that requires monomeric actin for barbed end association. *J Cell Biol* **191**:571–584. doi:10.1083/jcb.201003014
- Jenzora A, Behrendt B, Small JV, Stradal TEB. 2005. PREL1 provides a link from Ras signalling to the actin cytoskeleton via Ena / VASP proteins **579**:455–463. doi:10.1016/j.febslet.2004.10.110
- Jiang G, Giannone G, Critchley DR, Fukumoto E, Sheetz MP. 2003. Two-piconewton slip

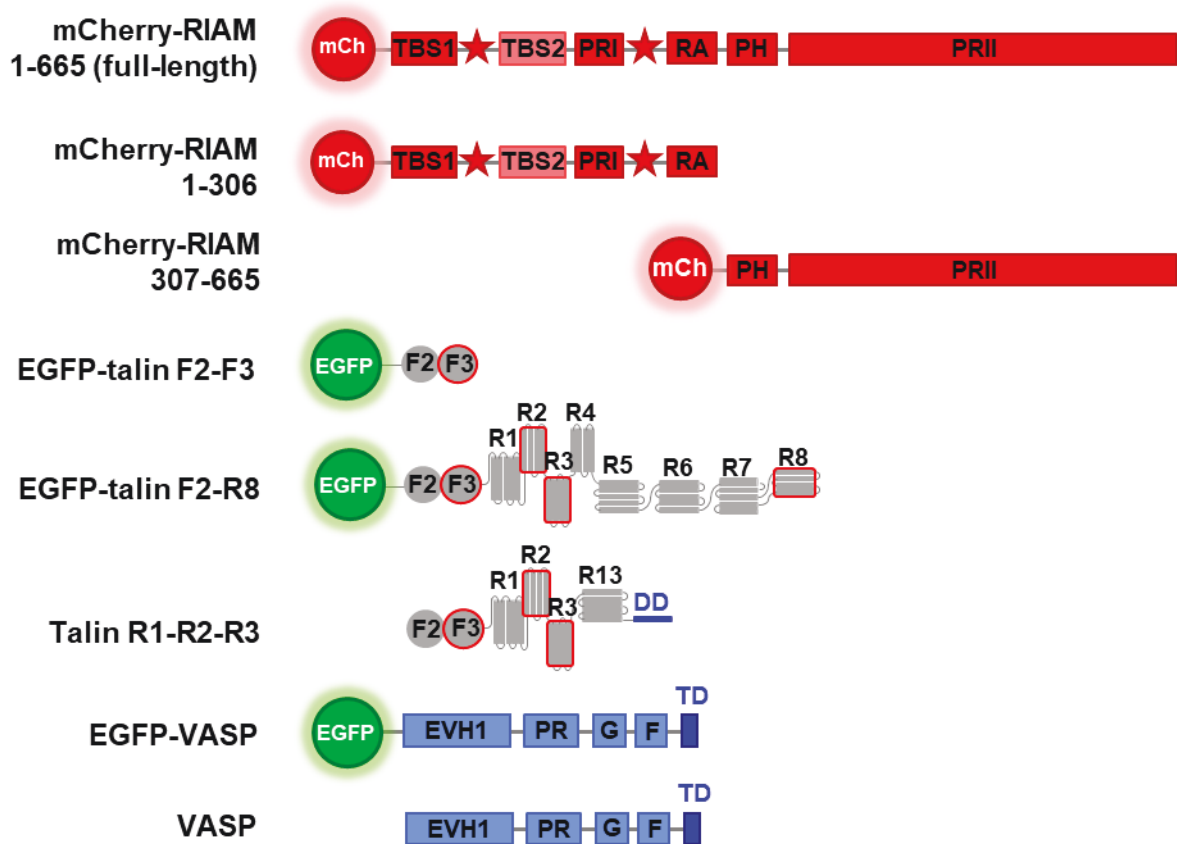
- bond between fibronectin and the cytoskeleton depends on talin. *Nature* **424**:334–337. doi:10.1038/nature01805
- Kouyama T, Mihashi K. 1981. Fluorimetry Study of N-(1-Pyrenyl)iodoacetamide-Labelled F-Actin. *Eur J Biochem* **114**:33–38. doi:10.1111/j.1432-1033.1981.tb06167.x
- Krause M, Leslie JD, Stewart M, Lafuente EM, Valderrama F, Jagannathan R, Strasser GA, Rubinson DA, Liu H, Way M, Yaffe MB, Boussiotis VA, Gertler FB. 2004. Lamellipodin, an Ena / VASP Ligand, Is Implicated in the Regulation of Lamellipodial Dynamics **7**:571–583.
- Lafuente EM, van Puijenbroek AAFL, Krause M, Carman C V., Freeman GJ, Berezovskaya A, Constantine E, Springer TA, Gertler FB, Boussiotis VA. 2004. RIAM, an Ena/VASP and profilin ligand, interacts with Rap1-GTP and mediates Rap1-induced adhesion. *Dev Cell* **7**:585–595. doi:10.1016/j.devcel.2004.07.021
- Lagarrigue F, Kim C, Ginsberg MH. 2016. The Rap1-RIAM-talin axis of integrin activation and blood cell function. *Blood* **128**:479–487. doi:10.1182/blood-2015-12-638700
- Lagarrigue F, Vikas Anekal P, Lee H-S, Bachir AI, Ablack JN, Horwitz AF, Ginsberg MH. 2015. A RIAM/lamellipodin–talin–integrin complex forms the tip of sticky fingers that guide cell migration. *Nat Commun* **6**:8492. doi:10.1038/ncomms9492
- Laurent V, Loisel TP, Harbeck B, Wehman A, Gröbe L, Jockusch BM, Wehland J, Gertler FB, Carlier M-F. 1999. Role of Proteins of the Ena/VASP Family in Actin-based Motility of *Listeria monocytogenes*. *J Cell Biol* **144**:1245–1258. doi:10.1083/jcb.144.6.1245
- Law A, Vehlow A, Kotini M, Dodgson L, Soong D, Theveneau E, Bodo C, Taylor E, Navarro C, Perera U, Michael M, Dunn GA, Bennett D, Mayor R, Krause M. 2013. Lamellipodin and the Scar/WAVE complex cooperate to promote cell migration in vivo **203**:673–689. doi:10.1083/jcb.201304051
- Le Clainche C, Carlier M-F. 2008. Regulation of Actin Assembly Associated With Protrusion and Adhesion in Cell Migration. *Physiol Rev* **88**:489–513. doi:10.1152/physrev.00021.2007
- Le Clainche C, Carlier M-F. 2004. Actin-Based Motility Assay Current Protocols in Cell Biology. Hoboken, NJ, USA: John Wiley & Sons, Inc. pp. 1–20. doi:10.1002/0471143030.cb1207s24
- Lee H-S, Lim CJ, Puzon-McLaughlin W, Shattil SJ, Ginsberg MH. 2009. RIAM Activates Integrins by Linking Talin to Ras GTPase Membrane-targeting Sequences. *J Biol Chem* **284**:5119–5127. doi:10.1074/jbc.M807117200
- Martel V, Racaud-Sultan C, Dupe S, Marie C, Paulhe F, Galmiche A, Block MR, Albiges-Rizo C. 2001. Conformation, Localization, and Integrin Binding of Talin Depend on Its Interaction with Phosphoinositides. *J Biol Chem* **276**:21217–21227. doi:10.1074/jbc.M102373200
- Paul A, Pollard T. 2008. The Role of the FH1 Domain and Profilin in Formin-Mediated Actin-Filament Elongation and Nucleation. *Curr Biol* **18**:9–19. doi:10.1016/j.cub.2007.11.062
- Pernier J, Shekhar S, Jegou A, Guichard B, Carlier MF. 2016. Profilin Interaction with Actin Filament Barbed End Controls Dynamic Instability, Capping, Branching, and Motility. *Dev Cell* **36**:201–214. doi:10.1016/j.devcel.2015.12.024
- Pollard TD. 1982. Chapter 22 Myosin Purification and Characterization Methods in Cell Biology. pp. 333–371. doi:10.1016/S0091-679X(08)60665-2
- Pollard TD, Cooper JA. 1984. Quantitative analysis of the effect of *Acanthamoeba* profilin on actin filament nucleation and elongation. *Biochemistry* **23**:6631–6641. doi:10.1021/bi00321a054
- Pring M, Weber A, Bubb MR. 1992. Profilin-actin complexes directly elongate actin filaments at the barbed end. *Biochemistry* **31**:1827–1836. doi:10.1021/bi00121a035
- Rottner K, Behrendt B, Small JV, Wehland J. 1999. VASP dynamics during lamellipodia protrusion. *Nat Cell Biol* **1**:321–322. doi:10.1038/13040
- Saltel F, Mortier E, Hytönen VP, Jacquier MC, Zimmermann P, Vogel V, Liu W, Wehrle-Haller B. 2009. New PI(4,5)P<sub>2</sub>- and membrane proximal integrin-binding motifs in the talin head control  $\beta$ 3-integrin clustering. *J Cell Biol* **187**:715–731. doi:10.1083/jcb.200908134
- Svitkina TM, Bulanova EA, Chaga OY, Vignjevic DM, Kojima S, Vasiliev JM, Borisy GG. 2003. Mechanism of filopodia initiation by reorganization of a dendritic network. *J Cell*

- Biol* **160**:409–421. doi:10.1083/jcb.200210174
- Vigouroux C, Henriot V, Le Clainche C. 2020. Talin dissociates from RIAM and associates to vinculin sequentially in response to the actomyosin force. *Nat Commun* **11**:3116. doi:10.1038/s41467-020-16922-1
- Weinberger A, Tsai F-C, Koenderink GH, Schmidt TF, Itri R, Meier W, Schmatko T, Schröder A, Marques C. 2013. Gel-Assisted Formation of Giant Unilamellar Vesicles. *Biophys J* **105**:154–164. doi:10.1016/j.bpj.2013.05.024
- Wiesner S. 2006. Purification of Skeletal Muscle Actin *Cell Biology*. Elsevier. pp. 173–175. doi:10.1016/B978-012164730-8/50097-6
- Wynne JP, Wu J, Su W, Mor A, Patsoukis N, Boussiotis VA, Hubbard SR, Philips MR. 2012. Rap1-interacting adapter molecule (RIAM) associates with the plasma membrane via a proximity detector. *J Cell Biol* **199**:317–330. doi:10.1083/jcb.201201157
- Yang J, Zhu L, Zhang H, Hirbawi J, Fukuda K, Dwivedi P, Liu J, Byzova T, Plow EF, Wu J, Qin J. 2014. Conformational activation of talin by RIAM triggers integrin-mediated cell adhesion. *Nat Commun* **5**:5880. doi:10.1038/ncomms6880
- Zhang H, Chang Y-C, Brennan ML, Wu J. 2014. The structure of Rap1 in complex with RIAM reveals specificity determinants and recruitment mechanism. *J Mol Cell Biol* **6**:128–139. doi:10.1093/jmcb/mjt044
- Zhang J, Robson RM, Schmidt JM, Stromer MH. 1996. Talin can crosslink actin filaments into both networks and bundles. *Biochem Biophys Res Commun*. doi:10.1006/bbrc.1996.0095

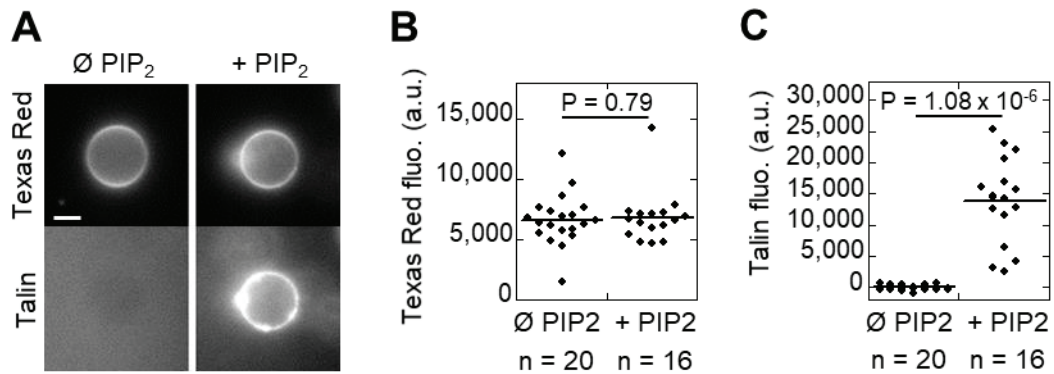
# **The PIP<sub>2</sub>-talin-RIAM-VASP pathway controls actin polymerization and organization.**

Vigouroux et al.

**Supplementary Figures.**

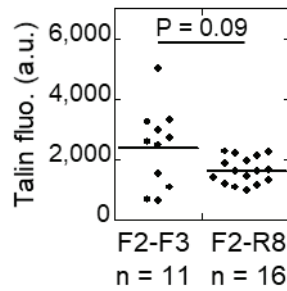


**Supplementary Figure 1. Proteins used in the study.** mCh, mCherry; TBS, talin-binding site; red star, coiled-coil; PR, proline-rich domain; RA, Ras-association domain; PH, plekstrin-homogy domain; EGFP, enhanced green fluorescent protein; F2 and F3, talin FERM domains 2 and 3; R1 to R13, talin rod bundles 1 to 13; DD, dimerization domain; EVH1, Ena/VASP homology 1; G, G-actin-binding domain; F, F-actin-binding domain; TD, tetramerization domain. RIAM-binding sites in talin are highlighted with red boxes.

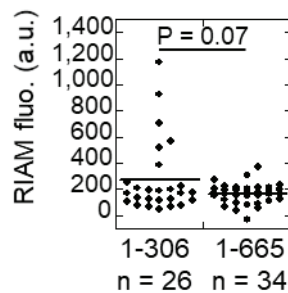


**Supplementary Figure 2. Talin is recruited to the surface of PIP<sub>2</sub>-containing GUVs. (A)** Representative epifluorescence images of EGFP-talin F2-R8 (3  $\mu$ M) incubated with GUVs, composed of EPC and 0.1% SR101-DHPE lipids (Texas Red) ( $\emptyset$  PIP<sub>2</sub>) or EPC, 0.1% SR101-DHPE, supplemented with 10% PIP<sub>2</sub> (+ PIP<sub>2</sub>). The final solution contains 50 mM salt (KCl + NaCl) to maintain 200 mOsmol. Scale bar = 5  $\mu$ m. **(B)** Fluorescence of SR101-DHPE lipids in the conditions described in (A). **(C)** Fluorescence of EGFP-talin F2-R8 in the conditions described in (A). One point represents a vesicle, the bar indicates the mean. P-value obtained by a two-tailed t-test.

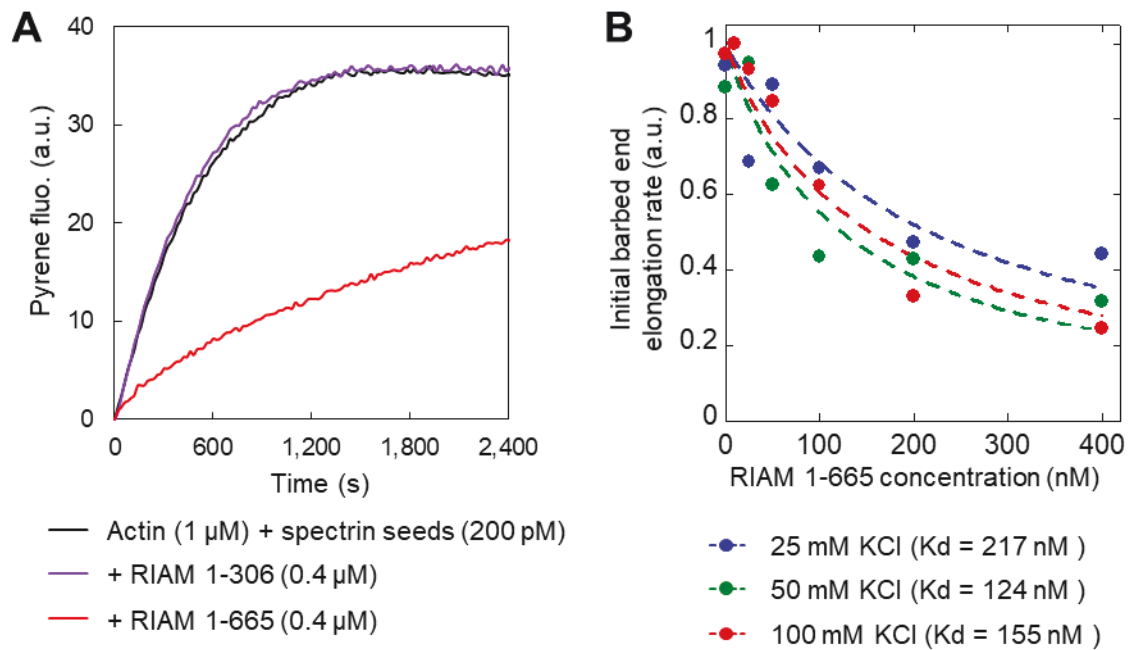




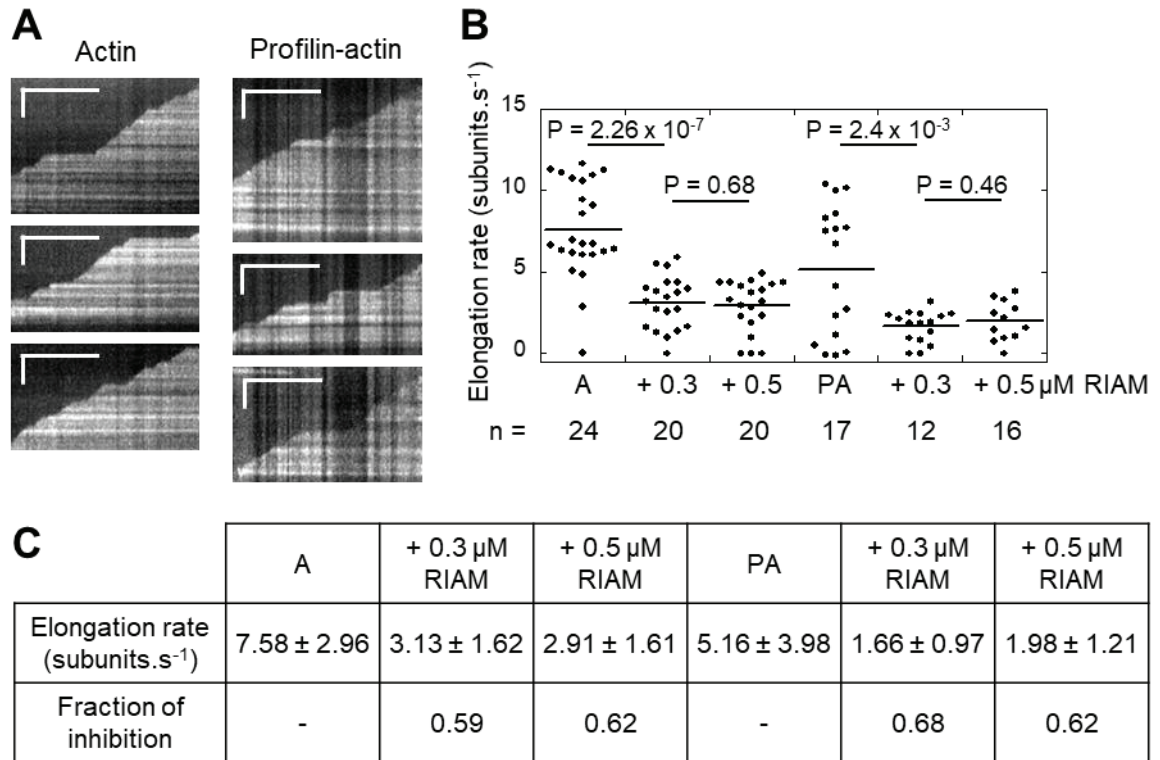
**Supplementary Figure 3. Talin F2-F3 and F2-R8 are equally recruited to the surface of PIP<sub>2</sub>-containing GUVs in the presence of RIAM.** Quantification of the fluorescence of EGFP-talin (5  $\mu$ M) F2-F3 or F2-R8 at the surface of PIP<sub>2</sub>-containing GUVs in the presence of mCherry-RIAM 1-665 (0.125  $\mu$ M) in the conditions described in Figure 1A. One point represents a vesicle, the bar indicates the mean. P-value obtained by a two-tailed t-test.



**Supplementary Figure 4. RIAM 1-306 and 1-665 are equally recruited to the surface of PIP<sub>2</sub>-containing GUVs in the presence of talin and VASP.** Quantification of the fluorescence of mCherry-RIAM 1-306 or 1-665 (0.2  $\mu$ M) at the surface of PIP<sub>2</sub>-containing GUVs in the presence of talin R1-R2-R3 (3  $\mu$ M) and EGFP-VASP (0.2  $\mu$ M) in the conditions described in Figure 1D. One point represents a vesicle, the bar indicates the mean. P-value obtained by a two-tailed t-test.



**Supplementary Figure 5. RIAM inhibits actin filament barbed-end elongation. (A)** Barbed-end elongation was measured in the presence of 200 pM spectrin-actin seeds, 1  $\mu\text{M}$  G-actin (10% pyrenyl-labeled) in the absence of RIAM and in the presence of 0.4  $\mu\text{M}$  mCherry-RIAM 1-306 or 1-665. **(B)** Quantification of the initial rates of barbed-end elongation was plotted versus the concentration of mCherry-RIAM full-length in buffers of various salt concentration (25, 50 and 100 mM KCl).



**Supplementary Figure 6. RIAM barbed-end capping activity is not sensitive to profilin.**

**(A)** Kymographs of single actin filaments (1  $\mu$ M, 10% Alexa488-labeled, alone or pre-incubated with 2  $\mu$ M profilin) observed in TIRF microscopy in the presence of 0.5  $\mu$ M mCherry-RIAM 1-665. The assay was performed in 100 mM salt (20.5 mM KCl, 79.5 mM NaCl). Horizontal bar = 500s, vertical bar = 5  $\mu$ m. **(B)** Quantification of the elongation rate of single actin filaments (expressed in actin subunits incorporated per second). Conditions: 1  $\mu$ M actin (10% Alexa488-labeled), 2  $\mu$ M profilin, 0, 0.3 and 0.5  $\mu$ M mCherry-RIAM 1-665. **(C)** Mean elongation rate value from (B). A, actin; PA, profilin-actin. One point represents a filament, the bar indicates the mean. P-values obtained by a two-tailed t-test.

## **Legends of Supplementary Movies.**

**Supplementary Movie 1. RIAM inhibits actin filaments barbed end elongation through its C-terminal half.** Elongation of Alexa488-labelled actin filaments observed in spinning disks confocal microscopy in the absence and presence of mCherry-RIAM 1-306 and 1-665. Conditions: 300 nM mCherry-RIAM constructs, 0.6  $\mu$ M actin (5% Alexa488-labeled). Scale bar = 5  $\mu$ M.

## IV.2 ARTICLE 2: TALIN DISSOCIATES FROM RIAM AND ASSOCIATES TO VINCULIN SEQUENTIALLY IN RESPONSE TO THE ACTOMYOSIN FORCE (VIGOUROUX ET AL., 2020)

Cell-matrix adhesion complexes sense changes in intra- and extracellular mechanical properties. During cell migration, they mature to reinforce adhesion strength and cytoskeleton anchoring in response to the increasing actomyosin force. In this process, the mechanical stretching of the actin-binding protein talin exposes cryptic vinculin-binding sites, allowing the talin-vinculin complex to reinforce actin anchoring. The force-dependent conformational change of talin might be the initial switch that triggers the maturation of short-lived nascent adhesions into stable focal adhesions. The binding of RIAM to talin could regulate this mechanism. However, the mechanosensitivity of the talin-RIAM interaction has never been reported. Whether RIAM association with talin controls the force-dependent binding of vinculin to talin is also not known. Finally, several helical bundles of talin, that interact with both RIAM and vinculin, could react to actomyosin force differently.

To determine the force-dependence, sequence and interdependence of these molecular events, we developed a quantitative in vitro microscopy assay, in which the actomyosin force controls RIAM and vinculin binding to a talin-micropatterned surface. We revealed for the first time that actomyosin is sufficient to stretch talin bundles and induce RIAM dissociation. We also demonstrated that actomyosin triggers the sequential exchange of RIAM for vinculin on several talin bundles. Moreover, RIAM affects the mechanosensitivity of the RIAM-binding talin bundles differently. RIAM protects some talin-bundles from unfolding, implying that RIAM increases the threshold force for exposing the cryptic vinculin-binding sites located in these bundles.

Talin interacts with many binding partners other than RIAM and vinculin. We hypothesize that this high number of combinations of talin partners, associated with specific mechanically-stretched talin conformations, provides the cell with a very precise means of encoding variations in intra- and extracellular forces.

I have carried out and quantified all the experiments presented in this article. I purified proteins. V. Henriot constructed the plasmids encoding for mouse mCherry-RIAM 1-306 and human talin R1-R2-R3. This article was published in June 2020 in Nature Communications.



ARTICLE



<https://doi.org/10.1038/s41467-020-16922-1>

OPEN

# Talin dissociates from RIAM and associates to vinculin sequentially in response to the actomyosin force

Clémence Vigouroux<sup>1</sup>, Véronique Henriot<sup>1</sup> & Christophe Le Clainche<sup>1</sup>  

Cells reinforce adhesion strength and cytoskeleton anchoring in response to the actomyosin force. The mechanical stretching of talin, which exposes cryptic vinculin-binding sites, triggers this process. The binding of RIAM to talin could regulate this mechanism. However, the mechanosensitivity of the talin-RIAM complex has never been tested. It is also not known whether RIAM controls the mechanosensitivity of the talin-vinculin complex. To address these issues, we designed an in vitro microscopy assay with purified proteins in which the actomyosin force controls RIAM and vinculin-binding to talin. We demonstrate that actomyosin triggers RIAM dissociation from several talin domains. Actomyosin also provokes the sequential exchange of RIAM for vinculin on talin. The effect of RIAM on this force-dependent binding of vinculin to talin varies from one talin domain to another. This mechanism could allow talin to biochemically code a wide range of forces by selecting different combinations of partners.

<sup>1</sup> Université Paris-Saclay, CEA, CNRS, Institute for Integrative Biology of the Cell (I2BC), 91198 Gif-sur-Yvette, France. ✉email: [christophe.leclainche@i2bc.paris-saclay.fr](mailto:christophe.leclainche@i2bc.paris-saclay.fr)

**M**echanical cues govern a variety of biological processes. During migration, cells sense and respond to changes in intracellular and extracellular forces by adapting their shape, dynamics, and adhesion. Focal adhesions (FAs), that play a major role in this mechanosensitive process, are composed of transmembrane integrins that mechanically couple the extracellular matrix (ECM) to the actomyosin cytoskeleton, via actin-binding proteins (ABPs)<sup>1–6</sup>. The mechanosensitivity of FAs allows cells to adapt adhesion strength to the internal force of the actomyosin cytoskeleton and to the physical properties of the ECM<sup>7–13</sup>. However, the biochemical mechanisms that govern FA mechanosensitivity remain largely unexplored.

Several lines of evidence indicate that the force-dependent conformational change of the actin-binding protein talin might be the initial switch that triggers the maturation of short-lived nascent adhesions into stable FAs, which withstand higher adhesion and actomyosin traction force<sup>3,14–16</sup>. Although it is thought that distinct force-dependent conformations of talin select specific binding partners to trigger appropriate mechanical responses, a limited number of these mechanisms have been discovered.

The mechanosensitive talin–vinculin interaction has long been the hallmark of FA maturation<sup>3</sup>. Experiments of mechanical stretching of talin by atomic force microscopy and magnetic tweezers revealed how force exposes one or more of the 11 cryptic vinculin-binding sites (VBSs) located in the 13 helical bundles of the talin rod domain (R1–R13, Fig. 1a)<sup>14,17–20</sup>. Using an *in vitro* reconstitution strategy, we demonstrated that the actomyosin force is sufficient to stretch talin, allowing its binding to vinculin<sup>21,22</sup>. A series of cellular and biochemical studies showed that the force-dependent formation of the talin–vinculin complex reinforces actin anchoring to FAs<sup>21,23–26</sup>. This reinforcement is further enhanced by the stability of the talin–vinculin complex in which vinculin locks talin in its stretched conformation<sup>20,21</sup>.

Less is known about the specific talin-binding partners in nascent adhesions. First observations in cells showed that the Rap1-GTP-interacting adaptor molecule (RIAM) is localized at the leading edge of migrating cells, where it cooperates with talin and Ena/VASP proteins to promote the formation of actin-based membrane protrusions<sup>27,28</sup>. During this early phase, RIAM could bind to the F3 domain of talin head, which disrupts the autoinhibition of talin, allowing it to activate integrins<sup>29,30</sup>. Interestingly, RIAM, which is initially enriched in nascent adhesions, is replaced by vinculin in mature FAs, that are known to experience higher traction force<sup>31,32</sup>. Structural studies showed that RIAM also interacts with exposed residues in the talin helical bundles R2, R3, R8, and R11<sup>33</sup>. In R2, R3, and R8, RIAM-binding sites and VBSs overlap<sup>33–35</sup>, suggesting a complex interplay between RIAM, vinculin, and talin.

Altogether these observations suggest that the actomyosin force triggers the mechanosensitive transition between nascent adhesions and FAs by controlling the binding of RIAM and vinculin to talin. However, the mechanosensitivity of the talin–RIAM complex has never been tested. It is also not known whether RIAM-binding to talin controls the mechanosensitive formation of the talin–vinculin complex. Furthermore, several domains of talin that interact with RIAM and vinculin may respond to force differently. To determine the mechanosensitivity, sequence and interdependence of these talin-associated reactions, we designed an *in vitro* microscopy assay with purified proteins. In this assay, the actomyosin force controls the binding of RIAM and vinculin to a micropatterned surface coated with talin constructs, which contain variable RIAM- and vinculin-binding sites (Fig. 1a).

## Results

***In vitro* reconstitution of talin–RIAM complexes.** The stoichiometry of the talin–RIAM complex was a major problem to

start this study. RIAM contains two talin-binding site (TBS1 and TBS2). TBS1 binds to the R2, R3, R8, and R11 helix bundles of the talin rod and to the subdomain F3 of the head<sup>30,33,35</sup> (Fig. 1a). TBS2 has a very low affinity for talin<sup>35</sup>. However, TBS2 could reinforce TBS1 anchoring by binding to a neighboring site if available. Hence, RIAM TBS1–TBS2 interacts with talin R2–R3 with a 2:2 stoichiometry and a higher affinity than the TBS1–R3 complex<sup>33</sup>. Based on this information, we designed a fluorescent mCherry–RIAM 1-306 protein, encompassing TBS1 and TBS2, to visualize the RIAM–talin interaction in microscopy (Fig. 1a, Supplementary Fig. 1a, b). We also designed a series of minimal talin constructs, made of the F2–F3 domains of the head, that anchor the protein to a micropatterned surface<sup>21</sup>, followed by an exchangeable cassette containing variable RIAM-binding sites, and the C-terminal actin-binding domain ABD3 (R13) that binds to the actomyosin cytoskeleton (Fig. 1a, Supplementary Fig. 1a, b). We selected the three following RIAM-binding regions for insertion in our minimal talin constructs: R1–R2–R3 that includes the high affinity R2–R3 part, R7–R8 in which the RIAM-binding R8 bundle is inserted in R7, and the single helical bundle R11 (Supplementary Fig. 1a). We found that RIAM binds specifically and with high affinity to disk-shaped micropatterns coated with these three talin constructs (Fig. 1b, c). In contrast, RIAM does not bind to talin F2–F3 alone, whereas it binds to the same construct fused to R1–R2–R3 (Supplementary Fig. 2). This result indicates that, in our experimental setup, talin F3 does not interact with RIAM because it is masked by its interaction with the surface or because, as reported by others, its affinity is too low ( $K_d = 32 \mu\text{M}$ )<sup>30</sup>.

## Actomyosin-dependent binding of vinculin to talin bundles.

Before testing the effect of actomyosin on talin–RIAM interactions, we first established the mechanosensitivity of our minimal talin constructs using the approach that we developed previously<sup>21,22</sup>. In this method, the force applied to disk-shaped talin-coated micropatterns is sufficient to expose cryptic vinculin-binding sites in talin and recruit fluorescent EGFP–vinculin head (Vh) (Fig. 1a). Here, the force is produced by the association of myosin II with slowly polymerizing actin filaments and applied to talin through its actin-binding domain (R13). Although actomyosin self-organizes transiently, it remains in the disks for at least 1000 s. In this assay, talin R1–R2–R3 shows a strong binding to Vh in the presence of actomyosin, compared with the low constitutive binding measured in the absence of actomyosin (Fig. 2a, b, e, Supplementary Movie 1). Using a procedure that we have already validated for full-length talin<sup>21</sup>, we confirmed that the actomyosin-dependent increase in Vh–talin interaction depends on myosin II and not on the bundling and polymerization of the actin network, even for a minimal talin like R1–R2–R3 (Supplementary Fig. 3a, b). We also observed the actomyosin-dependent binding of Vh to talin R11 (Fig. 2c, f, Supplementary Movie 2). R1–R2–R3 recruits more Vh than R11 because it contains five VBSs, whereas R11 contains only one (Supplementary Fig. 1a). However, talin R7–R8 does not bind to Vh in the presence of the same concentration of actin and myosin used to stimulate R1–R2–R3 and R11 (Fig. 2d, g, Supplementary Movie 3). The fact that R7–R8 does not bind Vh at all in the presence of actomyosin also rules out the mechanical exposure of the single VBS of ABD3 in our series of three constructs (Fig. 2d, g). Altogether, our data showed that the actomyosin force is efficiently transmitted to talin through ABD3 to stretch R1–R2–R3 and R11 but not R7–R8.

**Actomyosin-dependent dissociation of RIAM from talin.** To test the mechanosensitivity of the three talin–RIAM complexes,

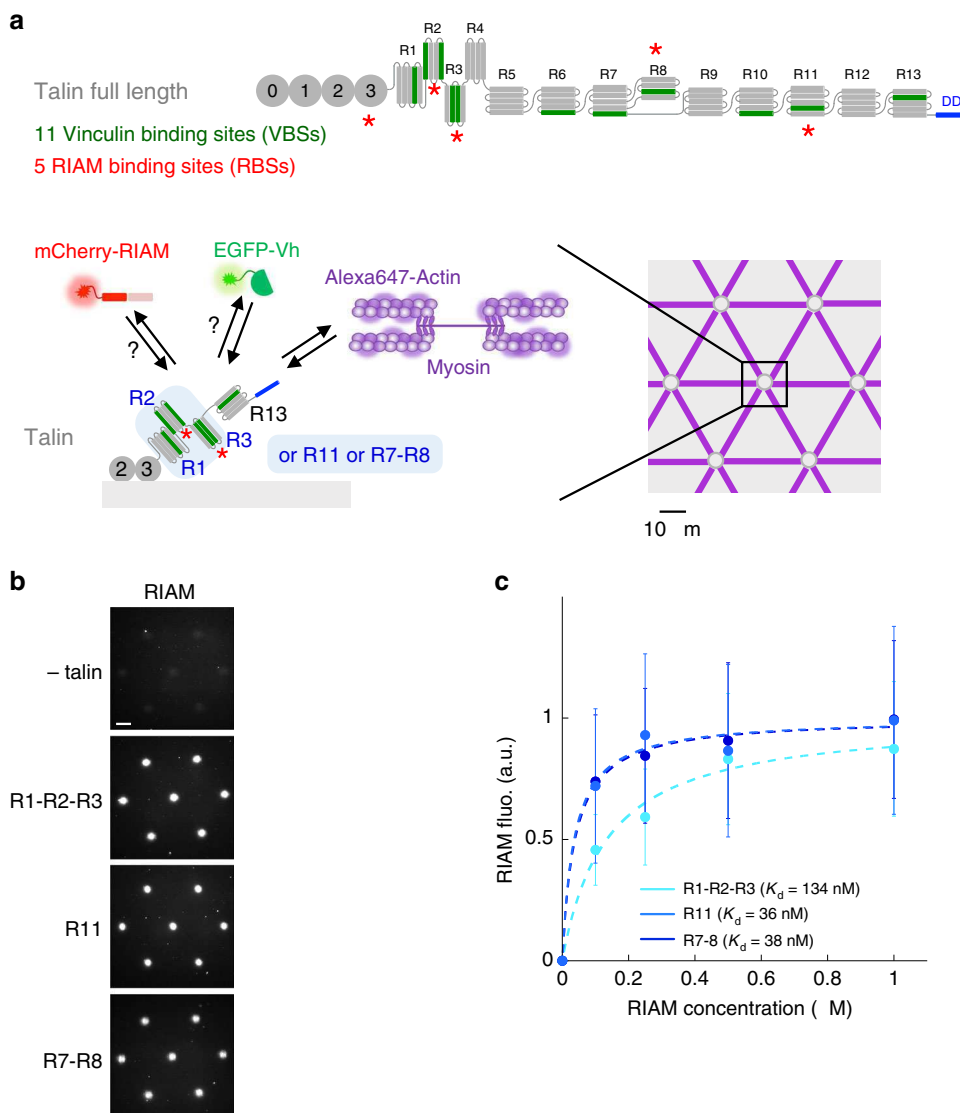


**Fig. 1 In vitro reconstitution of talin-RIAM complexes.** **a** Top panel: organization of full-length talin featuring RIAM- and vinculin-binding sites. The vinculin-binding sites (VBSs) are the dark green helices. RIAM binds to the R2, R3, R8, and R11 domains of talin. R13 is the C-terminal actin-binding domain (ABD) of talin. Bottom panels: basic principle of the in vitro microscopy assay. Alexa647-labeled actin and myosin II self-assemble to apply force to talin R1-R2-R3, R11, or R7-R8 immobilized in micropatterns, which controls the binding of EGFP-vinculin head (EGFP-Vh) and mCherry-RIAM. Talin is represented as a monomer for convenience but it contains a dimerization domain (DD). **b** Representative images of the fluorescence of mCherry-RIAM 1-306 (1  $\mu$ M) in non-coated control disks and disks coated with 1  $\mu$ M talin R1-R2-R3 or R11, or R7-R8. Scale bar = 10  $\mu$ m. This experiment was repeated three times independently with the same results. **c** Binding of RIAM to disks coated with talin R1-R2-R3, R11, and R7-R8. Conditions: 0-1  $\mu$ M mCherry-RIAM 1-306, 1  $\mu$ M of talin during the coating step. Data are mean  $\pm$  SD.  $n = 150$  disks all points, except (R1-R2-R3 + 0.5  $\mu$ M RIAM)  $n = 137$  disks. Source data are provided as a Source data file.

we measured the variation in fluorescence of mCherry-RIAM in talin-coated disks submitted to the force of the actomyosin cytoskeleton. Here, the delay of actomyosin accumulation in the disks makes the onset of force application easy to correlate with force-dependent events. The time lapses and the kymographs revealed that RIAM starts to dissociate from talin R1-R2-R3-coated disks as soon as actomyosin accumulates (Fig. 3a, b, e, Supplementary Movie 4). At the end of the kinetics, 50% of RIAM is dissociated from talin (Fig. 3e). As a control, we also showed that the fluorescence of RIAM bound to talin R1-R2-R3 is stable in the absence of actomyosin (Fig. 3a, b, e, Supplementary Movie 4). Like the actomyosin-dependent binding of Vh to talin constructs, the actomyosin-dependent dissociation of RIAM from this minimal talin does not require

the polymerization of actin, nor the formation of actomyosin bundles, and depends on the presence of myosin II in the assay (Supplementary Fig. 3c, d). This result demonstrates the mechanosensitivity of the talin-RIAM interaction. We used the same method to test the mechanosensitivity of the other two RIAM-binding sites of talin. Similarly, we observed that the actomyosin force triggers the efficient dissociation of RIAM from talin R11 (Fig. 3c, f, Supplementary Movie 5). However, we found that the actomyosin force only provokes a mild dissociation of RIAM from talin R7-R8 in the presence of the same concentration of actin and myosin used to stimulate R1-R2-R3 and R11 (Fig. 3d, g, Supplementary Movie 6). This result is in agreement with the weak mechanosensitivity of talin R7-R8 observed in Fig. 2g.



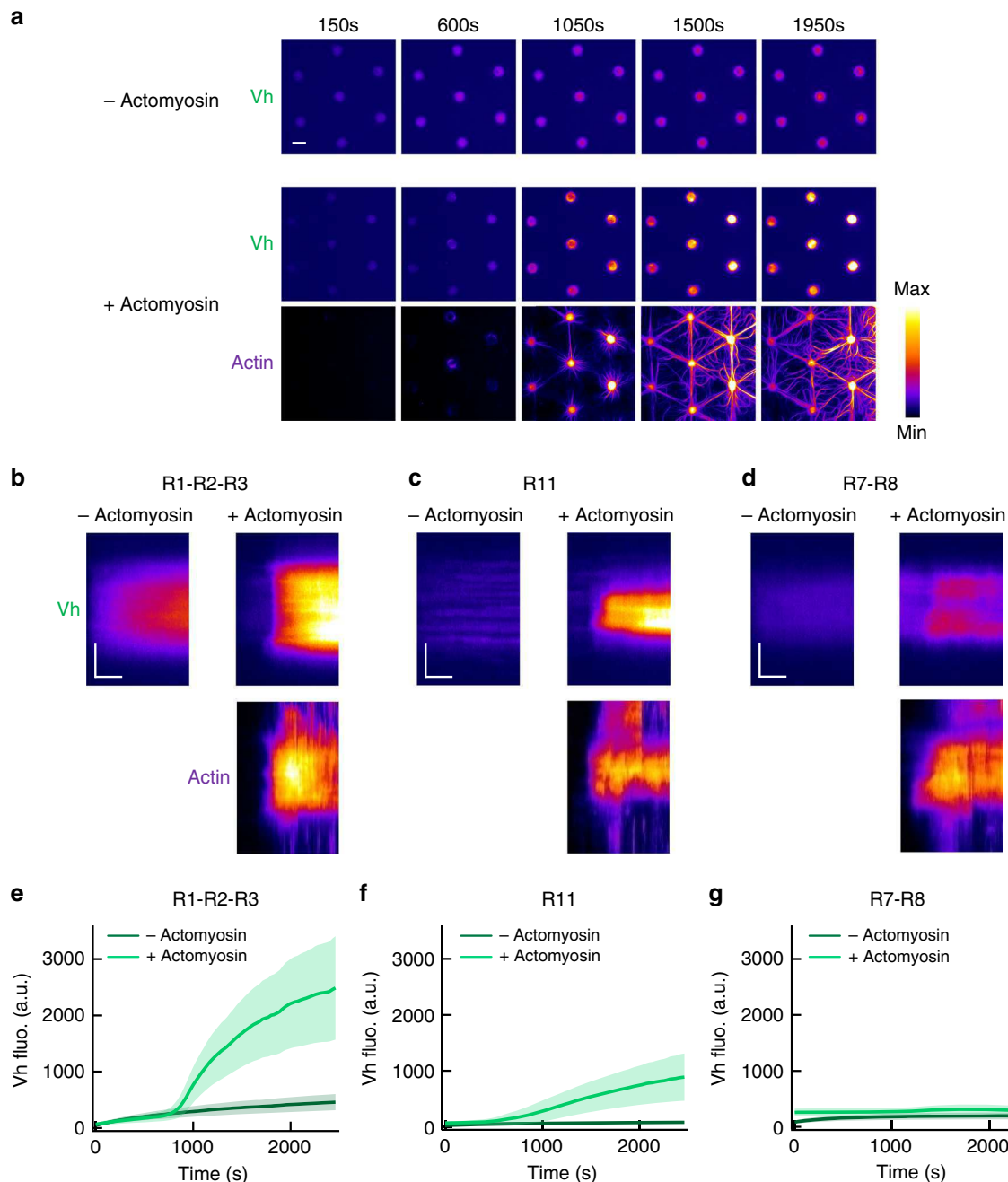


**Fig. 2 Talin domains bind to vinculin differently in response to the actomyosin force.** **a** Time lapses showing the recruitment of Vh to talin R1-R2-R3-coated disks in the absence (top) or presence of actomyosin (Vh is shown on the middle and actin on the bottom panel). This experiment was repeated five times independently with the same results. **b-d** Kymographs of EGFP-Vh (top) and actin (bottom) along a cross-section of a disk coated with talin R1-R2-R3 (**b**) or R11 (**c**) or R7-R8 (**d**) in the absence (left) or presence (right) of actomyosin. Conditions: 100 nM EGFP-Vh, 2.4  $\mu$ M actin (2% Alexa594-labeled), 50 nM myosin, and 1  $\mu$ M talin during the coating step. The images are color coded using the fire LUT of ImageJ. Scale bar in time lapses = 10  $\mu$ m. In kymographs, horizontal bar = 500 s, vertical bar = 5  $\mu$ m. **e-g** Kinetics of the mean fluorescence of EGFP-Vh corresponding to the conditions described in (**b-d**). Data are mean  $\pm$  SD. **e**  $n = 80$  (-actomyosin),  $n = 60$  disks (+actomyosin). **f**  $n = 60$  (-actomyosin),  $n = 75$  disks (+actomyosin). **g**  $n = 80$  (-actomyosin),  $n = 76$  disks (+actomyosin). Source data are provided as a Source data file. See Supplementary Movie 1, Supplementary Movie 2, and Supplementary Movie 3.

### Actomyosin-induced exchange of RIAM for vinculin on talin.

To determine the relationship between the mechanosensitive talin-RIAM and talin-vinculin interactions observed in Fig. 2 and Fig. 3, we compared the kinetics of RIAM, Vh, and actin in disks coated with talin R1-R2-R3 and talin R11 in our assay. The time lapses and the kymographs revealed that actomyosin

accumulation is associated with the concomitant RIAM dissociation and Vh association in disks coated with talin R1-R2-R3 (Fig. 4a, b, d, Supplementary Movie 7) and talin R11 (Fig. 4c, f, Supplementary Movie 8). The kinetics halftimes indicate a clear sequence in which actomyosin accumulation is followed by RIAM dissociation and Vh association (Fig. 4d, f). Our observations are

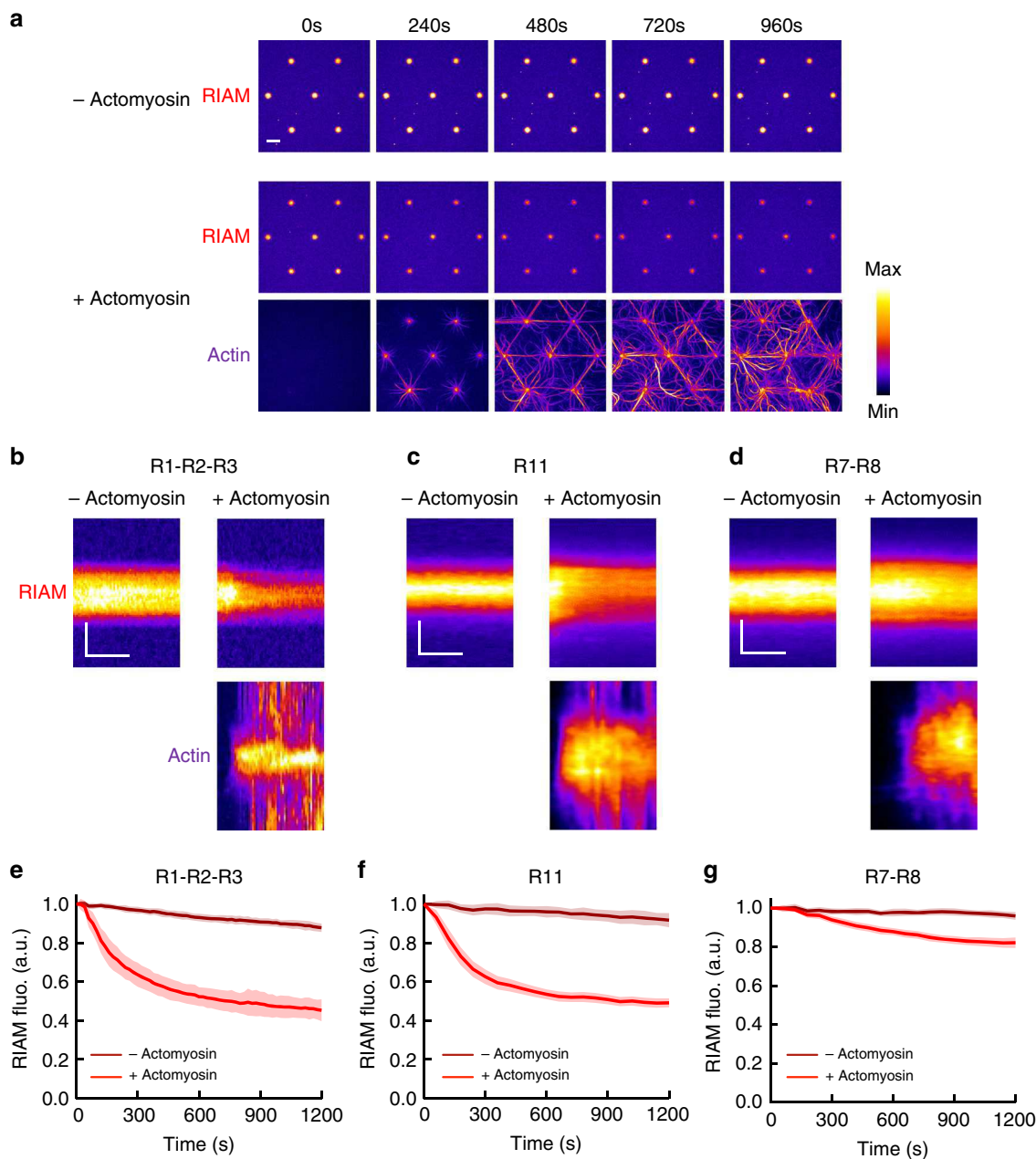


**Fig. 3 The actomyosin force provokes RIAM dissociation from several talin domains.** **a** Time lapses showing the binding of RIAM 1-306 to talin R1-R2-R3-coated disks in the absence (top) or presence of actomyosin (RIAM is shown on the middle and actin on the bottom panel). This experiment was repeated 11 times independently with the same results. **b-d** Kymographs of mCherry-RIAM 1-306 (top) and actin (bottom) along a cross-section of a disk coated with talin R1-R2-R3 (**b**) R11 (**c**) or R7-R8 (**d**) in the absence (left) or presence (right) of actomyosin. For better comparison, the fluorescence of mCherry-RIAM 1-306 in kymographs was normalized as the maximal fluorescence in the R11- and R7-R8-coated disks. Conditions: 100 nM mCherry-RIAM 1-306, 2.4  $\mu$ M actin (1% Alexa647-labeled for R1-R2-R3, 2% Alexa488 for R11 and R7-R8), 50 nM myosin, 1  $\mu$ M talin during the coating step. The images are color coded using the fire LUT of ImageJ. Scale bar in time lapses = 10  $\mu$ m. In kymographs, horizontal bar = 500 s, vertical bar = 5  $\mu$ m. **e-g** Kinetics of the mean fluorescence of mCherry-RIAM 1-306 corresponding to the conditions described in (**b-d**). Data are mean  $\pm$  SD. **e**  $n = 63$  (–actomyosin),  $n = 62$  disks (+actomyosin). **f**  $n = 50$  (–actomyosin),  $n = 60$  disks (+actomyosin). **g**  $n = 49$  (–actomyosin),  $n = 60$  disks (+actomyosin). Data were first normalized to 1 as the maximal mCherry-RIAM 1-306 fluorescence and synchronized using this maximal value as  $t_0$  before being averaged. Source data are provided as a Source data file. See Supplementary Movie 4, Supplementary Movie 5, and Supplementary Movie 6.

consistent with a mechanism in which talin switches from a RIAM-specific conformation to a vinculin-specific one. Alternatively, actomyosin could trigger a competition between RIAM and Vh for talin. However, Vh does not affect the dissociation rate of RIAM from talin R1-R2-R3 nor from talin R11 (Fig. 4e, g). The fact that Vh binding to talin follows RIAM dissociation, without influencing it, rules out a direct competition mechanism

and demonstrates that talin behaves as a force-dependent conformational switch.

**Effect of RIAM on the force-induced vinculin–talin complex.** Although Vh does not affect RIAM dissociation (Fig. 4e, g), RIAM could affect talin stretching and its subsequent binding to

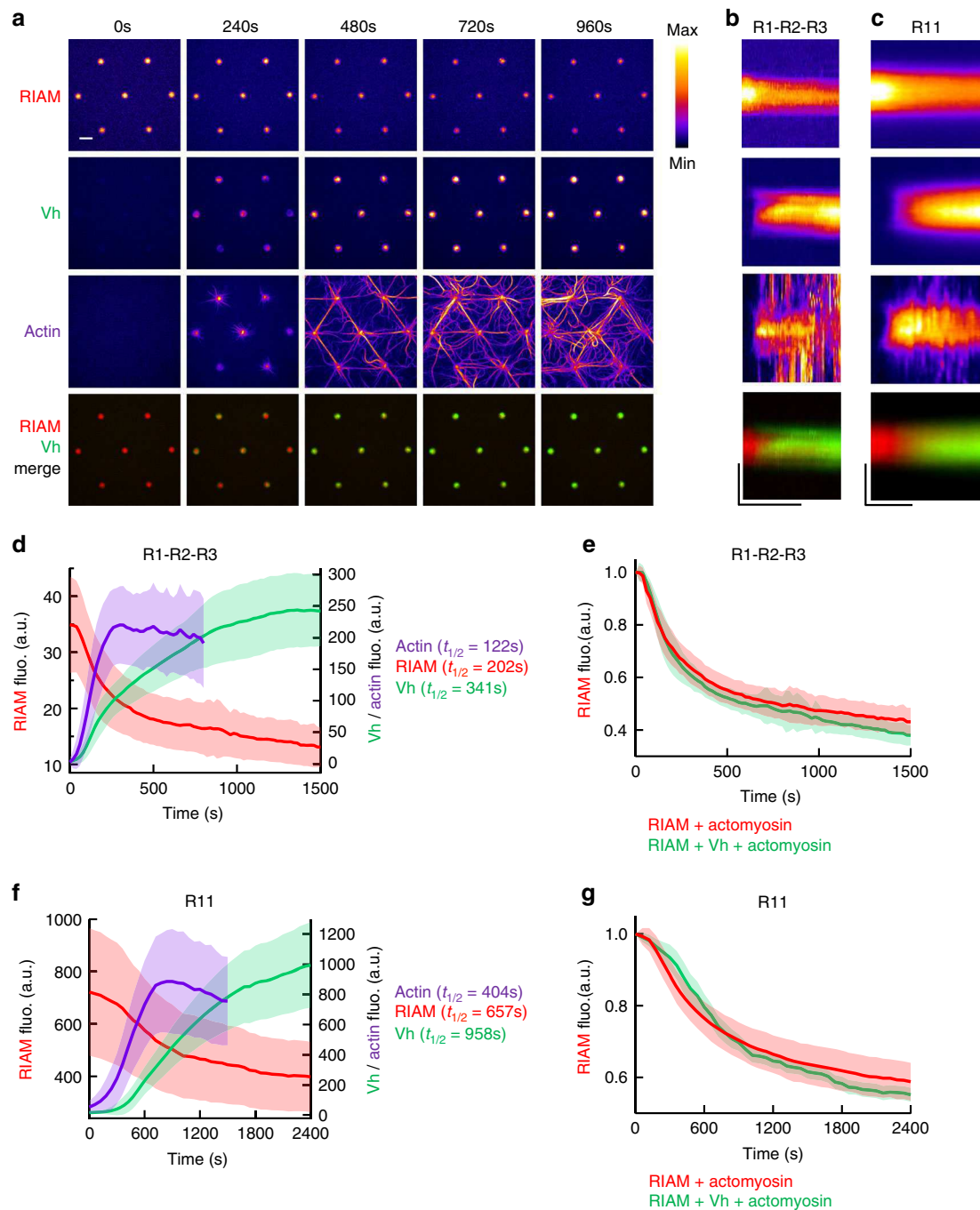


**Fig. 4** The actomyosin force provokes the sequential exchange of RIAM for vinculin on talin. **a** Time lapses showing the concomitant dissociation of RIAM 1-306, association of Vh, accumulation of actomyosin, and a Vh/RIAM merge in the same disks coated with talin R1-R2-R3. This experiment was repeated 4 times independently with the same results. **b, c** From top to bottom: kymographs of RIAM, Vh, actin, and Vh/RIAM merge along the cross-section of a disk coated with talin R1-R2-R3 (**b**) or R11 (**c**). Conditions: 100 nM mCherry-RIAM, 100 nM EGFP-Vh, 2.4  $\mu\text{M}$  actin (1% Alexa647-labeled), 50 nM myosin, and 1  $\mu\text{M}$  talin during the coating step. The images are color coded using the fire LUT of ImageJ. Scale bar in time lapses = 10  $\mu\text{m}$ . In kymographs, horizontal bar = 1000 s, vertical bar = 5  $\mu\text{m}$ . **d, f** Kinetics of the mean fluorescence of mCherry-RIAM 1-306, EGFP-Vh and Alexa647-labeled actin in disks coated with talin R1-R2-R3 (**d**) and R11 (**f**) corresponding to the conditions described in (**b**) and (**c**). Actin fluorescence is multiplied by 3. Data are mean  $\pm$  SD.  $n = 63$  (**d**),  $n = 59$  disks (**f**). **e** Kinetics of mCherry-RIAM 1-306 dissociation from disks coated with talin R1-R2-R3 in the presence of actomyosin with or without 100 nM EGFP-Vh as described in Fig. 3b and **b** respectively.  $n = 62$  (RIAM + actomyosin),  $n = 63$  disks (RIAM + Vh + actomyosin). **g** Kinetics of mCherry-RIAM 1-306 dissociation from disks coated with talin R11 in the presence of actomyosin with or without 100 nM EGFP-Vh as described in Fig. 3c and **c** respectively.  $n = 59$  disks. **e, g** Data are mean  $\pm$  SD. Data were first normalized to 1 as the maximal mCherry-RIAM 1-306 fluorescence and synchronized using this maximal value as  $t_0$  before being averaged. Source data are provided as a Source data file. See Supplementary Movie 7 and Supplementary Movie 8.

Vh. We therefore measured the effect of a high concentration of RIAM on the actomyosin-dependent binding of Vh to talin. A weak interaction between Vh and RIAM has been reported ( $K_d = 5 \mu\text{M}$ ) and could affect our interpretations<sup>33</sup>. However, this weak interaction cannot compete with the high affinity binding of Vh for a construct of talin corresponding to R1–R2–R3 in which one VBS (helix 12) is exposed ( $K_d = 140 \text{ nM}$ )<sup>36</sup>. Similarly, this weak interaction between Vh and RIAM is unlikely to affect the high affinity binding of RIAM 1–306 to our talin R1–R2–R3 and talin R11 ( $K_d = 36 \text{ nM}$  and  $134 \text{ nM}$  respectively, Fig. 1c). In addition, we showed that Vh does not affect the constitutive binding of RIAM to talin R1–R2–R3 in the absence of actomyosin (Supplementary Fig. 4), demonstrating that RIAM and Vh do not sequester each other through direct binding in our experimental conditions. After this clarification, we showed that the actomyosin-dependent binding of Vh to talin R1–R2–R3 is severely impaired by a high concentration of RIAM, compared with the control without RIAM (Fig. 5a, b, Supplementary Movie 9). Kinetic analysis and steady-state measurement confirmed that the final level of Vh bound to stretched talin is lower in the presence of RIAM (Fig. 5d, f), suggesting that the talin–RIAM complex requires a higher force for unfolding than talin alone. Our observations demonstrate that RIAM protects talin R2–R3 bundles from mechanical unfolding, which implies that the force-dependent dissociation of RIAM is a prerequisite for the exposure of VBSs in R2–R3. Surprisingly, RIAM does not affect the actomyosin-dependent binding of Vh to talin R11, at the concentration tested for talin R1–R2–R3 ( $0.5 \mu\text{M}$ ) and at a higher concentration ( $3 \mu\text{M}$ ) (Fig. 5c, e, g, Supplementary Movie 10). Therefore, unlike talin R1–R2–R3, the dissociation of RIAM from talin R11 is not a prerequisite for the force-dependent binding of vinculin.

## Discussion

Our *in vitro* reconstitution demonstrates that talin dissociates from RIAM and associates to vinculin sequentially in response to the actomyosin force. The force-dependent dissociation of the talin–RIAM interaction is one of the rare elementary mechanosensitive reactions of adhesion complexes which has been discovered. This process could control the mechanosensitive maturation of FAs (Fig. 6a).

We found that RIAM protects R2–R3 against stretching and its dissociation is a prerequisite for vinculin binding. Such a bistable mechanism is the desirable behavior for a mechanosensitive switch involved in a cellular decision-making process. This behavior likely results from the overlap between the RIAM-binding sites and VBSs in R2 and R3<sup>33</sup>. R1–R2–R3 is a key mechanosensitive part of talin, since a construct, almost identical to our talin R1–R2–R3, can rescue spreading, polarization and migration of talin null cells<sup>37</sup>. In this region of talin, R3 has a critical role, since mutations that destabilize this bundle affect ECM sensing<sup>38</sup>. The stretching of single molecules clearly revealed that R3 is the weakest bundle of the R1–R2–R3 region and should unfold first in response to force<sup>19,20</sup>. The inhibition of the mechanical exposure of VBSs in talin R1–R2–R3 by RIAM could therefore result from the stabilization of R3.

Our study reveals that talin R11 binds to vinculin in response to force. In contrast with talin R1–R2–R3, the mechanosensitive binding of R11 to vinculin is not affected by RIAM. Although the structure of the R11–RIAM complex is not known, our data suggest that the binding sites for RIAM and vinculin do not overlap in R11. Talin R11 can therefore dissociate from RIAM and associate to vinculin independently. Interestingly, simulations predicted that the first and last helices of the mechanically-stretched R11 should unfold first, leaving a 3-helix intermediate

bundle containing a cryptic VBS<sup>39</sup>. Whether RIAM dissociates after the detachment of these first and last helices of R11 remains to be determined.

The different effects of RIAM on talin R1–R2–R3 and R11 imply that RIAM increases the threshold force for the exposure of the VBSs located in R2–R3 but does not affect the exposure of the single VBS of R11. However, the sequential exchange of RIAM for vinculin on talin R11 implies that the force required to dissociate RIAM is lower than the one required to expose the single VBS of R11 (Fig. 6b).

R7–R8 is difficult to stretch in conditions that provoke both RIAM dissociation and vinculin association for R1–R2–R3 and R11 (Fig. 6b). In response to force, Vh does not bind to the two VBSs located in R7 and R8 for several possible reasons. The single VBS of R8 is probably not exposed because R8 is protected from unfolding by its insertion in R7. The single VBS of R7 could remain stably attached to R7 in response to force or, if exposed, its affinity for Vh is low as previously reported<sup>40</sup>. The weak dissociation of RIAM and the total absence of vinculin association suggest that the RIAM-binding site is disrupted at a level of force that is not sufficient to expose the single VBS of R8. Altogether, our observations are in agreement with a previous report showing that unfolding of isolated R8 occurs at a force of  $5 \text{ pN}$ , whereas unfolding of R7–R8 occurs at  $15 \text{ pN}$ , demonstrating that R8 is mechanically protected by its insertion in R7<sup>18</sup>. Mutations that prevent the mechanical stretching of R7 favor signaling cascades downstream of R8, revealing the importance of this mechanosensitive reaction controlled by a high threshold force<sup>41</sup>.

The mechanosensitivity of the domains of talin is influenced by their position relative to the ABDs in the full-length protein. By placing FRET sensors at different positions along talin, Ringer et al. revealed an intramolecular tension gradient characterized by high forces between the head and ABD2 and lower forces between ABD2 and ABD3<sup>42</sup>. However, we showed that a construct composed of R1–R2–R3 fused to ABD2 is not stretched compared with the same construct where ABD2 is replaced by ABD3 (Supplementary Fig. 5). This result can be easily explained by the fact that ABD2 is masked by R3 in talin<sup>23</sup>. The traction force applied to ABD3 would unfold R3, leading to the exposure of ABD2. The fact that R8 is the C-terminal part of ABD2 allows alternative interpretations of the weak mechanosensitivity of R7–R8<sup>23</sup>. Indeed, we cannot exclude that the binding of actin filaments stabilizes R8 and prevents RIAM dissociation and vinculin association. Alternatively, if actomyosin generates a pulling force on R13 (ABD3) and R7–R8 (ABD2) simultaneously, the apparent tension between R13 and R7–R8 could be reduced, as suggested by FRET measurement in cells<sup>42</sup>, leading to weak dissociation of RIAM and association of vinculin.

The structure of talin reveals auto-inhibitory contacts between F3 and R9, and also F2 and R12<sup>43,44</sup>. RIAM binding to the talin rod does not require the disruption of the F3–R9 autoinhibition<sup>35</sup>. In contrast, the release of the F3–R9 intramolecular contact appears critical to initiate talin–vinculin interaction independently of force application in nascent adhesion<sup>45</sup>. However, this talin conformation can be further stretched to recruit more vinculin in FAs. Whether the disruption of the talin auto-inhibitory contacts facilitates the stretching of individual bundles to dissociate RIAM and bind vinculin remains to be determined. It would also be interesting to determine whether the recently reported autoinhibition of RIAM controls its interaction with talin<sup>46</sup>.

Vinculin autoinhibition influences the mechanosensitivity of the talin–vinculin complex. Several biochemical, structural, and cellular studies compared the recruitment of the constitutively active Vh and the autoinhibited full-length vinculin (VFL) in FAs, leading to apparent discrepancies. In cells, Vh remains associated

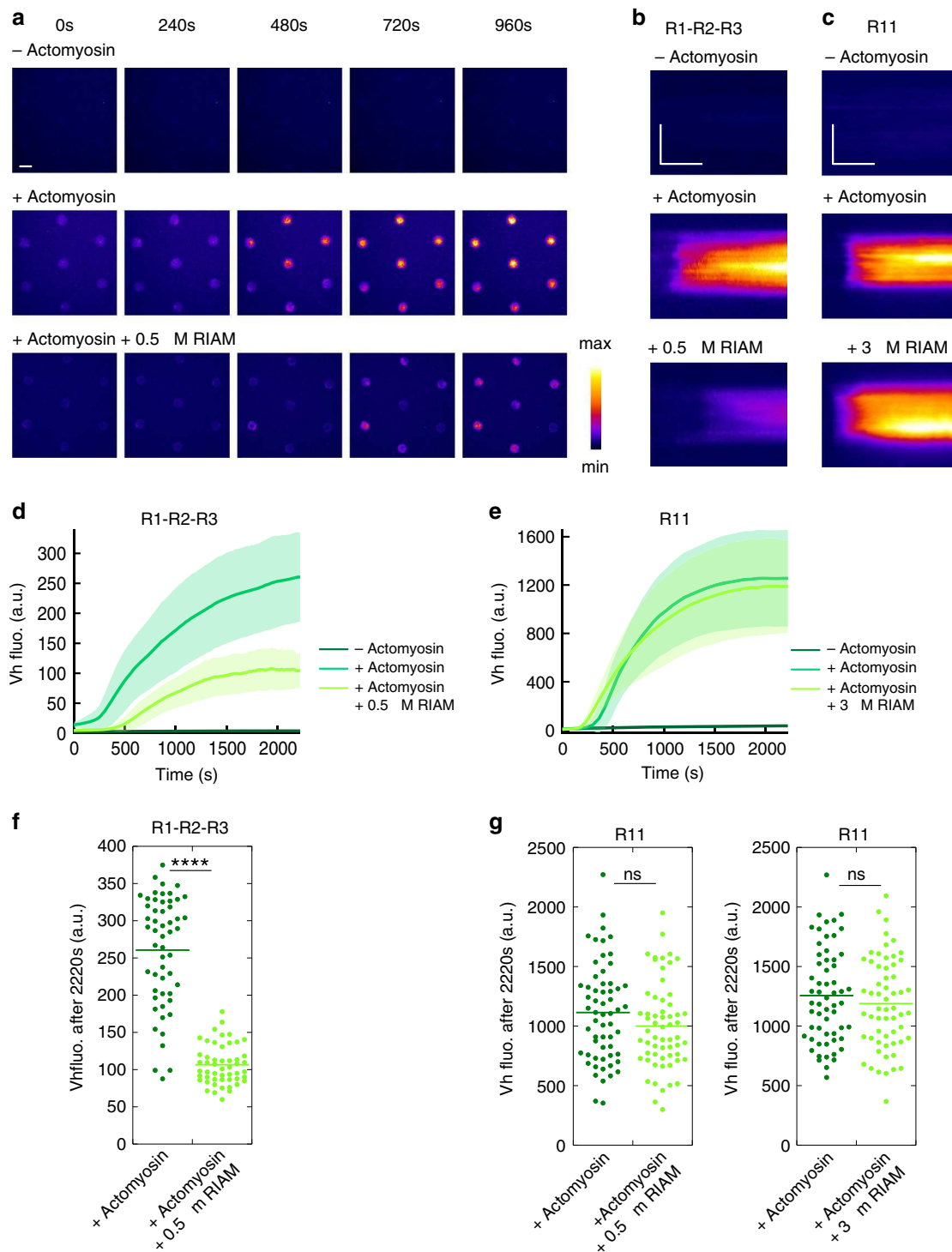


**Fig. 5** RIAM inhibits the actomyosin-dependent binding of vinculin to talin R1-R2-R3 but not to R11. **a** Time lapse showing the recruitment of Vh in disks coated with talin R1-R2-R3 in the absence of actomyosin (top), presence of actomyosin (middle), and presence of actomyosin and RIAM (bottom). This experiment was repeated twice independently with the same results. **b, c** Kymographs of EGFP-Vh along a cross-section of a disk coated with talin R1-R2-R3 (**b**) and R11 (**c**). Conditions: 100 nM EGFP-Vh, 2.4  $\mu$ M actin, 50 nM myosin, 500 nM (**b**) or 3  $\mu$ M (**c**) mCherry-RIAM, 1  $\mu$ M talin during the coating step. The images are color coded using the fire LUT of ImageJ. Scale bar in time lapses = 10  $\mu$ m. In kymographs, horizontal bar = 1000 s, vertical bar = 5  $\mu$ m. **d, e** Kinetics of the mean fluorescence of EGFP-Vh corresponding to the conditions described in (**b, c**). Data are mean  $\pm$  SD. **d**  $n = 54$  (–actomyosin) and (+actomyosin),  $n = 51$  disks (+actomyosin + 0.5  $\mu$ M RIAM). **e**  $n = 59$  disks. **f, g** Steady-state binding of Vh (2220 s after sealing the chamber) in disks coated with talin R1-R2-R3 (**f**) or R11 (**g**) in the absence and presence of RIAM. **f, g** Same conditions as in (**b, c**). Each data point represents the mean fluorescence of Vh in one disk. The bar shows the mean. **f**  $n = 54$  (+actomyosin),  $n = 51$  disks (+actomyosin + 0.5  $\mu$ M RIAM). A significant difference was found using a two-tailed  $t$  test ( $P = 3.95 \times 10^{-22}$ ). **g** Left panel:  $n = 60$ . No significant difference was found using a two-tailed  $t$  test ( $P = 0.1126$ ). Right panel:  $n = 59$  disks. No significant difference was found using a two-tailed  $t$  test ( $P = 0.3575$ ). \*\*\*\* $P < 0.0001$  using a two-tailed  $t$  test; ns nonsignificant. Source data are provided as a Source data file. See Supplementary Movie 9 and Supplementary Movie 10.

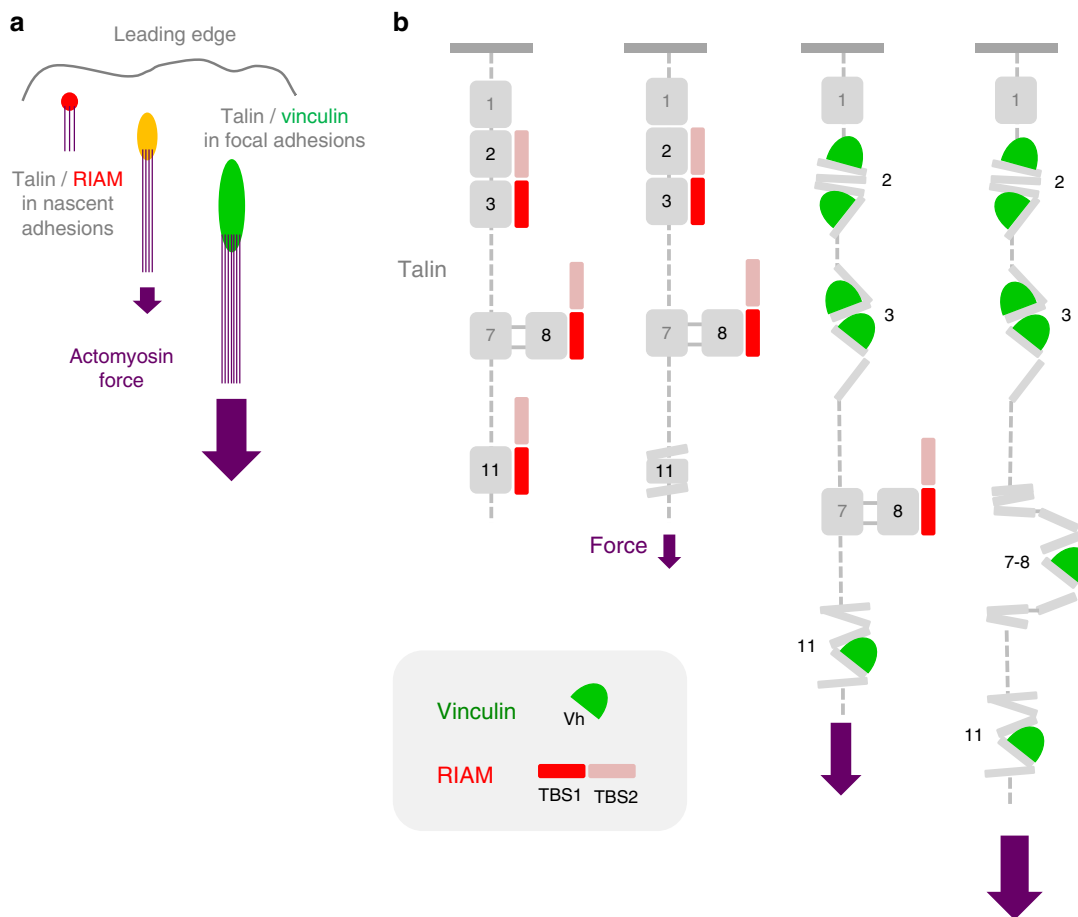


**Fig. 6 Model for the actomyosin-dependent binding of RIAM and vinculin to talin.** **a** Scheme illustrating that RIAM, which is initially enriched in nascent adhesions, is replaced by vinculin in mature FAs in response to the force exerted by the actomyosin stress fibers. **b** Model describing how talin dissociates from RIAM and associates to vinculin sequentially in response to the actomyosin force.

to talin in FAs after myosin inhibition by blebbistatin, whereas VFL dissociates<sup>24,47,48</sup>. The recruitment of VFL to FAs is restored by cell stretching, demonstrating the force-dependence of the talin–vinculin interaction, whereas Vh binding is not increased<sup>24</sup>. The slow dissociation of Vh from talin after force release, observed *in vitro*<sup>20,21</sup>, could explain the slow dissociation of Vh in cells after blebbistatin treatment, whereas the fast dissociation of VFL could result from the reassociation of the tail to the head of vinculin in the absence of actomyosin. Indeed, actomyosin force acts on vinculin to maintain the active open conformation of vinculin<sup>48,49</sup>. The saturation of talin by Vh would explain why talin does not recruit more Vh after cell stretching. Thus, *in vitro*, and probably in cells, the mechanosensitivity of the talin–Vh interaction depends on Vh concentration. Because Vh is not autoinhibited like VFL, it binds to partially exposed VBSs in the least stable helical bundles of non-stretched talin, provided that Vh concentration is high enough<sup>21</sup>. At the low concentration of Vh used in our past and present *in vitro* studies (22–100 nM), Vh mimics VFL by displaying a very weak constitutive binding, which is greatly enhanced by the application of actomyosin force to talin (Fig. 2e).

Talin bundles have several binding partners other than RIAM and vinculin. Interestingly, talin R7 interacts with KANK and R8 interacts with both DLC and paxillin<sup>33,41,50,51</sup>. The catch-to-slip bond switching behavior of the R7–KANK complex is thought to control KANK recruitment at FAs<sup>52</sup>. The mechanical unfolding of R8 should provoke the dissociation of DLC from talin, leading to upregulation of actomyosin contractility, and acceleration of

cell migration<sup>41</sup>. Interestingly, R11 interacts with the  $\beta$ -subunit of integrins. However, it is not known whether R11, like the F3 subdomain of the head, promotes the inside–out activation of integrins and whether this activity is influenced by the force-dependent dissociation of RIAM and association of vinculin. This high number of combinations of talin partners, associated with specific mechanically-stretched talin conformations, provides the cell with a precise means of informing itself about variations in intracellular and extracellular forces. Conversely, the binding of talin partners, as exemplified by the present study on RIAM, can modify the mechanosensitivity of talin bundles differently, leading to a change in the hierarchy of their response to force.

**Methods**

**cDNA constructs.** All talin constructs are derived from a cDNA encoding for human talin-1 containing a C-terminal His<sub>6</sub> tag. Talin R1–R2–R3, corresponding to F2–F3–R1–R2–R3–R13, was cloned into a pETM plasmid with an N-terminal StrepTagII and a C-terminal His<sub>6</sub> tag. This construct was made in three steps. First the R2–R3 fragment was PCR amplified using primers 1 and 2 and cloned into the KpnI/BamHI sites of pETM, leading to the intermediate plasmid pETM–R2–R3. R13 was PCR amplified using primers 3 and 4 and cloned into the BamHI/EcoRI sites of pETM–R2–R3, leading to the intermediate plasmid pETM–R2–R3–R13. Finally, F2–F3–R1–R2–R3 was PCR amplified using primers 5 and 6 and cloned into the KpnI/NcoI sites of the pETM–R2–R3–R13, leading to pETM–F2–F3–R1–R2–R3–R13. Talin R11, corresponding to F2–F3–R11–R13 and talin R7–R8, corresponding to talin F2–F3–R7–R8–R13 were cloned into a pET–29a(+) plasmid with an N-terminal StrepTagII and a C-terminal His<sub>6</sub> tag. Talin R7–R8 and R11 have been synthesized by Genscript. The cDNAs encoding for talin F2–F3 (talin 196–405), talin F2–F3–R1–R2–R3 (talin 196–911), and talin R1–R8 (talin 196–1659) were PCR amplified using the primer pairs 7–8, 7–9, 7–10 and cloned into the BamH/XhoI, BamHI/EcoRI, and BamHI/EcoRI sites, respectively, of a

pGEX6P1 plasmid (GE Healthcare) with an N-terminal GST tag and a C-terminal His<sub>6</sub> tag. Our constructs do not include the F0 and F1 subdomains of the head (talin 1–195) because this part of talin reduces the expression quality in our hands and is not involved in the binding of RIAM and vinculin. A preexisting cDNA encoding for human vinculin 1–851, corresponding to Vh, was cloned into the Sall/NotI sites of a homemade pGEX-6P1-EGFP plasmid. The cDNA encoding for mouse RIAM 1-306 was PCR amplified using primers 11 and 12, and cloned into the BamHI/XhoI sites of a homemade pGEX-6P2-mCherry plasmid with a C-terminal His<sub>6</sub> tag. Primers used for cloning the DNA constructs in this study are listed in Supplementary Table 1.

**Protein purification.** All the recombinant proteins were expressed in *Escherichia coli* (BL21 DE3, Invitrogen). After transformation, bacteria were grown in 4–12 l of LB medium containing 0.1 mg ml<sup>-1</sup> of ampicillin or kanamycin at 37 °C until absorbance reached 0.8 at 600 nm. The recombinant proteins were expressed upon addition of 1 mM isopropyl-β-D-thiogalactoside for 16 h at 16 °C. After centrifugation, the bacterial pellet was submitted to specific purification steps<sup>22</sup>.

Talin R1–R2–R3, R11, and R7–R8 were bound to Ni-NTA (Ni<sup>2+</sup>-nitrilotriacetic acid)-Agarose (Macherey-Nalge), washed with 50 mM Tris pH 7.8, 500 mM NaCl, 20 mM imidazole, 1 mM β-mercaptoethanol (BME), eluted with 50 mM Tris pH 7.8, 500 mM NaCl, 250 mM imidazole, 1 mM BME, dialyzed in 20 mM Tris pH 7.8, 100 mM KCl, 1 mM DTT, frozen in liquid nitrogen, and stored at –80 °C.

mCherry-RIAM 1-306, talin F2–F3, F2–F3–R1–R2–R3, R1–R8, and EGFP-Vh containing a N-terminal GST (Glutathione-S-transferase) tag, were bound to glutathione-Sepharose (GE Healthcare), washed with 50 mM Tris pH 7.8, 500 mM NaCl, and eluted with 50 mM Tris pH 7.8, 500 mM NaCl and 50 mM reduced L-Glutathione (Sigma-Aldrich). For mCherry-RIAM 1-306 and EGFP-Vh, GST was cleaved by PreScission protease (GE Healthcare) in 50 mM Tris pH 7.8 and 500 mM NaCl and GST was eliminated by Glutathione-Sepharose chromatography. mCherry-RIAM 1-306 and talin F2–F3, F2–F3–R1–R2–R3, and R1–R8 were then bound to Ni-NTA-Agarose, washed with 50 mM Tris pH 7.8, 500 mM NaCl, 20 mM imidazole, eluted with 50 mM Tris pH 7.8, 500 mM NaCl, 250 mM imidazole, dialyzed in 20 mM Tris pH 7.8, 100 mM KCl, 1 mM DTT, frozen in liquid nitrogen and stored at –80 °C. EGFP-Vh was further centrifuged at 300,000 × g for 30 min, purified by gel filtration (Superdex 200, 16/60, GE Healthcare) in 20 mM Tris pH 7.5, dialyzed in 20 mM Tris pH 7.8, 100 mM KCl, frozen in liquid nitrogen, and stored at –80 °C.

Actin was purified from rabbit skeletal muscle acetone powder. After cycles of polymerization and depolymerization, actin was gel filtered on a Superdex G-200 column (GE Healthcare) in 5 mM Tris pH 7.8, 0.2 mM ATP, 0.1 mM CaCl<sub>2</sub>, 1 mM DTT. Actin was labelled with Alexa Fluor 488, 594, and 647 Succinimidyl Ester (Invitrogen)<sup>22</sup>. Myosin II was extracted from rabbit skeletal muscles in a buffer containing 500 mM KCl, 100 mM K<sub>2</sub>HPO<sub>4</sub>. After grinding and centrifugation, the actin-containing pellet is discarded. The supernatant is submitted to cycles of precipitation in low-salt buffer, centrifugation, and resuspension in high-salt buffer. Finally, the protein was dialyzed in 20 mM KH<sub>2</sub>PO<sub>4</sub>/K<sub>2</sub>HPO<sub>4</sub> pH 7.5, 500 mM KCl, 1 mM EDTA, and stored at –20 °C after addition of 50% glycerol.

**Sample preparation for the in vitro assay.** Micropatterning was performed by modifying an existing method as follows<sup>53,54</sup>. Glass coverslips (22 mm × 32 mm, Thermo Scientific/Menzel-Glaser) were first washed with milliQ water and ethanol, sonicated and irradiated for 1 min under a deep UV lamp (Ossila). The coverslips were incubated for 2 h in 0.1 mg ml<sup>-1</sup> PLL-g-PEG (SuSoS) dissolved in 10 mM HEPES pH 7.8 and washed with milliQ water. The chrome-quartz photomask (Toppan, France), designed with disks of 5 μm in diameter, regularly spaced by 30 μm (Fig. 1a), was cleaned by deep UV irradiation for 1 min, placed on the PLL-g-PEG-coated coverslip, and exposed to deep UV for 3 min. The chamber was made of a micropatterned coverslip attached to a glass slide (Super Frost, Thermo Scientific) with double-sided adhesive tape. The volume of a typical chamber was 50 μl. The chamber was first incubated with talin (1 μM) for 5 min at room temperature. Unbound talin was washed out with 200 μl of F-buffer (10 mM Tris pH 7.8, 25 mM KCl, 1 mM MgCl<sub>2</sub>, 0.2 mM CaCl<sub>2</sub>, 1 mM DTT). The surface of the disks was passivated with 100 μl of F-buffer containing 10% BSA for 5 min at room temperature and washed with 200 μl F-buffer. Finally, 100 μl of the reaction was added and the chamber was sealed with VALAP (1:1:1 mixture of vaseline, lanolin, and paraffin). A typical reaction contained: 2.4 μM actin (containing 1% Alexa647-labeled or 2% Alexa488-labeled or 2% Alexa561-labeled actin), 50 nM myosin II, 1% BSA, a salt mix (2 mM MgCl<sub>2</sub>, 0.2 mM EGTA, and 25 mM KCl), and an ATP regenerating mix (2 mM ATP, 2 mM MgCl<sub>2</sub>, 10 mM creatine phosphate, 3.5 U/ml creatine kinase) in G-fluo buffer (10 mM Tris pH 7.8, 0.2 mM CaCl<sub>2</sub>, 0.4% methylcellulose, 5 mM DABCO and 20 mM DTT). Additional proteins such as EGFP-Vh and mCherry-RIAM 1-306 were also added. The gelsolin-capped actin filaments used in Supplementary Fig. 3 have been prepared by mixing the barbed-end capping protein gelsolin with actin filaments at a 1:600 gelsolin/actin molar ratio<sup>22</sup>.

**Microscopy observations.** Images were acquired with a Nikon Ti Eclipse E microscope equipped with a 60X oil immersion objective (Apochromat, 1.49 NA) and coupled to a sCMOS camera (Photometrics, Prime 95B or Hamamatsu, Orca

Flash04), using the spinning disk mode (Yokogawa CSU-X1-A1) or the TIRF mode. EGFP-Vh (or Alexa488-Actin), mCherry-RIAM 1-306 (or Alexa594-actin) and Alexa647-actin were excited with 488, 561, and 642 nm lasers, respectively.

**Data analysis.** Images were acquired with MetaMorph and analyzed with ImageJ. For steady-state data, each point of the dot plots represents the mean fluorescence of a single disk (background subtracted). The bar indicates the mean. Kinetics were obtained by averaging kinetics in a large number of single disks, after background subtraction, normalization, and synchronization on the maximal value of mCherry-RIAM for each disk (Figs. 3e–g, 4e, g), only synchronization (Fig. 4d, f), or only background subtraction (Figs. 2e–g, 5d, e, and Supplementary Fig. 5b, c).

The affinity of RIAM for talin constructs was obtained by plotting the average fluorescence of RIAM in a high number of talin-coated disks as a function of the total concentration of RIAM (Fig. 1c). Since we assumed that the amount of talin in the disks is negligible compared to the total concentration of RIAM in solution, we estimated the value of the K<sub>d</sub> as the concentration of RIAM at half saturation. Note that this assumption can only underestimate the affinity.

The graphs were assembled using Igor Pro or Kaleidagraph. Statistical analysis was performed using Student *t* test in Microsoft Excel. Experiments were reproduced 2–11 times with the same conclusions.

**Reporting summary.** Further information on research design is available in the Nature Research Reporting Summary linked to this article.

## Data availability

Data supporting this paper are available from the corresponding author upon reasonable request. A reporting summary for this article is available as a Supplementary Information file. The source data underlying Figs. 1c, 2e–g, 3e–g, 4d–g, 5d–g, and Supplementary Figs. 1b, 2, 3b, d, 4, 5b, c are provided as a Source data file. Source data are provided with this paper.

Received: 26 February 2020; Accepted: 26 May 2020;

Published online: 19 June 2020

## References

1. Le Clainche, C. & Carlier, M.-F. Regulation of actin assembly associated with protrusion and adhesion in cell migration. *Physiol. Rev.* **88**, 489–513 (2008).
2. Wehrle-Haller, B. Structure and function of focal adhesions. *Curr. Opin. Cell Biol.* **24**, 116–124 (2012).
3. Ciobanasu, C., Faivre, B. & Le Clainche, C. Integrating actin dynamics, mechanotransduction and integrin activation: the multiple functions of actin binding proteins in focal adhesions. *Eur. J. Cell Biol.* **92**, 339–348 (2013).
4. Schwarz, U. S. & Gardel, M. L. United we stand – integrating the actin cytoskeleton and cell–matrix adhesions in cellular mechanotransduction. *J. Cell Sci.* **125**, 3051–3060 (2012).
5. Bachmann, M., Kukkurainen, S., Hytönen, V. P. & Wehrle-Haller, B. Cell adhesion by integrins. *Physiol. Rev.* **99**, 1655–1699 (2019).
6. Romero, S., Le Clainche, C. & Gautreau, A. M. Actin polymerization downstream of integrins: signaling pathways and mechanotransduction. *Biochem. J.* **477**, 1–21 (2020).
7. Gardel, M. L., Schneider, I. C., Aratyn-Schaus, Y. & Waterman, C. M. Mechanical integration of actin and adhesion dynamics in cell migration. *Annu. Rev. Cell Dev. Biol.* **26**, 315–333 (2010).
8. Wolfenson, H., Yang, B. & Sheetz, M. P. Steps in mechanotransduction pathways that control cell morphology. *Annu. Rev. Physiol.* **81**, 585–605 (2019).
9. Humphrey, J. D., Dufresne, E. R. & Schwartz, M. A. Mechanotransduction and extracellular matrix homeostasis. *Nat. Rev. Mol. Cell Biol.* **15**, 802–812 (2014).
10. Wolfenson, H., Lavelin, I. & Geiger, B. Dynamic regulation of the structure and functions of integrin adhesions. *Dev. Cell* **24**, 447–458 (2013).
11. Sun, Z., Guo, S. S. & Fässler, R. Integrin-mediated mechanotransduction. *J. Cell Biol.* **215**, 445–456 (2016).
12. Geiger, B., Spatz, J. P. & Bershadsky, A. D. Environmental sensing through focal adhesions. *Nat. Rev. Mol. Cell Biol.* **10**, 21–33 (2009).
13. Jansen, K. A., Atherton, P. & Ballestrem, C. Mechanotransduction at the cell–matrix interface. *Semin. Cell Dev. Biol.* **71**, 75–83 (2017).
14. Haining, A. W. M., Lieberthal, T. J., Hernández, A. & del, R. Talin: a mechanosensitive molecule in health and disease. *FASEB J.* **30**, 2073–2085 (2016).
15. Gough, R. E. & Goult, B. T. The tale of two talins—two isoforms to fine-tune integrin signalling. *FEBS Lett.* **592**, 2108–2125 (2018).
16. Goult, B. T., Yan, J. & Schwartz, M. A. Talin as a mechanosensitive signaling hub. *J. Cell Biol.* **217**, 3776–3784 (2018).

17. del Rio, A. et al. Stretching single talin rod molecules activates vinculin binding. *Science* **323**, 638–641 (2009).
18. Yao, M. et al. The mechanical response of talin. *Nat. Commun.* **7**, 11966 (2016).
19. Haining, A. W. M., von Essen, M., Attwood, S. J., Hytönen, V. P. & del Río Hernández, A. All subdomains of the talin rod are mechanically vulnerable and may contribute to cellular mechanosensing. *ACS Nano* **10**, 6648–6658 (2016).
20. Yao, M. et al. Mechanical activation of vinculin binding to talin locks talin in an unfolded conformation. *Sci. Rep.* **4**, 4610 (2015).
21. Ciobanaru, C., Faivre, B. & Le Clairche, C. Actomyosin-dependent formation of the mechanosensitive talin–vinculin complex reinforces actin anchoring. *Nat. Commun.* **5**, 3095 (2014).
22. Ciobanaru, C., Faivre, B. & Le Clairche, C. Reconstituting actomyosin-dependent mechanosensitive protein complexes in vitro. *Nat. Protoc.* **10**, 75–89 (2015).
23. Atherton, P. et al. Vinculin controls talin engagement with the actomyosin machinery. *Nat. Commun.* **6**, 10038 (2015).
24. Hirata, H., Tatsumi, H., Lim, C. T. & Sokabe, M. Force-dependent vinculin binding to talin in live cells: a crucial step in anchoring the actin cytoskeleton to focal adhesions. *Am. J. Physiol. Cell Physiol.* **306**, C607–C620 (2014).
25. Austen, K. et al. Extracellular rigidity sensing by talin isoform-specific mechanical linkages. *Nat. Cell Biol.* **17**, 1597–1606 (2015).
26. Thievesen, I. et al. Vinculin–actin interaction couples actin retrograde flow to focal adhesions, but is dispensable for focal adhesion growth. *J. Cell Biol.* **202**, 163–177 (2013).
27. Lafuente, E. M. et al. RIAM, an Ena/VASP and profilin ligand, interacts with Rap1-GTP and mediates Rap1-induced adhesion. *Dev. Cell* **7**, 585–595 (2004).
28. Lagarrigue, F. et al. A RIAM/lamellipodin–talin–integrin complex forms the tip of sticky fingers that guide cell migration. *Nat. Commun.* **6**, 8492 (2015).
29. Han, J. et al. Reconstructing and deconstructing agonist-induced activation of integrin  $\alpha$ Ib $\beta$ 3. *Curr. Biol.* **16**, 1796–1806 (2006).
30. Yang, J. et al. Conformational activation of talin by RIAM triggers integrin-mediated cell adhesion. *Nat. Commun.* **5**, 5880 (2014).
31. Lagarrigue, F., Kim, C. & Ginsberg, M. H. The Rap1-RIAM-talin axis of integrin activation and blood cell function. *Blood* **128**, 479–487 (2016).
32. Lee, H.-S., Anekal, P., Lim, C. J., Liu, C.-C. & Ginsberg, M. H. Two modes of integrin activation form a binary molecular switch in adhesion maturation. *Mol. Biol. Cell* **24**, 1354–1362 (2013).
33. Goult, B. T. et al. RIAM and vinculin binding to talin are mutually exclusive and regulate adhesion assembly and turnover. *J. Biol. Chem.* **288**, 8238–8249 (2013).
34. Baxter, N. J., Zacharchenko, T., Barsukov, I. L. & Williamson, M. P. Pressure-dependent chemical shifts in the r3 domain of talin show that it is thermodynamically poised for binding to either vinculin or RIAM. *Structure* **25**, 1856–1866.e2 (2017).
35. Chang, Y.-C. et al. Structural and mechanistic insights into the recruitment of talin by RIAM in integrin signaling. *Structure* **22**, 1810–1820 (2014).
36. Patel, B. et al. The activity of the vinculin binding sites in talin is influenced by the stability of the helical bundles that make up the talin rod. *J. Biol. Chem.* **281**, 7458–7467 (2006).
37. Rahikainen, R., Öhman, T., Turkki, P., Varjosalo, M. & Hytönen, V. P. Talin-mediated force transmission and talin rod domain unfolding independently regulate adhesion signaling. *J. Cell Sci.* **132**, jcs226514 (2019).
38. Rahikainen, R. et al. Mechanical stability of talin rod controls cell migration and substrate sensing. *Sci. Rep.* **7**, 3571 (2017).
39. Mykuliak, V. V., Haining, A. W. M., von Essen, M., del Río Hernández, A. & Hytönen, V. P. Mechanical unfolding reveals stable 3-helix intermediates in talin and  $\alpha$ -catenin. *PLoS Comput. Biol.* **14**, e1006126 (2018).
40. Gingras, A. R. et al. Mapping and consensus sequence identification for multiple vinculin binding sites within the talin rod. *J. Biol. Chem.* **280**, 37217–37224 (2005).
41. Haining, A. W. M. et al. Mechanotransduction in talin through the interaction of the R8 domain with DLC1. *PLoS Biol.* **16**, e2005599 (2018).
42. Ringer, P. et al. Multiplexing molecular tension sensors reveals piconewton force gradient across talin-1. *Nat. Methods* **14**, 1090–1096 (2017).
43. Dedden, D. et al. The architecture of talin1 reveals an autoinhibition mechanism. *Cell* **179**, 120–131 (2019). e13.
44. Goult, B. T. et al. The structure of an interdomain complex that regulates talin activity. *J. Biol. Chem.* **284**, 15097–15106 (2009).
45. Atherton, P. et al. Relief of talin autoinhibition triggers a force-independent association with vinculin. *J. Cell Biol.* **219**. <https://doi.org/10.1083/jcb.201903134> (2020).
46. Chang, Y.-C. et al. Molecular basis for autoinhibition of RIAM regulated by FAK in integrin activation. *Proc. Natl Acad. Sci.* **116**, 3524–3529 (2019).
47. Humphries, J. D. et al. Vinculin controls focal adhesion formation by direct interactions with talin and actin. *J. Cell Biol.* **179**, 1043–1057 (2007).
48. Carisey, A. et al. Vinculin regulates the recruitment and release of core focal adhesion proteins in a force-dependent manner. *Curr. Biol.* **23**, 271–281 (2013).
49. Grashoff, C. et al. Measuring mechanical tension across vinculin reveals regulation of focal adhesion dynamics. *Nature* **466**, 263–266 (2010).
50. Bouchet, B. P. et al. Talin-KANK1 interaction controls the recruitment of cortical microtubule stabilizing complexes to focal adhesions. *Elife* **5**. <https://doi.org/10.7554/eLife.18124> (2016).
51. Zacharchenko, T. et al. LD motif recognition by talin: structure of the talin-DLC1 complex. *Structure* **24**, 1130–1141 (2016).
52. Yu, M. et al. Force-dependent regulation of talin-KANK1 complex at focal adhesions. *Nano Lett.* **19**, 5982–5990 (2019).
53. Reymann, A.-C. et al. Nucleation geometry governs ordered actin networks structures. *Nat. Mater.* **9**, 827–832 (2010).
54. Azioune, A., Storch, M., Bornens, M., Théry, M. & Piel, M. Simple and rapid process for single cell micro-patterning. *Lab Chip* **9**, 1640–1642 (2009).

### Acknowledgements

This work was supported by Agence Nationale pour la Recherche Grants ANR-16-CE13-0007-02 PHAGOMECA and ANR-18-CE13-0026-01 RECAMECA (to C.L.C.). The present work has benefited from the Light Microscopy facility of Imagerie-Gif, (<http://www.i2bc.paris-saclay.fr>), member of IBISA (<http://www.ibisa.net>), supported by “France-BiImaging” (ANR-10-INBS-04-01), and the Labex “Saclay Plant Sciences” (ANR-10-LABX-0040-SPS). We thank Annabelle Fente for initial observations of mCherry-RIAM binding to talin, Jun Qin (Cleveland Clinic, USA) for the gift of the mouse RIAM cDNA. We thank Florence Niedergang and the members of the “Cytoskeleton Dynamics and Motility” team for helpful discussions.

### Author contributions

C.V. performed the microscopy experiments, analyzed the data, and prepared the figures. V.H. cloned cDNAs. C.V., V.H., and C.L.C. purified and characterized the proteins used in this study. C.L.C. designed the experiments, supervised the project, and wrote the paper.

### Competing interests

The authors declare no competing interests.

### Additional information

**Supplementary information** is available for this paper at <https://doi.org/10.1038/s41467-020-16922-1>.

**Correspondence** and requests for materials should be addressed to C.L.C.

**Peer review information** *Nature Communications* thanks Masahiro Sokabe and the other, anonymous, reviewer(s) for their contribution to the peer review of this work. Peer reviewer reports are available.

**Reprints and permission information** is available at <http://www.nature.com/reprints>

**Publisher's note** Springer Nature remains neutral with regard to jurisdictional claims in published maps and institutional affiliations.



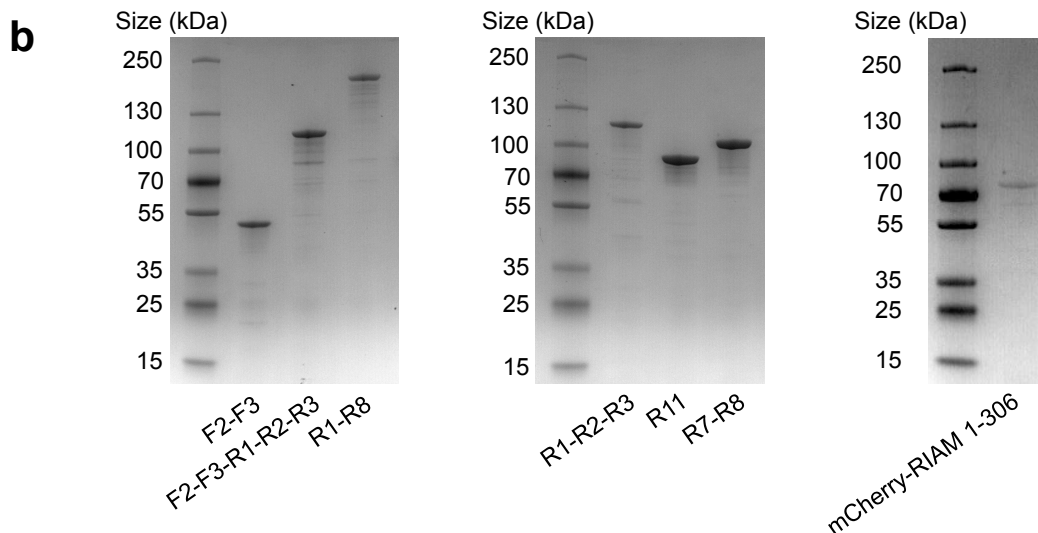
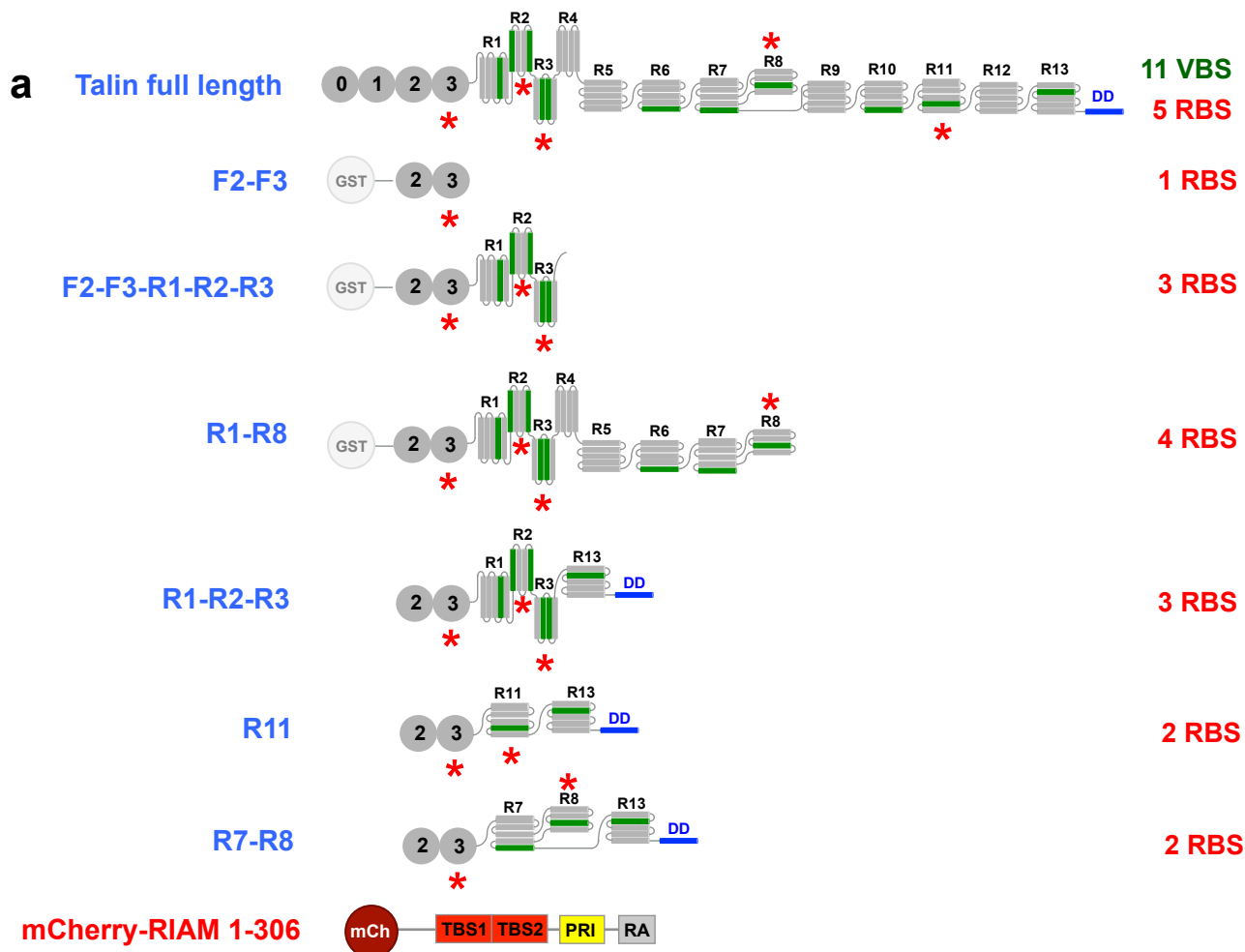
**Open Access** This article is licensed under a Creative Commons Attribution 4.0 International License, which permits use, sharing, adaptation, distribution and reproduction in any medium or format, as long as you give appropriate credit to the original author(s) and the source, provide a link to the Creative Commons license, and indicate if changes were made. The images or other third party material in this article are included in the article's Creative Commons license, unless indicated otherwise in a credit line to the material. If material is not included in the article's Creative Commons license and your intended use is not permitted by statutory regulation or exceeds the permitted use, you will need to obtain permission directly from the copyright holder. To view a copy of this license, visit <http://creativecommons.org/licenses/by/4.0/>.

© The Author(s) 2020

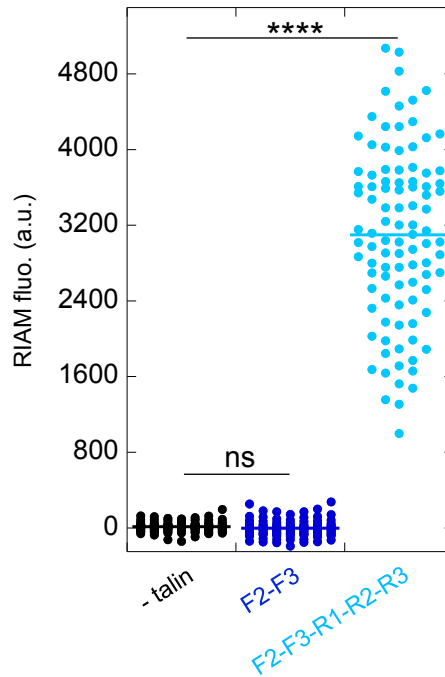


# **Talin dissociates from RIAM and associates to vinculin sequentially in response to the actomyosin**

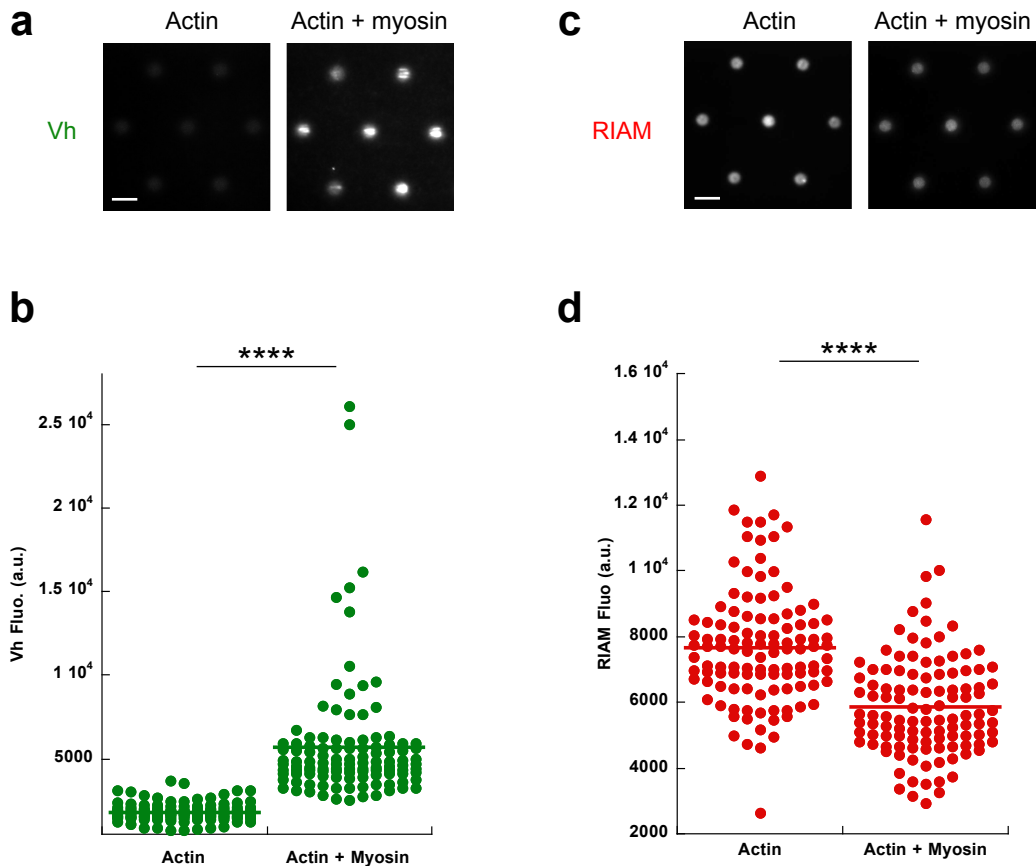
Vigouroux et al.



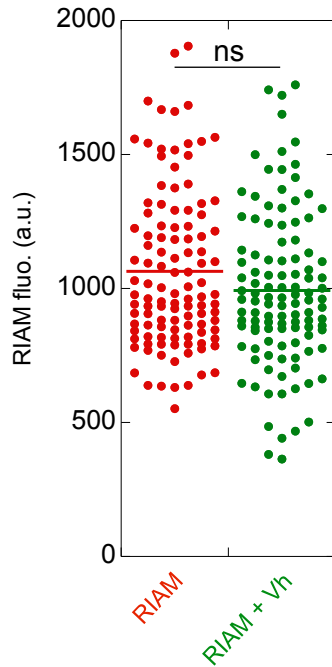
**Supplementary Figure 1. Proteins used in the study. (a)** Constructs used in this study. The talin domains named 0, 1, 2 and 3 are the F0, F1, F2 and F3 subdomains of the FERM (four-point-one, ezrin, radixin, moesin). R1 to R13 are the helix bundles along the rod domains of talin. DD is the dimerization domain of talin. Red stars show the RIAM binding sites (RBS) of talin. Dark green helices show the vinculin binding sites (VBS) of talin. mCherry-RIAM 1-306 contains a N-terminal mCherry tag (mCh), two talin-binding site (TBS1 and TBS2), a Ras-association domain (RA) and a Plekstrin-homology domain (PH). **(b)** SDS-PAGE of the purified proteins used in this work, stained with Coomassie blue. Proteins were purified 3 times independently with similar results on SDS PAGE. Source data are provided as a Source Data file.



**Supplementary Figure 2. The F3 subdomain of micropattern-bound talin does not bind to RIAM.** Recruitment of RIAM 1-306 in non-coated disks and disks coated with talin F2-F3 or talin F2-F3-R1-R2-R3. Conditions: 1  $\mu$ M mCherry-RIAM 1-306, 3  $\mu$ M of each talin construct during the coating step. Each data point represents the mean fluorescence of a single disk. The bar shows the mean.  $n = 105$ ,  $105$  and  $98$  disks for - talin, F2-F3 and F2-F3-R1-R2-R3 respectively. No significant difference (ns) was found between '- talin' and 'F2-F3' ( $P = 0.0940$ ), a significant difference was found between '- talin' and 'F2-F3-R1-R2-R3' ( $P = 1.69 \times 10^{-55}$ ) using a two-tailed t-test. \*\*\*\*,  $P < 0.0001$ . Source data are provided as a Source Data file.

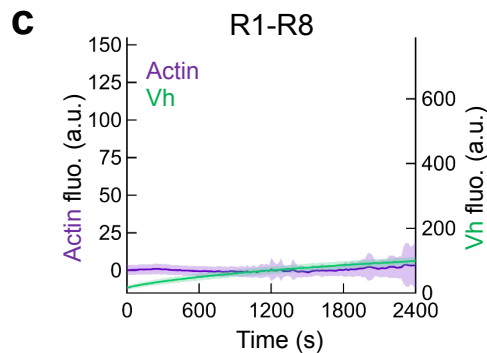
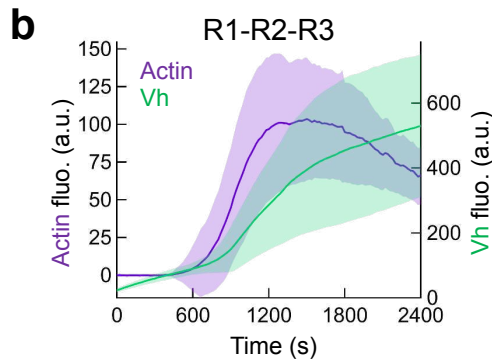
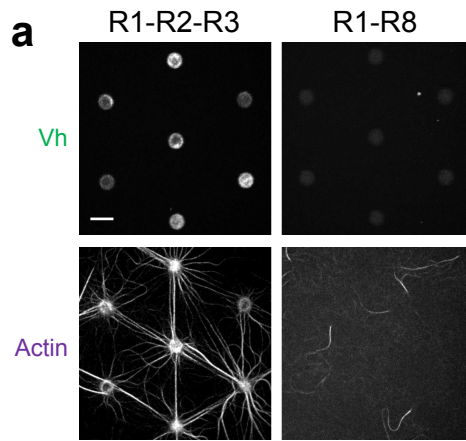


**Supplementary Figure 3. Myosin II promotes the binding of Vh to talin R1-R2-R3 and the dissociation of RIAM from talin R1-R2-R3.** (a, c) Representative images of the recruitment of Vh (a) or RIAM (c) in disks coated with talin R1-R2-R3 in the presence of short non polymerizing actin filaments alone (left) or with myosin II (right). Conditions: 100 nM EGFP-Vh (a) or 100 nM mCherry-RIAM 1-306 (c), 4.8  $\mu$ M pre-formed gelsolin-capped short actin filaments, 25 nM myosin II, 1  $\mu$ M of talin R1-R2-R3 during the coating step. Scale bar = 10  $\mu$ m. (b, d) The recruitment of Vh (b) or RIAM (d) is quantified in the conditions described in (a) and (c) respectively. Each data point represents the mean fluorescence of a single disk, the bar shows the mean.  $n = 112$  disks. A significant difference was found between 'Vh + actin' and 'Vh + actin + myosin' ( $P = 4.28 \times 10^{-23}$ ) and between 'RIAM + actin' and 'RIAM + actin + myosin' ( $P = 8.08 \times 10^{-15}$ ) using a two-tailed t-test. \*\*\*\*,  $P < 0.0001$ . The experiment was repeated 4 times (a) and 3 times (c) independently with similar results. Source data are provided as a Source Data file.



**Supplementary Figure 4. Vh does not prevent RIAM binding to talin in the absence of actomyosin.**

The recruitment of RIAM 1-306 is quantified in disks coated with talin R1-R2-R3 in the absence (left) and presence of Vh (right). Conditions: 100nM mCherry-RIAM 1-306, 500 nM EGFP-Vh and 1  $\mu$ M of talin during the coating step. Each data point represents the mean fluorescence of a single disk. The bar shows the mean. n = 112 disks. No significant difference (ns) was found using a two-tailed t-test ( $P = 0.0677$ ). Source data are provided as a Source Data file.



**Supplementary Figure 5. The central actin-binding domain of talin (ABD2) is not capable of anchoring actin filaments to stretch talin and induce vinculin binding.**

(a) Representative images of the recruitment of Vh (top) and actin (bottom) in disks coated with talin R1-R2-R3 (left) or talin R1-R8 (right) after 1000s. Talin R1-R2-R3 contains the C-terminal ABD3 (R13) whereas talin R1-R8 contains the same R1-R2-R3 domain followed by the central ABD2 (R4-R8). Conditions: 100 nM EGFP-Vh, 2.4  $\mu$ M actin (1% Alexa647-labeled), 50 nM myosin, 1  $\mu$ M of talin during the coating step. Scale bar = 10  $\mu$ m. The experiment was repeated twice independently with similar results. (b, c) Average of the kinetics of EGFP-Vh and Alexa647-labeled actin presented in (a). Data are mean  $\pm$  SD. (b) n = 54 disks. (c) n = 48 disks. Source data are provided as a Source Data file.



## V DISCUSSION AND PERSPECTIVES

---

### V.1 RIAM REGULATES ACTIN ASSEMBLY IN NASCENT ADHESIONS

#### V.1.1 The MIT complex assembles at the tip of adherent protrusions

A complex containing MRL proteins, active integrins and talin (MIT) forms at the tip of lamellipodia and filopodia, called “sticky fingers” (Galbraith et al., 2007). The MIT complex contains active unligated integrins and stimulates actin polymerization, likely by recruiting Ena/VASP proteins (Lagarrigue et al., 2015) (Figure 44). Sticky fingers, which propel active integrins through actin polymerization, could probe the extracellular matrix in search for new adhesion sites. This mechanism could be particularly important for directing haptotactic cell migration (Galbraith et al., 2007). However, the molecular mechanism underlying the assembly of the MIT complex, preceding the activation of integrins at the plasma membrane, and its actin polymerization activity, remained unclear before this study.

#### V.1.2 Formation of a PIP<sub>2</sub>-talin-RIAM-VASP complex requires the release of layers of autoinhibition

In adhesion complexes, a chain reaction, in which autoinhibited proteins are activated sequentially, leads to the activation of integrins by the F3 domain of talin at the plasma membrane (Khan and Goult, 2019) (part I.3.4.1). These autoinhibitions are released by post-translational modifications, protein-protein interactions or mechanical forces.

Activation of integrins by talin requires the release of talin autoinhibition, which exposes its F3 domain, and its recruitment to the plasma membrane. In addition to the already known interaction between R9 and F3 (Goult et al., 2009) (Figure 15), the structure of inactive talin, obtained in cryo-EM, revealed a second intramolecular contact between R12 and F2 (Dedden et al., 2019). The mechanisms by which the autoinhibitory contacts of talin are disrupted remain blurry.



## Discussion and perspectives

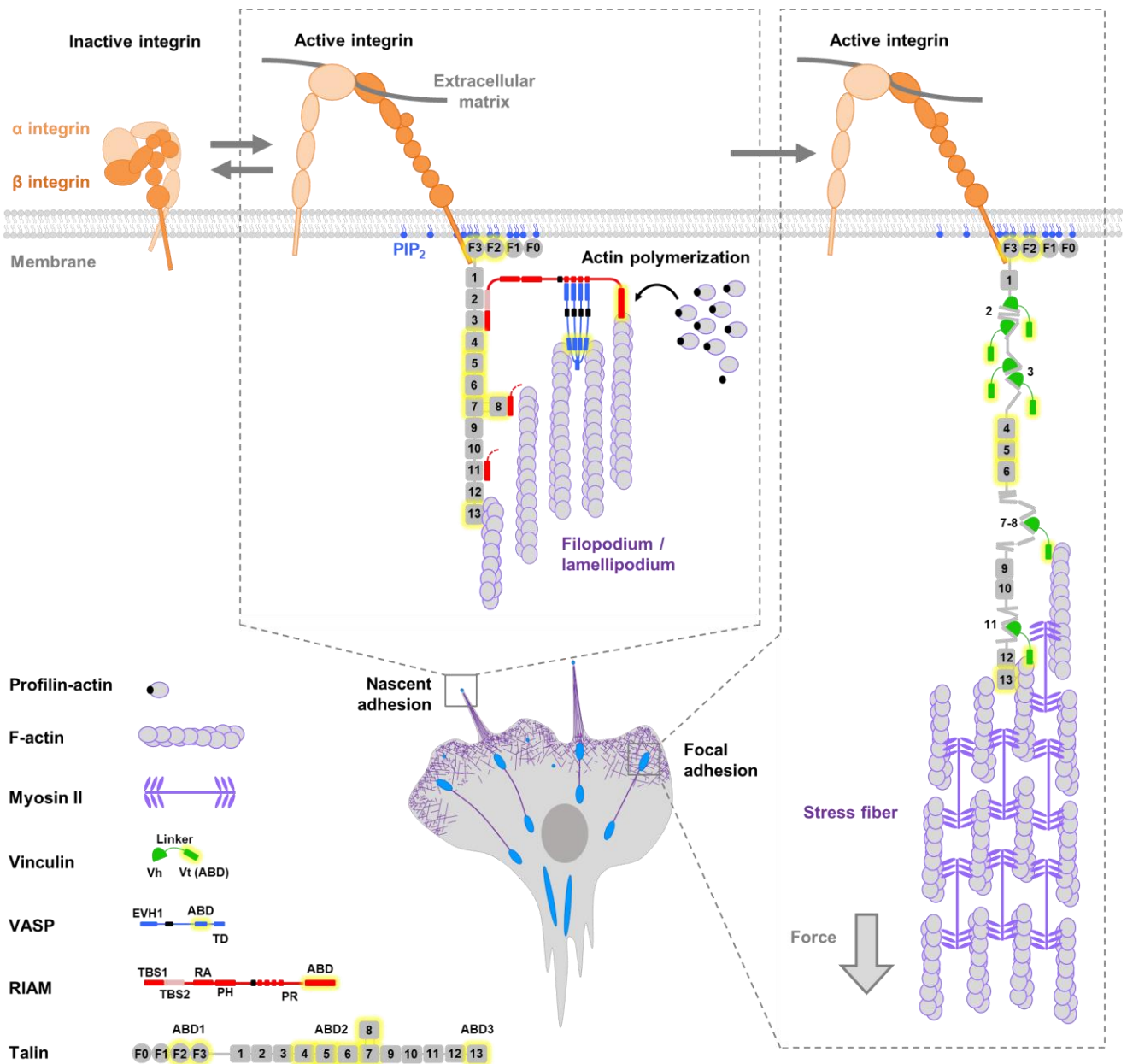


**Figure 44. The actomyosin force triggers the change of talin-binding partners during the maturation of nascent adhesions into focal adhesions.**

In migrating cells, talin is first recruited to the membrane to activate integrins, leading to the formation of nascent adhesions. Talin, RIAM and VASP form a complex which stimulates actin polymerization in nascent adhesions, contributing to the formation of filopodia and lamellipodia. Deeper in the cell, actin filaments associate with myosin II filaments to form tensile stress fibers. The force applied by these stress fibers to talin unfolds a series of  $\alpha$ -helix bundles that are bound to RIAM, leading to the sequential dissociation of RIAM and association of vinculin., which reinforces actin anchoring. This change in talin-binding partners allows the maturation of nascent adhesions into focal adhesions. RIAM contains two consecutive talin-binding sites (TBSs), a ras-association domain (RA), a pleckstrin-homology domain (PH) and a C-terminal proline rich region (PR) that contains four FPPPP, five profilin-binding motifs and the actin-binding domain (ABD). VASP contains an EVH1 (Ena/VASP homology 1) domain that interacts with RIAM FPPPP motifs, a profilin-binding domain, a G-actin and a F-actin-binding domain, and a tetramerization domain (TD). Profilin-binding sites in RIAM and VASP are represented in black. Talin FERM domains F0 to F3 and rod bundles 1 to 13 are indicated. The ABDs in all proteins are highlighted in yellow.

The Rap1-RIAM complex plays a key role in the regulation of talin during integrin activation. Structural studies revealed that RIAM TBS1 binds to talin F3 and disrupts the F3-R9 interaction to form a ternary complex between RIAM TBS1, talin F3 and integrin  $\beta$  (Yang et al., 2014). However, the low affinity of RIAM TBS1 for F3 ( $K_d = 32 \mu\text{M}$ ) suggests the existence of additional mechanisms for RIAM to mediate talin-dependent integrin activation. Structural studies also showed that RIAM binds to talin R8, which could destabilize the F3-R9 intramolecular interaction of talin (Chang et al., 2014; Zhang et al., 2016a). Cryo-EM applied to the talin-RIAM complex would help to determine if RIAM is sufficient to break talin autoinhibition.

Interestingly, RIAM can participate in the activation of integrins by talin only after the release of an intramolecular contact between TBS2 and RA (Chang et al., 2019) (Figure 45). Releasing this autoinhibition would allow RA to target RIAM to a Rap1-bound membrane surface, and TBS2 to bind talin with high affinity. In this model, TBS2 would cooperate with TBS1 to establish a stronger interaction with two adjacent talin bundles like R2 and R3 as suggested previously (Goult et al., 2013b). However, our full-length and 1-306 RIAM constructs, which comprise the RA-TBS2 intramolecular contact, interact with talin on GUVs and micropatterns with an apparent high affinity, suggesting that TBS2 is not required for high affinity binding. RIAM autoinhibition might be broken through phosphorylation by FAK (Chang et al., 2019). Rap1 itself might also be able to release the intramolecular contact in RIAM (Chang et al., 2019).

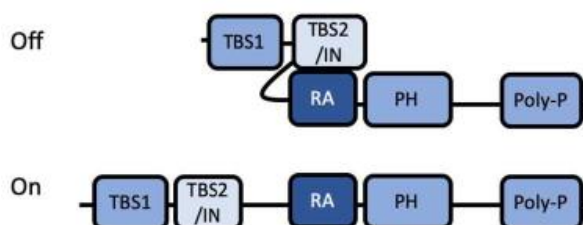


**Figure 45. Autoinhibited (off) and activated (on) forms of RIAM.**

RIAM comprises two Talin-Binding Sites (TBS1 and TBS2), an Inhibition motif (IN) in TBS2, a Ras-Association domain (RA), a Pleckstrin Homology (PH) and a Poly-proline (Poly-P) motif (Khan and Goult, 2019).

Alternative models suggest that talin can be activated by Rap1 independently of RIAM. Indeed, the F0 subdomain of talin head has been shown to directly interact with Rap1 (Goult et al., 2010). The relative importance of the RIAM-dependent and independent pathways to recruit talin at the membrane and activate it remains unclear. Although studies suggest that the Rap1-RIAM pathway might be crucial in leukocyte integrin  $\beta_2$  activation (Bromberger et al., 2018), it is accessory for  $\alpha_{IIb}\beta_3$  activation in platelets for example (Stritt et al., 2015). These apparent discrepancies may result from individual differences among integrins and cell types. In addition, other proteins can release talin intramolecular contacts and localize it to the membrane. For example,  $G\alpha_{13}$  (guanine nucleotide-binding protein  $\alpha$  13) interacts with talin, releases its autoinhibitory contacts and induces integrin activation (Schiemer et al., 2016), while FAK is

involved in talin recruitment to the membrane (Lawson et al., 2012). Kindlin is also localized at the membrane and synergizes with talin to activate integrins (Sun et al., 2019). Kindlin role should thus be considered in the mechanism by which talin is anchored at the plasma membrane. Finally, the binding of PIP<sub>2</sub> to the head domain of talin releases of the F3-R9 intramolecular contact to expose the integrin-binding site in talin F3 and target talin to the membrane (Goksoy et al., 2008; Martel et al., 2001; Saltel et al., 2009). This PIP<sub>2</sub>-talin interaction seems essential for integrin activation and focal adhesions formation (Chinthalapudi et al., 2018; Orłowski et al., 2015). Interestingly, the phosphatidylinositol phosphate kinase type 1  $\gamma$  (PIP1K1 $\gamma$ ) produces PIP<sub>2</sub> and binds to talin F3 (Di Paolo et al., 2002). Talin and PIP1K1 $\gamma$  might interact first and then translocate to the membrane, leading to a local enrichment in PIP<sub>2</sub> by PIP1K1 $\gamma$  after talin binding (Goksoy et al., 2008). PIP<sub>2</sub> may act synergistically with Rap1 (directly or via RIAM) to activate talin (Bromberger et al., 2019).

Altogether, these observations demonstrate that talin activation and localization at the membrane can be achieved by multiple mechanisms. The relative importance of each pathway needs to be further addressed. Rap1 and RIAM are likely needed to specify the spatiotemporal recruitment of talin and release its auto-inhibitions. However, once talin is recruited to the membrane, the binding of the talin head to PIP<sub>2</sub> is a critical part of the mechanism that induces the extended conformation of integrin. To mimic this configuration in the first study, and bypass the requirement of Rap1, we used a constitutively active talin construct, called R1-R2-R3, deleted from R9 and R12. In addition to its role in talin activation, RIAM also appears to be involved in the regulation of actin assembly by recruiting VASP. Talin R1-R2-R3, comprises two RIAM-binding sites. As mentioned earlier, RIAM full-length needs to be activated to interact with talin-bound GUVs containing PIP<sub>2</sub>. In addition, we found that RIAM binds to PIP<sub>2</sub>-containing GUVs through talin, but does not require its PH domain, in contrast with previous reports (Lafuente et al., 2004; Zhang et al., 2014). The binding of VASP to the C-terminal half of RIAM appears constitutive, suggesting that the EVH1 domains of VASP are exposed, as is the C-terminal proline-rich domain of RIAM which is often considered unstructured. We could finally reconstitute actin assembly by the PIP<sub>2</sub>-talin-RIAM-VASP-profilin machinery at the surface of GUVs. In the future, it could be interesting to use this approach to determine the relative contribution of Rap1, RIAM and PIP<sub>2</sub> to talin recruitment and integrin activation at the surface of GUVs containing purified transmembrane integrins.

### V.1.3 The talin-RIAM-VASP complex promotes actin polymerization

Once assembled at the plasma membrane, the MRL protein-integrin-talin complex promotes the actin-based propulsion of the tip of sticky fingers (Lagarrigue et al., 2015) (Figure 44).

## Discussion and perspectives

Although they were not directly identified in the MIT complex, Ena/VASP proteins are thought to associate to FPPPP motifs present in MRL proteins, via their EVH1 domain, to provide an actin polymerization activity to the complex ([Lagarrigue et al., 2015](#)). MRL proteins would thus act as a bridge between active integrins, via talin, and the actin cytoskeleton, via Ena/VASP proteins (Figure 44). Whether VASP is a permanent member of this complex or only transiently associates to stimulate actin elongation remains to be established.

Our mechanistic study revealed that, surprisingly, the actin polymerization activity of the complex was not solely the result of VASP activity, even if its contribution is important. Indeed, our results show that RIAM interacts with actin filaments and inhibits actin polymerization by capping the barbed ends of actin filaments. We have also shown that talin head inhibits actin polymerization by a similar capping mechanism in a previous study (See Appendix). However, under the experimental conditions used for the study of the talin-RIAM-VASP complex, the concentration of talin is too low and the ionic strength too high, making this activity negligible. It would have been interesting to perform the experiments in conditions where talin also inhibits actin assembly. The reason for the present choice comes from the limitations inherent in the use of GUVs. Indeed, the osmolarity, and thus the ionic strength, of the solution cannot be different from that inside the GUVs to keep their stability.

The measurement of the activity of all the combinations of talin, RIAM and VASP, first showed only additive effects. For example, the stimulation of actin assembly by VASP is decreased by RIAM in the same proportions as the inhibition of spontaneous actin assembly by RIAM alone. A major finding in this study is the critical role of the actin-binding protein profilin. In cells, the pool of monomeric actin is predominantly bound to profilin, which prevents spontaneous nucleation, helps direct actin monomers to the barbed end of filaments, and assists other actin regulators containing profilin-binding motifs ([Pollard and Cooper, 1984](#)). In contrast to the additive effects observed in the absence of profilin, the addition of profilin allows talin, RIAM and VASP to stimulate actin assembly synergistically. The mechanism of this profilin-induced change in activity is not fully elucidated in this study. It is already known that profilin increases actin filament barbed end elongation by human VASP, which contains binding sites for profilin ([Hansen and Mullins, 2010](#)). However, the effect of profilin on RIAM is less clear. In the presence of profilin, RIAM slightly stimulates actin assembly, whereas in the absence of profilin, RIAM inhibits the elongation of actin filament barbed ends. We first hypothesized that profilin, which transiently associates with the barbed ends of actin filaments, could simply inhibit the capping activity of RIAM. However, the observation of single actin filaments reveals that profilin does not modify the capping activity of RIAM. Although further experiments are needed to

determine the effect of profilin on RIAM, we propose that profilin stimulates the nucleation of actin filaments by RIAM.

In addition to understanding the contribution of each component, it will also be necessary to decipher whether the complex behaves like a machine in which talin, RIAM, VASP and profilin participate in a single activity that stimulates actin assembly by a mechanism yet to be determined, or whether the kinetic observations result from the sum of several distinct activities. Direct observations in TIRF microscopy of actin filaments in the presence of fluorescent talin, RIAM, VASP and profilin will provide more precise information on the molecular mechanism than global observations in solution using pyrene-actin assays. We could also more accurately determine the activity of the talin-RIAM-VASP complex in the presence of profilin by assembling it on the surface of polystyrene microscopic beads, like it has been first performed to elucidate how pathogens form actin comet tails to propel themselves in the host cell ([Loisel et al., 1999](#)). Breitsprecher used a similar system to demonstrate the processivity of VASP when clustered on the surface of beads ([Breitsprecher et al., 2008](#)). Injecting actin monomers labelled with two different fluorophores at two different time points or performing FRAP (fluorescence recovery after photobleaching) would reveal the direction in which actin filaments grow and therefore their orientation respective to the bead, and thus to the protein complex. A nucleation-release mechanism would result in filaments growing with their barbed ends outwards, while processive elongation would result in the elongation of the filaments with their barbed ends facing the bead. We can then elucidate the function of this complex by assembling it on the surface of GUVs containing fluorescent lipids to assess whether the complex can generate a protrusive force sufficient to deform the membrane, or whether additional components are needed.

#### V.1.4 RIAM and lamellipodin have non-overlapping functions

The fact that RIAM is expressed broadly, both in immune and non-immune tissues, while its paralog lamellipodin is most highly expressed in brain, heart, ovary, and developing embryo, and totally absent from leukocytes, suggests that both proteins have non redundant functions (Krause et al., 2004; Lafuente et al., 2004). The MIT complex, localized at the tip of protrusions, contains either RIAM or lamellipodin, but little evidence points out the role of lamellipodin in integrin activation. Lamellipodin contributes to activate  $\alpha_{IIb}\beta_3$  integrins, but independently of the Rap1 pathway (Krause et al., 2004; Watanabe et al., 2008). In fact, Rap1 interacts with the RA domain of RIAM much more strongly than that of lamellipodin (Zhang et al., 2014). The lamellipodin-dependent integrin activation could be mediated by another pathway involving Rac or Ras GTPases (Lee et al., 2009; Quinn et al., 2006). The poor affinity of lamellipodin for PIP<sub>2</sub> may also restrict its translocation to the membrane and its binding to Rap1 (Chang et al., 2013). Surprisingly, lamellipodin has also been shown to negatively affect inside-out integrin signaling (Lafuente et al., 2004), highlighting even more strongly the differences between both paralogs. Additional work would be needed to refine the differential contribution of RIAM and lamellipodin to integrin activation.

The comparison of our results on RIAM with published results on lamellipodin reinforces the idea that they act through different mechanisms. Lamellipodin was first described to bind actin filaments through a C-terminal cluster of positively-charged amino acids (Hansen and Mullins, 2015), which were not found in RIAM. Generally, the C-terminal regions of MRL proteins is not conserved. RIAM was thus not predicted to interact with actin. Our discovery that RIAM directly binds actin filaments in vitro and caps their barbed ends adds to the knowledge on MRL proteins. The fact that RIAM binding to actin is not sensitive to ionic strength, unlike the lamellipodin-actin interaction (Hansen and Mullins, 2015), confirms that RIAM activity does not involve positively-charged amino-acids. In addition, lamellipodin decreases the rate of actin filament elongation by sequestering actin monomers (Hansen and Mullins, 2015), while we unveiled that RIAM caps their barbed ends. Another difference is the much stronger affinity of talin for RIAM than for lamellipodin (Chang et al., 2014). In contrast with the talin-RIAM interaction, much less information is available on the interaction between talin and lamellipodin. RIAM interacts with talin through a N-terminal TBS1 domain, followed by a TBS2 that is thought to reinforce the interaction (Goult et al., 2013b). Lamellipodin also contains a N-terminal talin-binding region similar to RIAM TBS1. It also possesses another helical region similar to RIAM TBS2, but its contribution has not been described (Chang et al., 2014). Replacing RIAM TBS1 by the corresponding domain of lamellipodin greatly reduced the affinity of RIAM

for talin, suggesting that lamellipodin has a weaker affinity for talin than RIAM (Chang et al., 2014).

Given the differences between RIAM and lamellipodin, it could be interesting to compare the actin polymerization activity of talin-RIAM-VASP and talin-lamellipodin-VASP complexes.

### V.1.5 Does the clustering of the multivalent proteins talin, RIAM and VASP influence actin assembly?

The discovery that VASP promotes the processive elongation of actin filaments from a surface where it is immobilized at very high density revealed that an actin polymerization activity can emerge from the collective behavior of molecules that individually do not possess this activity (Breitsprecher et al., 2008). The fact that artificial dimers of lamellipodin enhance the clustering and processive activity of VASP supports this view (Cheng and Mullins, 2020; Hansen and Mullins, 2015).

We expected that the multivalent proteins talin, RIAM and VASP would form large clusters on membrane surfaces. Indeed, talin dimers, linked by RIAM dimers, themselves bound to VASP tetramers, can theoretically diffuse in the 2D plane of the PIP<sub>2</sub>-rich membrane to cluster. From these clusters could then emerge an unexpected actin polymerization activity.

At this stage, we were able to find the conditions to observe the formation of an actin network on the surface of GUVs and correlate it with some of the actin-binding proteins mentioned above. Although some observations suggest the formation of clusters of proteins associated with actin over-densities, it would be premature to conclude that protein clustering influences actin assembly. If clusters do form, their size could be limited, as our data suggest that the four EVH1 of a VASP tetramer binds to the four FPPPP domains of the same RIAM protein or are not available to additional RIAM molecules, which does not allow VASP to bridge different RIAM proteins. Complementary experiments will be necessary to demonstrate the formation of such clusters. For example, FRAP experiments could reveal the immobilization of talin, RIAM and VASP in zones of protein over-densities on the surface of GUVs.

Although we have not demonstrated the formation of clusters on GUVs, other experiments demonstrated the ability of talin, RIAM and VASP to form multivalent actin-binding networks in solution that bundle actin filaments. The relevance of bundling observed in vitro in solution is always to be taken with caution. Indeed, in cells, the proteins talin, RIAM and VASP are present at the tip of filopodia but they do not colocalize with actin along these protrusions. The talin-RIAM-VASP complex could initiate bundling at the plasma membrane, while other

proteins, such as fascin, would bundle the filaments along the entire length of filopodia. In this mechanism, actin filaments bundling is not only a consequence of protein clustering but it can also promote clustering.

## V.2 RIAM CONTROLS THE MATURATION OF NASCENT ADHESIONS INTO MATURE FOCAL ADHESIONS

The talin-RIAM-VASP complex coordinates actin assembly and integrin activation in nascent adhesions at the leading edge of migrating cells (Figure 44). After discovering a role for RIAM in the regulation of actin assembly during this process, we studied the role of RIAM in the irreversible maturation of these nascent adhesions into force-bearing focal adhesions.

### V.2.1 The actomyosin force destabilizes the talin-RIAM interaction

Our *in vitro* reconstitution demonstrated that the actomyosin assembly provokes the dissociation of RIAM from talin-coated discs micropatterned on a glass surface. This actomyosin-dependent dissociation of the talin-RIAM complex is followed by the recruitment of vinculin to talin. This sequence of events recapitulates the exchange of major binding partners of talin during the maturation of nascent adhesions into focal adhesions in response to the force applied by actomyosin stress fibers (Figure 44). A series of single molecule experiments, structural studies and simulation showed that, in this process, talin is mechanically stretched, which is expected to disrupt the RIAM binding sites and expose cryptic vinculin-binding sites (Del Rio et al., 2009; Goult et al., 2013b; Haining et al., 2016b; Hytönen and Vogel, 2008; Mykuliak et al., 2018; Yao et al., 2016, 2014).

Talin contains five RIAM-binding sites and eleven vinculin-binding sites. These domains may have different affinities and respond to force differently, which makes the study of the exchange of RIAM for vinculin on talin highly challenging. Therefore, we designed mini-talin constructs containing only one (or two) RIAM-binding sites. We found that RIAM protects R2-R3 from unfolding, and that RIAM dissociation is a prerequisite for vinculin binding. Such a mechanism could act as a mechanical switch to control the force-dependent maturation of focal adhesions. In fact, R1-R2-R3 is one of the key mechanosensitive part of talin, as a talin construct lacking the R4 to R12 bundles, similar to our R1-R2-R3 talin, can rescue spreading, polarization and migration in talin-null cells (Rahikainen et al., 2017). R3 is the weakest of all bundles and should unfold first, as demonstrated from single talin molecule stretching experiments (Yao et al., 2014). Force sensing by talin R3 is particularly important, since expression of a mutant that destabilizes the R3 bundle leads to decreased migration rates and



traction force generation ([Rahikainen et al., 2017](#)). It can be hypothesized that the strength of the interaction between RIAM and R3 partly determines the threshold force at which R3 unfolds and exposes its cryptic sites for vinculin. Therefore, the biochemical signals that affect the affinity of RIAM for R3 directly control the mechanosensitivity of talin.

Much less is known about the RIAM-binding site located in the R11 bundle of talin. The structure of R11 in complex with RIAM is not known and the residues interacting with RIAM have not been mapped yet. Like for R1-R2-R3, we found that actomyosin is sufficient to induce RIAM dissociation from R11. Interestingly, the expression in talin-null cells of a talin construct deleted from R1 to R10, comparable to our R11 talin, is also able to rescue adhesion reinforcement, cell polarization and migration, revealing that, like for R3, mechanosensing through R11 plays an important role ([Rahikainen et al., 2019](#)). However, for R11, in contrary to R1-R2-R3, we observed that RIAM-binding does not affect the mechanosensitive recruitment of vinculin, implying that RIAM does not protect R11 from unfolding. Actomyosin-induced RIAM dissociation and vinculin association to R11 happen sequentially and do not influence each other. Simulations predicted that the first and last helices of R11 would unfold first, leaving a 3-helix intermediate conformation of the bundle ([Mykuliak et al., 2018](#)), which would expose the cryptic VBS. Whether RIAM dissociates after this first step of unfolding would need to be addressed. Importantly, the 4<sup>th</sup>  $\alpha$ -helix of R11, that is a VBS, also interacts with integrins. Structural studies suggest that integrin binding to R11 favors vinculin binding ([Yogeshha et al., 2012](#)). RIAM interaction with R11 could therefore play a role in talin-mediated integrin activation or clustering.

In contrast to talin R1-R2-R3 and R11, we found that R8 dissociation from RIAM and association to vinculin are only mildly affected by actomyosin. This difference likely results from the insertion of R8 between the 3<sup>rd</sup> and 4<sup>th</sup> helix of R7, which protects R8 from unfolding. Simulations and single molecule stretching experiments showed that isolated R8 unfolds at 5 pN, while a R7-R8 talin fragment unfolds in one step at 15 pN, confirming that R8 unfolds when R7 is disrupted ([Yao et al., 2016](#)). In our experimental conditions, the force generated by actomyosin might be sufficient to unfold R3 and R11 and disrupt their RIAM-binding interface, but not sufficient to unfold R7-R8. In cells an artificial clamp in R7, which precludes R8 opening, leads to a decrease migration and force generation ([Haining et al., 2018](#)), indicating that R8 is also a critical mechanosensitive module that likely responds to higher forces compared to R3 and R11.

## V.2.2 The various actin-binding domains of talin contribute differently to the mechanosensitivity of talin

The mechanosensitivity of talin domains depends on their localization relative to the three actin-binding domains (ABDs) that transmit the actomyosin force. Insertion of FRET sensors at different locations along talin revealed that tension is higher between the N-terminal ABD1 and the central ABD2 than between ABD2 and the C-terminal ABD3 (Ringer et al., 2017). Therefore, the bundles R1-R2-R3, which are located between ABD1 and ABD2, are submitted to the highest tension along the rod. It is interesting to remember that these three bundles of talin, which comprise half of talin VBSs, are also the weakest along the rod (Yao et al., 2016). Altogether, these observations highlight the important role of the R1-R2-R3 bundles for the mechanosensitive properties of talin.

We determined the relative importance of the three ABDs of talin in our in vitro assay. Previous work from our laboratory determined that talin ABD1 is bound to the micropatterns and unable to interact with actin filaments. ABD1 does not transmit the actomyosin force and therefore does not contribute to talin mechanosensitivity in our experimental conditions. However, ABD2 (when present) and ABD3 are available to bind actin filaments. ABD3 is thought to provide the major bond between talin and the tensile actomyosin cytoskeleton because super-resolution microscopy shows that talin C-terminus colocalizes with stress fibers (Kanchanawong et al., 2010). We also demonstrate that a mini-talin construct containing ABD3, as the only available ABD, anchors actomyosin efficiently. ABD2 is often described to span from R4 to R8. Actually ABD2 is made of two independent domains located in R4 and R8 respectively (Atherton et al., 2015a). In addition to binding actin filaments, R8 contains both RIAM- and vinculin-binding sites. RIAM and vinculin binding to R8 could prevent actin association, and vice versa. Alternatively, actin association to both ABD2 and ABD3 could modify the tension experienced by the various talin bundles. In full-length talin, pulling both on ABD2 and ABD3 might release the tension between these two domains. In our setup, though, a talin construct containing ABD2, but lacking ABD3, is not sufficient to recruit actin filaments, even in the absence of RIAM and vinculin. ABD2 thus cannot mediate talin stretching and induce vinculin recruitment. The fact that ABD2 is masked by R3 could explain this result (Atherton et al., 2015a). However, others found that ABD2 is available in full-length talin (Dedden et al., 2019). Further experiments are needed to better understand the contribution of ABD2 to talin function.

### V.3 TALIN CONTROLS THE TRANSITION BETWEEN POLYMERIZING AND CONTRACTILE ACTIN NETWORKS

Several studies have reported a link between actin polymerization at the leading edge, actomyosin contractility and adhesion formation ([Giannone et al., 2007, 2004](#)). My PhD project highlights the importance of talin-containing complexes in these highly coordinated processes. The talin-RIAM-VASP complex initiates actin polymerization and activates integrins in nascent adhesions at the leading edge of membrane protrusions, while the talin-vinculin complex couples contractile actomyosin stress fibers to active integrins in mature focal adhesions (Figure 44). RIAM is a marker of nascent adhesions submitted to low traction forces. When the tension stays low, nascent adhesions quickly disassemble. However, when the threshold force is reached, they quickly mature into focal adhesions in an irreversible manner. The main roles of RIAM in this process is first to initiate cell-matrix adhesions, by contributing to the release of talin autoinhibition and its localization to the membrane. RIAM also controls very precisely the irreversible growth of these adhesions into mature focal adhesions by protecting talin rod bundles from stretching. The mechanical stability of the talin-RIAM complex plays a critical role in the decision to switch from a polymerizing to a contractile actin network during adhesion growth. Our discovery of a direct link between RIAM and actin suggests the existence of a feedback loop in which RIAM contributes, together with talin and VASP, to actin assembly, which strengthen the talin-bound actomyosin network, leading to its own dissociation from talin (Figure 44).

### V.4 DECIPHERING THE TALIN CODE

The control of talin stretching by RIAM represents, however, only a small part of the entire picture in the cellular context. In cells, multiple force-dependent conformations of talin are recognized by specific binding partners. This mechanism allows talin to encode a broad range of mechanical cues into the biochemical signaling pathways that control cell adaptation. The talin interactome underlying this complex mechanism has been termed “talin code” ([Goult et al., 2018](#)) (Figure 46).

Among the talin-binding partners, the conserved proteins of the KANK family have received attention recently ([Bouchet et al., 2016](#); [Chen et al., 2018](#); [Sun et al., 2016](#); [Yu et al., 2019](#)) (Figure 46). Like the interaction of RIAM with R2, R3, R8 and R11, the interaction of KANK1 with R7 is disrupted by talin stretching ([Yu et al., 2019](#)). Perturbation of the talin-KANK1 interaction

by point mutations abolishes the association of microtubule-stabilizing complexes with focal adhesions (Bouchet et al., 2016). Additionally, KANK proteins are also involved in talin activation, and thus integrin activation (Sun et al., 2016). Another talin partner, DLC1, binds to the R8 bundle of unstretched talin (Zacharchenko et al., 2016) (Figure 46). Mutations that prevent the sequential unfolding of R7-R8 revealed the crucial importance of the R8-DLC1 interaction (Haining et al., 2018). Interestingly, RIAM and DLC1 interact with talin R8 in a mutually exclusive manner, but differently (Chang et al., 2014; Zacharchenko et al., 2016). The differential expression of RIAM and DLC1 in cells likely confers a different sensitivity to mechanical cues.

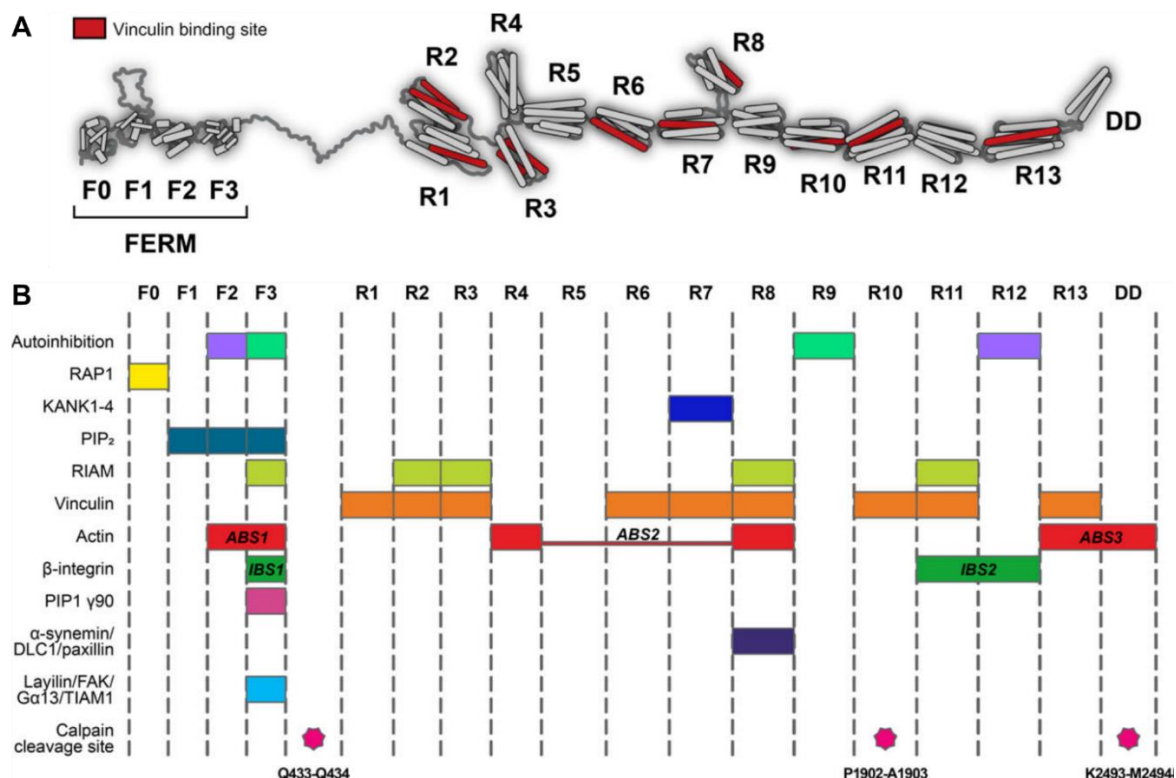


**Figure 46. The talin code: talin domains interact with various proteins.**

**(A)** Structural model of the domain arrangement of talin. The scheme indicates the position of the F0, F1, F2 and F3 domains of the FERM domain, the 13 helical bundles (R1 to R13) of the rod and the dimerization domain (DD). **(B)** Talin binding partners are shown for each domain, as well as the domains involved in the autoinhibitions and the calpain cleavage sites. ABS (actin-binding site), IBS (integrin-binding site) (Adapted from Gough and Goult, 2018).

In the future, it will important to determine with certainty the mechanosensitivity of the different bundles of talin for their partner proteins. Our assay, that reconstitutes talin stretching in response to actomyosin, is an important step in this process, because it partly mimics the cellular context. However, single molecule stretching experiments are necessary to determine the force thresholds necessary for protein unfolding, and for this reason these techniques perfectly complement our approach. It now appears crucial to correlate force measurements, real-time observation of talin stretching and the association/dissociation

## Discussion and perspectives

dynamics of protein interactions with talin. To this aim, we will have to transfer our reconstituted assay to a deformable micropatterned surface, or flexible micropillars, allowing the measurement of traction force and simultaneously observe the dynamics of fluorophore-labeled talin partners. In addition, inserting a FRET sensor into talin would allow measuring its elongation. Finally, designing and characterizing new mutants of the different bundles of talin, to facilitate or prevent stretching, such as the 4S and IVVI mutants of R3 respectively ([Rahikainen et al., 2017](#); [Yao et al., 2014](#)), will be informative and easy in our assay. Such tools will make it possible to determine the importance of the stretching of these bundles, or their combination, in cells placed in environments of variable mechanical properties.

## BIBLIOGRAPHY

---

- Anthis NJ, Wegener KL, Critchley DR, Campbell ID. 2010. Structural Diversity in Integrin/Talin Interactions. *Structure* **18**:1654–1666. doi:10.1016/j.str.2010.09.018
- Anthis NJ, Wegener KL, Ye F, Kim C, Goult BT, Lowe ED, Vakonakis I, Bate N, Critchley DR, Ginsberg MH, Campbell ID. 2009. The structure of an integrin/talin complex reveals the basis of inside-out signal transduction. *EMBO J* **28**:3623–3632. doi:10.1038/emboj.2009.287
- Aota SI, Nomizu M, Yamada KM. 1994. The short amino acid sequence Pro-His-Ser-Arg-Asn in human fibronectin enhances cell-adhesive function. *J Biol Chem* **269**:24756–24761.
- Atherton P, Stutchbury B, Wang D-Y, Jethwa D, Tsang R, Meiler-Rodriguez E, Wang P, Bate N, Zent R, Barsukov IL, Goult BT, Critchley DR, Ballestrem C. 2015a. Vinculin controls talin engagement with the actomyosin machinery. *Nat Commun* **6**:10038. doi:10.1038/ncomms10038
- Atherton P, Stutchbury B, Wang DY, Jethwa D, Tsang R, Meiler-Rodriguez E, Wang P, Bate N, Zent R, Barsukov IL, Goult BT, Critchley DR, Ballestrem C. 2015b. Vinculin controls talin engagement with the actomyosin machinery. *Nat Commun* **6**:1–12. doi:10.1038/ncomms10038
- Austen K, Ringer P, Mehlich A, Chrostek-Grashoff A, Kluger C, Klingner C, Sabass B, Zent R, Rief M, Grashoff C. 2015. Extracellular rigidity sensing by talin isoform-specific mechanical linkages. *Nat Cell Biol* **17**:1597–1606. doi:10.1038/ncb3268
- Azioune A, Carpi N, Tseng Q, Théry M, Piel M. 2010. Protein Micropatterns **97**:133–146. doi:10.1016/s0091-679x(10)97008-8
- Azioune A, Storch M, Bornens M, Théry M, Piel M. 2009. Simple and rapid process for single cell micro-patterning. *Lab Chip* **9**:1640. doi:10.1039/b821581m
- Bachmann C, Fischer L, Walter U, Reinhard M. 1999. The EVH2 domain of the vasodilator-stimulated phosphoprotein mediates tetramerization, F-actin binding, and actin bundle formation. *J Biol Chem* **274**:23549–23557. doi:10.1074/jbc.274.33.23549
- Bachmann M, Kukkurainen S, Hytönen VP, Wehrle-Haller B. 2019. Cell Adhesion by Integrins. *Physiol Rev* **99**:1655–1699. doi:10.1152/physrev.00036.2018
- Bakolitsa C, Cohen DM, Bankston LA, Bobkov AA, Dadwell GW, Jennings L, Critchley DR, Craig SW, Liddington RC. 2004. Structural basis for vinculin activation at sites of cell adhesion. *Nature* **430**:583–586. doi:10.1038/nature02610
- Bao G. 2013. Protein Conformational Change In: Mofrad MRK, Kamm RD, editors. Cellular Mechanotransduction. Cambridge: Cambridge University Press. pp. 269–285. doi:10.1017/CBO9781139195874.013
- Bate N, Gingras AR, Bachir A, Horwitz R, Ye F, Patel B, Goult BT, Critchley DR. 2012. Talin contains a C-terminal calpain2 cleavage site important in focal adhesion dynamics. *PLoS One* **7**:e34461. doi:10.1371/journal.pone.0034461
- Bays JL, DeMali KA. 2017. Vinculin in cell–cell and cell–matrix adhesions. *Cell Mol Life Sci* **74**:2999–3009. doi:10.1007/s00018-017-2511-3

## Bibliography

- Bear JE, Loureiro JJ, Libova I, Fässler R, Wehland J, Gertler FB. 2000. Negative regulation of fibroblast motility by Ena/VASP proteins. *Cell* **101**:717–728. doi:10.1016/S0092-8674(00)80884-3
- Bear JE, Svitkina TM, Krause M, Schafer DA, Loureiro JJ, Strasser GA, Maly I V., Chaga OY, Cooper JA, Borisy GG, Gertler FB. 2002. Antagonism between Ena/VASP proteins and actin filament capping regulates fibroblast motility. *Cell* **109**:509–521. doi:10.1016/S0092-8674(02)00731-6
- Berrier AL, Yamada KM. 2007. Cell–matrix adhesion. *J Cell Physiol* **213**:565–573. doi:10.1002/jcp.21237
- Blanchoin L, Boujemaa-Paterski R, Sykes C, Plastino J. 2014. Actin Dynamics, Architecture, and Mechanics in Cell Motility. *Physiol Rev* **94**:235–263. doi:10.1152/physrev.00018.2013
- Blangy A. 2017. Tensins are versatile regulators of Rho GTPase signalling and cell adhesion. *Biol Cell* **109**:115–126. doi:10.1111/boc.201600053
- Bledzka K, Bialkowska K, Sossey-Alaoui K, Vaynberg J, Pluskota E, Qin J, Plow EF. 2016. Kindlin-2 directly binds actin and regulates integrin outside-in signaling. *J Cell Biol* **213**:97–108. doi:10.1083/jcb.201501006
- Borgon RA, Vornrhein C, Bricogne G, Bois PRJ, Izard T. 2004. Crystal Structure of Human Vinculin. *Structure* **12**:1189–1197. doi:10.1016/j.str.2004.05.009
- Böttcher RT, Veelders M, Rombaut P, Faix J, Theodosiou M, Stradal TE, Rottner K, Zent R, Herzog F, Fässler R. 2017. Kindlin-2 recruits paxillin and Arp2/3 to promote membrane protrusions during initial cell spreading. *J Cell Biol* **216**:3785–3798. doi:10.1083/jcb.201701176
- Bouaouina M, Lad Y, Calderwood DA. 2008. The N-terminal domains of talin cooperate with the phosphotyrosine binding-like domain to activate  $\beta$ 1 and  $\beta$ 3 integrins. *J Biol Chem* **283**:6118–6125. doi:10.1074/jbc.M709527200
- Bouchet BP, Gough RE, Ammon Y-C, van de Willige D, Post H, Jacquemet G, Altelaar AM, Heck AJR, Goult BT, Akhmanova A. 2016. Talin-KANK1 interaction controls the recruitment of cortical microtubule stabilizing complexes to focal adhesions. *Elife* **5**:1–23. doi:10.7554/eLife.18124
- Bouvard D, Pouwels J, De Franceschi N, Ivaska J. 2013. Integrin inactivators: balancing cellular functions in vitro and in vivo. *Nat Rev Mol Cell Biol* **14**:430–442. doi:10.1038/nrm3599
- Breitsprecher D, Kiesewetter AK, Linkner J, Urbanke C, Resch GP, Small JV, Faix J. 2008. Clustering of VASP actively drives processive, WH2 domain-mediated actin filament elongation. *EMBO J* **27**:2943–2954. doi:10.1038/emboj.2008.211
- Breitsprecher D, Kiesewetter AK, Linkner J, Vinzenz M, Stradal TEB, Small JV, Curth U, Dickinson RB, Faix J. 2011. Molecular mechanism of Ena/VASP-mediated actin-filament elongation. *EMBO J* **30**:456–467. doi:10.1038/emboj.2010.348
- Bromberger T, Klapproth S, Rohwedder I, Zhu L, Mittmann L, Reichel CA, Sperandio M, Qin J, Moser M. 2018. Direct Rap1/Talin1 interaction regulates platelet and neutrophil integrin activity in mice. *Blood* **132**:2754–2762. doi:10.1182/blood-2018-04-846766

## Bibliography

- Bromberger T, Zhu L, Klapproth S, Qin J, Moser M. 2019. Rap1 and membrane lipids cooperatively recruit talin to trigger integrin activation. *J Cell Sci* **132**:jcs.235531. doi:10.1242/jcs.235531
- Brühmann S, Ushakov DS, Winterhoff M, Dickinson RB, Curth U, Faix J. 2017. Distinct VASP tetramers synergize in the processive elongation of individual actin filaments from clustered arrays. *Proc Natl Acad Sci* **114**:E5815–E5824. doi:10.1073/pnas.1703145114
- Burridge K, Connell L. 1983. A new protein of adhesion plaques and ruffling membranes. *J Cell Biol* **97**:359–367. doi:10.1083/jcb.97.2.359
- Burridge K, Wittchen ES. 2013. The tension mounts: Stress fibers as force-generating mechanotransducers. *J Cell Biol* **200**:9–19. doi:10.1083/jcb.201210090
- Calderwood DA, Campbell ID, Critchley DR. 2013. Talins and kindlins: Partners in integrin-mediated adhesion. *Nat Rev Mol Cell Biol* **14**:503–517. doi:10.1038/nrm3624
- Carisey A, Tsang R, Greiner AM, Nijenhuis N, Heath N, Nazgiewicz A, Kemkemer R, Derby B, Spatz J, Ballestrem C. 2013. Vinculin regulates the recruitment and release of core focal adhesion proteins in a force-dependent manner. *Curr Biol* **23**:271–281. doi:10.1016/j.cub.2013.01.009
- Carlier M-F. 2015. Control of polarized assembly of actin filaments in cell motility. *Cell Mol Life Sci* **72**:3051–3067. doi:10.1007/s00018-015-1914-2
- Carlier M-F, Laurent V, Santolini J, Melki R, Didry D, Xia G-X, Hong Y, Chua N-H, Pantaloni D. 1997. Actin Depolymerizing Factor (ADF/Cofilin) Enhances the Rate of Filament Turnover: Implication in Actin-based Motility. *J Cell Biol* **136**:1307–1322. doi:10.1083/jcb.136.6.1307
- Case LB, Waterman CM. 2015. Integration of actin dynamics and cell adhesion by a three-dimensional, mechanosensitive molecular clutch. *Nat Cell Biol* **17**:955–963. doi:10.1038/ncb3191
- Casella JF, Maack DJ, Lin S. 1986. Purification and initial characterization of a protein from skeletal muscle that caps the barbed ends of actin filaments. *J Biol Chem* **261**:10915–21.
- Chang Y-C, Su W, Cho E, Zhang H, Huang Q, Philips MR, Wu J. 2019. Molecular basis for autoinhibition of RIAM regulated by FAK in integrin activation. *Proc Natl Acad Sci* **116**:3524–3529. doi:10.1073/pnas.1818880116
- Chang Y-C, Zhang H, Brennan ML, Wu J. 2013. Crystal structure of Lamellipodin implicates diverse functions in actin polymerization and Ras signaling. *Protein Cell* **4**:211–219. doi:10.1007/s13238-013-2082-5
- Chang YC, Zhang H, Franco-Barraza J, Brennan ML, Patel T, Cukierman E, Wu J. 2014. Structural and mechanistic insights into the recruitment of talin by RIAM in integrin signaling. *Structure* **22**:1810–1820. doi:10.1016/j.str.2014.09.020
- Chen H, Choudhury DM, Craig SW. 2006. Coincidence of actin filaments and talin is required to activate vinculin. *J Biol Chem* **281**:40389–40398. doi:10.1074/jbc.M607324200
- Chen H, Cohen DM., Choudhury DM., Kioka N, Craig SW. 2005. Spatial distribution and functional significance of activated vinculin in living cells. *J Cell Biol* **169**:459–470. doi:10.1083/jcb.200410100



## Bibliography

- Chen N-P, Sun Z, Fässler R. 2018. The Kank family proteins in adhesion dynamics. *Curr Opin Cell Biol* **54**:130–136. doi:10.1016/j.ceb.2018.05.015
- Chen NT, Lo SH. 2005. The N-terminal half of talin2 is sufficient for mouse development and survival. *Biochem Biophys Res Commun* **337**:670–676. doi:10.1016/j.bbrc.2005.09.100
- Chen WT, Singer SJ. 1982. Immunoelectron microscopic studies of the sites of cell-substratum and cell-cell contacts in cultured fibroblasts. *J Cell Biol* **95**:205–222. doi:10.1083/jcb.95.1.205
- Cheng KW, Mullins RD. 2020. Initiation and disassembly of filopodia tip complexes containing VASP and lamellipodin. *Mol Biol Cell* **31**:2021–2034. doi:10.1091/mbc.E20-04-0270
- Chinthalapudi K, Rangarajan ES, Izard T. 2018. The interaction of talin with the cell membrane is essential for integrin activation and focal adhesion formation. *Proc Natl Acad Sci* **115**:10339–10344. doi:10.1073/pnas.1806275115
- Chodniewicz D, Klemke RL. 2004. Regulation of integrin-mediated cellular responses through assembly of a CAS/Crk scaffold. *Biochim Biophys Acta - Mol Cell Res* **1692**:63–76. doi:10.1016/j.bbamcr.2004.03.006
- Chorev DS, Moscovitz O, Geiger B, Sharon M. 2014. Regulation of focal adhesion formation by a vinculin-Arp2/3 hybrid complex. *Nat Commun* **5**. doi:10.1038/ncomms4758
- Ciobanasu C, Faivre B, Le Clainche C. 2015. Reconstituting actomyosin-dependent mechanosensitive protein complexes in vitro. *Nat Protoc* **10**:75–89. doi:10.1038/nprot.2014.200
- Ciobanasu C, Faivre B, Le Clainche C. 2014. Actomyosin-dependent formation of the mechanosensitive talin–vinculin complex reinforces actin anchoring. *Nat Commun* **5**:3095. doi:10.1038/ncomms4095
- Ciobanasu C, Faivre B, Le Clainche C. 2013. Integrating actin dynamics, mechanotransduction and integrin activation: The multiple functions of actin binding proteins in focal adhesions. *Eur J Cell Biol* **92**. doi:10.1016/j.ejcb.2013.10.009
- Ciobanasu C, Faivre B, Le Clainche C. 2012. Actin Dynamics Associated with Focal Adhesions. *Int J Cell Biol* **2012**:1–9. doi:10.1155/2012/941292
- Ciobanasu C, Wang H, Henriot V, Mathieu C, Fente A, Csillag S, Vigouroux C, Faivre B, Le Clainche C. 2018. Integrin-bound talin head inhibits actin filament barbed-end elongation. *J Biol Chem* **293**:2586–2596. doi:10.1074/jbc.M117.808204
- Cohen DM, Kutscher B, Chen H, Murphy DB, Craig SW. 2006. A conformational switch in vinculin drives formation and dynamics of a talin–vinculin complex at focal adhesions. *J Biol Chem* **281**:16006–16015. doi:10.1074/jbc.M600738200
- Coló GP, Lafuente EM, Teixidó J. 2012. The MRL proteins: Adapting cell adhesion, migration and growth. *Eur J Cell Biol* **91**:861–868. doi:10.1016/j.ejcb.2012.03.001
- Cossart P, Kocks C. 1994. The actin-based motility of the facultative intracellular pathogen *Listeria monocytogenes*. *Mol Microbiol* **13**:395–402. doi:10.1111/j.1365-2958.1994.tb00434.x
- Critchley DR. 2009. Biochemical and Structural Properties of the Integrin-Associated

## Bibliography

- Cytoskeletal Protein Talin. *Annu Rev Biophys* **38**:235–254.  
doi:10.1146/annurev.biophys.050708.133744
- Damiano-Guercio J, Kurzawa L, Mueller J, Dimchev G, Schaks M, Nemethova M, Pokrant T, Brühmann S, Linkner J, Blanchoin L, Sixt M, Rottner K, Faix J. 2020. Loss of Ena/VASP interferes with lamellipodium architecture, motility and integrin-dependent adhesion. *Elife* **9**:1–31. doi:10.7554/eLife.55351
- Debrand E, Conti FJ, Bate N, Spence L, Mazzeo D, Pritchard CA, Monkley SJ, Critchley DR. 2012. Mice carrying a complete deletion of the talin2 coding sequence are viable and fertile. *Biochem Biophys Res Commun* **426**:190–195. doi:10.1016/j.bbrc.2012.08.061
- Dedden D, Schumacher S, Kelley CF, Zacharias M, Biertümpfel C, Fässler R, Mizuno N. 2019. The Architecture of Talin1 Reveals an Autoinhibition Mechanism. *Cell* **179**:120–131.e13. doi:10.1016/j.cell.2019.08.034
- Del Rio A, Perez-Jimenez R, Liu R, Roca-Cusachs P, Fernandez JM, Sheetz MP. 2009. Stretching Single Talin Rod Molecules Activates Vinculin Binding. *Science (80- )* **323**:638–641. doi:10.1126/science.1162912
- DeMali KA, Barlow CA, Burrridge K. 2002. Recruitment of the Arp2/3 complex to vinculin: Coupling membrane protrusion to matrix adhesion. *J Cell Biol* **159**:881–891. doi:10.1083/jcb.200206043
- Di Paolo G, Pellegrini L, Letinic K, Cestra G, Zoncu R, Voronov S, Chang S, Guo J, Wenk MR, De Camilli P. 2002. Recruitment and regulation of phosphatidylinositol phosphate kinase type 1 $\gamma$  by the FERM domain of talin. *Nature* **420**:85–89. doi:10.1038/nature01147
- Doyle AD, Yamada KM. 2013. Cellular Mechanotransduction: Interactions with the Extracellular Matrix In: Mofrad MRK, Kamm RD, editors. Cellular Mechanotransduction. Cambridge: Cambridge University Press. pp. 120–160. doi:10.1017/CBO9781139195874.006
- Dumbauld DW, Lee TT, Singh A, Scrimgeour J, Gersbach CA, Zamir EA, Fu J, Chen CS, Curtis JE, Craig SW, Garcia AJ. 2013. How vinculin regulates force transmission. *Proc Natl Acad Sci* **110**:9788–9793. doi:10.1073/pnas.1216209110
- Elosegui-Artola A, Trepas X, Roca-Cusachs P. 2018. Control of Mechanotransduction by Molecular Clutch Dynamics. *Trends Cell Biol* **28**:356–367. doi:10.1016/j.tcb.2018.01.008
- Ermekeva KS, Zambrano N, Linn H, Minopoli G, Gertler F, Russo T, Sudol M. 1997. The WW Domain of Neural Protein FE65 Interacts with Proline-rich Motifs in Mena, the Mammalian Homolog of Drosophila Enabled. *J Biol Chem* **272**:32869–32877. doi:10.1074/jbc.272.52.32869
- Faix J, Rottner K. 2006. The making of filopodia. *Curr Opin Cell Biol* **18**:18–25. doi:10.1016/j.ceb.2005.11.002
- Fillingham I, Gingras AR, Papagrigoriou E, Patel B, Emsley J, Critchley DR, Roberts GCK, Barsukov IL. 2005. A vinculin binding domain from the talin rod unfolds to form a complex with the vinculin head. *Structure* **13**:65–74. doi:10.1016/j.str.2004.11.006
- Foster DS, Jones RE, Ransom RC, Longaker MT, Norton JA. 2018. The evolving relationship of wound healing and tumor stroma. *JCI Insight* **3**. doi:10.1172/jci.insight.99911

## Bibliography

- Franco-Chuaire ML, Magda Carolina S-C, Chuaire-Noack L. 2013. Epithelial-mesenchymal transition (EMT): principles and clinical impact in cancer therapy. *Invest Clin* **54**:186–205.
- Frischknecht F, Moreau V, Röttger S, Gonfloni S, Reckmann I, Superti-Furga G, Way M. 1999. Actin-based motility of vaccinia virus mimics receptor tyrosine kinase signalling. *Nature* **401**:926–929. doi:10.1038/44860
- Funk J, Merino F, Venkova L, Heydenreich L, Kierfeld J, Vargas P, Raunser S, Piel M, Bieling P. 2019. Profilin and formin constitute a pacemaker system for robust actin filament growth. *Elife* **8**:1–34. doi:10.7554/eLife.50963
- Galbraith CG, Yamada KM, Galbraith JA. 2007. Polymerizing Actin Fibers Position Integrins Primed to Probe for Adhesion Sites. *Science (80- )* **315**:992–995. doi:10.1126/science.1137904
- Gammill LS, Bronner-Fraser M. 2003. Neural crest specification: migrating into genomics. *Nat Rev Neurosci* **4**:795–805. doi:10.1038/nrn1219
- Garcia-Arcos JM, Chabrier R, Deygas M, Nader G, Barbier L, Sáez PJ, Mathur A, Vargas P, Piel M. 2019. Reconstitution of cell migration at a glance. *J Cell Sci*. doi:10.1242/jcs.225565
- Gardel ML, Schneider IC, Aratyn-Schaus, Y, Waterman CM. 2010. Mechanical Integration of Actin and Adhesion Dynamics in Cell Migration. *Annu Rev Cell Dev Biol* **26**:315–333. doi:10.1146/annurev.cellbio.011209.122036
- Geiger T, Zaidel-Bar R. 2012. Opening the floodgates: proteomics and the integrin adhesome. *Curr Opin Cell Biol* **24**:562–568. doi:10.1016/j.ceb.2012.05.004
- Georgiadou M, Ivaska J. 2017. Tensins: Bridging AMP-Activated Protein Kinase with Integrin Activation. *Trends Cell Biol* **27**:703–711. doi:10.1016/j.tcb.2017.06.004
- Giannone G, Dubin-Thaler BJ, Döbereiner H-G, Kieffer N, Bresnick AR, Sheetz MP. 2004. Periodic Lamellipodial Contractions Correlate with Rearward Actin Waves. *Cell* **116**:431–443. doi:10.1016/S0092-8674(04)00058-3
- Giannone G, Dubin-Thaler BJ, Rossier O, Cai Y, Chaga O, Jiang G, Beaver W, Döbereiner H-G, Freund Y, Borisy G, Sheetz MP. 2007. Lamellipodial Actin Mechanically Links Myosin Activity with Adhesion-Site Formation. *Cell* **128**:561–575. doi:10.1016/j.cell.2006.12.039
- Giannone G, Jiang G, Sutton DH, Critchley DR, Sheetz MP. 2003. Talin1 is critical for force-dependent reinforcement of initial integrin–cytoskeleton bonds but not tyrosine kinase activation. *J Cell Biol* **163**:409–419. doi:10.1083/jcb.200302001
- Gingras AR, Bate N, Goult BT, Patel B, Kopp PM, Emsley J, Barsukov IL, Roberts GCK, Critchley DR. 2010. Central region of talin has a unique fold that binds vinculin and actin. *J Biol Chem* **285**:29577–29587. doi:10.1074/jbc.M109.095455
- Gingras AR, Ziegler WH, Frank R, Barsukov IL, Roberts GCK, Critchley DR, Emsley J. 2005. Mapping and consensus sequence identification for multiple vinculin binding sites within the talin rod. *J Biol Chem* **280**:37217–37224. doi:10.1074/jbc.M508060200
- Ginsberg MH, Partridge A, Shattil SJ. 2005. Integrin regulation. *Curr Opin Cell Biol* **17**:509–516. doi:10.1016/j.ceb.2005.08.010
- Goksoy E, Ma YQ, Wang X, Kong X, Perera D, Plow EF, Qin J. 2008. Structural Basis for the

## Bibliography

- Autoinhibition of Talin in Regulating Integrin Activation. *Mol Cell* **31**:124–133. doi:10.1016/j.molcel.2008.06.011
- Gough RE, Goult BT. 2018. The tale of two talins - two isoforms to fine-tune integrin signalling. *FEBS Lett* **592**:2108–2125. doi:10.1002/1873-3468.13081
- Goult BT, Bate N, Anthis NJ, Wegener KL, Gingras AR, Patel B, Barsukov IL, Campbell ID, Roberts GCK, Critchley DR. 2009. The structure of an interdomain complex that regulates Talin activity. *J Biol Chem* **284**:15097–15106. doi:10.1074/jbc.M900078200
- Goult BT, Bouaouina M, Elliott PR, Bate N, Patel B, Gingras AR, Grossmann JG, Roberts GCK, Calderwood DA, Critchley DR, Barsukov IL. 2010. Structure of a double ubiquitin-like domain in the talin head: A role in integrin activation. *EMBO J* **29**:1069–1080. doi:10.1038/emboj.2010.4
- Goult BT, Xu XP, Gingras AR, Swift M, Patel B, Bate N, Kopp PM, Barsukov IL, Critchley DR, Volkmann N, Hanein D. 2013a. Structural studies on full-length talin1 reveal a compact auto-inhibited dimer: Implications for talin activation. *J Struct Biol* **184**:21–32. doi:10.1016/j.jsb.2013.05.014
- Goult BT, Yan J, Schwartz MA. 2018. Talin as a mechanosensitive signaling hub. *J Cell Biol* **217**:3776–3784. doi:10.1083/jcb.201808061
- Goult BT, Zacharchenko T, Bate N, Tsang R, Hey F, Gingras AR, Elliott PR, Roberts GCK, Ballestrem C, Critchley DR, Barsukov IL. 2013b. RIAM and Vinculin Binding to Talin Are Mutually Exclusive and Regulate Adhesion Assembly and Turnover. *J Biol Chem* **288**:8238–8249. doi:10.1074/jbc.M112.438119
- Grashoff C, Hoffman BD, Brenner MD, Zhou R, Parsons M, Yang MT, McLean MA, Sligar SG, Chen CS, Ha T, Schwartz MA. 2010. Measuring mechanical tension across vinculin reveals regulation of focal adhesion dynamics. *Nature* **466**:263–266. doi:10.1038/nature09198
- Haeger A, Wolf K, Zegers MM, Friedl P. 2015. Collective cell migration: Guidance principles and hierarchies. *Trends Cell Biol*. doi:10.1016/j.tcb.2015.06.003
- Haining AWM, Lieberthal TJ, Hernández A del R. 2016a. Talin: a mechanosensitive molecule in health and disease. *FASEB J* **30**:2073–2085. doi:10.1096/fj.201500080R
- Haining AWM, Rahikainen R, Cortes E, Lachowski D, Rice A, von Essen M, Hytönen VP, Del Río Hernández A. 2018. Mechanotransduction in talin through the interaction of the R8 domain with DLC1. *PLOS Biol* **16**:e2005599. doi:10.1371/journal.pbio.2005599
- Haining AWM, von Essen M, Attwood SJ, Hytönen VP, del Río Hernández A. 2016b. All Subdomains of the Talin Rod Are Mechanically Vulnerable and May Contribute To Cellular Mechanosensing. *ACS Nano* **10**:6648–6658. doi:10.1021/acsnano.6b01658
- Han J, Lim CJ, Watanabe N, Soriani A, Ratnikov B, Calderwood DA, Puzon-McLaughlin W, Lafuente EM, Boussiotis VA, Shattil SJ, Ginsberg MH. 2006. Reconstructing and Deconstructing Agonist-Induced Activation of Integrin  $\alpha$ IIb $\beta$ 3. *Curr Biol* **16**:1796–1806. doi:10.1016/j.cub.2006.08.035
- Hansen SD, Mullins RD. 2015. Lamellipodin promotes actin assembly by clustering Ena/VASP proteins and tethering them to actin filaments. *Elife* **4**:1–29. doi:10.7554/eLife.06585

## Bibliography

- Hansen SD, Mullins RD. 2010. VASP is a processive actin polymerase that requires monomeric actin for barbed end association. *J Cell Biol* **191**:571–584. doi:10.1083/jcb.201003014
- Haydari Z, Shams H, Jahed Z, Mofrad MRK. 2020. Kindlin Assists Talin to Promote Integrin Activation. *Biophys J* **118**:1977–1991. doi:10.1016/j.bpj.2020.02.023
- Hemmings L, Rees DJG, Ohanian V, Bolton SJ, Gilmore AP, Patel B, Priddle H, Trevithick JE, Hynes RO, Critchley DR. 1996. Talin contains three actin-binding sites each of which is adjacent to a vinculin-binding site. *J Cell Sci* **109**:2715–2726.
- Hervy M, Hoffman L, Beckerle MC. 2006. From the membrane to the nucleus and back again: bifunctional focal adhesion proteins. *Curr Opin Cell Biol* **18**:524–532. doi:10.1016/j.ceb.2006.08.006
- Hirata H, Tatsumi H, Lim CT, Sokabe M. 2014. Force-dependent vinculin binding to talin in live cells: a crucial step in anchoring the actin cytoskeleton to focal adhesions. *Am J Physiol Cell Physiol* **306**:607–620. doi:10.1152/ajpcell.00122.2013.-Mechanical
- Hotulainen P, Lappalainen P. 2006. Stress fibers are generated by two distinct actin assembly mechanisms in motile cells. *J Cell Biol* **173**:383–394. doi:10.1083/jcb.200511093
- Hu K, Ji L, Applegate KT, Danuser G, Waterman-Storer CM. 2007. Differential Transmission of Actin Motion Within Focal Adhesions. *Science (80- )* **315**:111–115. doi:10.1126/science.1135085
- Huang DL, Bax NA, Buckley CD, Weis WI, Dunn AR. 2017. Vinculin forms a directionally asymmetric catch bond with F-actin. *Science (80- )* **357**:703–706. doi:10.1126/science.aan2556
- Humphries JD, Wang P, Streuli C, Geiger B, Humphries MJ, Ballestrem C. 2007. Vinculin controls focal adhesion formation by direct interactions with talin and actin. *J Cell Biol* **179**:1043–1057. doi:10.1083/jcb.200703036
- Hytönen VP, Vogel V. 2008. How force might activate talin's vinculin binding sites: SMD reveals a structural mechanism. *PLoS Comput Biol* **4**. doi:10.1371/journal.pcbi.0040024
- Inagaki T, Suzuki S, Miyamoto T, Takeda T, Yamashita K, Komatsu A, Yamauchi K, Hashizume K. 2003. The Retinoic Acid-responsive Proline-rich Protein Is Identified in Promyeloleukemic HL-60 Cells. *J Biol Chem* **278**:51685–51692. doi:10.1074/jbc.M308016200
- Janoštiak R, Brábek J, Auernheimer V, Tatárová Z, Lautscham LA, Dey T, Gemperle J, Merkel R, Goldmann WH, Fabry B, Rösel D. 2014a. CAS directly interacts with vinculin to control mechanosensing and focal adhesion dynamics. *Cell Mol Life Sci* **71**:727–744. doi:10.1007/s00018-013-1450-x
- Janoštiak R, Pataki AC, Brábek J, Rösel D. 2014b. Mechanosensors in integrin signaling: The emerging role of p130Cas. *Eur J Cell Biol* **93**:445–454. doi:10.1016/j.ejcb.2014.07.002
- Jansen KA, Atherton P, Ballestrem C. 2017. Mechanotransduction at the cell-matrix interface. *Semin Cell Dev Biol* **71**:75–83. doi:10.1016/j.semcdb.2017.07.027
- Jenzora A, Behrendt B, Small JV, Stradal TEB. 2005. PREL1 provides a link from Ras signalling to the actin cytoskeleton via Ena / VASP proteins **579**:455–463. doi:10.1016/j.febslet.2004.10.110

## Bibliography

- Jiang G, Giannone G, Critchley DR, Fukumoto E, Sheetz MP. 2003. Two-piconewton slip bond between fibronectin and the cytoskeleton depends on talin. *Nature* **424**:334–337. doi:10.1038/nature01805
- Johnson RP, Craig SW. 1995. F-actin binding site masked by the intramolecular association of vinculin head and tail domains. *Nature* **373**:261–264. doi:10.1038/373261a0
- Johnson RP, Craig SW. 1994. An intramolecular association between the head and tail domains of vinculin modulates talin binding. *J Biol Chem* **269**:12611–12619.
- Kadry YA, Calderwood DA. 2020. Chapter 22: Structural and signaling functions of integrins. *Biochim Biophys Acta - Biomembr* **1862**:183206. doi:10.1016/j.bbamem.2020.183206
- Kanchanawong P, Shtengel G, Pasapera AM, Ramko EB, Davidson MW, Hess HF, Waterman CM. 2010. Nanoscale architecture of integrin-based cell adhesions. *Nature* **468**:580–584. doi:10.1038/nature09621
- Kechagia JZ, Ivaska J. 2019. Integrins as biomechanical sensors of the microenvironment. *Nat Rev Mol Cell Biol* **20**. doi:10.1038/s41580-019-0134-2
- Khan RB, Goult BT. 2019. Adhesions Assemble!—Autoinhibition as a Major Regulatory Mechanism of Integrin-Mediated Adhesion. *Front Mol Biosci* **6**:1–16. doi:10.3389/fmolb.2019.00144
- Kong F, García AJ, Mould AP, Humphries MJ, Zhu C. 2009. Demonstration of catch bonds between an integrin and its ligand. *J Cell Biol* **185**:1275–1284. doi:10.1083/jcb.200810002
- Kostic A, Sheetz MP. 2006. Fibronectin Rigidity Response through Fyn and p130Cas Recruitment to the Leading Edge. *Mol Biol Cell* **17**:2684–2695. doi:10.1091/mbc.e05-12-1161
- Kouyama T, Mihashi K. 1981. Fluorimetry Study of N-(1-Pyrenyl)iodoacetamide-Labelled F-Actin. *Eur J Biochem* **114**:33–38. doi:10.1111/j.1432-1033.1981.tb06167.x
- Kovar DR, Harris ES, Mahaffy R, Higgs HN, Pollard TD. 2006. Control of the Assembly of ATP- and ADP-Actin by Formins and Profilin. *Cell* **124**:423–435. doi:10.1016/j.cell.2005.11.038
- Krammer A, Lu H, Isralewitz B, Schulten K, Vogel V. 1999. Forced unfolding of the fibronectin type III module reveals a tensile molecular recognition switch. *Proc Natl Acad Sci U S A* **96**:1351–1356. doi:10.1073/pnas.96.4.1351
- Krause M, Leslie JD, Stewart M, Lafuente EM, Valderrama F, Jagannathan R, Strasser GA, Rubinson DA, Liu H, Way M, Yaffe MB, Boussiotis VA, Gertler FB. 2004. Lamellipodin , an Ena / VASP Ligand , Is Implicated in the Regulation of Lamellipodial Dynamics **7**:571–583.
- Kuo JC, Han X, Hsiao C Te, Yates JR, Waterman CM. 2011. Analysis of the myosin-II-responsive focal adhesion proteome reveals a role for  $\beta$ -Pix in negative regulation of focal adhesion maturation. *Nat Cell Biol* **13**:383–395. doi:10.1038/ncb2216
- Kuroda M, Wada H, Kimura Y, Ueda K, Kioka N. 2017. Vinculin promotes nuclear localization of TAZ to inhibit ECM stiffness-dependent differentiation into adipocytes. *J Cell Sci* **130**:989–1002. doi:10.1242/jcs.194779
- Ladoux B, Mège RM. 2017. Mechanobiology of collective cell behaviours. *Nat Rev Mol Cell Biol*. doi:10.1038/nrm.2017.98

## Bibliography

- Lafuente EM, van Puijenbroek AAFL, Krause M, Carman C V., Freeman GJ, Berezovskaya A, Constantine E, Springer TA, Gertler FB, Boussiotis VA. 2004. RIAM, an Ena/VASP and profilin ligand, interacts with Rap1-GTP and mediates Rap1-induced adhesion. *Dev Cell* **7**:585–595. doi:10.1016/j.devcel.2004.07.021
- Lagarrigue F, Kim C, Ginsberg MH. 2017. The Rap1-RIAM-talin axis of integrin activation and blood cell function. *Blood* **128**:479–488. doi:10.1182/blood-2015-12-638700.cyttoplasmic
- Lagarrigue F, Vikas Anekal P, Lee H-S, Bachir AI, Ablack JN, Horwitz AF, Ginsberg MH. 2015. A RIAM/lamellipodin–talin–integrin complex forms the tip of sticky fingers that guide cell migration. *Nat Commun* **6**:8492. doi:10.1038/ncomms9492
- Laurent V, Loisel TP, Harbeck B, Wehman A, Gröbe L, Jockusch BM, Wehland J, Gertler FB, Carlier M-F. 1999. Role of Proteins of the Ena/VASP Family in Actin-based Motility of *Listeria monocytogenes*. *J Cell Biol* **144**:1245–1258. doi:10.1083/jcb.144.6.1245
- Law A, Vehlow A, Kotini M, Dodgson L, Soong D, Theveneau E, Bodo C, Taylor E, Navarro C, Perera U, Michael M, Dunn GA, Bennett D, Mayor R, Krause M. 2013. Lamellipodin and the Scar/WAVE complex cooperate to promote cell migration in vivo **203**:673–689. doi:10.1083/jcb.201304051
- Lawson C, Lim S-T, Uryu S, Chen XL, Calderwood DA, Schlaepfer DD. 2012. FAK promotes recruitment of talin to nascent adhesions to control cell motility. *J Cell Biol* **196**:223–232. doi:10.1083/jcb.201108078
- Le Clainche C, Carlier M-F. 2008. Regulation of Actin Assembly Associated With Protrusion and Adhesion in Cell Migration. *Physiol Rev* **88**:489–513. doi:10.1152/physrev.00021.2007
- Le Clainche C, Carlier M-F. 2004. Actin-Based Motility Assay Current Protocols in Cell Biology. Hoboken, NJ, USA: John Wiley & Sons, Inc. pp. 1–20. doi:10.1002/0471143030.cb1207s24
- Le Clainche C, Dwivedi SP, Didry D, Carlier M-F. 2010. Vinculin Is a Dually Regulated Actin Filament Barbed End-capping and Side-binding Protein. *J Biol Chem* **285**:23420–23432. doi:10.1074/jbc.M110.102830
- Lee H-S, Anekal P, Lim CJ, Liu C-C, Ginsberg MH. 2013. Two modes of integrin activation form a binary molecular switch in adhesion maturation. *Mol Biol Cell* **24**:1354–1362. doi:10.1091/mbc.e12-09-0695
- Lee H-S, Lim CJ, Puzon-McLaughlin W, Shattil SJ, Ginsberg MH. 2009. RIAM Activates Integrins by Linking Talin to Ras GTPase Membrane-targeting Sequences. *J Biol Chem* **284**:5119–5127. doi:10.1074/jbc.M807117200
- Lee SE, Kamm RD, Mofrad MRK. 2007. Force-induced activation of Talin and its possible role in focal adhesion mechanotransduction. *J Biomech* **40**:2096–2106. doi:10.1016/j.jbiomech.2007.04.006
- Letort G, Ennomani H, Gressin L, Théry M, Blanchoin L. 2015. Dynamic reorganization of the actin cytoskeleton. *F1000Research* **4**:940. doi:10.12688/f1000research.6374.1
- Li G, Du X, Vass WC, Papageorge AG, Lowy DR, Qian X. 2011. Full activity of the deleted in liver cancer 1 (DLC1) tumor suppressor depends on an LD-like motif that binds talin and focal adhesion kinase (FAK). *Proc Natl Acad Sci* **108**:17129–17134. doi:10.1073/pnas.1112122108

## Bibliography

- Li S, Guan J-L, Chien S. 2005. Biochemistry and Biomechanics of Cell Motility. *Annu Rev Biomed Eng* **7**:105–150. doi:10.1146/annurev.bioeng.7.060804.100340
- Liu J, Das M, Yang J, Ithychanda SS, Yakubenko VP, Plow EF, Qin J. 2015. Structural mechanism of integrin inactivation by filamin. *Nat Struct Mol Biol* **22**:383–391. doi:10.1038/nsmb.2999
- Liu J, Fukuda K, Xu Z, Ma Y-Q, Hirbawi J, Mao X, Wu C, Plow EF, Qin J. 2011. Structural Basis of Phosphoinositide Binding to Kindlin-2 Protein Pleckstrin Homology Domain in Regulating Integrin Activation. *J Biol Chem* **286**:43334–43342. doi:10.1074/jbc.M111.295352
- Liu J, Wang Y, Goh WI, Goh H, Baird MA, Ruehland S, Teo S, Bate N, Critchley DR, Davidson MW, Kanchanawong P. 2015. Talin determines the nanoscale architecture of focal adhesions. *Proc Natl Acad Sci* **112**:E4864–E4873. doi:10.1073/pnas.1512025112
- Lo SH, Weisberg E, Chen LB. 1994. Tensin: A potential link between the cytoskeleton and signal transduction. *BioEssays* **16**:817–823. doi:10.1002/bies.950161108
- Lock JG, Wehrle-Haller B, Strömblad S. 2008. Cell-matrix adhesion complexes: Master control machinery of cell migration. *Semin Cancer Biol* **18**:65–76. doi:10.1016/j.semcancer.2007.10.001
- Loisel TP, Boujemaa R, Pantaloni D, Carlier M-F. 1999. Reconstitution of actin-based motility of *Listeria* and *Shigella* using pure proteins. *Nature* **401**:613–616. doi:10.1038/44183
- Lowery LA, Vactor D Van. 2009. The trip of the tip: understanding the growth cone machinery. *Nat Rev Mol Cell Biol* **10**:332–343. doi:10.1038/nrm2679
- Lu C, Wu F, Qiu W, Liu R. 2013. P130Cas substrate domain is intrinsically disordered as characterized by single-molecule force measurements. *Biophys Chem* **180–181**:37–43. doi:10.1016/j.bpc.2013.06.008
- Luo B-H, Carman C V., Springer TA. 2007. Structural Basis of Integrin Regulation and Signaling. *Annu Rev Immunol* **25**:619–647. doi:10.1146/annurev.immunol.25.022106.141618
- Machesky LM, Mullins RD, Higgs HN, Kaiser DA, Blanchoin L, May RC, Hall ME, Pollard TD. 1999. Scar, a WASp-related protein, activates nucleation of actin filaments by the Arp2/3 complex. *Proc Natl Acad Sci* **96**:3739–3744. doi:10.1073/pnas.96.7.3739
- Maciver SK, Zot HG, Pollard TD. 1991. Characterization of actin filament severing by actophorin from *Acanthamoeba castellanii*. *J Cell Biol* **115**:1611–1620. doi:10.1083/jcb.115.6.1611
- Margadant F, Chew LL, Hu X, Yu H, Bate N, Zhang X, Sheetz M. 2011. Mechanotransduction in vivo by repeated talin stretch-relaxation events depends upon vinculin. *PLoS Biol* **9**. doi:10.1371/journal.pbio.1001223
- Martel V, Rocaud-Sultan C, Dupe S, Marie C, Paulhe F, Galmiche A, Block MR, Albiges-Rizo C. 2001. Conformation, Localization, and Integrin Binding of Talin Depend on Its Interaction with Phosphoinositides. *J Biol Chem* **276**:21217–21227. doi:10.1074/jbc.M102373200
- McCleverty CJ, Lin DC, Liddington RC. 2007. Structure of the PTB domain of tensin1 and a model for its recruitment to fibrillar adhesions. *Protein Sci* **16**:1223–1229. doi:10.1110/ps.072798707



## Bibliography

- Michael M, Parsons M. 2020. New perspectives on integrin-dependent adhesions. *Curr Opin Cell Biol* **63**:31–37. doi:10.1016/j.ceb.2019.12.008
- Monkley SJ, Zhou XH, Kinston SJ, Giblett SM, Hemmings L, Priddle H, Brown JE, Pritchard CA, Critchley DR, Fässler R. 2000. Disruption of the talin gene arrests mouse development at the gastrulation stage. *Dev Dyn* **219**:560–574.  
doi:https://anatomypubs.onlinelibrary.wiley.com/doi/10.1002/1097-0177(2000)9999:9999%3C::AID-DVDY1079%3E3.0.CO;2-Y
- Murphy CT, Rock RS, Spudich JA. 2001. A myosin II mutation uncouples ATPase activity from motility and shortens step size. *Nat Cell Biol* **3**:311–315. doi:10.1038/35060110
- Mykuliak V V., Haining AWM, von Essen M, Del Río Hernández A, Hytönen VP. 2018. Mechanical unfolding reveals stable 3-helix intermediates in talin and  $\alpha$ -catenin. *PLOS Comput Biol* **14**:e1006126. doi:10.1371/journal.pcbi.1006126
- Niebuhr K. 1997. A novel proline-rich motif present in ActA of *Listeria monocytogenes* and cytoskeletal proteins is the ligand for the EVH1 domain, a protein module present in the Ena/VASP family. *EMBO J* **16**:5433–5444. doi:10.1093/emboj/16.17.5433
- Niedergang F, Grinstein S. 2018. How to build a phagosome: new concepts for an old process. *Curr Opin Cell Biol* **50**:57–63. doi:10.1016/j.ceb.2018.01.009
- Ohashi T, Kiehart DP, Erickson HP. 1999. Dynamics and elasticity of the fibronectin matrix in living cell culture visualized by fibronectin-green fluorescent protein. *Proc Natl Acad Sci U S A* **96**:2153–2158. doi:10.1073/pnas.96.5.2153
- Orłowski A, Kukkurainen S, Pöyry A, Rissanen S, Vattulainen I, Hytönen VP, Róg T. 2015. PIP2 and Talin Join Forces to Activate Integrin. *J Phys Chem B* **119**:12381–12389. doi:10.1021/acs.jpcc.5b06457
- Patel B, Gingras AR, Bobkov AA, Fujimoto LM, Zhang M, Liddington RC, Mazzeo D, Emsley J, Roberts GCK, Barsukov IL, Critchley DR. 2006. The activity of the vinculin binding sites in talin is influenced by the stability of the helical bundles that make up the talin rod. *J Biol Chem* **281**:7458–7467. doi:10.1074/jbc.M508058200
- Patla I, Volberg T, Elad N, Hirschfeld-Warneken V, Grashoff C, Fässler R, Spatz JP, Geiger B, Medalia O. 2010. Dissecting the molecular architecture of integrin adhesion sites by cryo-electron tomography. *Nat Cell Biol* **12**:909–915. doi:10.1038/ncb2095
- Patsoukis N, Bardhan K, Weaver JD, Sari D, Torres-Gomez A, Li L, Strauss L, Lafuente EM, Boussiotis VA. 2017. The adaptor molecule RIAM integrates signaling events critical for integrin-mediated control of immune function and cancer progression. *Sci Signal* **10**:eaam8298. doi:10.1126/scisignal.aam8298
- Paul A, Pollard T. 2008. The Role of the FH1 Domain and Profilin in Formin-Mediated Actin-Filament Elongation and Nucleation. *Curr Biol* **18**:9–19. doi:10.1016/j.cub.2007.11.062
- Pernier J, Shekhar S, Jegou A, Guichard B, Carlier MF. 2016. Profilin Interaction with Actin Filament Barbed End Controls Dynamic Instability, Capping, Branching, and Motility. *Dev Cell* **36**:201–214. doi:10.1016/j.devcel.2015.12.024
- Plow EF, Qin J. 2019. The Kindlin Family of Adapter Proteins. *Circ Res* **124**:202–204. doi:10.1161/CIRCRESAHA.118.314362

## Bibliography

- Pollard TD. 2016. Actin and Actin-Binding Proteins. *Cold Spring Harb Perspect Biol* **8**:1–18. doi:10.1101/cshperspect.a018226
- Pollard TD. 1982. Chapter 22 Myosin Purification and Characterization Methods in Cell Biology. pp. 333–371. doi:10.1016/S0091-679X(08)60665-2
- Pollard TD, Cooper JA. 1984. Quantitative analysis of the effect of Acanthamoeba profilin on actin filament nucleation and elongation. *Biochemistry* **23**:6631–6641. doi:10.1021/bi00321a054
- Pring M, Weber A, Bubb MR. 1992. Profilin-actin complexes directly elongate actin filaments at the barbed end. *Biochemistry* **31**:1827–1836. doi:10.1021/bi00121a035
- Quinn CC, Pfeil DS, Chen E, Stovall EL, Harden M V., Gavin MK, Forrester WC, Ryder EF, Soto MC, Wadsworth WG. 2006. UNC-6/Netrin and SLT-1/Slit Guidance Cues Orient Axon Outgrowth Mediated by MIG-10/RIAM/Lamellipodin. *Curr Biol* **16**:845–853. doi:10.1016/j.cub.2006.03.025
- Rahikainen R, Öhman T, Turkki P, Varjosalo M, Hytönen VP. 2019. Talin-mediated force transmission and talin rod domain unfolding independently regulate adhesion signaling. *J Cell Sci* **132**:jcs226514. doi:10.1242/jcs.226514
- Rahikainen R, von Essen M, Schaefer M, Qi L, Azizi L, Kelly C, Ihalainen TO, Wehrle-Haller B, Bastmeyer M, Huang C, Hytönen VP. 2017. Mechanical stability of talin rod controls cell migration and substrate sensing. *Sci Rep* **7**:3571. doi:10.1038/s41598-017-03335-2
- Rausch V, Hansen CG. 2020. The Hippo Pathway, YAP/TAZ, and the Plasma Membrane. *Trends Cell Biol* **30**:32–48. doi:10.1016/j.tcb.2019.10.005
- Razinia Z, Mäkelä T, Ylännä J, Calderwood DA. 2012. Filamins in Mechanosensing and Signaling. *Annu Rev Biophys* **41**:227–246. doi:10.1146/annurev-biophys-050511-102252
- Reymann A-C, Martiel J-L, Cambier T, Blanchoin L, Boujemaa-Paterski R, Théry M. 2010. Nucleation geometry governs ordered actin networks structures. *Nat Mater* **9**:827–832. doi:10.1038/nmat2855
- Reymann AC, Boujemaa-Paterski R, Martiel JL, Guérin C, Cao W, Chin HF, De La Cruz EM, Théry M, Blanchoin L. 2012. Actin network architecture can determine myosin motor activity. *Science (80- )* **336**:1310–1314. doi:10.1126/science.1221708
- Ringer P, Colo G, Fässler R, Grashoff C. 2017. Sensing the mechano-chemical properties of the extracellular matrix. *Matrix Biol* **64**:6–16. doi:10.1016/j.matbio.2017.03.004
- Riveline D, Zamir E, Balaban NQ, Schwarz US, Ishizaki T, Narumiya S, Kam Z, Geiger B, Bershadsky AD. 2001. Focal contacts as mechanosensors: Externally applied local mechanical force induces growth of focal contacts by an mDia1-dependent and ROCK-independent mechanism. *J Cell Biol* **153**:1175–1185. doi:10.1083/jcb.153.6.1175
- Romero S, Le Clainche C, Didry D, Egile C, Pantaloni D, Carlier M-F. 2004. Formin Is a Processive Motor that Requires Profilin to Accelerate Actin Assembly and Associated ATP Hydrolysis. *Cell* **119**:419–429. doi:10.1016/j.cell.2004.09.039
- Romero S, Le Clainche C, Gautreau AM. 2020. Actin polymerization downstream of integrins: signaling pathways and mechanotransduction. *Biochem J* **477**:1–21.

## Bibliography

doi:10.1042/BCJ20170719

Rossier O, Oceau V, Sibarita JB, Leduc C, Tessier B, Nair D, Gatterdam V, Destaing O, Albigès-Rizo C, Tampé R, Cognet L, Choquet D, Lounis B, Giannone G. 2012. Integrins  $\beta$  1 and  $\beta$  3 exhibit distinct dynamic nanoscale organizations inside focal adhesions. *Nat Cell Biol* **14**:1057–1067. doi:10.1038/ncb2588

Rottner K, Behrendt B, Small JV, Wehland J. 1999. VASP dynamics during lamellipodia protrusion. *Nat Cell Biol* **1**:321–322. doi:10.1038/13040

Rottner K, Faix J, Bogdan S, Linder S, Kerkhoff E. 2017. Actin assembly mechanisms at a glance. *J Cell Sci* **130**:3427–3435. doi:10.1242/jcs.206433

Saltel F, Mortier E, Hytönen VP, Jacquier MC, Zimmermann P, Vogel V, Liu W, Wehrle-Haller B. 2009. New PI(4,5)P<sub>2</sub>- and membrane proximal integrin-binding motifs in the talin head control  $\beta$ 3-integrin clustering. *J Cell Biol* **187**:715–731. doi:10.1083/jcb.200908134

Sarangi BR, Gupta M, Doss BL, Tissot N, Lam F, Mè R, Borghi N, Ladoux B. 2017. Coordination between Intra-and Extracellular Forces Regulates Focal Adhesion Dynamics. *Nano Lett* **17**:399–406. doi:10.1021/acs.nanolett.6b04364

Sawada Y, Tamada M, Dubin-thaler BJ, Cherniavskaya O, Sakai R, Tanaka S, Sheetz MP. 2006. Force Sensing by Extension of the Src Family Kinase Substrate, p130Cas. *Cell* **127**:1015–1026. doi:10.1016/j.cell.2006.09.044.Force

Schiemer J, Bohm A, Lin L, Merrill-Skoloff G, Flaumenhaft R, Huang J-S, Le Breton GC, Chishti AH. 2016.  $\alpha$ 13 Switch Region 2 Relieves Talin Autoinhibition to Activate  $\alpha$ 11 $\beta$ 3 Integrin. *J Biol Chem* **291**:26598–26612. doi:10.1074/jbc.M116.747279

Schiller HB, Hermann MR, Polleux J, Vignaud T, Zanivan S, Friedel CC, Sun Z, Raducanu A, Gottschalk KE, Théry M, Mann M, Fässler R. 2013.  $\beta$  1 - And  $\alpha$  v -class integrins cooperate to regulate myosin II during rigidity sensing of fibronectin-based microenvironments. *Nat Cell Biol* **15**:625–636. doi:10.1038/ncb2747

Serrels B, Serrels A, Brunton VG, Holt M, McLean GW, Gray CH, Jones GE, Frame MC. 2007. Focal adhesion kinase controls actin assembly via a FERM-mediated interaction with the Arp2/3 complex. *Nat Cell Biol* **9**:1046–1056. doi:10.1038/ncb1626

Shekhar S, Pernier J, Carlier M. 2016. Regulators of actin filament barbed ends at a glance. *J Cell Sci* **129**:1085–1091. doi:10.1242/jcs.179994

Shen K, Tolbert CE, Guilluy C, Swaminathan VS, Berginski ME, Burrridge K, Superfine R, Campbell SL. 2011. The Vinculin C-terminal Hairpin Mediates F-actin Bundle Formation, Focal Adhesion, and Cell Mechanical Properties. *J Biol Chem* **286**:45103–45115. doi:10.1074/jbc.M111.244293

Shroff H, Galbraith CG, Galbraith JA, White H, Gillette J, Olenych S, Davidson MW, Betzig E. 2007. Dual-color superresolution imaging of genetically expressed probes within individual adhesion complexes. *Proc Natl Acad Sci* **104**:20308–20313. doi:10.1073/pnas.0710517105

Smith MA, Blankman E, Gardel ML, Luettjohann L, Waterman CM, Beckerle MC. 2010. A Zyxin-Mediated Mechanism for Actin Stress Fiber Maintenance and Repair. *Dev Cell* **19**:365–376. doi:10.1016/j.devcel.2010.08.008

## Bibliography

- Steffen A, Faix J, Resch GP, Linkner J, Wehland J, Small JV, Rottner K, Stradal TEB. 2006. Filopodia Formation in the Absence of Functional WAVE- and Arp2/3-Complexes. *Mol Biol Cell* **17**:2581–2591. doi:10.1091/mbc.e05-11-1088
- Stein H, Spindler S, Bonakdar N, Wang C, Sandoghdar V. 2017. Production of isolated giant unilamellar vesicles under high salt concentrations. *Front Physiol* **8**:1–16. doi:10.3389/fphys.2017.00063
- Stritt S, Wolf K, Lorenz V, Vögtle T, Gupta S, Bösl MR, Nieswandt B. 2015. Rap1-GTP–interacting adaptor molecule (RIAM) is dispensable for platelet integrin activation and function in mice. *Blood* **125**:219–222. doi:10.1182/blood-2014-08-597542
- Sun N, Critchley DR, Paulin D, Li Z, Robson RM. 2008. Identification of a repeated domain within mammalian  $\alpha$ -synemin that interacts directly with talin. *Exp Cell Res* **314**:1839–1849. doi:10.1016/j.yexcr.2008.01.034
- Sun Z, Costell M, Fässler R. 2019. Integrin activation by talin, kindlin and mechanical forces. *Nat Cell Biol* **21**:25–31. doi:10.1038/s41556-018-0234-9
- Sun Z, Tseng H-Y, Tan S, Senger F, Kurzawa L, Dedden D, Mizuno N, Wasik AA, Thery M, Dunn AR, Fässler R. 2016. Kank2 activates talin, reduces force transduction across integrins and induces central adhesion formation. *Nat Cell Biol* **18**:941–953. doi:10.1038/ncb3402
- Suraneni P, Rubinstein B, Unruh JR, Durnin M, Hanein D, Li R. 2012. The Arp2/3 complex is required for lamellipodia extension and directional fibroblast cell migration. *J Cell Biol* **197**:239–251. doi:10.1083/jcb.201112113
- Svitkina TM, Bulanova EA, Chaga OY, Vignjevic DM, Kojima S, Vasiliev JM, Borisy GG. 2003. Mechanism of filopodia initiation by reorganization of a dendritic network. *J Cell Biol* **160**:409–421. doi:10.1083/jcb.200210174
- Swaminathan V, Fischer RS, Waterman CM. 2016. The FAK–Arp2/3 interaction promotes leading edge advance and haptosensing by coupling nascent adhesions to lamellipodia actin. *Mol Biol Cell* **27**:1085–1100. doi:10.1091/mbc.E15-08-0590
- Theodosiou M, Widmaier M, Böttcher RT, Rognoni E, Veelders M, Bharadwaj M, Lambacher A, Austen K, Müller DJ, Zent R, Fässler R. 2016. Kindlin-2 cooperates with talin to activate integrins and induces cell spreading by directly binding paxillin. *Elife* **5**:1–24. doi:10.7554/eLife.10130
- Théry M, Racine V, Piel M, Pepin A, Dimitrov A, Chen Y, Sibarita J-B, Bornens M. 2006. Anisotropy of cell adhesive microenvironment governs cell internal organization and orientation of polarity. *Proc Natl Acad Sci* **103**:19771–19776. doi:10.1073/pnas.0609267103
- Thiam HR, Vargas P, Carpi N, Crespo CL, Raab M, Terriac E, King MC, Jacobelli J, Alberts AS, Stradal T, Lennon-Dumenil AM, Piel M. 2016. Perinuclear Arp2/3-driven actin polymerization enables nuclear deformation to facilitate cell migration through complex environments. *Nat Commun* **7**. doi:10.1038/ncomms10997
- Thievessen I, Thompson PM, Berlemont S, Plevock KM, Plotnikov S, Zemljic-Harpf A, Ross RS, Davidson MW, Danuser G, Campbell SL, Waterman CM. 2013. Vinculin–actin interaction couples actin retrograde flow to focal adhesions, but is dispensable for focal adhesion growth. *J Cell Biol* **202**:163–177. doi:10.1083/jcb.201303129

## Bibliography

- Thoss F, Dietrich F, Punkt K, Illenberger S, Rottner K, Himmel M, Ziegler WH. 2013. Metavinculin: New insights into functional properties of a muscle adhesion protein. *Biochem Biophys Res Commun* **430**:7–13. doi:10.1016/j.bbrc.2012.11.013
- Tilney LG, Portnoy DA. 1989. Actin filaments and the growth, movement, and spread of the intracellular bacterial parasite, *Listeria monocytogenes*. *J Cell Biol* **109**:1597–1608. doi:10.1083/jcb.109.4.1597
- Tojkander S, Gateva G, Husain A, Krishnan R, Lappalainen P. 2015. Generation of contractile actomyosin bundles depends on mechanosensitive actin filament assembly and disassembly. *Elife* **4**:1–28. doi:10.7554/eLife.06126
- Tojkander S, Gateva G, Schevzov G, Hotulainen P, Naumanen P, Martin C. 2011. Article A Molecular Pathway for Myosin II Recruitment to Stress Fibers. *Curr Biol* **21**:539–550. doi:10.1016/j.cub.2011.03.007
- Trichet L, Le Digabel J, Hawkins RJ, Vedula SRK, Gupta M, Ribault C, Hersen P, Voituriez R, Ladoux B. 2012. Evidence of a large-scale mechanosensing mechanism for cellular adaptation to substrate stiffness. *Proc Natl Acad Sci* **109**:6933–6938. doi:10.1073/pnas.1117810109
- Vicente-Manzanares M, Ma X, Adelstein RS, Horwitz AR. 2009. Non-muscle myosin II takes centre stage in cell adhesion and migration. *Nat Rev Mol Cell Biol* **10**:778–790. doi:10.1038/nrm2786
- Vigouroux C, Henriot V, Le Clainche C. 2020. Talin dissociates from RIAM and associates to vinculin sequentially in response to the actomyosin force. *Nat Commun* **11**:3116. doi:10.1038/s41467-020-16922-1
- Vogel V, Thomas WE, Craig DW, Krammer A, Baneyx G. 2001. Structural insights into the mechanical regulation of molecular recognition sites. *Trends Biotechnol* **19**:416–423. doi:10.1016/S0167-7799(01)01737-1
- Watanabe N, Bodin L, Pandey M, Krause M, Coughlin S, Boussiotis VA, Ginsberg MH, Shattil SJ. 2008. Mechanisms and consequences of agonist-induced talin recruitment to platelet integrin  $\alpha\text{IIb}\beta\text{3}$ . *J Cell Biol* **181**:1211–1222. doi:10.1083/jcb.200803094
- Wehrle-Haller B, Imhof BA. 2003. Integrin-dependent pathologies. *J Pathol* **200**:481–487. doi:10.1002/path.1399
- Weinberger A, Tsai F-C, Koenderink GH, Schmidt TF, Itri R, Meier W, Schmatko T, Schröder A, Marques C. 2013. Gel-Assisted Formation of Giant Unilamellar Vesicles. *Biophys J* **105**:154–164. doi:10.1016/j.bpj.2013.05.024
- Wen KK, Rubenstein PA, DeMali KA. 2009. Vinculin nucleates actin polymerization and modifies actin filament structure. *J Biol Chem* **284**:30463–30473. doi:10.1074/jbc.M109.021295
- Wiesner S. 2006. Purification of Skeletal Muscle Actin. *Cell Biology*. Elsevier. pp. 173–175. doi:10.1016/B978-012164730-8/50097-6
- Wioland H, Guichard B, Senju Y, Myram S, Lappalainen P, Jégou A, Romet-Lemonne G. 2017. ADF/Cofilin Accelerates Actin Dynamics by Severing Filaments and Promoting Their Depolymerization at Both Ends. *Curr Biol* **27**:1956–1967.e7. doi:10.1016/j.cub.2017.05.048

## Bibliography

- Wynne JP, Wu J, Su W, Mor A, Patsoukis N, Boussiotis VA, Hubbard SR, Philips MR. 2012. Rap1-interacting adapter molecule (RIAM) associates with the plasma membrane via a proximity detector. *J Cell Biol* **199**:317–330. doi:10.1083/jcb.201201157
- Xu W, Baribault H, Adamson ED. 1998. Vinculin knockout results in heart and brain defects during embryonic development. *Development* **125**:327–337.
- Yang J, Antin P, Berx G, Blanpain C, Brabletz T, Bronner M, Campbell K, Cano A, Casanova J, Christofori G, Dedhar S, Derynck R, Ford HL, Fuxe J, García de Herreros A, Goodall GJ, Hadjantonakis A-K, Huang RJY, Kalcheim C, Kalluri R, Kang Y, Khew-Goodall Y, Levine H, Liu J, Longmore GD, Mani SA, Massagué J, Mayor R, McClay D, Mostov KE, Newgreen DF, Nieto MA, Puisieux A, Runyan R, Savagner P, Stanger B, Stemmler MP, Takahashi Y, Takeichi M, Theveneau E, Thiery JP, Thompson EW, Weinberg RA, Williams ED, Xing J, Zhou BP, Sheng G. 2020. Guidelines and definitions for research on epithelial–mesenchymal transition. *Nat Rev Mol Cell Biol* **21**:341–352. doi:10.1038/s41580-020-0237-9
- Yang J, Zhu L, Zhang H, Hirbawi J, Fukuda K, Dwivedi P, Liu J, Byzova T, Plow EF, Wu J, Qin J. 2014. Conformational activation of talin by RIAM triggers integrin-mediated cell adhesion. *Nat Commun* **5**:5880. doi:10.1038/ncomms6880
- Yao M, Goult BT, Chen H, Cong P, Sheetz MP, Yan J. 2014. Mechanical activation of vinculin binding to talin locks talin in an unfolded conformation. *Sci Rep* **4**:4610. doi:10.1038/srep04610
- Yao M, Goult BT, Klapholz B, Hu X, Toseland CP, Guo Y, Cong P, Sheetz MP, Yan J. 2016. The mechanical response of talin. *Nat Commun* **7**:1–11. doi:10.1038/ncomms11966
- Ye F, Petrich BG, Anekal P, Lefort CT, Kasirer-Friede A, Shattil SJ, Ruppert R, Moser M, Fässler R, Ginsberg MH. 2013. The Mechanism of Kindlin-Mediated Activation of Integrin  $\alpha$ IIb $\beta$ 3. *Curr Biol* **23**:2288–2295. doi:10.1016/j.cub.2013.09.050
- Yogesha SD, Rangarajan ES, Vonrhein C, Bricogne G, Izard T. 2012. Crystal structure of vinculin in complex with vinculin binding site 50 (VBS50), the integrin binding site 2 (IBS2) of talin. *Protein Sci* **21**:583–588. doi:10.1002/pro.2041
- Yu M, Le S, Ammon Y, Goult BT, Akhmanova A, Yan J. 2019. Force-Dependent Regulation of Talin–KANK1 Complex at Focal Adhesions. *Nano Lett* **19**:5982–5990. doi:10.1021/acs.nanolett.9b01732
- Zacharchenko T, Qian X, Goult BT, Jethwa D, Almeida TB, Ballestrem C, Critchley DR, Lowy DR, Barsukov IL. 2016. LD Motif Recognition by Talin: Structure of the Talin-DLC1 Complex. *Structure* **24**:1130–1141. doi:10.1016/j.str.2016.04.016
- Zhang H, Chang Y-C, Brennan ML, Wu J. 2014. The structure of Rap1 in complex with RIAM reveals specificity determinants and recruitment mechanism. *J Mol Cell Biol* **6**:128–139. doi:10.1093/jmcb/mjt044
- Zhang H, Chang Y, Huang Q, Brennan ML, Zhang H, Chang Y, Huang Q, Brennan ML, Wu J. 2016a. Structural and Functional Analysis of a Talin Triple-Domain Module Suggests an Alternative Talin Autoinhibitory Configuration Article Structural and Functional Analysis of a Talin Triple-Domain Module Suggests an Alternative Talin Autoinhibitory Configura. *Struct Des* **24**:721–729. doi:10.1016/j.str.2016.02.020

## Bibliography

Zhang H, Chang YC, Huang Q, Brennan ML, Wu J. 2016b. Structural and Functional Analysis of a Talin Triple-Domain Module Suggests an Alternative Talin Autoinhibitory Configuration. *Structure* **24**:721–729. doi:10.1016/j.str.2016.02.020

Zhang X, Jiang G, Cai Y, Monkley SJ, Critchley DR, Sheetz MP. 2008. Talin depletion reveals independence of initial cell spreading from integrin activation and traction. *Nat Cell Biol* **10**:1062–1068. doi:10.1038/ncb1765

## APPENDIX

---

### ARTICLE 3: INTEGRIN-BOUND TALIN HEAD INHIBITS ACTIN FILAMENT BARBED END ELONGATION (CIOBANASU ET AL., 2018)

In this study, we found that the N-terminal actin-binding domain of talin blocks actin-filaments barbed-end elongation via a positively charged surface that is partially masked by its intramolecular interaction with talin R9. I characterized a construction of talin in Figure 3B. This article was published in December 2017 in The Journal of Biological Chemistry.



# Integrin-bound talin head inhibits actin filament barbed-end elongation

Received for publication, July 28, 2017, and in revised form, December 15, 2017. Published, Papers in Press, December 24, 2017, DOI 10.1074/jbc.M117.808204

Corina Ciobanasu<sup>1,2</sup>, Hong Wang<sup>1,3</sup>, Véronique Henriot<sup>1</sup>, Cécile Mathieu, Annabelle Fente, Sandrine Csillag, Clémence Vigouroux, Bruno Faivre, and Christophe Le Clairche<sup>4</sup>

From the Institute for Integrative Biology of the Cell (I2BC), CEA, CNRS, Université Paris-Sud, Université Paris-Saclay, 91198 Gif-sur-Yvette cedex, France

Edited by Norma M. Allewell

Focal adhesions (FAs) mechanically couple the extracellular matrix to the dynamic actin cytoskeleton, via transmembrane integrins and actin-binding proteins. The molecular mechanisms by which protein machineries control force transmission along this molecular axis (*i.e.* modulating integrin activation and controlling actin polymerization) remain largely unknown. Talin is a major actin-binding protein that controls both the inside-out activation of integrins and actin filament anchoring and thus plays a major role in the establishment of the actin-extracellular matrix mechanical coupling. Talin contains three actin-binding domains (ABDs). The N-terminal head domain contains both the F3 integrin-activating domain and ABD1, whereas the C-terminal rod contains the actin-anchoring ABD2 and ABD3. Integrin binding is regulated by an intramolecular interaction between the N-terminal head and a C-terminal five-helix bundle (R9). Whether talin ABDs regulate actin polymerization in a constitutive or regulated manner has not been fully explored. Here, we combine kinetics assays using fluorescence spectroscopy and single actin filament observation in total internal reflection fluorescence microscopy, to examine relevant functions of the three ABDs of talin. We find that the N-terminal ABD1 blocks actin filament barbed-end elongation, whereas ABD2 and ABD3 do not show any activity. By mutating residues in ABD1, we find that this activity is mediated by a positively charged surface that is partially masked by its intramolecular interaction with R9. Our results also demonstrate that, once this intramolecular interaction is released, the integrin-bound talin head retains the ability to inhibit actin assembly.

Cell adhesion to the extracellular matrix plays a critical role in many physiological functions, such as cell migration, invasion, or epithelial basement membrane attachment. Among the multiple adhesion structures, focal adhesions (FAs)<sup>5</sup> play a

major role (1, 2). These multiprotein complexes couple various extracellular matrices to the actin cytoskeleton via the transmembrane heterodimeric  $\alpha\beta$  integrins and actin-binding proteins (ABPs) (3, 4). The control of actin polymerization by ABPs is thought to play an important role to initiate the formation of the actomyosin stress fibers and control their tension by modulating their elongation. We showed previously that vinculin blocks actin filament barbed-end elongation (5), whereas others reported that VASP promotes the elongation of actin filament barbed ends in a processive-like manner (6, 7). Several formins may also play a role in the formation and elongation of stress fibers (8). However, despite these isolated characterizations, the respective roles of the multiple ABPs and their coordination in this process are poorly understood.

The actin-binding protein talin plays a major role in FAs (9) (Fig. S1). First, it acts very early to activate integrins. In this process, the N-terminal PTB (phosphotyrosine-binding) domain, located in the head domain of talin, also known as the F3 subdomain of the FERM (four-point-one, ezrin, radixin, moesin) domain, binds to the cytoplasmic tail of the  $\beta$  subunit of integrins to induce an allosteric conformational change through the membrane, leading to the binding of the extracellular domains to ECM with high affinity (10, 11). Talin head is not constitutively active because F3 is buried by an intramolecular interaction with the R9 five-helix bundle of the rod (12, 13). Several mechanisms have been proposed to explain talin head exposure in FAs. The binding of the N-terminal head of talin to a PIP2-enriched membrane or to the RIAM (Rap1-GTP-interacting adaptor molecule) protein could disrupt the F3-R9 interaction to expose F3, allowing integrin binding (13–16). Talin head is also released by calpain-mediated proteolytic cleavage (17). The isolated head domain of talin, resulting from calpain cleavage, regulates adhesion dynamics (18).

In addition to its role in the inside-out activation of integrins, talin anchors the actin cytoskeleton to FAs (19). Talin contains three actin-binding domains (ABDs), also named actin-binding sites (ABSs) (20). ABD1 spans along the F2 and F3 subdomains of the FERM domain (21). ABD2 is located in the center of the rod (22). ABD3, also known as THATCH (talin/HIP1R/Slp2p actin-tethering C-terminal homology), is located at the C terminus of the protein (23). The nanoscale organization of mature FAs, revealed by superresolution, showed that the

This work was supported in part by Agence Nationale pour la Recherche Grants ANR-09-JCJC-0111 ADERACTIN (to C. L. C.) and ANR-16-CE13-0007-02 PHAGOMECHANISME (to C. L. C.). The authors declare that they have no conflicts of interest with the contents of this article.

This article contains Figs. S1–S8 and Movies S1 and S2.

<sup>1</sup> These authors contributed equally to this work.

<sup>2</sup> Present address: Interdisciplinary Research Dept., Alexandru I. Cuza University, Blvd. Carol I, no. 11, Iasi, RO-700506, Romania.

<sup>3</sup> Supported by a Ph.D. fellowship from the China Scholarship Council (CSC).

<sup>4</sup> To whom correspondence should be addressed. E-mail: christophe.leclairche@i2bc.paris-saclay.fr.

<sup>5</sup> The abbreviations used are: FA, focal adhesion; ABP, actin-binding protein; VASP, vasodilator-stimulated phosphoprotein; ABD, actin-binding domain;

ABS, actin-binding site; TIRF, total internal reflection fluorescence; PMSF, phenylmethylsulfonyl fluoride; a.u., arbitrary units; PLL, poly-L-lysine.

N-terminal ABD1 of talin is located proximal to the membrane, whereas ABD3 extends deeper in the cell to anchor actomyosin stress fibers (24). In this conformation, talin behaves as a mechanosensor to transduce the force conveyed by the actin cytoskeleton to FAs (25). These properties allow talin to sense the rigidity of the ECM (26). Single molecule experiments showed that force transduction involves the mechanical stretching of the talin rod domain, which exposes cryptic vinculin-binding sites (27). Our previous work showed that vinculin binding to mechanically stretched talin exposes its ABD, known as vinculin tail, and reinforces actin anchoring (28, 29). In cells, actomyosin force acts on talin via its ABD3 to expose vinculin-binding sites and ABD2, locking talin into an actin-binding configuration that stabilizes FAs (30).

Although actin binding to talin plays a major role in the establishment of the actin-ECM mechanical coupling, the contribution of the three ABDs of talin to the regulation of actin polymerization is poorly understood. Here, we report the detailed characterization of the ABDs of talin. We found that the N-terminal ABD1 blocks actin filament barbed-end elongation, whereas ABD2 and ABD3 do not show any activity. This activity is masked by the intramolecular interaction between the F3 subdomain of ABD1 and R9. When ABD1 is exposed, it associates with the cytoplasmic tail of integrin- $\beta$ 3 and inhibits actin filament barbed-end elongation. Our study reveals a new activity of talin and paves the way to understand the complex regulation of actin assembly in FAs.

## Results

### Talin ABD1 inhibits actin filament barbed-end elongation

To determine the ability of talin constructs to regulate actin assembly (Fig. S1, A and C), we first monitored barbed-end elongation by measuring the increase in pyrenyl-labeled actin fluorescence upon polymerization in the presence of spectrin-actin seeds (5). In cells, multiple parameters can modify the activity of proteins, such as the charge of membrane lipids, the addition of phosphate groups by kinases, local gradients of pH and cations, crowding effects, or the binding of partners. Hence, in many instances, it proved informative to screen a variety of physico-chemical conditions, including a mild reduction in ionic strength, before establishing the activity of actin-binding proteins, such as formins, VASP, or vinculin (5, 31, 32). Here, varying the ionic strength was sufficient to reveal a new inhibitory activity of ABD1 (Fig. 1A). This activity of ABD1 is higher at low ionic strength, with a half-maximum effect at 50 mM KCl (Fig. S2), which is the KCl concentration used by many groups to establish the activity of actin-binding proteins (33). In conditions where ABD1 inhibited actin polymerization, full-length talin, ABD2, and ABD3 remained inactive (Fig. 1A).

The inhibition curve displays a sigmoidal shape (Fig. 1B), suggesting a cooperative mode of binding. Alternatively, at low concentration, ABD1 could be sequestered along the side of the filaments, preventing it from altering barbed-end dynamics. ABD1 abolished the elongation of spectrin-actin seeds but did not inhibit, or slightly enhanced, the pointed-end elongation of barbed-end capped gelsolin-actin complexes, indicating that

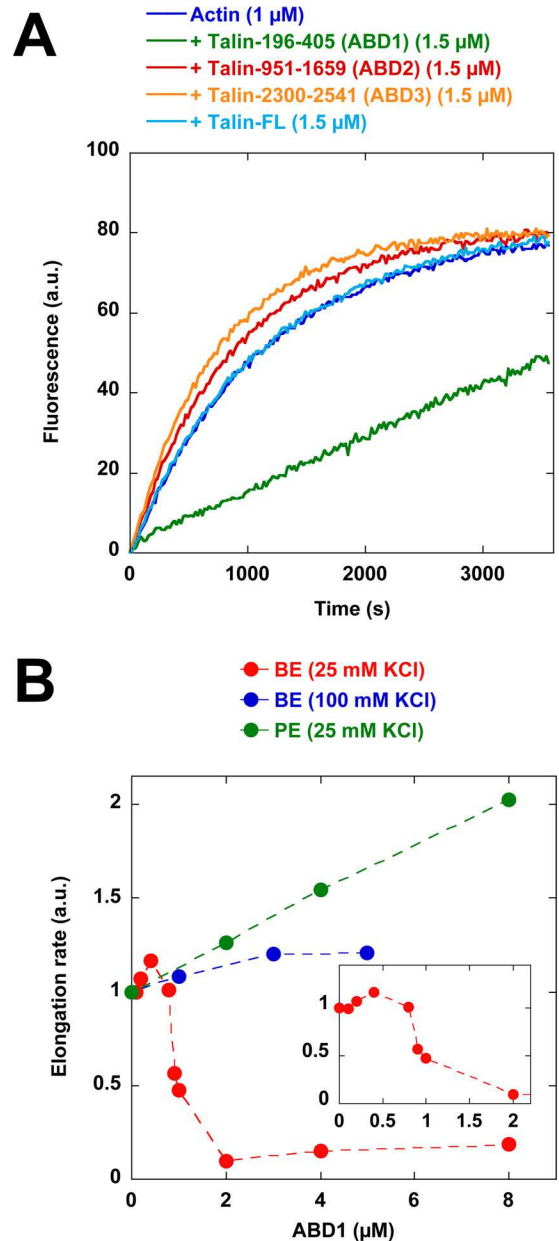


**Figure 1. Talin ABD1 inhibits actin filament barbed-end elongation.** A, barbed-end elongation was measured in the presence of 100  $\mu$ M spectrin-actin seeds, 1  $\mu$ M Mg-ATP-G-actin (10% pyrenyl-labeled) in the absence of talin and in the presence of 1.5  $\mu$ M full-length talin, 1.5  $\mu$ M ABD1, 1.5  $\mu$ M ABD2, and 1.5  $\mu$ M ABD3. This assay was performed at 25 mM KCl. B, barbed-end (BE) elongation was measured in the presence of 100  $\mu$ M spectrin-actin seeds, 1  $\mu$ M Mg-ATP-G-actin (10% pyrenyl-labeled), and increasing concentrations of ABD1 in the presence of 25 mM KCl (red points) and 100 mM KCl (blue points). Pointed end (PE) elongation was measured in the presence of 25 nM gelsolin-actin complex, 2  $\mu$ M Mg-ATP-G-actin (10% pyrenyl-labeled), and increasing concentrations of ABD1 (green points). The initial rates of pointed-end and barbed-end elongation were plotted versus the concentration of ABD1. The inset shows the detail of the red curve labeled BE (25 mM KCl) between 0 and 2  $\mu$ M ABD1.

ABD1 blocks the elongation of actin filament barbed ends specifically (Fig. 1B).

For the activity of isolated ABD1 to play a physiological role, a significant amount of ABD1-containing talin head, produced by calpain-mediated proteolysis, must exist in cells. To verify this point, we performed the biochemical fractionation of chicken gizzard tissue, extensively used in studies on FA pro-

## Talin head inhibits actin assembly

teins, followed by Western blotting with an antibody directed against talin head (Fig. S3A). We detected talin head in the cytosolic (S1) and membrane (P1) fractions, whereas full-length talin was found associated with the membrane fraction (P1) only. In mild extraction conditions, full-length talin dissociated from the membrane fraction (S2), whereas a large amount of talin head remained associated with the membrane (P2) (Fig. S3, B and C). These observations indicate that ABD1 probably plays a role independent of the context of the full-length protein.

The inhibition of barbed-end elongation is usually the signature of actin filament barbed-end capping proteins. However, our kinetic assays did not rule out the possibility that talin inhibitory activity results from the sequestration of actin monomers. Our results, showing that the saturation of the actin filaments by phalloidin completely abolished ABD1 activity, indicate that ABD1 acts on the filaments and not on the monomers (Fig. S4A). The effect of ABD1 on the linear relationship between the elongation rate and the concentration of polymerizing actin can also provide valuable information about the mechanism. In this assay, a capping protein is expected to decrease the slope of the curve, whereas a monomer-sequestering protein is expected to shift the curve without affecting the slope. We observed that, at nearly saturating concentrations of ABD1, the elongation rate is dramatically reduced (Fig. S4B). The abscissa intercept, which gives the critical concentration for actin assembly, is slightly shifted toward the critical concentration of the free pointed end, which is the usual signature of a barbed-end capping protein, but not further, ruling out an actin-monomer sequestering activity.

In cells, profilin-actin is the main polymerizable actin species, and profilin can participate in several mechanisms as a co-factor in an unpredictable manner. It was therefore important to determine whether ABD1 inhibits the elongation of actin filament barbed ends in the presence of a saturating amount of profilin. We found that profilin did not affect ABD1 activity or slightly enhanced its activity (Fig. S4A).

Finally, we directly observed the effect of ABD1 on the elongation of single actin filaments in total internal reflection fluorescence (TIRF) microscopy. In this assay, 5% biotin-labeled actin filaments are trapped on a streptavidin-biotin-PEG-coated surface to facilitate the quantification of the barbed-end elongation rate. In these conditions, we also observed that ABD1 inhibits actin assembly. At the single filament level, the details of the elongation clearly show that pauses occur in the presence of ABD1, resulting in the presence of blocked small filaments, whereas filaments elongate at the rate of the control between pauses (Fig. 2 (A–C) and Movies S1 and S2). In the presence of ABD1, the fraction of blocked filaments increases with time to reach 50% after 600 s at 2  $\mu\text{M}$  ABD1 (Fig. 2D). Altogether, these observations clearly show that ABD1 blocks actin filament barbed-end elongation in a capping-like manner.

### ABD1 activity is masked by an intramolecular interaction with R9

Interestingly, full-length talin, in contrast with isolated ABD1, remained inactive (Fig. 1A), suggesting that ABD1 activ-

ity is masked by an intramolecular interaction. To identify the domain that inhibits ABD1 activity, we compared the activity of talin constructs encompassing the N-terminal ABD1 domain and various deletions of the rod domain. We found that a talin construct (talin 196–1822) ending after the R9 five-helix bundle was almost inactive, whereas a talin construct (talin 196–1659) ending before R9 was fully active (Fig. 3, A and B). These observations indicate that R9 plays a critical role to keep ABD1 inactive. Talin constructs, containing combinations of exposed ABD1 and ABD2 (talin 196–1659) or exposed ABD1 and ABD3 (196–2541- $\Delta$ 912–2299), inhibit actin assembly, indicating that ABD1 activity does not combine with ABD2 or ABD3 to create a different activity (Fig. 3B).

To determine whether R9 was sufficient to inhibit ABD1, we expressed R9 as an isolated protein and tested its role on the inhibitory activity of isolated ABD1. Our results demonstrated that R9 is sufficient to reverse the activity of ABD1, whereas R9 alone did not affect actin assembly (Fig. 4, A and B). This result, indicating that actin and R9 binding to ABD1 are mutually exclusive, was confirmed by a co-sedimentation experiment in which increasing amounts of R9 efficiently displaced ABD1 from actin filaments (Fig. 4, C and D), without binding to actin (Fig. S5).

To define the ABD1-actin binding interface involved in the barbed-end capping-like activity, we performed a systematic mutagenesis analysis of ABD1. Because the sensitivity of ABD1 activity to ionic strength indicates that the ABD1-actin interaction is mainly electrostatic, we restricted this analysis to acidic and basic amino acids. We verified that our mutants were not unfolded by showing that they all retained the ability to interact with the side of actin filaments in a co-sedimentation assay (Fig. S6). Interestingly, we found several point mutations in basic residues that abolish ABD1 activity (Fig. 5, A and B). We also showed that the ABD1 K324E mutant, which is defective for barbed-end inhibition but not for side binding (Fig. 5 (A and B) and Fig. S6), reverses the inhibitory activity of the wildtype form of ABD1 in a kinetic assay (Fig. S7). This result indicates that actin filament side binding is necessary but not sufficient for the inhibitory activity of ABD1, which requires an additional set of basic residues to alter barbed-end dynamics.

Because most of these basic residues have been found by previous studies (14) to be involved in PIP2 binding, we tested the effect of PIP2 micelles and found that they reverse the activity of ABD1 (Fig. 5C). When placed on the known crystal structure of ABD1 (talin F2F3), these residues form a clear binding surface that spans along the F2 and F3 subdomains of ABD1 (Fig. 5D). Interestingly, several of these basic residues of F3 were also found to interact with R9 in the crystal structure of the F3-R9 complex (12) (Fig. 5E), explaining why R9 binding to ABD1 interferes with the activity of ABD1 on actin assembly (Fig. 4).

### Evidence for an integrin-talin complex that inhibits actin assembly

Previous reports also showed that R9 and the cytoplasmic tail of integrin- $\beta$  compete for ABD1 binding (12). Whether the binding of integrin- $\beta$  to ABD1 can release the R9-ABD1 auto-

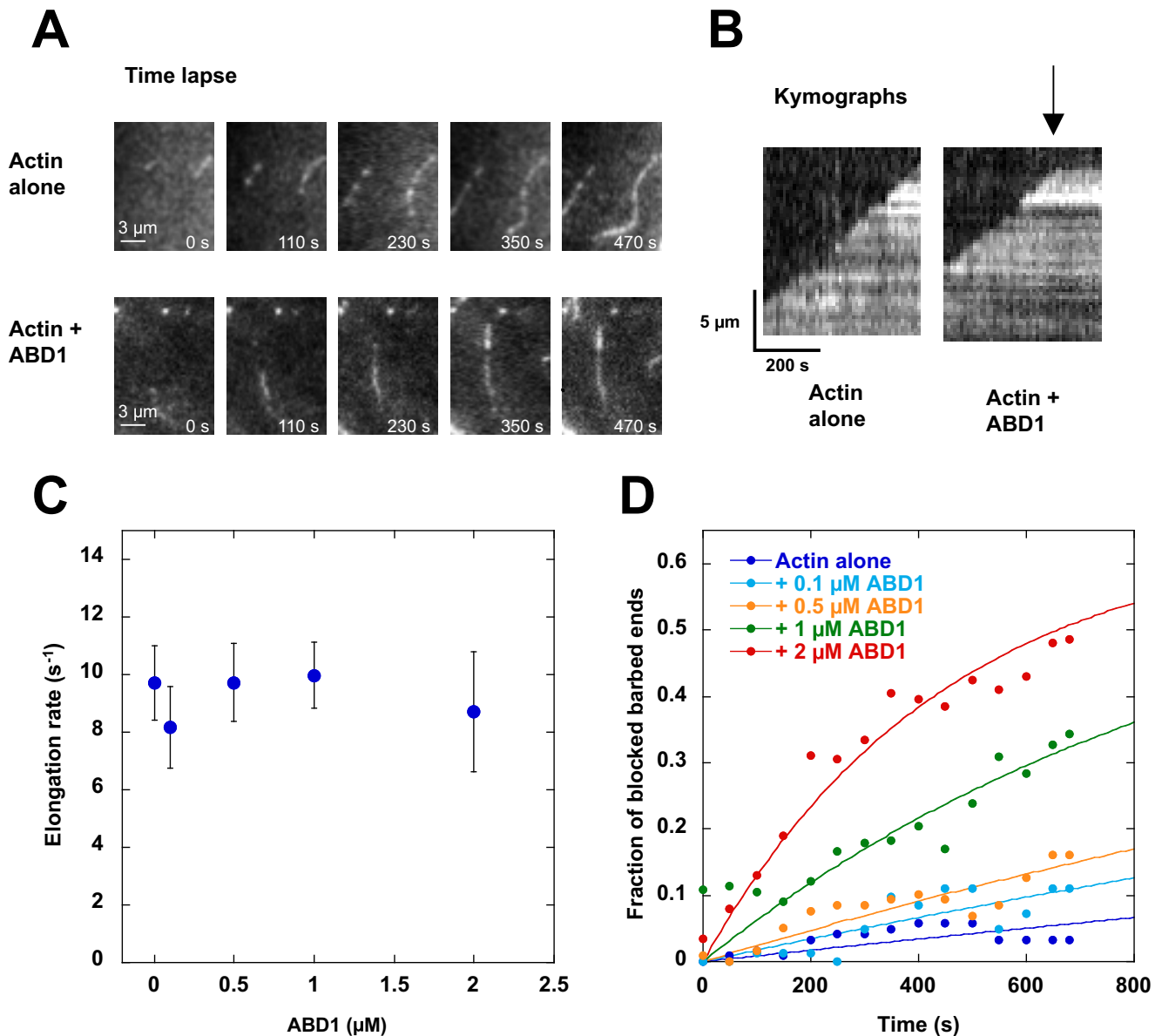


**Figure 2. Real-time observation and quantification of the inhibition of barbed-end elongation by talin ABD1 in TIRF microscopy.** Conditions were as follows: 1.5  $\mu M$  Mg-G-actin (5% Alexa 488- and 5% biotin-labeled) in 5 mM Tris, pH 7.8, 200  $\mu M$  ATP, 0.8% methylcellulose, 1 mM 1,4-diazabicyclo(2,2,2)-octane, 25 mM KCl, 1 mM MgCl<sub>2</sub>, 200  $\mu M$  EGTA, 10 mM DTT supplemented with 0, 0.1, 0.5, 1, and 2  $\mu M$  of talin ABD1. *A*, time lapse of the elongation of single actin filaments in the absence (*top*) or presence (*bottom*) of 1  $\mu M$  ABD1. Scale bar, 3  $\mu m$ . See the corresponding [Movie S1](#) and [Movie S2](#). *B*, kymographs of the filaments shown in *A*. The fluorescence intensity was measured along the length of a single filament (*vertical axis*) for each frame of the time lapse (*horizontal axis*). In contrast with the linear elongation of the control filaments (*left*), pauses (*arrow*) were observed in the presence of talin ABD1, indicating barbed-end capping-like events (*right*). *C*, elongation rate ( $s^{-1}$ ) of the filaments during the growing periods (between pauses), in the presence of the indicated concentrations of talin ABD1. Data are mean  $\pm$  S.D. (*error bars*). *D*, quantification of the data shown in *A* and *B*. The fraction of blocked filaments is plotted as a function of time in the absence or presence of the indicated concentrations of talin ABD1. For *C* and *D*, the number of filaments that we analyzed are  $n = 121$  (0  $\mu M$  ABD1),  $n = 82$  (0.1  $\mu M$  ABD1),  $n = 118$  (0.5  $\mu M$  ABD1),  $n = 324$  (1  $\mu M$  ABD1),  $n = 200$  (2  $\mu M$  ABD1).

inhibitory contact or keep it dissociated after talin activation to form an integrin-talin complex that inhibits barbed-end elongation is not known. Studying the binding of the cytoplasmic tail of integrin- $\beta$  to talin head in our assays is difficult because the affinity is very low ( $K_d = 273 \mu M$  for talin-1-integrin- $\beta$ , (34)). In cells, integrin clustering could favor the binding of integrin to talin through an avidity effect. To determine the activity of an integrin-talin-actin complex, we designed a synthetic peptide of integrin- $\beta$  carrying mutations (DTAN)/(VE) between the membrane-distal (MD) and membrane-proximal (MP) regions that are expected to increase the integrin-talin

affinity by a factor of 1000, according to similar mutations performed in integrin- $\beta$ 1D (34) (Fig. S1B). We tested the ability of this integrin peptide to reverse the ABD1-R9 interaction, using the inhibition of actin assembly as a readout of ABD1 exposure. First, we showed that integrin restores the ability of ABD1 to inhibit actin assembly in the presence of a saturating concentration of R9, indicating the existence of an active integrin-ABD1-actin ternary complex that is protected from R9 inhibition (Fig. 6A). We also tested the ability of this integrin peptide to activate longer autoinhibited constructs, such as full-length talin and talin 196–1822. This peptide induced the inhibition of

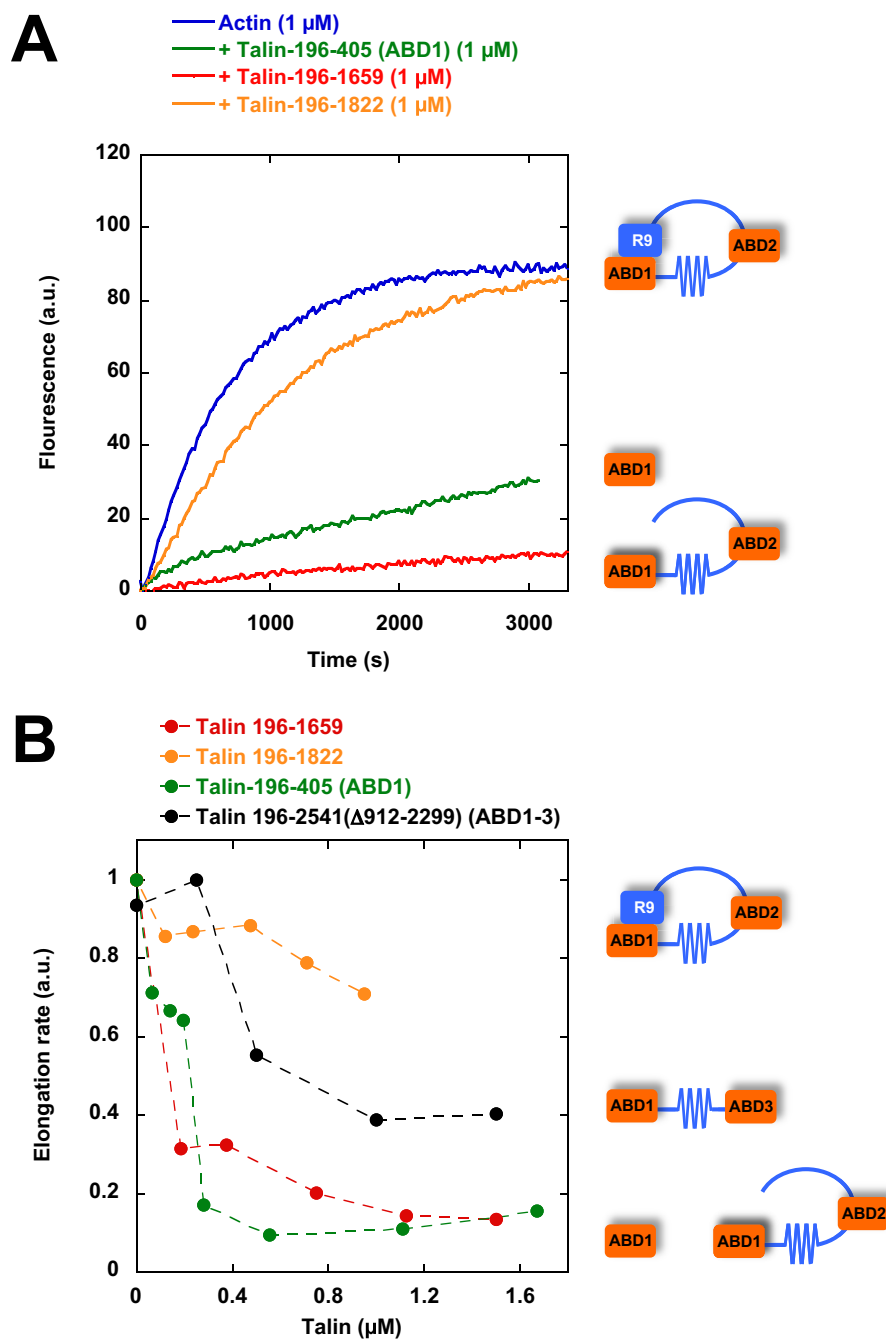


**Figure 3. The activity of talin ABD1 is masked by R9.** *A*, barbed-end elongation was measured in the presence of 100 pM spectrin-actin seeds, 1  $\mu\text{M}$  Mg-ATP-G-actin (10% pyrenyl-labeled) in the absence and in the presence of 1  $\mu\text{M}$  talin ABD1 196–405, 196–1659, and 196–1822. *B*, the initial rates of barbed-end elongation were plotted versus the concentration of talin-ABD1 196–405, 196–1659, and 196–1822 and talin-ABD1-3 (196–2541 $\Delta$ 912–2299). The conditions used in *B* are described in *A*.

actin assembly by talin 196–1822 (Fig. 6, *B* and *C*). However, this peptide could activate neither full-length talin nor full-length talin carrying the E1770A mutation, previously described to break the ABD1-R9 interaction (12), suggesting that the dimerization of full-length talin, together with additional autoinhibitory contacts, stabilizes the inactive conformation of talin (Fig. S8). We also found that the integrin- $\beta$ 3 peptide phosphorylated on tyrosine 747 of the NPLY motif was slightly less efficient at activating talin 196–1822 than the non-phosphorylated one (Fig. 6*C*), in agreement with previous find-

ings showing that this phosphorylation reduces talin-integrin binding (35).

## Discussion

Our study revealed that talin ABD1 inhibits actin filament barbed-end elongation in a regulated manner (Fig. 7, *A* and *B*). Talin adds to the list of proteins that target actin filaments barbed ends in FAs, including VASP, vinculin, tensin, and formins (5, 7, 8, 36). Like vinculin tail, talin ABD1 binds to the side of actin filaments and inhibits barbed-end elongation. In

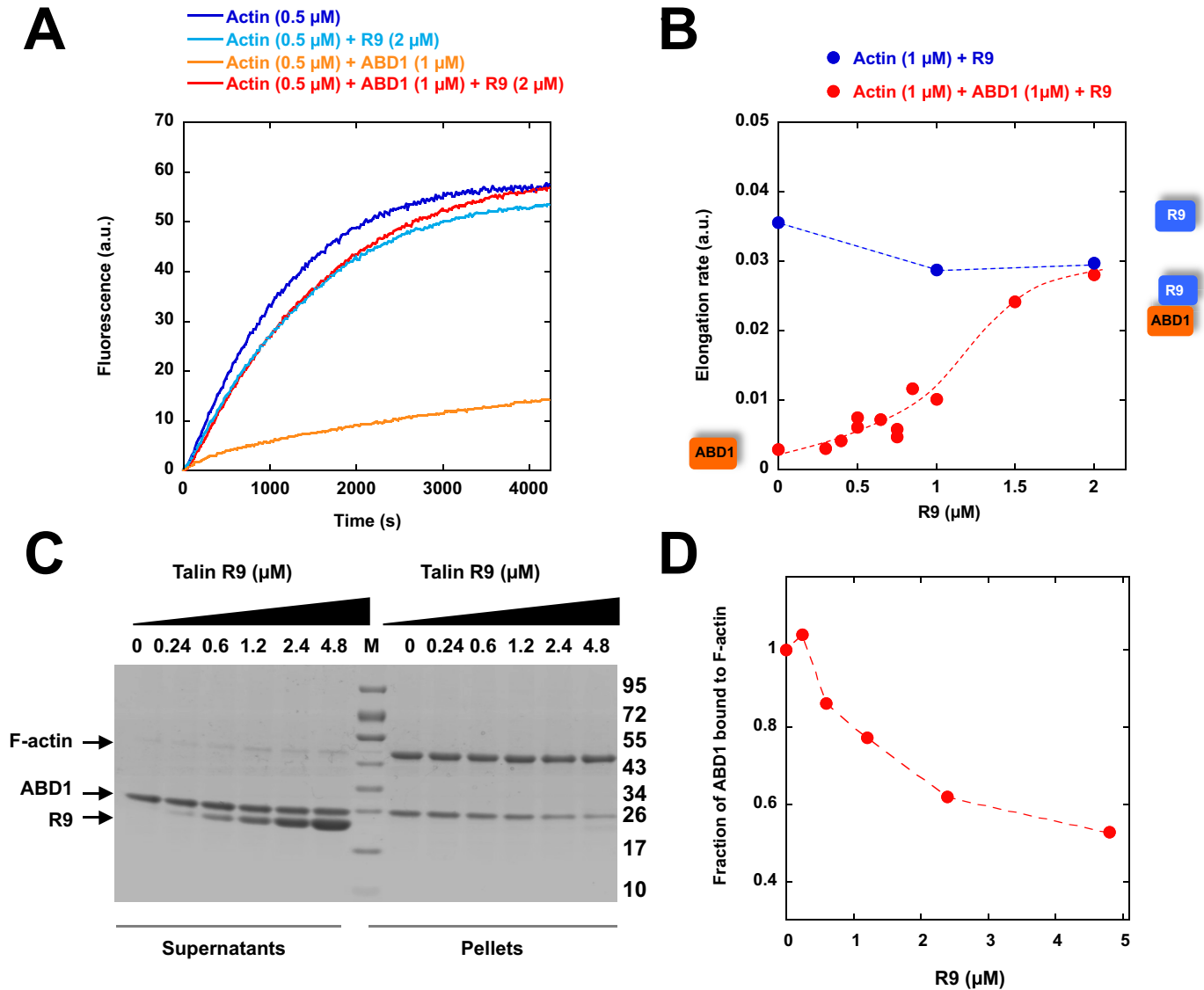


**Figure 4. The ability of talin ABD1 to bind to actin filaments and inhibit polymerization is regulated by the ABD1-R9 intramolecular interaction.** *A*, barbed-end elongation was measured in the presence of 100 pM spectrin-actin seeds, 0.5  $\mu\text{M}$  Mg-ATP-G-actin (10% pyrenyl-labeled) alone (dark blue) and in the presence of 2  $\mu\text{M}$  R9 alone (light blue), 1  $\mu\text{M}$  ABD1 alone (orange), and 1  $\mu\text{M}$  ABD1 + 2  $\mu\text{M}$  R9 (red). *B*, quantification of the elongation rate as a function of R9 concentration. *C*, co-sedimentation of ABD1 (2.3  $\mu\text{M}$ ) with actin filaments (5  $\mu\text{M}$ ) in the presence of increasing concentrations of R9 as indicated. Supernatant and pellet fractions were resolved by SDS-PAGE and stained by Coomassie Blue. *M*, molecular weight markers. *D*, quantification of the fraction of ABD1 bound to actin filaments as a function of R9 concentration.

both mechanisms, barbed-end inhibition requires amino acids that are not necessary for side binding. Determining the result of the combination of these similar activities in the force-dependent talin-vinculin complex will be the subject of future studies.

In FAs, the elongation of actin filaments is expected to release the actomyosin-based tension in stress fibers. Conversely, the stable anchoring provided by actin filament barbed-end capping in FAs could be a means to increase the traction force applied by stress fibers on FAs and ECM. Another interesting possibility is that all the barbed-end capping proteins mentioned above, including talin, anchor the filaments with their barbed ends facing FAs and their pointed ends pointing outward, to create the appropriate orientation for actomyosin contraction.

Interestingly, we identified four lysines in the F3 part of ABD1 (Lys-318, Lys-320, Lys-322, and Lys-324) that are involved in the inhibitory activity and that were previously described in the F3-R9 autoinhibitory interaction (12, 13). This observation explains why an autoinhibited construct of talin (residues 196–1822 or full-length) does not inhibit actin polymerization (Fig. 7A). Although we used a high-affinity mutant of integrin- $\beta$ 3 to disrupt this interaction, as a tool to demonstrate the existence of an integrin-talin-actin complex, the affinity of the wildtype integrin- $\beta$ 3 tail for talin ( $K_d = 273 \mu\text{M}$  (34)) is probably not sufficient to break the ABD1-R9 intramolecular interaction. It is more likely that other regulators, such as RIAM, synergize with integrin to disrupt the ABD1-R9 interaction of the autoinhibited conformation (16), allowing ABD1 to bind actin. Alternatively, the calpain-mediated cleavage of

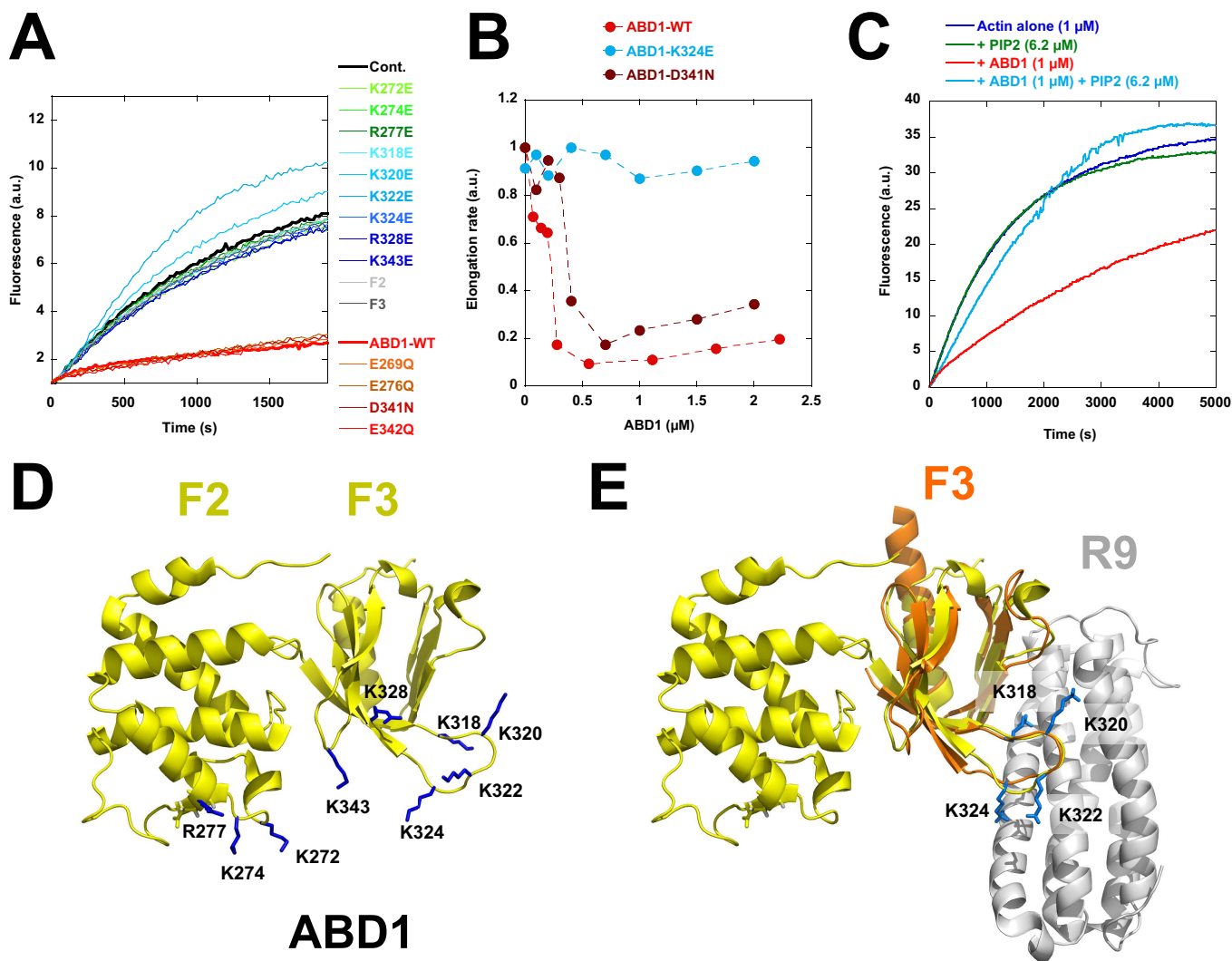


**Figure 5. Systematic mutagenesis of charged amino acids in ABD1 reveals the ABD1-actin binding interface and explains the mechanism by which R9 masks ABD1 activity.** *A*, barbed-end elongation was measured in the presence of  $100\ \mu\text{M}$  spectrin-actin seeds,  $1\ \mu\text{M}$  Mg-ATP-G-actin ( $10\%$  pyrenyl-labeled) in the absence (*cont.*) and in the presence of  $1.5\ \mu\text{M}$  talin-ABD1-WT; the point mutants E269Q, K272E, K274E, E276Q, R277E, K318E, K320E, K322E, K324E, R328E, D341N, E342Q, and K343E; and the F2 and F3 domains. *B*, the initial rates of barbed-end elongation were plotted *versus* the concentration of talin-ABD1 WT, K324E, and D341N. The conditions used in *B* are described in *A*. *C*, the inhibition of barbed-end elongation observed in the presence of ABD1 ( $1\ \mu\text{M}$ ) is abrogated by PIP2 ( $6.2\ \mu\text{M}$ ). *D*, the amino acids whose mutation affects the activity of ABD1 are represented on the known structure (side chains in *blue*) (43). *E*, overlay of ABD1 (F2F3) (*yellow*) and the complex formed by F3 (*orange*) and R9 (*gray*) (12, 43). The four basic amino acids (Lys-318, -320, -322, and -324) in F3 (side chains in *blue*) involved in the inhibition of actin polymerization are also involved in the autoinhibitory contact between ABD1 and R9. The representations of the known structures in *D* and *E* have been generated by PyMOL (Schroedinger, LLC, New York).

the region linking the head and the rod of talin produces enough talin head that constitutively interacts with both integrin and actin (18).

Our findings also shed light on the mechanism by which actin could modulate integrin activation by talin (Fig. 7). Integrin activation occurs through outside-in and inside-out mechanisms. The outside-in mechanism involves the binding of ECM to integrin, inducing integrin extension. The inside-out mechanism involves the binding of talin F3 to the cytoplasmic tail of integrin- $\beta$ . Talin first interacts with the integrin MD site, inducing its ordering (37). This first step is followed by the binding of the lysine 324 of F3 (Lys-327 in talin-2) to an acidic residue of the integrin MP site (Asp-723 in integrin- $\beta$ 3 or Asp-729 in integrin- $\beta$ 1). This interaction brings the positively charged interface, made of basic residues of F2 and F3, in close proximity to the negative charges of PIP2 heads at the inner face

of the plasma membrane (Fig. 7C). The interaction between talin Lys-324 and integrin- $\beta$ 3 Asp-723 also disrupts the salt bridge between this acidic residue and a basic residue of the  $\alpha$  subunit (Arg-995 in  $\alpha$ IIb), allowing the dissociation of the  $\alpha$  and  $\beta$  subunits and their extension in a high-affinity conformation for ECM (38). In this conformation, talin F3 interacts with integrin MD and MP sites, and both F2 and F3 are anchored to the PIP2-containing membrane surface. The actin-binding surface that we identified along F2 and F3 is nearly identical to the one that interacts with PIP2-containing membranes, because all of the mutations that reverse the inhibition of actin assembly by ABD1 have also been described to alter the binding of PIP2 to liposomes *in vitro* (14). Our results confirm that PIP2 prevents ABD1 to inhibit actin polymerization. Interestingly, our mutagenesis study, showing that the lysine Lys-324 interacts with actin barbed ends, implies that actin prevents lysine

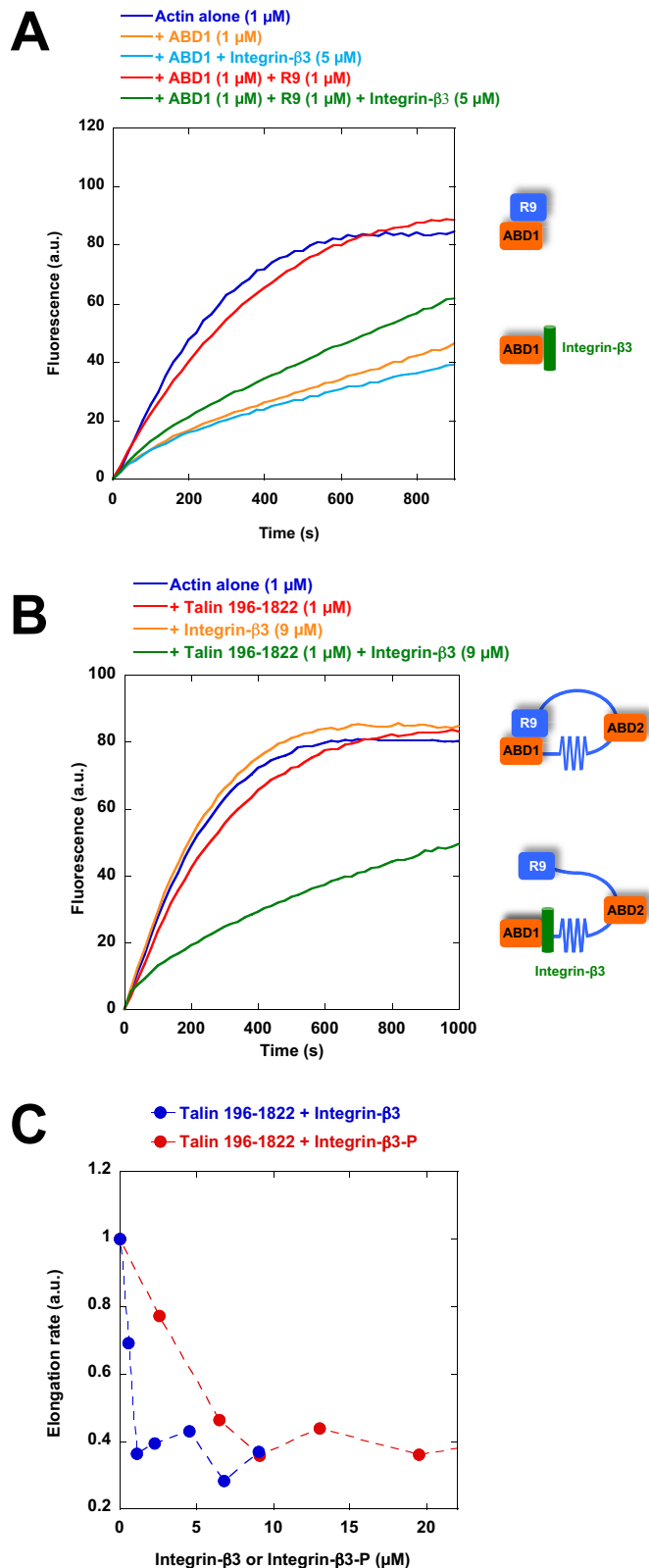


**Figure 6. Evidence for an integrin-talin-actin ternary complex that inhibits actin assembly.** A, barbed-end elongation was measured in the presence of 100 pM spectrin-actin seeds and 1  $\mu\text{M}$  Mg-ATP-G-actin (10% pyrenyl-labeled) alone (dark blue) and in the presence of 1  $\mu\text{M}$  talin ABD1 alone (orange), 1  $\mu\text{M}$  ABD1 + 5  $\mu\text{M}$  integrin- $\beta$ 3 (DTAN)/(VE) peptide (light blue), 1  $\mu\text{M}$  ABD1 + 1  $\mu\text{M}$  R9 (red), 1  $\mu\text{M}$  ABD1 + 1  $\mu\text{M}$  R9 + 5  $\mu\text{M}$  integrin- $\beta$ 3 (DTAN)/(VE) peptide (green). B, barbed-end elongation was measured in the presence of 100 pM spectrin-actin seeds and 1  $\mu\text{M}$  Mg-ATP-G-actin (10% pyrenyl-labeled) alone

324 from interacting with the MP site, which is normally required for integrin activation. Therefore, in the integrin-ABD1-actin complex, integrin would remain inactive because the F3 part of ABD1 only associates with the integrin MD site, whereas the MP site remains dissociated. In this conformation, ABD1 would not associate with the PIP<sub>2</sub>-containing membrane leaflet, leaving enough space for an actin filament to bind. In support of this hypothesis, the interaction between talin F3 and the isolated integrin MD site has been reported by others (37, 39). In addition, mutations in the MP region of integrin, including a K324D charge swapping, similar to the K324E we used, abolish integrin activation in cells and abrogate talin binding to the MP site but not to the MD site (37, 38).

It is generally believed that, in FAs, the ABD1-containing talin head lies on the membrane, where it activates integrin by the inside-out pathway (11), whereas the C-terminal ABD3 domain senses the actomyosin force to induce the formation of the mechanosensitive talin-vinculin complex, which is the first step toward the maturation of FAs (9). More recently, ABD2 has been involved in force transmission too (30). Our findings suggest an alternative mechanism to couple integrin to the actin cytoskeleton through the N-terminal ABD1. In this conformation, the talin rod does not sense force, and the integrin MP region cannot contribute to the inside-out integrin activation. This mechanism would allow the retrograde actin flow to drag inactive integrins inside FAs. The mechanism that we identified could also prevent inactive integrins from diffusing away from FAs between two activation events, which appears necessary for a very dynamic and adaptive process like integrin activation. Finally, it is also possible that the integrin-ABD1-actin complex transmits enough force to induce the mechanically induced transition from the closed to the open high-affinity conformation of integrin (40, 41).

### Experimental procedures

#### Recombinant cDNA constructs and peptides

cDNAs encoding for human talin-1 196–405 (ABD1), 196–309 (F2), 309–405 (F3), 196–1659, 196–1822, 951–1659 (ABD2), 1655–1822 (R9), and 2300–2541 (ABD3) were constructed by PCR amplification of the full-length talin cDNAs and subcloning of the resulting DNA in a pGEX6P1 plasmid (GE Healthcare). An N-terminal glutathione S-transferase (GST) tag is present in the pGEX6P1, and a C-terminal His<sub>6</sub> tag was introduced by PCR for talin 196–1659, talin 196–1822, and ABD2. Talin 196–2541 $\Delta$ 912–2299 (ABD1–3) was cloned into a pETM plasmid with an N-terminal StrepTagII and a C-terminal His<sub>6</sub> tag. Full-length talin carrying E1770A was generated from full-length talin cloned into pET101-TOPO (28, 29). The following integrin- $\beta$ 3 peptides were synthesized by ProteoGenix (France): KLLITIHDRKEFAKFEERARAKWVENPLYPKATSTFTNITYRGTC and KLLITIHDRKEFAKFEERARA-

(blue) and in the presence of 1  $\mu\text{M}$  talin 196–1822 (red), 9  $\mu\text{M}$  of integrin- $\beta$ 3 (DTAN)/(VE) peptide (orange), and 1  $\mu\text{M}$  talin 196–1822 + 9  $\mu\text{M}$  of integrin- $\beta$ 3 (DTAN)/(VE) peptide (green). C, the initial rates of barbed-end elongation obtained in the conditions described in B were plotted as a function of the concentration of integrin- $\beta$ 3 (DTAN)/(VE) or phosphorylated integrin- $\beta$ 3 (DTAN)/(VE) peptides.



## Talin head inhibits actin assembly

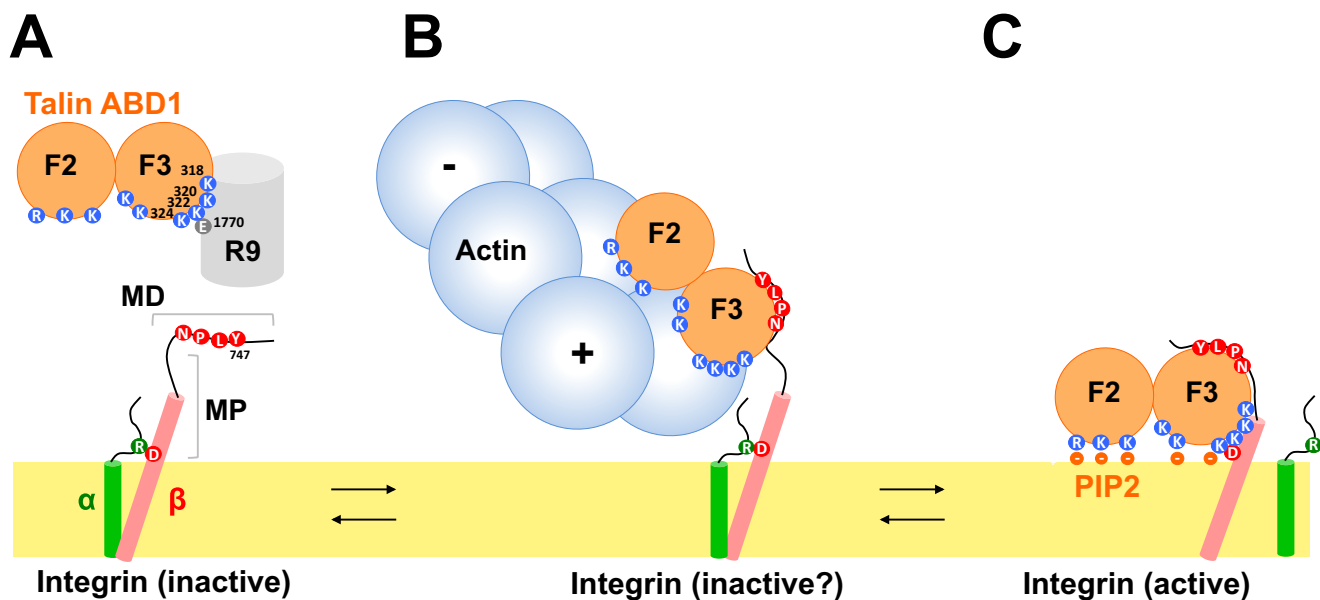


**Figure 7. Working model for the activity and regulation of talin.** *A*, schematic representation of talin showing only ABD1, made of F2 and F3, in contact with R9 (top) and integrin (cytoplasmic and transmembrane domains only) in its inactive conformation. The important amino acids are featured. *B*, the integrin MD site, ABD1, and actin form a ternary complex. In this complex, ABD1 inhibits actin filament barbed-end (+) elongation. In this situation, integrin is inactive, and the  $\alpha$  and  $\beta$  subunits remain associated. *C*, ABD1 binding to a PIP2-containing membrane allows its binding with integrin MD and MP sites. In this situation, integrin is active, and the  $\alpha$  and  $\beta$  subunits are dissociated. Actin cannot interact with ABD1.

KWVENPL<sub>p</sub>YPKEATSTFTNITYRGTC (where pY represents phosphotyrosine).

### Protein purification

All of the recombinant proteins were expressed using a similar protocol. First, the plasmid of interest was transformed in *Escherichia coli* (BL21 DE3, Invitrogen). Typically, transformed bacteria were grown in 4–8 liter of LB medium containing the appropriate antibiotics at 37 °C until the absorbance measured at 600 nm reached 0.6–0.8. The culture was then incubated on ice until the temperature reached 16 °C precisely. The expression of the recombinant proteins of interest was induced by adding 1 mM isopropyl 1-thio- $\beta$ -D-galactopyranoside to the medium during 16 h at 16 °C. After centrifugation, the pellet was lysed by sonication in 50 mM Tris, pH 7.8, 500 mM NaCl, 1% Triton X-100, 1 mM  $\beta$ -mercaptoethanol, 10  $\mu$ g/ml benzamidine, and 1 mM PMSF.

The proteins expressed as N-terminal GST fusions were bound to glutathione-Sepharose (GE Healthcare) during 2 h at 4 °C on a rotating wheel and washed with 50 mM Tris, pH 7.8, 500 mM NaCl, 1 mM  $\beta$ -mercaptoethanol. The protein of interest was cleaved from its GST tag by the PreScission protease (GE Healthcare) during 16 h at 4 °C on a rotating wheel and recovered in the supernatant after a low-speed centrifugation. Proteins containing a C-terminal His<sub>6</sub> tag (ABD2, 196–1659, and 196–1822) were further bound to Ni<sup>2+</sup>-nitrilotriacetic acid–agarose (Macherey-Nalge); washed with 50 mM Tris, pH 7.8, 500 mM NaCl, 20 mM imidazole, 1 mM  $\beta$ -mercaptoethanol; and eluted with 50 mM Tris, pH 7.8, 500 mM NaCl, 250 mM imidazole, 1 mM  $\beta$ -mercaptoethanol. Talin 196–2541 $\Delta$ 912–2299 (ABD1–3) was bound to Ni<sup>2+</sup>-nitrilotriacetic acid–agarose (Macherey-Nalge), washed with 50 mM Tris, pH 7.8, 500 mM NaCl, 20 mM imidazole, 1 mM  $\beta$ -mercaptoethanol and eluted with 50 mM Tris, pH 7.8, 500 mM NaCl, 250 mM imidaz-

ole, 1 mM  $\beta$ -mercaptoethanol. Proteins were finally dialyzed in 20 mM Tris, pH 7.8, 100 mM KCl, 1 mM  $\beta$ -mercaptoethanol; frozen in liquid nitrogen; and stored at –80 °C. Full-length talin and the E1770A mutant were expressed and purified as described previously (28, 29).

### Chicken gizzard fractionation

To fractionate chicken gizzards, we adapted the beginning of the classic protocol used for talin purification (42). Chicken gizzards (7 g) were mixed in 70 ml of ice-cold buffer (5 mM Tris, pH 7.0, 1 mM PMSF (protease inhibitor), and 5 mM EGTA) and homogenized in a Waring blender with three 10-s bursts at full speed. The suspension was centrifuged at 4 °C for 10 min at 10,000  $\times$  g. The supernatant (S1) was kept. The pellet (P1) was resuspended in 70 ml of ice-cold buffer (50 mM Tris, pH 9.0, 1 mM PMSF, and 5 mM EGTA) and homogenized in a Waring blender with three 10-s bursts at full speed. The suspension was then incubated at 37 °C for 30 min and centrifuged at 4 °C for 10 min at 10,000  $\times$  g to separate the soluble FA proteins (S2) and the membrane-associated proteins (P2). Comparable samples of S1, P1, S2, and P2 were submitted to Western blot analysis with an antibody directed against talin head (TA205, Bio-Rad). This experiment was reproduced twice with the same results.

### F-actin co-sedimentation assay

We performed co-sedimentation assays to measure the competition between actin filaments and R9 for talin ABD1. Increasing concentrations of R9 (0–4.8  $\mu$ M) were incubated with 2.3  $\mu$ M ABD1 and 5  $\mu$ M F-actin in 5 mM Tris, pH 7.8, 25 mM KCl, 1 mM MgCl<sub>2</sub>, 200  $\mu$ M ATP, 1 mM DTT for 15 min at room temperature. After centrifugation at 90,000 rpm in a TL100 centrifuge (Beckman), the pellets and supernatants were separated, loaded on SDS-PAGE, and quantified using the ImageJ

software. This experiment was reproduced three times in similar conditions with the same results.

### Polymerization assay

Actin polymerization was monitored by the increase in fluorescence of 10% pyrenyl-labeled actin. Actin polymerization was induced by the addition of 25 mM KCl (unless specified), 1 mM MgCl<sub>2</sub>, and 0.2 mM EGTA to a solution of 10% pyrenyl-labeled Ca-ATP-G-actin containing the proteins of interest. Fluorescence measurements were carried out in a Xenius spectrofluorimeter (Safas, Monaco). For kinetic experiments, 100 pM spectrin-actin seeds were added to the reaction for barbed-end elongation measurements, and 25 nM gelsolin-actin (1:2) complexes were added for pointed-end elongation measurements. All of the experiments have been reproduced two or three times with the same conclusions.

### Observation and measurement of single actin filament elongation by TIRF microscopy

Our protocol is a modification of the protocol used to study vinculin activity (5). To force the filaments to grow at the surface of the coverslip, we first irradiated coverslips with deep UV radiation for 1 min and incubated them with 10% biotin-labeled PLL-PEG for 1 h at room temperature. The coverslip was then washed extensively with water and dried with a nitrogen stream. Flow cells containing 40–60 μl of liquid were prepared by sticking the PLL-PEG-coated coverslip to a slide with double-faced adhesive spacers. The chamber was first incubated with 0.1 mg/ml streptavidin for 5 min and washed with washing buffer (5 mM Tris, pH 7.8, 200 μM ATP, 10 mM DTT, 1 mM MgCl<sub>2</sub>, 25 mM KCl). The chamber was then saturated with 10% BSA for 5 min and washed with washing buffer. The final reaction was then injected into the chamber. A typical reaction was composed of 1.5 μM 5% Alexa 488, 5% biotin-labeled Mg-G-actin in 5 mM Tris, pH 7.8, 200 μM ATP, 0.8% methylcellulose, 1 mM 1,4-diazabicyclo(2,2,2)-octane, 25 mM KCl, 1 mM MgCl<sub>2</sub>, 200 μM EGTA, 10 mM DTT supplemented with 0, 0.1, 0.5, 1, or 2 μM talin ABD1. Finally, we sealed the flow chamber with VALAP (a mixture of Vaseline, lanolin, and paraffin) and observed the reaction on an Olympus AX71 inverted microscope equipped with a ×60 (numerical aperture 1.45) objective (Olympus) and a Blues 473-nm laser (Cobolt). The time-lapse videos were acquired by Metamorph and subsequently analyzed by the ImageJ software.

**Author contributions**—C. C. identified the activity of talin, purified proteins, and performed some of the experiments shown in Figs. 1 and 4. H. W. performed the experiments and analyzed the data shown in Fig. 2. V. H. made cDNA constructs, purified proteins, and performed the experiments shown in Fig. 5. C. M. performed some of the experiments shown in Fig. 4. A. F. performed some of the experiments shown in Fig. 3. S. C. performed some of the experiments shown in Fig. 1 and Fig. S2. C. V. performed some of the experiments shown in Fig. 3. B. F. made cDNA constructs and purified proteins (Fig. S1). C. L. C. performed some of the experiments shown in Figs. 3 and 6 and Figs. S3–S8, conceived and coordinated the study, and wrote the paper.

**Acknowledgments**—We thank Pierre Montaville for help with structure representations and all the members of the “Cytoskeleton Dynamics and Motility” team for helpful discussions.

### References

- Wehrle-Haller, B. (2012) Structure and function of focal adhesions. *Curr. Opin. Cell Biol.* **24**, 116–124 [CrossRef Medline](#)
- Wehrle-Haller, B. (2012) Assembly and disassembly of cell matrix adhesions. *Curr. Opin. Cell Biol.* **24**, 569–581 [CrossRef Medline](#)
- Ciobanaru, C., Faivre, B., and Le Clainche, C. (2012) Actin dynamics associated with focal adhesions. *Int. J. Cell Biol.* **2012**, 941292 [Medline](#)
- Ciobanaru, C., Faivre, B., and Le Clainche, C. (2013) Integrating actin dynamics, mechanotransduction and integrin activation: the multiple functions of actin binding proteins in focal adhesions. *Eur. J. Cell Biol.* **92**, 339–348 [CrossRef Medline](#)
- Le Clainche, C., Dwivedi, S. P., Didry, D., and Carlier, M. F. (2010) Vinculin is a dually regulated actin filament barbed end-capping and side-binding protein. *J. Biol. Chem.* **285**, 23420–23432 [CrossRef Medline](#)
- Breitsprecher, D., Kieseewetter, A. K., Linkner, J., and Faix, J. (2009) Analysis of actin assembly by *in vitro* TIRF microscopy. *Methods Mol. Biol.* **571**, 401–415 [CrossRef Medline](#)
- Breitsprecher, D., Kieseewetter, A. K., Linkner, J., Urbanke, C., Resch, G. P., Small, J. V., and Faix, J. (2008) Clustering of VASP actively drives processive, WH2 domain-mediated actin filament elongation. *EMBO J.* **27**, 2943–2954 [CrossRef Medline](#)
- Skau, C. T., Plotnikov, S. V., Doyle, A. D., and Waterman, C. M. (2015) Inverted formin 2 in focal adhesions promotes dorsal stress fiber and fibrillar adhesion formation to drive extracellular matrix assembly. *Proc. Natl. Acad. Sci. U.S.A.* **112**, E2447–E2456 [CrossRef Medline](#)
- Calderwood, D. A., Campbell, I. D., and Critchley, D. R. (2013) Talins and kindlins: partners in integrin-mediated adhesion. *Nat. Rev. Mol. Cell Biol.* **14**, 503–517 [CrossRef Medline](#)
- Tadokoro, S., Shattil, S. J., Eto, K., Tai, V., Liddington, R. C., de Pereda, J. M., Ginsberg, M. H., and Calderwood, D. A. (2003) Talin binding to integrin beta tails: a final common step in integrin activation. *Science* **302**, 103–106 [CrossRef Medline](#)
- Calderwood, D. A., Zent, R., Grant, R., Rees, D. J., Hynes, R. O., and Ginsberg, M. H. (1999) The Talin head domain binds to integrin β subunit cytoplasmic tails and regulates integrin activation. *J. Biol. Chem.* **274**, 28071–28074 [CrossRef Medline](#)
- Goult, B. T., Bate, N., Anthis, N. J., Wegener, K. L., Gingras, A. R., Patel, B., Barsukov, I. L., Campbell, I. D., Roberts, G. C., and Critchley, D. R. (2009) The structure of an interdomain complex that regulates talin activity. *J. Biol. Chem.* **284**, 15097–15106 [CrossRef Medline](#)
- Goksoy, E., Ma, Y. Q., Wang, X., Kong, X., Perera, D., Plow, E. F., and Qin, J. (2008) Structural basis for the autoinhibition of talin in regulating integrin activation. *Mol. Cell* **31**, 124–133 [CrossRef Medline](#)
- Saltel, F., Mortier, E., Hytönen, V. P., Jacquier, M. C., Zimmermann, P., Vogel, V., Liu, W., and Wehrle-Haller, B. (2009) New PI(4,5)P<sub>2</sub>- and membrane proximal integrin-binding motifs in the talin head control β3-integrin clustering. *J. Cell Biol.* **187**, 715–731 [CrossRef Medline](#)
- Lee, H. S., Lim, C. J., Puzon-McLaughlin, W., Shattil, S. J., and Ginsberg, M. H. (2009) RIAM activates integrins by linking talin to ras GTPase membrane-targeting sequences. *J. Biol. Chem.* **284**, 5119–5127 [CrossRef Medline](#)
- Yang, J., Zhu, L., Zhang, H., Hirbawi, J., Fukuda, K., Dwivedi, P., Liu, J., Byzova, T., Plow, E. F., Wu, J., and Qin, J. (2014) Conformational activation of talin by RIAM triggers integrin-mediated cell adhesion. *Nat. Commun.* **5**, 5880 [CrossRef Medline](#)
- O'Halloran, T., Beckerle, M. C., and Burridge, K. (1985) Identification of talin as a major cytoplasmic protein implicated in platelet activation. *Nature* **317**, 449–451 [CrossRef Medline](#)
- Franco, S. J., Rodgers, M. A., Perrin, B. J., Han, J., Bennin, D. A., Critchley, D. R., and Huttenlocher, A. (2004) Calpain-mediated proteolysis of talin regulates adhesion dynamics. *Nat. Cell Biol.* **6**, 977–983 [CrossRef Medline](#)

## Talin head inhibits actin assembly

19. Jiang, G., Giannone, G., Critchley, D. R., Fukumoto, E., and Sheetz, M. P. (2003) Two-piconewton slip bond between fibronectin and the cytoskeleton depends on talin. *Nature* **424**, 334–337 [CrossRef Medline](#)
20. Hemmings, L., Rees, D. J., Ohanian, V., Bolton, S. J., Gilmore, A. P., Patel, B., Priddle, H., Trevithick, J. E., Hynes, R. O., and Critchley, D. R. (1996) Talin contains three actin-binding sites each of which is adjacent to a vinculin-binding site. *J. Cell Sci.* **109**, 2715–2726 [Medline](#)
21. Lee, H. S., Bellin, R. M., Walker, D. L., Patel, B., Powers, P., Liu, H., Garcia-Alvarez, B., de Pereda, J. M., Liddington, R. C., Volkmann, N., Hanein, D., Critchley, D. R., and Robson, R. M. (2004) Characterization of an actin-binding site within the talin FERM domain. *J. Mol. Biol.* **343**, 771–784 [CrossRef Medline](#)
22. Gingras, A. R., Bate, N., Goult, B. T., Patel, B., Kopp, P. M., Emsley, J., Barsukov, I. L., Roberts, G. C., and Critchley, D. R. (2010) Central region of talin has a unique fold that binds vinculin and actin. *J. Biol. Chem.* **285**, 29577–29587 [CrossRef Medline](#)
23. Gingras, A. R., Bate, N., Goult, B. T., Hazelwood, L., Canestrelli, I., Grossmann, J. G., Liu, H., Putz, N. S., Roberts, G. C., Volkmann, N., Hanein, D., Barsukov, I. L., and Critchley, D. R. (2008) The structure of the C-terminal actin-binding domain of talin. *EMBO J.* **27**, 458–469 [CrossRef Medline](#)
24. Kanchanawong, P., Shtengel, G., Pasapera, A. M., Ramko, E. B., Davidson, M. W., Hess, H. F., and Waterman, C. M. (2010) Nanoscale architecture of integrin-based cell adhesions. *Nature* **468**, 580–584 [CrossRef Medline](#)
25. Haining, A. W., Lieberthal, T. J., and Del Río Hernández, A. (2016) Talin: a mechanosensitive molecule in health and disease. *FASEB J.* **30**, 2073–2085 [CrossRef Medline](#)
26. Austen, K., Ringer, P., Mehlich, A., Chrostek-Grashoff, A., Kluger, C., Klingner, C., Sabass, B., Zent, R., Rief, M., and Grashoff, C. (2015) Extracellular rigidity sensing by talin isoform-specific mechanical linkages. *Nat. Cell Biol.* **17**, 1597–1606 [CrossRef Medline](#)
27. del Rio, A., Perez-Jimenez, R., Liu, R., Roca-Cusachs, P., Fernandez, J. M., and Sheetz, M. P. (2009) Stretching single talin rod molecules activates vinculin binding. *Science* **323**, 638–641 [CrossRef Medline](#)
28. Ciobanasu, C., Faivre, B., and Le Clairche, C. (2014) Actomyosin-dependent formation of the mechanosensitive talin-vinculin complex reinforces actin anchoring. *Nat. Commun.* **5**, 3095 [Medline](#)
29. Ciobanasu, C., Faivre, B., and Le Clairche, C. (2015) Reconstituting actomyosin-dependent mechanosensitive protein complexes *in vitro*. *Nat. Protoc.* **10**, 75–89 [Medline](#)
30. Atherton, P., Stutchbury, B., Wang, D. Y., Jethwa, D., Tsang, R., Meiler-Rodriguez, E., Wang, P., Bate, N., Zent, R., Barsukov, I. L., Goult, B. T., Critchley, D. R., and Ballestrem, C. (2015) Vinculin controls talin engagement with the actomyosin machinery. *Nat. Commun.* **6**, 10038 [CrossRef Medline](#)
31. Romero, S., Le Clairche, C., Didry, D., Egile, C., Pantaloni, D., and Carlier, M. F. (2004) Formin is a processive motor that requires profilin to accelerate actin assembly and associated ATP hydrolysis. *Cell* **119**, 419–429 [CrossRef Medline](#)
32. Laurent, V., Loisel, T. P., Harbeck, B., Wehman, A., Gröbe, L., Jockusch, B. M., Wehland, J., Gertler, F. B., and Carlier, M. F. (1999) Role of proteins of the Ena/VASP family in actin-based motility of *Listeria monocytogenes*. *J. Cell Biol.* **144**, 1245–1258 [CrossRef Medline](#)
33. Doolittle, L. K., Rosen, M. K., and Padrick, S. B. (2013) Measurement and analysis of *in vitro* actin polymerization. *Methods Mol. Biol.* **1046**, 273–293 [CrossRef Medline](#)
34. Anthis, N. J., Wegener, K. L., Critchley, D. R., and Campbell, I. D. (2010) Structural diversity in integrin/talin interactions. *Structure* **18**, 1654–1666 [CrossRef Medline](#)
35. Anthis, N. J., Haling, J. R., Oxley, C. L., Memo, M., Wegener, K. L., Lim, C. J., Ginsberg, M. H., and Campbell, I. D. (2009)  $\beta$  integrin tyrosine phosphorylation is a conserved mechanism for regulating talin-induced integrin activation. *J. Biol. Chem.* **284**, 36700–36710 [CrossRef Medline](#)
36. Chuang, J. Z., Lin, D. C., and Lin, S. (1995) Molecular cloning, expression, and mapping of the high affinity actin-capping domain of chicken cardiac tensin. *J. Cell Biol.* **128**, 1095–1109 [CrossRef Medline](#)
37. Wegener, K. L., Partridge, A. W., Han, J., Pickford, A. R., Liddington, R. C., Ginsberg, M. H., and Campbell, I. D. (2007) Structural basis of integrin activation by talin. *Cell* **128**, 171–182 [CrossRef Medline](#)
38. Anthis, N. J., Wegener, K. L., Ye, F., Kim, C., Goult, B. T., Lowe, E. D., Vakonakis, I., Bate, N., Critchley, D. R., Ginsberg, M. H., and Campbell, I. D. (2009) The structure of an integrin/talin complex reveals the basis of inside-out signal transduction. *EMBO J.* **28**, 3623–3632 [CrossRef Medline](#)
39. Ling, K., Doughman, R. L., Iyer, V. V., Firestone, A. J., Bairstow, S. F., Mosher, D. F., Schaller, M. D., and Anderson, R. A. (2003) Tyrosine phosphorylation of type I $\gamma$  phosphatidylinositol phosphate kinase by Src regulates an integrin-talin switch. *J. Cell Biol.* **163**, 1339–1349 [CrossRef Medline](#)
40. Friedland, J. C., Lee, M. H., and Boettiger, D. (2009) Mechanically activated integrin switch controls  $\alpha 5\beta 1$  function. *Science* **323**, 642–644 [CrossRef Medline](#)
41. Zhu, J., Luo, B. H., Xiao, T., Zhang, C., Nishida, N., and Springer, T. A. (2008) Structure of a complete integrin ectodomain in a physiologic resting state and activation and deactivation by applied forces. *Mol. Cell* **32**, 849–861 [CrossRef Medline](#)
42. O'Halloran, T., Molony, L., and Burridge, K. (1986) Purification and assay of vinculin, metavinculin, and talin. *Methods Enzymol.* **134**, 69–77 [CrossRef Medline](#)
43. García-Alvarez, B., de Pereda, J. M., Calderwood, D. A., Ulmer, T. S., Critchley, D., Campbell, I. D., Ginsberg, M. H., and Liddington, R. C. (2003) Structural determinants of integrin recognition by talin. *Mol. Cell* **11**, 49–58 [CrossRef Medline](#)

**Integrin-bound talin head inhibits actin filament barbed-end elongation**  
Corina Ciobanasu, Hong Wang, Véronique Henriot, Cécile Mathieu, Annabelle Fente,  
Sandrine Csillag, Clémence Vigouroux, Bruno Faivre and Christophe Le Clainche

*J. Biol. Chem.* 2018, 293:2586-2596.

doi: 10.1074/jbc.M117.808204 originally published online December 24, 2017

---

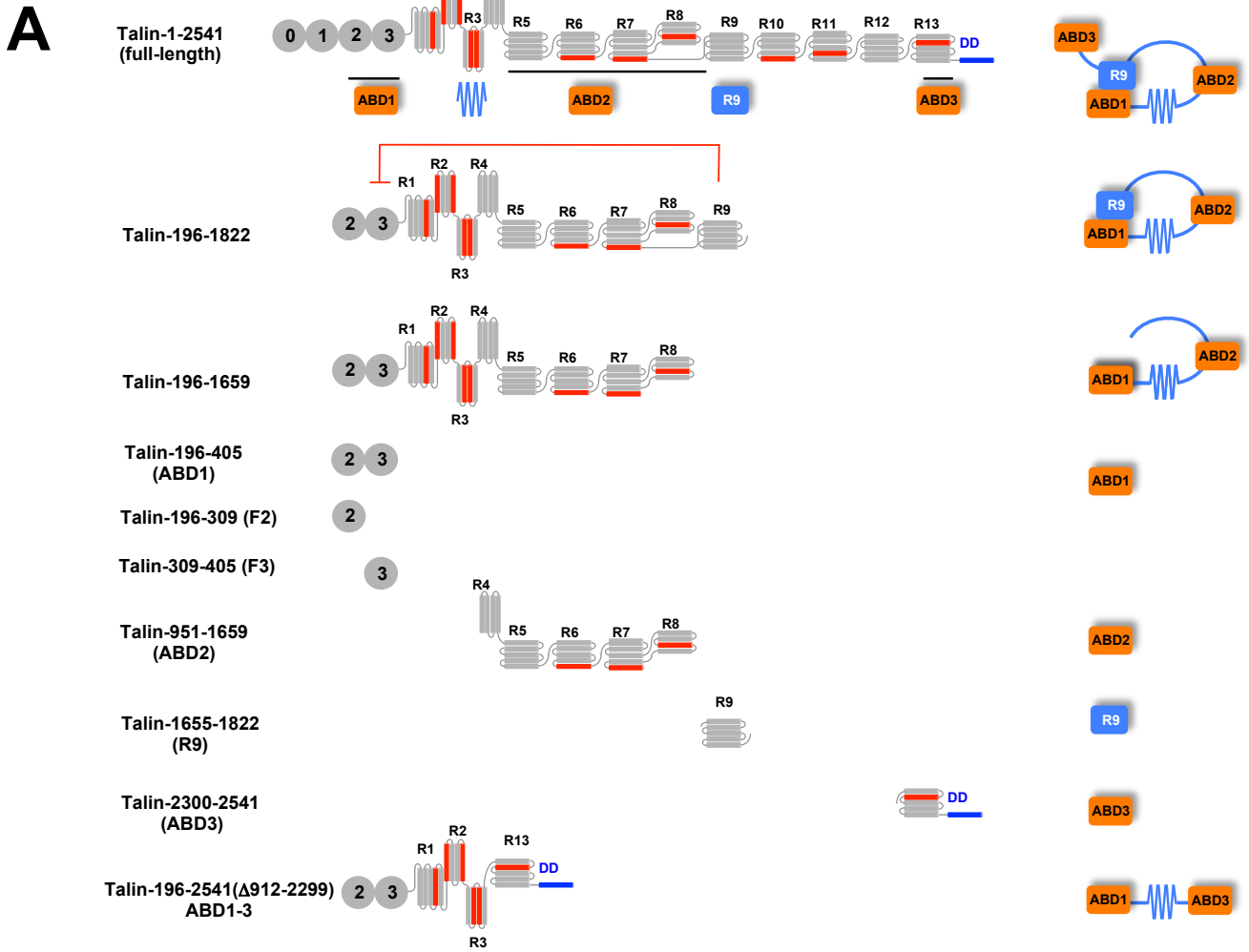
Access the most updated version of this article at doi: [10.1074/jbc.M117.808204](https://doi.org/10.1074/jbc.M117.808204)

Alerts:

- [When this article is cited](#)
- [When a correction for this article is posted](#)

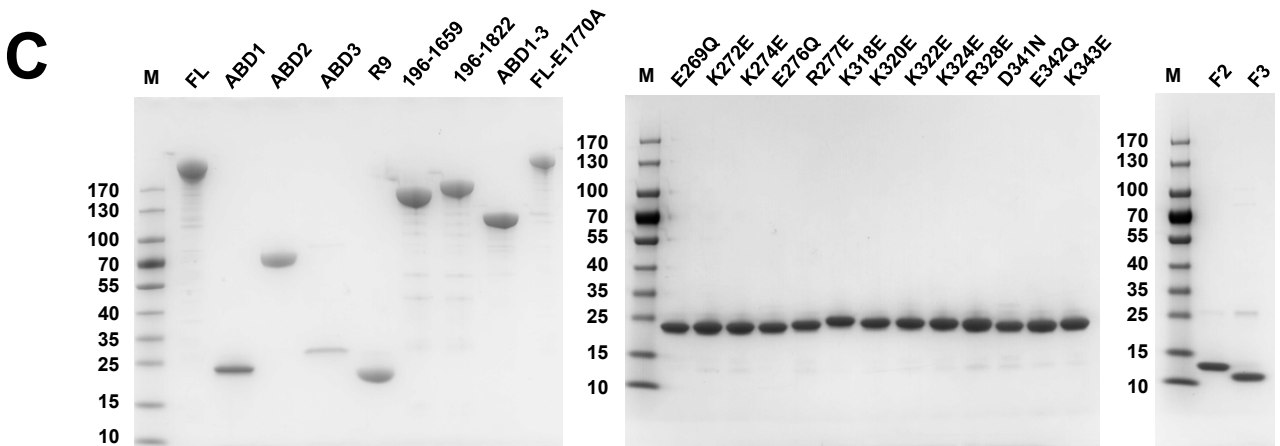
[Click here](#) to choose from all of JBC's e-mail alerts

This article cites 43 references, 15 of which can be accessed free at  
<http://www.jbc.org/content/293/7/2586.full.html#ref-list-1>

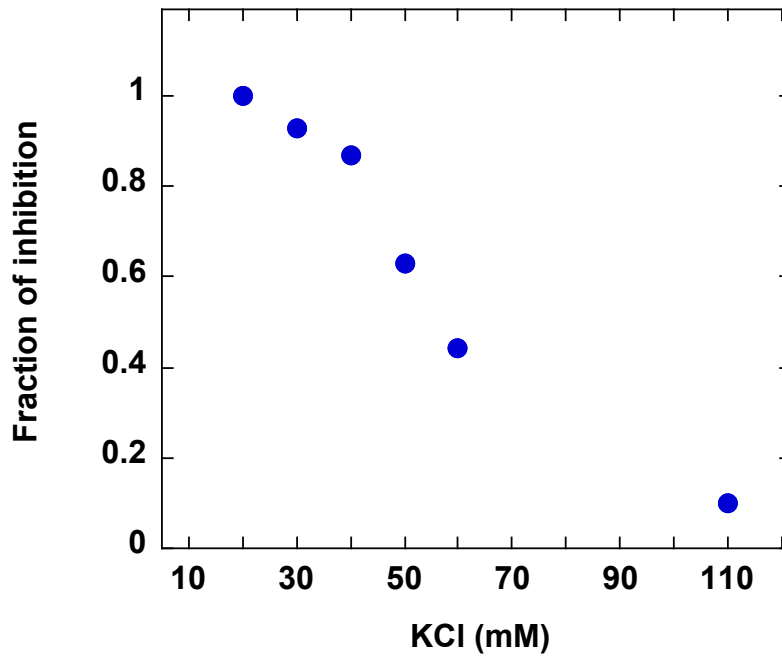


**B**

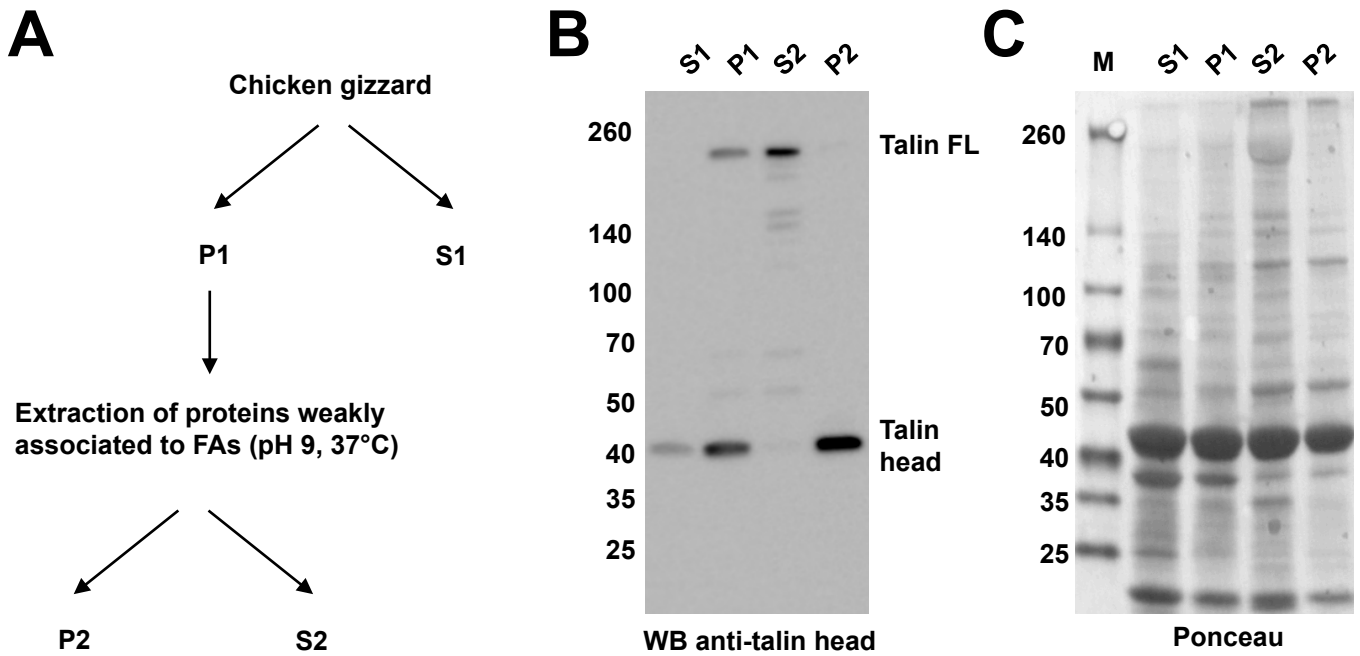
Integrin-β3	716	LLITITIHDRKEFAKFEFEERARAKWDTANNPLY	KEATSTFTNITYRGT	762
Integrin-β3 DTAN/VE		LLITITIHDRKEFAKFEFEERARAKW--VENPLY	KEATSTFTNITYRGT	
Integrin-β3-P DTAN/VE		LLITITIHDRKEFAKFEFEERARAKW--VENPLY <sub>p</sub>	KEATSTFTNITYRGT	



**Figure S1. Proteins used in the study.** (A) Constructs used in this study. A schematized version of each construct is shown on the right side. (B) Sequence of the integrin-β3 (DTAN/VE) peptides used in this study. The Y747 phosphorylation is indicated. (C) SDS-PAGE of the purified proteins used in this work stained with Coomassie blue. M indicates the molecular weight markers.

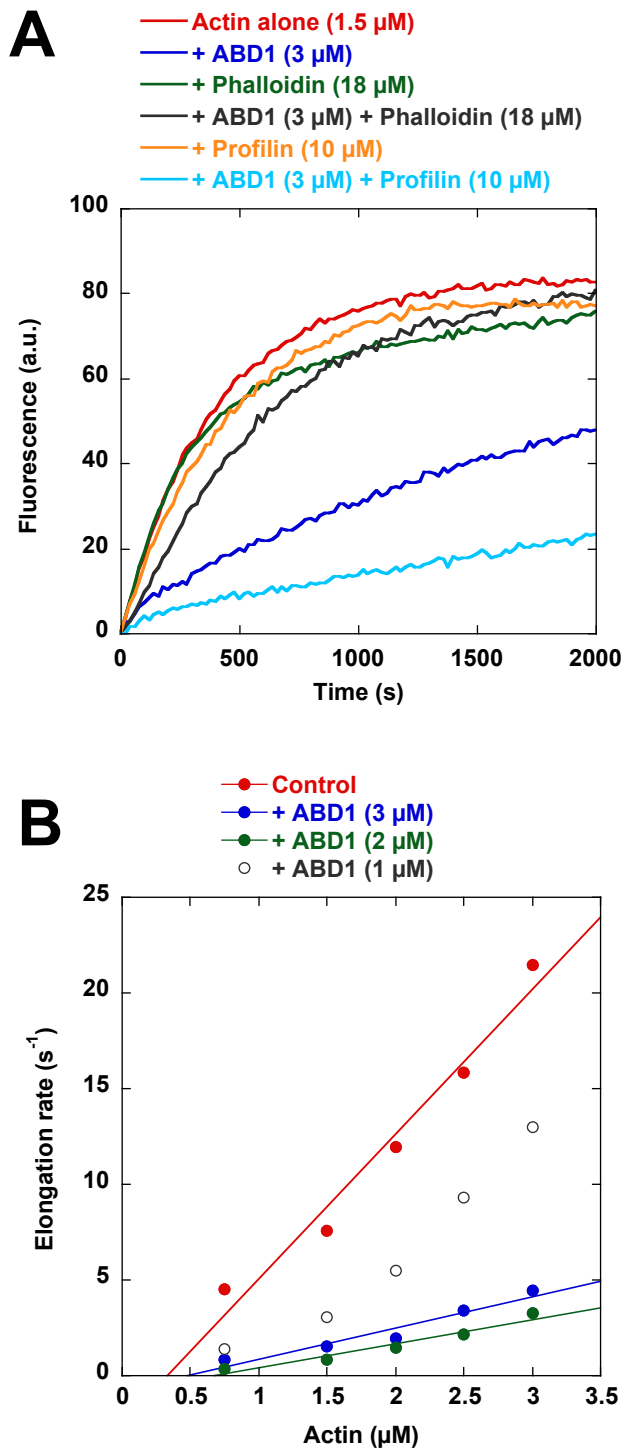


**Figure S2. ABD1 is sensitive to ionic strength** Actin was polymerized in the presence of 100 pM spectrin actin seeds, 1.5  $\mu$ M Mg-ATP-G-actin, in the absence (control) and presence of 3  $\mu$ M ABD1 and increasing concentrations of KCl. The initial slopes of barbed end growth were measured and the fraction of inhibition by ABD1 (relative to the control) was plotted as a function of the indicated concentrations of KCl.



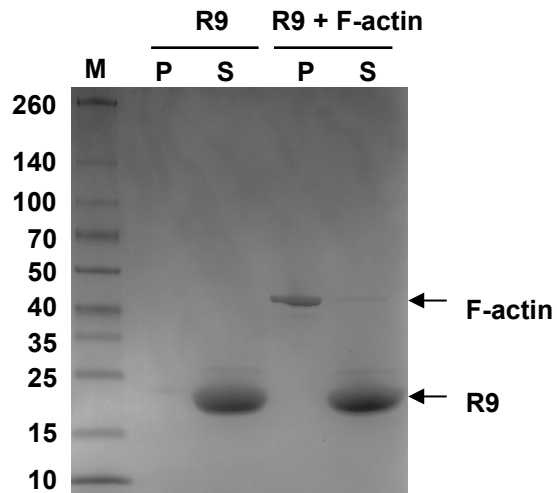
**Figure S3. Detection of talin head in biochemical fractions of chicken gizzard tissue.**

(A) Scheme of the biochemical fractionation. (B) All fractions were resolved by 4-15 % SDS-PAGE and talin was detected by western blotting with an antibody directed against talin head. (C) Ponceau red staining of the membrane probed in (B). M indicates the molecular weight markers.

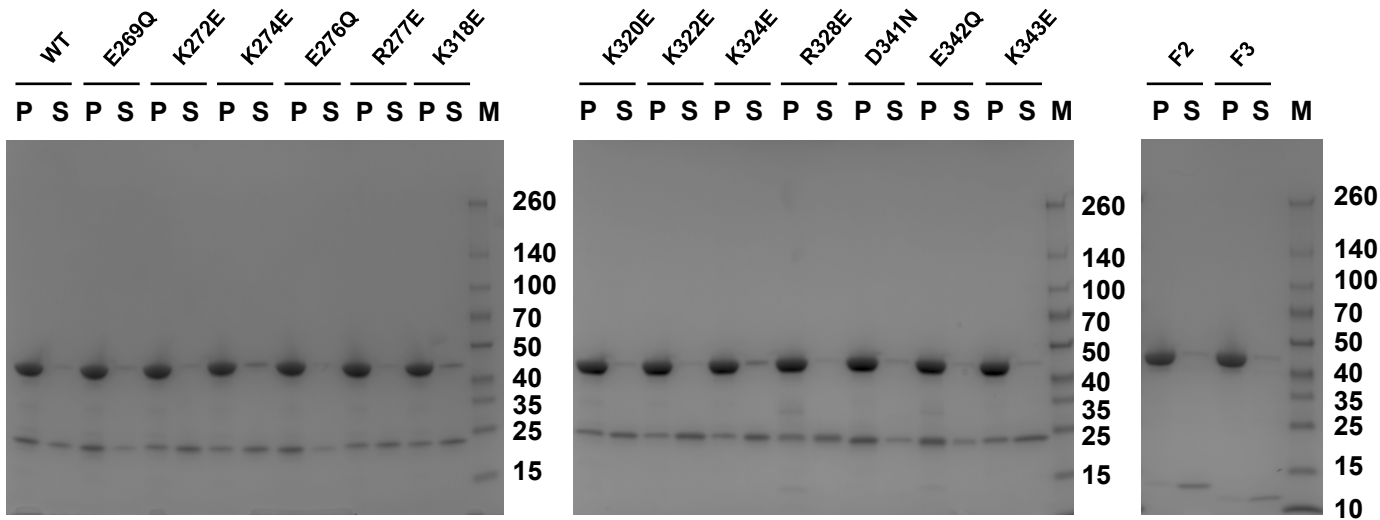
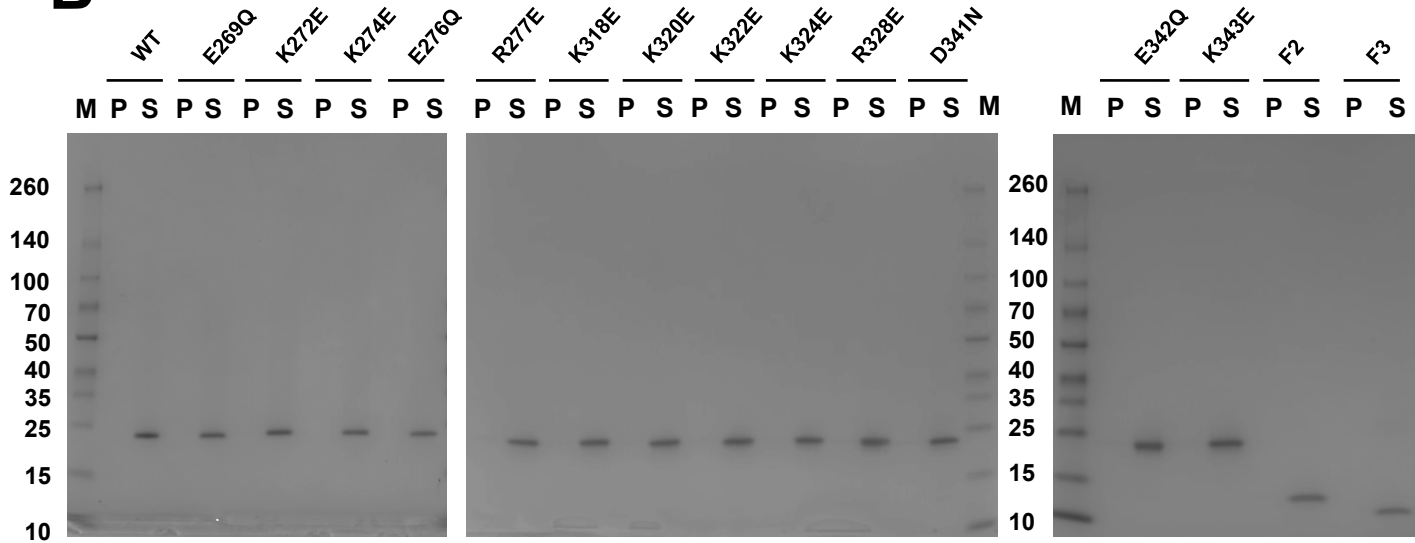


**Figure S4. ABD1 acts on actin filaments.** (A) Barbed-end elongation was measured in the presence of 100 pM spectrin-actin seeds, 1.5  $\mu\text{M}$  Mg-ATP-G-actin (10% pyrenyl-labeled) in the absence and in the presence of 3  $\mu\text{M}$  ABD1, 10  $\mu\text{M}$  profilin, 18  $\mu\text{M}$  phalloidin, ABD1 and profilin, ABD1 and phalloidin as indicated. (B) Barbed-end elongation was measured in the presence of 100 pM spectrin-actin seeds, 0.6, 1.5, 2, 2.5 and 3  $\mu\text{M}$  Mg-ATP-G-actin (10% pyrenyl-labeled) in the absence and in the presence of 1, 2 and 3  $\mu\text{M}$  ABD1.





**Figure S5. R9 does not bind to actin filaments.** R9 (10 $\mu$ M) was incubated with and without pre-polymerized actin (F-actin, 5  $\mu$ M) for 15 min at room temperature, centrifuged at 90,000 rpm for 30 min. The pellet (P) and supernatant (S) fractions were resolved by 4-15 % SDS-PAGE and detected by Coomassie blue. M indicates the molecular weight markers.

**A****B**

**Figure S6. ABD1 mutants bind to actin filaments in co-sedimentation assay.** (A) ABD1 and the indicated mutants (2  $\mu$ M) were incubated with pre-polymerized actin (20  $\mu$ M) for 15 min at room temperature and centrifuged at 90,000 rpm for 30 min. The pellet (P) and supernatant (S) fractions were resolved by 4-15 % SDS-PAGE and stained with Coomassie blue. (B) As a control, ABD1 and the indicated mutants (2  $\mu$ M) were incubated without actin for 15 min at room temperature, centrifuged at 90,000 rpm for 30 min. The pellet and supernatant were resolved by 4-15 % SDS-PAGE and stained with Coomassie blue. M indicates the molecular weight markers.

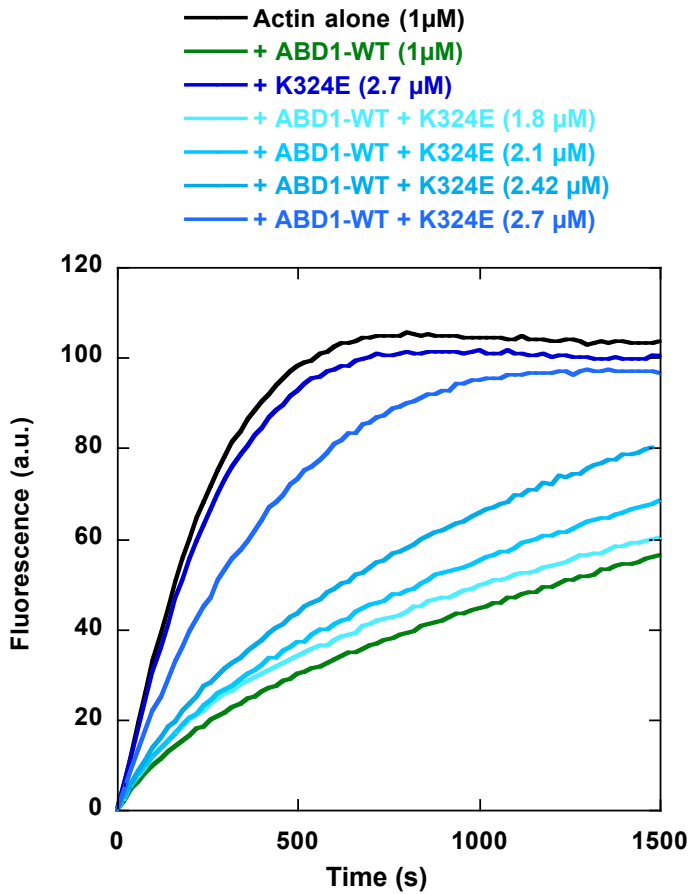


**Figure S7. ABD1 K324E competes with wild-type ABD1.** Barbed-end elongation was measured in the presence of 100 pM spectrin-actin seeds, 1  $\mu$ M Mg-ATP-G-actin (10% pyrenyl-labeled) in the absence and presence of 1  $\mu$ M wild-type ABD1 alone, 2.7  $\mu$ M ABD1 K324E alone and 1  $\mu$ M wild-type ABD1 and increasing concentrations of ABD1 K324E.

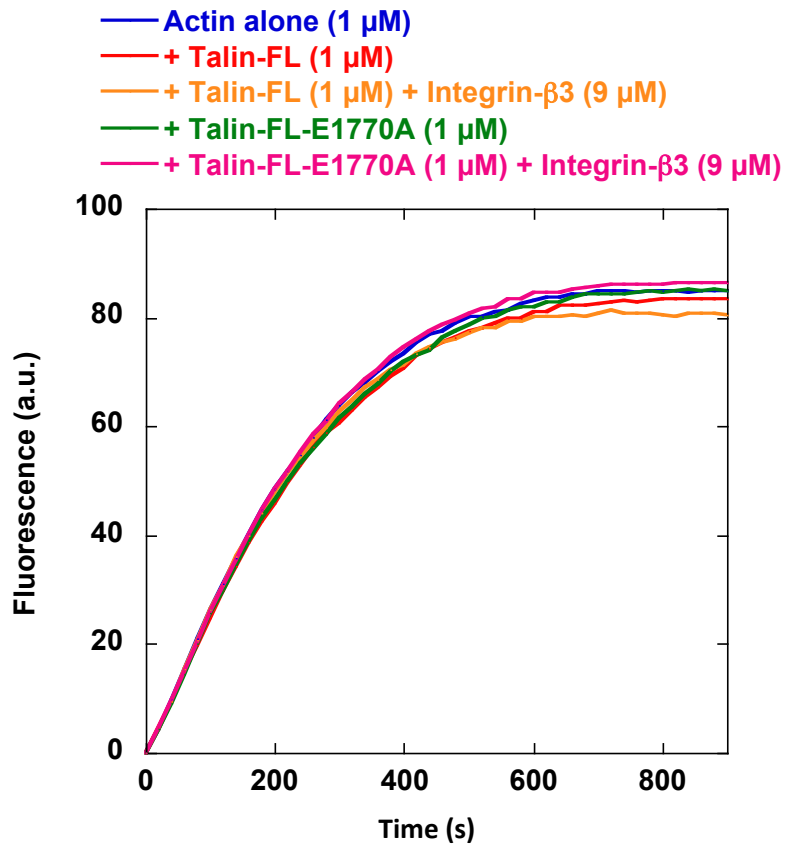


**Figure S8. Full-length talin and the E1770A mutant are inactive and are not activated by the integrin-β3 (DTAN/VE) peptide.** Barbed-end elongation was measured in the presence of 100 pM spectrin-actin seeds and 1 μM Mg-ATP-G-actin (10% pyrenyl-labeled) alone (dark blue) and in the presence of 1 μM full-length talin (red), 1 μM full-length talin + 9 μM of integrin-β3 (DTAN/VE) peptide (orange), 1 μM talin E1770A (green) and 1 μM talin E1770A + 9 μM of integrin-β3 (DTAN/VE) peptide (pink).

## LEGENDS OF SUPPLEMENTARY MOVIES

**Movie S1. Direct real-time observation of actin filament barbed elongation in TIRF microscopy.** Conditions: 1.5  $\mu$ M MgG-actin (5 % Alexa488- and 5% Biotin-labeled) in 5 mM Tris pH7.8, 200  $\mu$ M ATP, 0.8% methyl-cellulose, 1 mM DABCO, 25 mM KCl, 1 mM MgCl<sub>2</sub>, 200  $\mu$ M EGTA, 10 mM DTT. This movie is the control of the Movie S2 without ABD1. The yellow rectangle corresponds to the selection shown in Figure 2A.

**Movie S2. Direct real-time observation of the barbed-end capping-like activity of talin ABD1 in TIRF microscopy.** Conditions: 1.5  $\mu$ M MgG-actin (5 % Alexa488- and 5% Biotin-labeled) and 1  $\mu$ M Talin ABD1 in 5 mM Tris pH7.8, 200  $\mu$ M ATP, 0.8% methyl-cellulose, 1 mM DABCO, 25 mM KCl, 1 mM MgCl<sub>2</sub>, 200  $\mu$ M EGTA, 10 mM DTT. The yellow rectangle corresponds to the selection shown in Figure 2A.

**Titre :** Régulation de l'assemblage de l'actine et de la mécano-transduction dans les complexes d'adhérence à la matrice extracellulaire par la protéine RIAM

**Mots clés :** cytosquelette, adhérence, mécano-transduction, actine, myosine

**Résumé :**

Lors de la migration cellulaire, les complexes d'adhérence contrôlent la production de force et l'adaptation aux propriétés mécaniques de l'environnement. Le but de ce projet était de comprendre les mécanismes moléculaires par lesquels ces complexes contrôlent la force produite par l'assemblage du cytosquelette d'actine et codent une information mécanique en réaction biochimique. La première étude montre que les protéines taline, RIAM et VASP s'assemblent à la surface d'une membrane pour stimuler l'assemblage de l'actine par un nouveau

mécanisme. La deuxième partie est basée sur la reconstitution de la machinerie mécano-sensible des complexes d'adhérence avec des protéines pures sur une surface micro-imprimée observée en microscopie. L'étude montre que la protéine étirable taline échange son partenaire RIAM contre la vinculine en réponse à la force du cytosquelette. La taline code donc l'information mécanique en recrutant les partenaires qui correspondent à son degré d'étirement.

**Title :** Regulation of actin assembly and mechanotransduction in cell-matrix adhesion complexes by the protein RIAM

**Keywords :** cytoskeleton, adhesion, mechanotransduction, actin, myosin

**Abstract :**

During cell migration, adhesion complexes control the production of force and the adaptation to the mechanical properties of the environment. The aim of this project was to understand the molecular mechanisms by which these complexes control the force produced by actin assembly and encode mechanical information into biochemical reactions. The first study shows that the proteins talin, RIAM and VASP assemble on the surface of a membrane to stimulate actin assembly by a novel

mechanism. The second part is based on the reconstitution of the mechanosensitive machinery of the adhesion complexes with pure proteins on a micropatterned surface observed in microscopy. The study reveals that the stretchable protein talin exchanges its partner RIAM for vinculin in response to the force transmitted by the actin cytoskeleton. Talin thus codes mechanical information by recruiting partners that correspond to its degree of stretch.